A NUMERICAL STUDY ON THE DEPTH OF ACTIVE ZONE IN SHRINK-SWELL SOIL PROBLEM

A Dissertation

by

YUE CHEN

Submitted to the Office of Graduate and Professional Studies of
Texas A&M University
in partial fulfillment of the requirements for the degree of

DOCTOR OF PHILOSOPHY

Chair of Committee,	Marcelo Sánchez
Co-Chair of Committee,	Jean-Louis Briaud
Committee Members,	Charles Aubeny
	Youjun Deng
Head of Department,	Robin Autenrieth

December 2020

Major Subject: Civil Engineering

ABSTRACT

The damage triggered by shrink-swell soil movements (SSSM) on structures built on top of them continues being a source of problems for the construction industry worldwide that can be measured in millions of dollars annually. In order to maintain the serviceability of the structure, special concerns on the SSSM are required during the design process. This research focuses on the estimation of the depth of active zone (DAZ), as one of the key parameters in when dealing with shrink-swell soils. A fully coupled hydro-mechanical finite element program CODE_BRIGHT is adopted to investigate the extent of the DAZ numerically. The analyses focused on the estimation of the DAZ under different conditions, such as, position of the water table, soil permeability and environmental conditions. Besides, a survey involving geotechnical consultants was conducted to learn about the local knowledge and practice about the determination of the DAZ in different cities in Texas. The DAZ values collected from the survey agree well with the DAZ results obtained from numerical models that replicated the local conditions reported in the survey. The simulation results also show a good correlation between the permeability, ground water table, weather history and the depth of the active zone.

DEDICATION

To

My parents

&

My brothers

Xie, R.-H., Chen, Y.-P.; Li, Q.-F.

ACKNOWLEDGEMENTS

Firstly, I would like to thank my committee chair and vice chair, as well as my mentors and supervisors Dr. Marcelo Sanchez and Dr. Jean-Louis Briaud for their guidance and support throughout my academic career in Texas A&M University. Dr. Sanchez's passion on the research inspires me keep fighting on my work and Dr. Briaud set a model for me on how to have a perfect time management.

My thanks also go to my committee member, Dr. Charles Aubeny and Dr. Youjun Deng for their valuable comments and suggestion on my research. These comments significantly expand the view of my research and enrich the content of it.

Special thanks go to Mr. Mike Linger, our laboratory technician who gave me generous support when I have difficulties in lab activities; Dr. Dong Wang, who provides valuable suggestion on my research and academic life from Australia. Dr. Michael Maedo, my friend I indebted to, had me back up on coding whenever I needed.

I would also like to thanks my friends Du, Yichi; Zhou, Bohan; Chen, Shi; Zhu, Yichuan; Luo, Xi; Wang, Yen-Chih; Shang, Zihao, Husham Al Janabi, Lee, Junho; Park, Jaechan and all my board members in Geo-Institute TAMU Chapter for 2019-2020. You had made my time in the College Station a great adventure. The time we spent together working, laughing are my precious memory during my stay here.

Last but not least, I would like to thank my parents and brothers, for their faithful encouragement, support and endless love.

CONTRIBUTORS AND FUNDING SOURCES

Contributors

This work was supervised by a dissertation committee consisting of Professor Dr. Marcelo Sanchez (advisor), Dr. Jean-Louis Briaud (co-advisor), Dr. Charles Aubeny of the Department of Civil and Environmental Engineering and Dr. Youjun Deng of the Department of Soil and Crop Sciences.

All other work conducted for the dissertation was completed by the student independently.

Funding Sources

Graduate study was supported by a fellowship from CERGEP (Consortium for Education and Research in Geo-Engineering Practice) in Texas A&M University and Graduate Teaching Fellowship from the Zachry Department of Civil and Environmental Engineering.

The contents in this dissertation are solely the responsibility of the authors and do not necessarily represent the official views of the Department of Civil and Environmental Engineering.

TABLE OF CONTENTS

Page

LIST OF FIGURES

Page

LIST OF TABLES

Page

1. INTRODUCTION

1.1. Background and objective of the research

Shrink-swell soil (SSS), also named expansive or swelling soils, is a type of soil that exhibits large volume changes when subjected to wetting or drying processes. Soils are usually considered SSS if variations in water content (or suction) induce volumetric changes > 10% (Chen, 1975; Nelson & Miller, 1997). SSS movements are the source of several and serious problems in buildings and civil infrastructures. SSS are very common in the USA and the other countries. They brought a worldwide challenge to the geotechnical engineering industry (Jones & Jefferson, 2012). Therefore there is a global ad growing interest to improve the current understanding of this complex type of soil and provide possible solutions for the related problems. The ASCE estimates that 1/4 damaged infrastructures were due to the movement of SSS, and the annual damage of infrastructures exceeds $22 billion, as presented in Table 1.1. Nelson and Miller (Nelson & Miller, 1997) point out that the SSS cost grater finical loss to the property owner and the combination of earthquake, floods, hurricane, and tornado. In other countries, the shrink-swell soil also brought a tremendous loss. Some of the reported examples are £400 million in the United Kingdom (Driscoll & Crilly, 2000), € 3.3 billion in France (L D Johnson, 1973), ¥100 million in China (Ng et al., 2003), and $150 million in Victoria, Australia (Osman et al., 2005).

Table 1.1 Annual lost due to soil movement (Jones Jr & Holtz, 1973)

Construction category	Estimated averaged annual loss [in millions of USD]
Single-family home	300
Commercial buildings	360
Multi-story buildings	80
Walks, drives. Parking areas	110
Highway and streets	1,140
Underground utilities and service	100
Airports	40
Urban landslides	25
Others	100
Total:	2,255

The United States has widespread shrink-swell soil. Particularly in the middle and east southern parts of the country, such as states of Texas, Arizona, New Mexico, and part of California (the blue and red in Figure 1.1). The geotechnical industry spared no effort to eliminate the damaging movement induced by the shrink-swell soil.

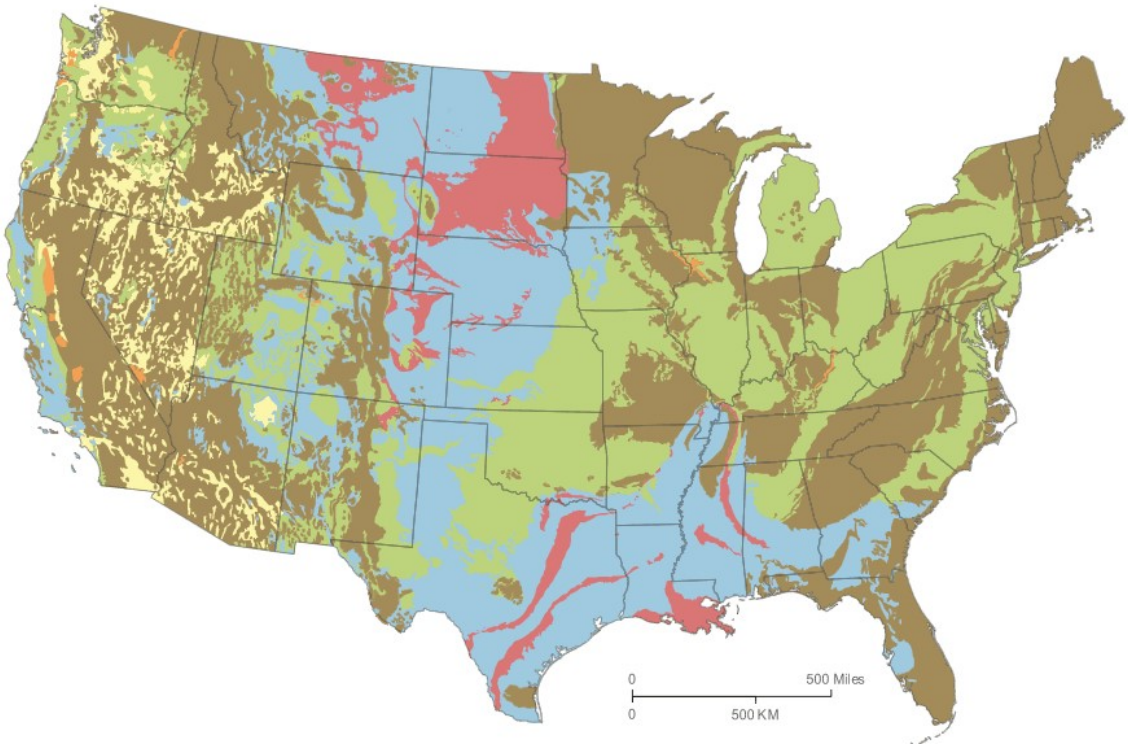

Figure 1.1 Swelling clay map of the United States (Olive et al., 1989)

At the present moment, numerous works had been conducted to seek an advanced understanding of shrink-swell soil behavior and further to carry out a more accurate prediction to solve such problem (e.g., Delwyn G. Fredlund, 1983; Delwyn G. Fredlund et al., 1980; Houston & Nelson, 2012; Lytton, 1994; Pedarla et al., 2016; Tu & Vanapalli, 2016; Vanapalli et al., 2010; Vu & Fredlund, 2004; Wray et al., 2005 but not limit). Two factors are considered as the main driven force to induce the shrink-swell soil movement, which are (1) suction (Aitchison & Martin, 1973; Alonso et al., 1990; Chiu & Ng, 2003; Fityus & Smith, 1998; Fredlund & Rahardjo, 1993) and (2) water content (Adem & Vanapalli, 2016; Briaud et al., 2003; J. Zhang et al., 2019; X. Zhang & Briaud, 2010). The suction driven movement relatives to the variation of stresses. Thus, the analysis of this movement problem can refer to other well-adopted constitutive models, which

makes suction driven analysis more popular among researches. The water content driven movement problem can be connected with the soil suction via the soil-water retention curve (SWRC) also known as soil-water characteristic curve (SWCC). The water content method is more practical and easier to operate in real projects as the water content measurement is one the most comment practice in geotechnical project. By considering the suction or water content variation, some of the semi-empirical methods had been proposed based on the researches on the surface movement of shrink-swell soil (BRAB, 1968; Nelson & Miller, 1997; Snowden, 1981a, 1996; Standards Association of Australia, 2011; Wang et al., 2016) and well accepted by the industry. These methods, which will be detail described in the following chapter, help to provide a logical framework on the analysis to the shrink-swell soil movement problem.

During the soil movement estimation, it is critical to determine the depth of soil to be considered, as known as the depth of active zone (DAZ). The role of the DAZ can be analogized to the zone of influence in the well-known soil settlement problem, which is the depth of soil that will affect by the suction/water content variation and induce movement. However, there are very few descriptions on how to estimate or determine the DAZ in the design methods mentioned previously or design standards. An over-estimated DAZ will lead to a costly conservatism design, while an under-estimated DAZ will induce a tremendous damage to the structure by a differential movement or distortion. Thus, a proper estimation value of DAZ is the first thing to do in the SSS movement problem.

The determination of the DAZ is challenging because of the fully-coupled hydro-mechanical analysis and the need to properly consider the in-situ conditions, such as, depth of water table, weather history, soil, water retention curve, saturated/unsaturated permeability, long-term analysis, among others. By assigning the depth of water table, soil properties, the numerical

simulation will provide a solution with the length of the weather history applied. The FEM result will help to determine the DAZ of the SSS through a period of time and will also estimate the corresponding surface movement.

Besides the depth of the active zone and the amount of movement (refers to swelling potential, P_s), the swelling pressure (SP) of soil is also important in the shrink-swell soil problem. The swelling pressure can analogy to the reaction force of a spring, depend on the type of spring, a small movement (P_s) can induce a large reaction force (SP). In this case, some of the methods eliminating the movement accomplish with additional surcharge may not be sufficient. Although the swelling potential is the most interested parameters in SSS problem, proper estimation method for the swelling pressure is also important in such the point of view.

1.2. Objectives

The underlying goal of this research is to advance the current understanding of the behavior of SSS, with particular emphasis on the depth of the depth of active zone. The DAZ is one of the most critical parameters when dealing with SSS, and its relevance can be assimilated to the stress influence zone when studying building settlements. The development of the active zone involves simultaneous and strongly coupled hydro-mechanical processes, as for example, unsaturated flow triggered by suction gradients, together with swelling/contraction processes associated with ability of this type of clay to absorb/release large amount of water during wetting/drying process. Suction gradients develop as a result of the interaction between the ground and the atmosphere. Therefore, proper estimation of the extent of the active zone requires long-term analysis and fully coupled hydraulic-mechanical analysis, where the local weather history provides the environmental (boundary) conditions to be used in the numerical model. This thesis integrates all of these components to achieve the main following objective:

- Gain a better understanding of the different factors and soil parameters affecting the behavior of SSS.
- Investigate the main factors affecting the extent of the active zone in SSS.
- Evaluate the impact of the DAZ and other factors on SSS movements.
- Proposed a quantitative definition for the depth of the active zone
- Validate the use of FEM analysis to determine the development of DAZ
- Prepare recommendations for remedial solutions and the design of foundations in SSS

1.3. Organization of the dissertation

This dissertation has nine sections. The main content of each section is introduced as follows:

Section 1 presents the introduction of the study. It states the study purpose, the overview, and the organization of this dissertation.

Section 2 is the literature review of comparative researches and works. This section includes some of the well-known design methods for foundations lying on shrink-swell soil. The surface movement is determined as the first step during the foundation design. Additional surface movement estimation methods are reviewed and compared to the corresponding part of the design methods. The mathematical framework in the porous medium problem is also introduced in this section. The mathematical framework adopts the mass balance equation to describe the mass flow within the medium and calculate the mechanical behavior simultaneously by constitutive equations. The constitutive model adopted in this works is the well-validated Modified Barcelona Basic (BBM), which is also described in this section.

Section 3 collected two cases history. The first case history is the foundation design on SSS. The design methods mentioned previously use the SI data of the first case history and perform foundation design. The design results are then compared to the actual design value of the foundation to present the conservative of different methods. The second case history focuses on the surface moment estimation. Again, the design methods are estimating the surface movement by using the SI data from the second case and then compared to the measured movement values.

Section 4 provides some comments and recommendations after revisiting the well-adopted methods mentioned in Section 2. Because of the particle methods had been used for a period of time, it is worth to take a back look into the methods again and discuss some of the assumptions

behind the processes. Additional explanations to the design methods are also included intend to have a better understanding of the design procedure is also included in this section.

Section 5 is devoted to the definition of the depth of the active zone. This section first compares the shrink-swell soil movement problem with the settlement problem to conclude a logical framework in solving the problem. By using the analogy result, the design procedure described in the previous section had been reorganized and demonstrated. The results point out that there is a consistency of the logic when considering the SSS problem and the settlement, and the importance of DAZ as well. Then, we summarized some of the definitions proposed in other literature. Based on our findings, we proposed a quantitative definition to the depth of the active zone. Although the criterion proposed in this work has a given value, they are not subjected to be fixed. Modification on the criterion for a more precise measurement or a rougher estimation is possible.

Section 6 presents a proposed empirical method to estimate the swelling pressure of the SSS. The swelling pressure is an important factor in the foundation design. A foundation lying on the shrink-swell soil is similar to a board sitting on a top of a vertical spring. The vertical displacement may be small, while the amount of reaction force may be large and damage the foundation. This section presents an empirical relationship between fundamental soil parameters and swelling pressure. Besides, some of the classification methods for the shrink-swell soil had been reviewed by using the data collected. The revision of the methods points out that with the same classification of the shrink-swell soil, the parameters such as swelling potential and swelling pressure may still be different.

Section 7 presents the numerical simulation to determine the depth of the active zone. The finite element code CODE_BRIGHT is adopted, and one of the most widely distributed

elastoplastic models for unsaturated soils, the Barcelona Basic Model (BBM), is implemented. The simulation is focusing on the sensitivity analysis of the soil parameter and weather conditions affecting on the DAZ. Further, by using the numerical tools, it is possible to investigate one of the remedial solutions of the SSS. The numerical tools can provide an economical solution to the SSS by replacing a certain amount of soil, such solution also refers to the optimum replacement depth.

Section 8 presents a summary of the practical value of DAZ within the State of Texas, collected from experienced consultant engineers. The empirical values may not be the best estimation value for the active zone depth but play as a reference value when there is no additional information provided. Also, the contour map of the collected data is presented to show the distribution of the DAZ. It will assist the site engineer in making a rough engineering judgment.

Section 9 is the overall conclusion of this work.

2. LITERATURE REVIEW

The literature review mainly divided into three part. The first part is the review of the empirical design methods for the slab-on-grade sitting on shrink-swell soil to resist the soil movement and maintain the serviceability of the infrastructure. The surface movement estimation is the first step among all the design methods, in the second part, alternative methods to estimate the surface movement are included. The third part is a general description of the numerical procedure adopted in the analysis.

2.1. Slab-on-Grade Design Methods

The design method BRAB method, proposed by the Building Research Advisory Board in 1957. It is the very first method dealing with the foundation design considering the soil movement. The WRI method proposed by Wire Reinforcement Institute in 1981 was developed based on the BRAB method and simplified

2.1.1. Building Research Advisory Board Method (BRAB Method)

2.1.1.1. Method Overview

The BRAB method was proposed in 1957 by the Building Research Advisory Board (BRAB) under a contract between the Federal Housing Administration and the National Academy of Sciences, to determine criteria for proper design and construction of slabs-on-ground to ensure structural soundness. In this report, only the depth of the stiffening beams is discussed. The design method is summarized as Figure 2.1 and detailed describe as follows,

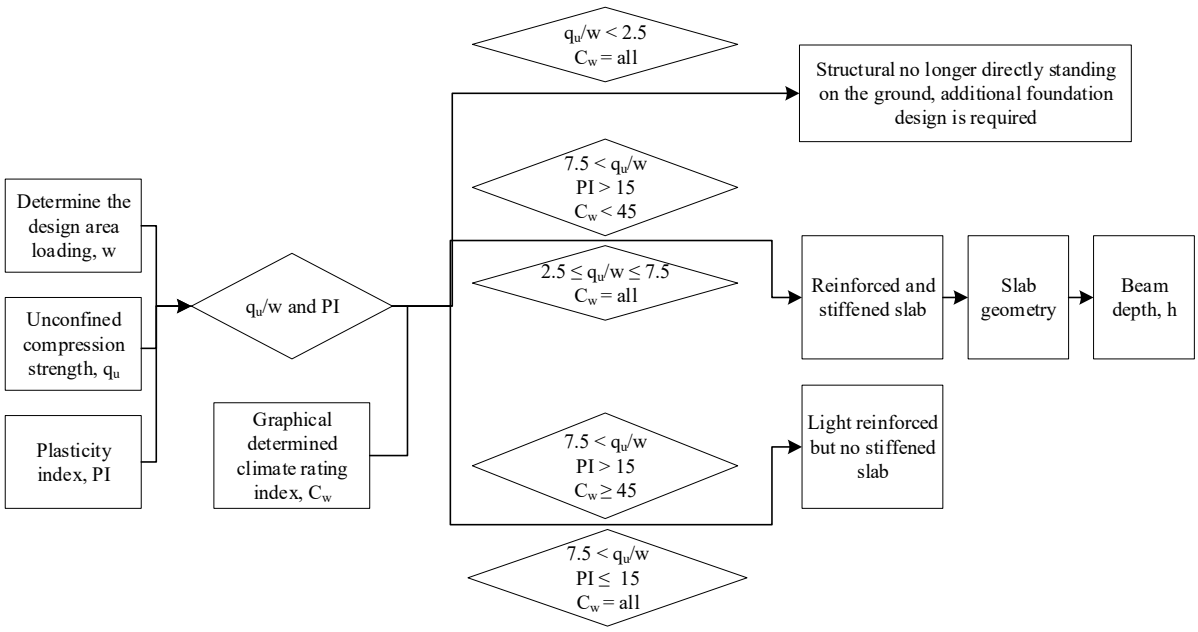

Figure 2.1 Design procedure of the BRAB method

2.1.1.1.1. Design Steps

- *Step 1 Site investigation*, at least one test boring should be performed per slab site to a depth of 15 feet below the existing ground surface or below the bottom of the slab. If the soil USCS classification is GW, GP, GM, GC, SW, SP, SM, SC, ML, MH, there is no need for stiffening beams.
- *Step 2 Determine the plasticity index (PI).* The plasticity index used in this method is a weighted average PI value over the 15 feet of soil immediately below the lowest elevation of the slab. The weight factors 3, 2, 1 are used for every 5 feet with depth. A sample calculation, as shown in Figure 2.2.

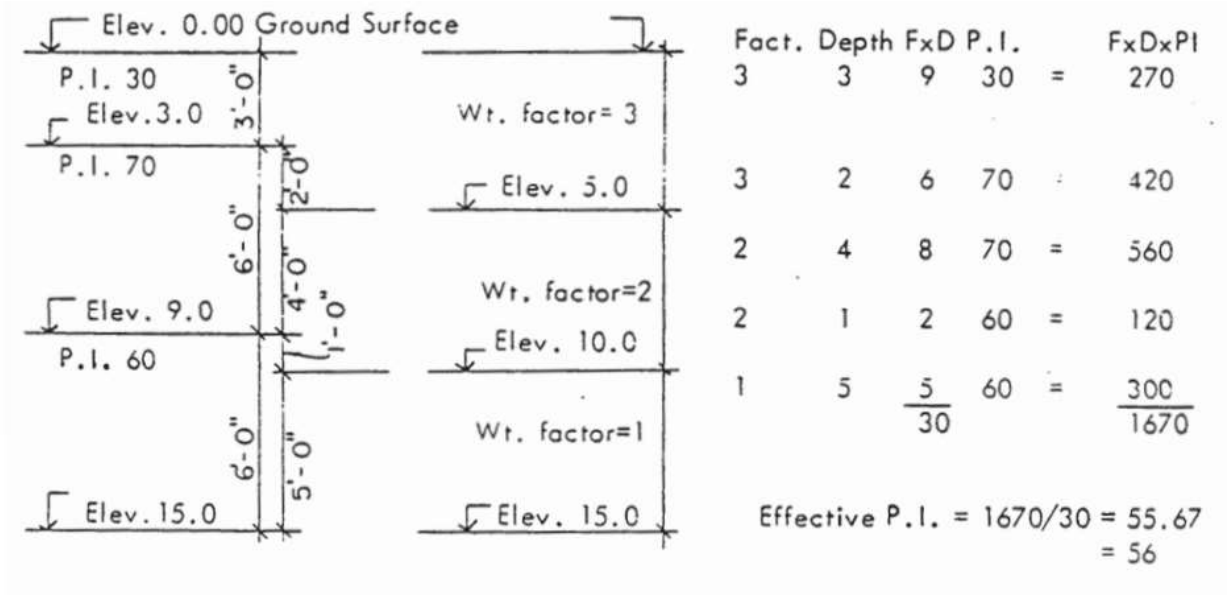

Figure 2.2 Hypothetical soil profile with variable PI (BRAB, 1968)

- *Step 3 Estimate the average total load* w (Unit converted)

$$w = w_d + w_s \tag{2.1}$$

w_d Dead load empirically determined as $w_d = L+1.5$ kPa
L Long side of the rectangular slab in m
w_s Superstructure load, 1 kPa of floor area, 0.5 kPa of roof area

- *Step 4 Determine the climate rating index* C_w based on the location of the construction project in Figure 2.3. The climate rating was determined from the U.S. Weather Bureau information, including the yearly annual precipitation, the number of times precipitation occurs, the duration of each occurrence and the amount of rainfall at each occurrence. The larger the numerical rating, the higher the abundance of moisture. (Nelson & Miller, 1997)

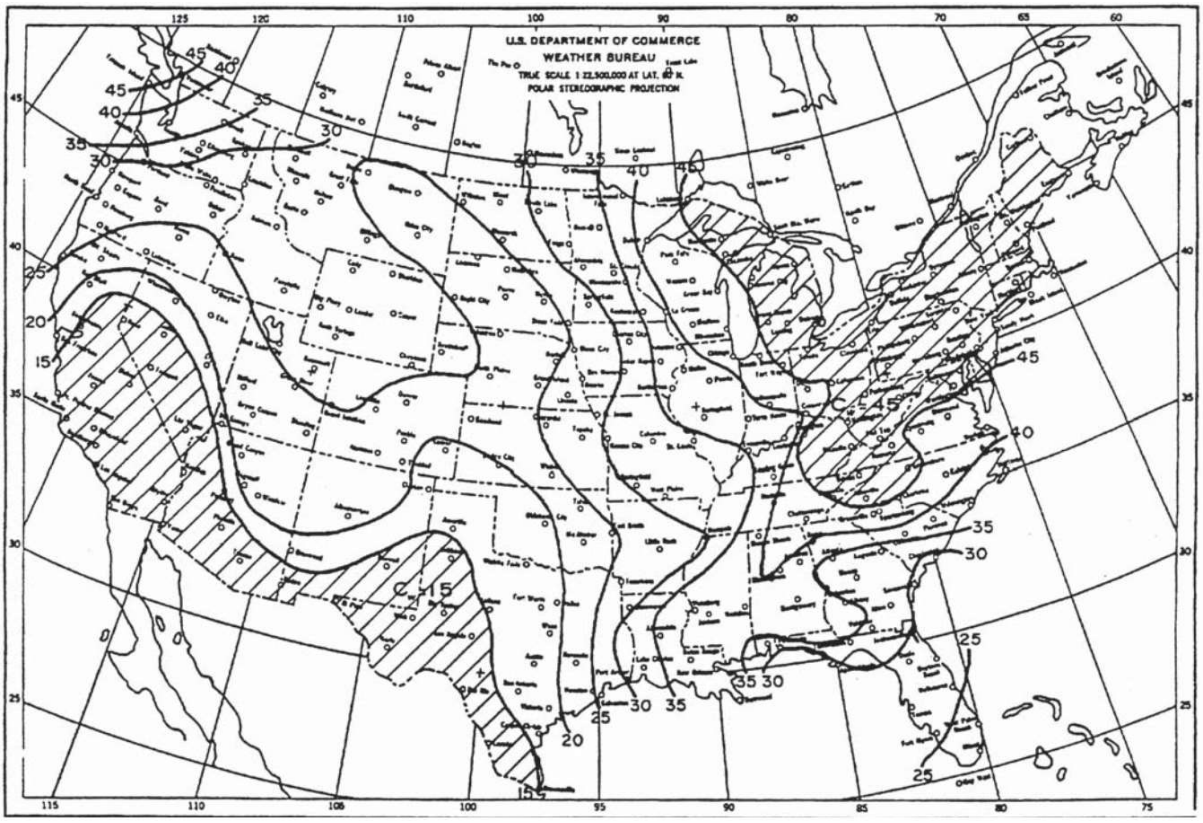

Figure 2.3 Climatic ratings C_w for the continental United States (shallow areas are extreme values) (BRAB, 1968)

- *Step 5 Determine the lowest unconfined compressive strength* q_u of undisturbed samples within the top 15 feet (4.5m) below the lowest point of the slab. Determine the type of foundation needed basing on the q_u/w value and the climate rating as follows.

Table 2.1 Foundation recommendations (BRAB, 1968)

q_u/w Value	Climate Rating	Recommendation of Foundation
< 2.5	All	Structural support (no longer directly support on the ground)
[2.5, 7.5]	All	Reinforced and stiffened
>7.5 & PI>15	C_w<45	
	C_w≥45	Lightly reinforced
>7.5 & PI≤15	All	

- *Step 6 Determine the support index* C of the soil according to the PI and C_w values according to Figure 2.4

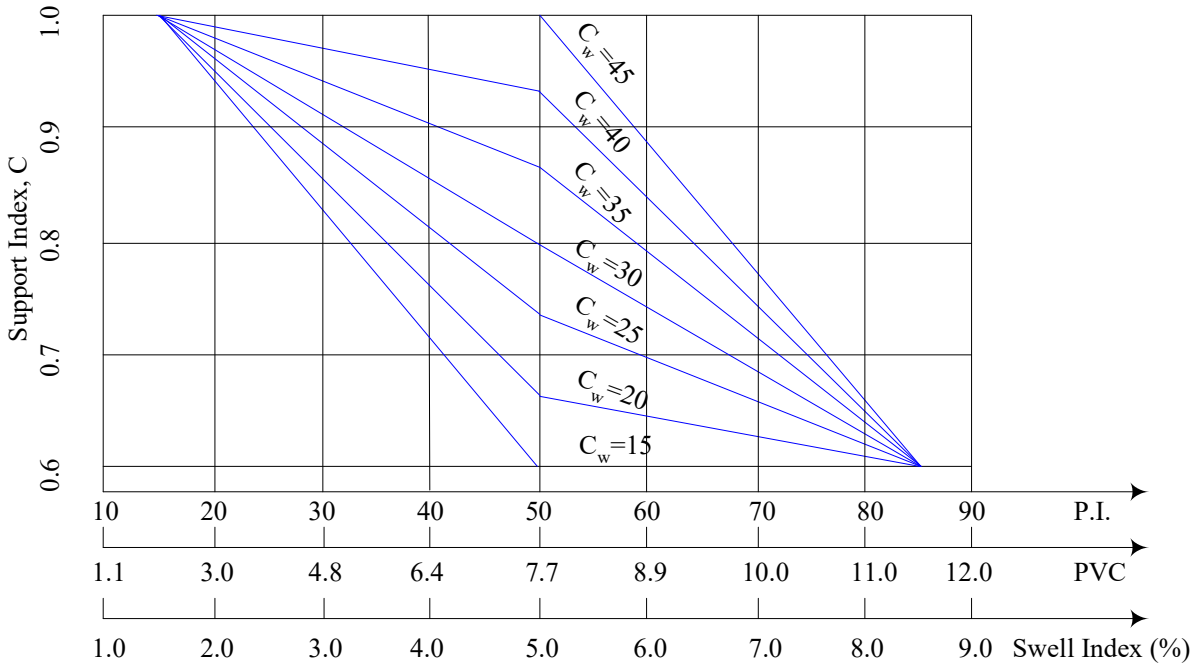

Figure 2.4 Support index C based on the criterion for soil sensitivity and climatic rating C_w (BRAB, 1968)

If the q_u/w value is within 2.5 to 7.5 ($q_u/w \in [2.5, 7.5]$), the support index C should be reduced to C_r as follows.

$$C_r = \left(2.5 - \frac{q_u}{w}\right)\left[0.13 - 0.2\left(\frac{w_c}{w} + C\right)\right] + \left(0.65 - \frac{w_c}{w}\right) \quad for \; C > 0.65 - \frac{w_c}{w} \tag{2.2}$$

$$C_r = C \quad for \quad C < 0.65 - \frac{w_c}{w} \tag{2.3}$$

q_u Unconfined compressive stress, in kPa
w_c Total concentrated dead and live loads distributed on the slab, in kPa
w Total slab dead and live load averaged over the entire slab area, in kPa

- *Step 7 Divide slabs of irregular shape* into overlapping rectangles with the long length of L and the short length of L'. Calculate the maximum bending moment, shear force, and deflection as follows.

$$M_{\max}\left[kN\cdot m\right]=\frac{wL^2L'\left(1-C\right)}{8}$$
$$V_{\max}\left[kN\right]=\frac{wLL'\left(1-C\right)}{2} \quad (2.4)$$
$$\Delta_{\max}\left[m\right]=\frac{wL^4L'\left(1-C\right)}{48EI}$$

- *Step 8 Design the beam depth* by limiting the deflection in Eq.(2.4) to an acceptable value.

2.1.1.2. Guidelines from the Texas ASCE (TxASCE, 2007)

In Eq. (2.4), the calculation involves the entire length of the slab. If the slab has a very long side, the design force would be considerable. Thus, the Texas ASCE guidelines recommend limiting the design by the BRAB method to a maximum of 50 ft. (Clause 5.2.2.1)

2.1.2. Wire Reinforcement Institute (WRI Method)

2.1.2.1. Method Overview

The WRI method was proposed by Walter L. Snowden (1981, 1996). It is an empirical method developed after observing slab performance and modifying equations to give results approximating the foundations that had been found to provide satisfactory results. The WRI method follows approximately the same procedure as the BRAB method mentioned previously. However, Snowden (Snowden, 1981b) suggested that the beam depth by the BRAB method might become extremely large because it considers the entire length of the slab. Thus, in the WRI method, new design charts are proposed to maintain a reasonable ratio between cost and efficiency. The design method of the slab is summarized as Figure 2.5 and detailed describe as follows.

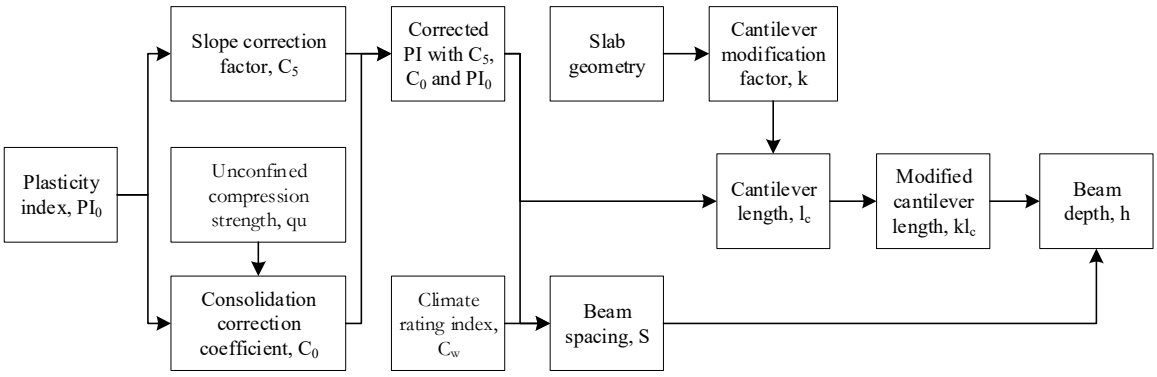

Figure 2.5 Design procedure of WRI method

2.1.2.1.1. Design Steps

- *Step 1 Site investigation*. A minimum of one boring is recommended for each isolated site and at least two borings where shrink-swell clay is found. Samples are taken at 0.5m intervals to a depth of at least 4.5m or deeper. The unconfined compression strength of at least 95 kPa is usually sufficient for single-story frame houses with 190 kPa usually adequate for commercial buildings and multi-story dwellings.

- *Step 2 Determine the "effective PI."* First, determine the weighted average PI within the top 15 feet as in the BRAB method shown in Figure 2.2. Second, consider the effect of the slope of the natural ground and the increase in unconfined compression strength due to the consolidation process. Figures 8 and 9 give the slope correction coefficient C_s and consolidation correction coefficient C_0.

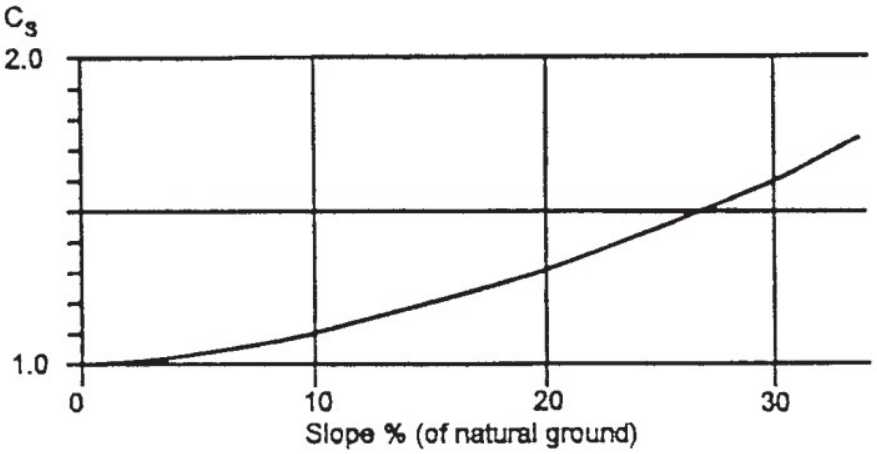

Figure 2.6 Slope of natural ground vs. slope correction coefficient (Snowden, 1981)

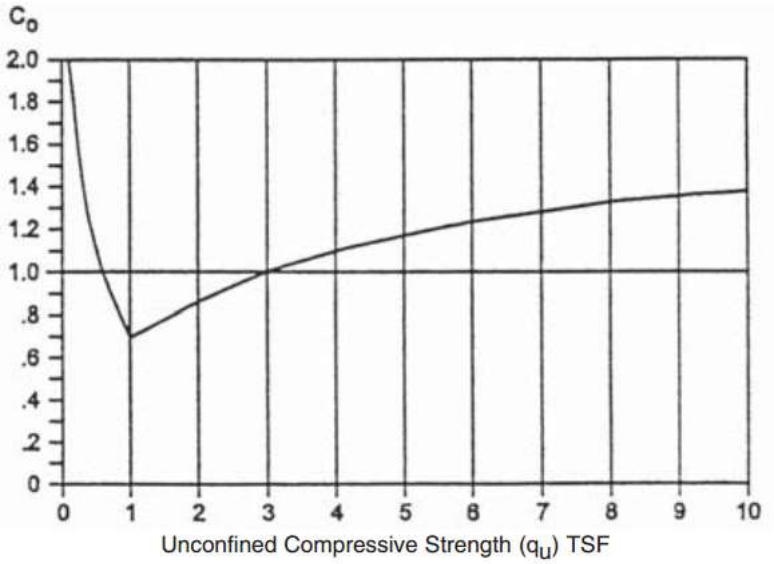

Figure 2.7 Unconfined compressive strength vs. consolidation correction coefficient (Snowden, 1981)

The effective PI is then

$$PI_o = PI_{Equivalent} \times C_5 \times C_o \tag{2.5}$$

C_5 Slope correction coefficient
C_0 Consolidation correction coefficient

For example,

The equivalent (or weighted) PI =30
10% ground slope (C_5) =1.1
Unconfined compression strength (C_0) =1.2

Then the effective plasticity index PI_o is

$$PI_o = 30 \times 1.1 \times 1.2 = 39.6 (use\ 40)$$

- *Step 3 Determine the loading conditions*. A uniform load assumption is considered adequate for 1 to 3 stories of a wood-frame building. Attention should be paid when there are large concentrated loads and numerous columns.

- *Step 4 Determine the climate rating index C_w*. This is the same index as in the BRAB method (Figure 2.3), based on the location of the project.

- *Step 5 Determine the cantilever length l_c*, beam spacing s, based on the climate rating index $C_{w,}$ and the effective PI in Figure 10.

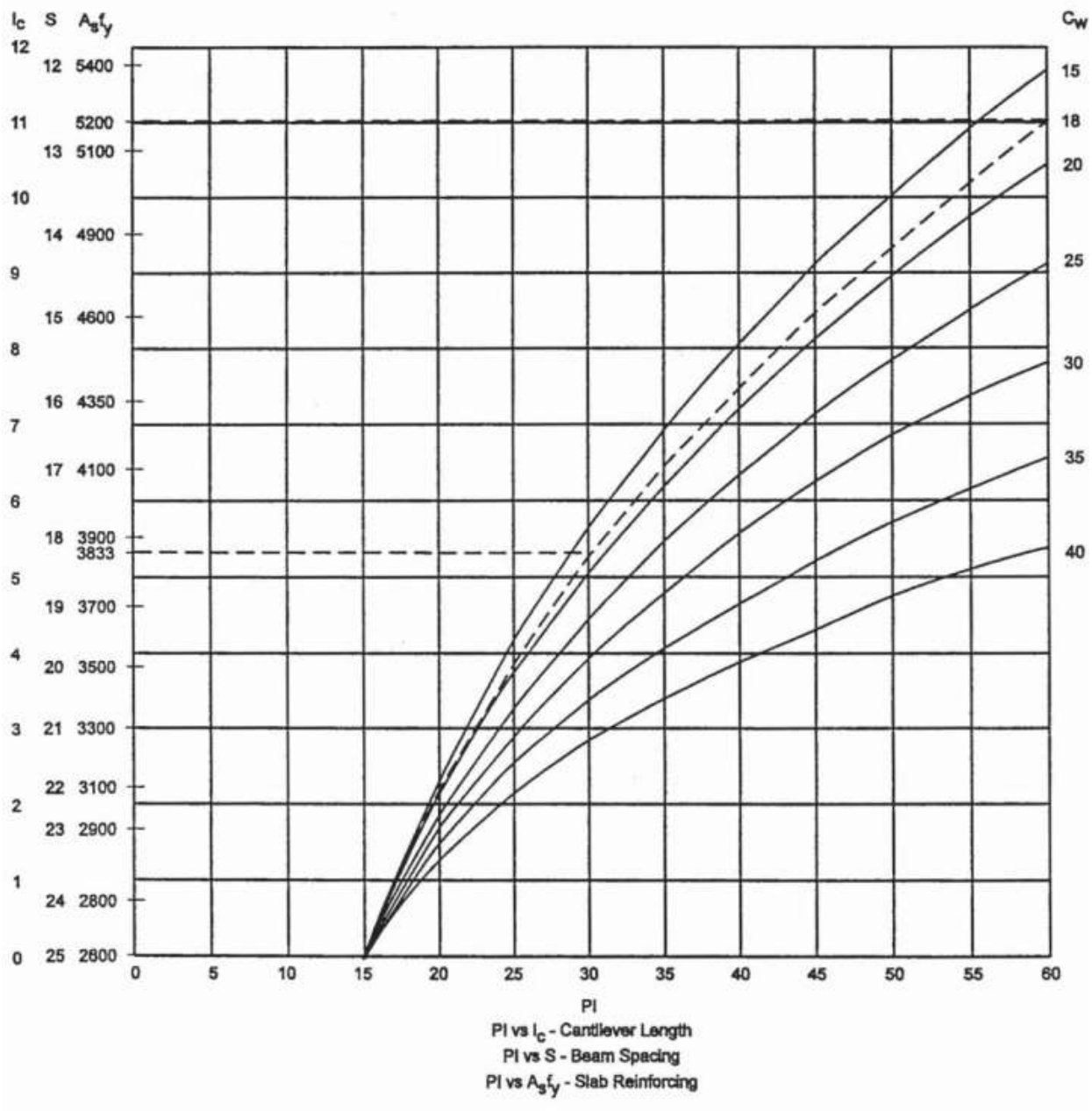

Figure 2.8 PI_0 vs. Cantilever length (l_c, ft), beam spacing (s, ft) and slab reinforcement ($A_s \times f_y$) (Snowden, 1981)

- *Step 6 Determine the modification factor for cantilever length k.* In this step, slabs of irregular shape are divided into overlapping rectangles with long length L and short length L'. Then find the k value from Figure 11. Use the designation k_L for the k value corresponding to the long length L and k_s for the length L'.

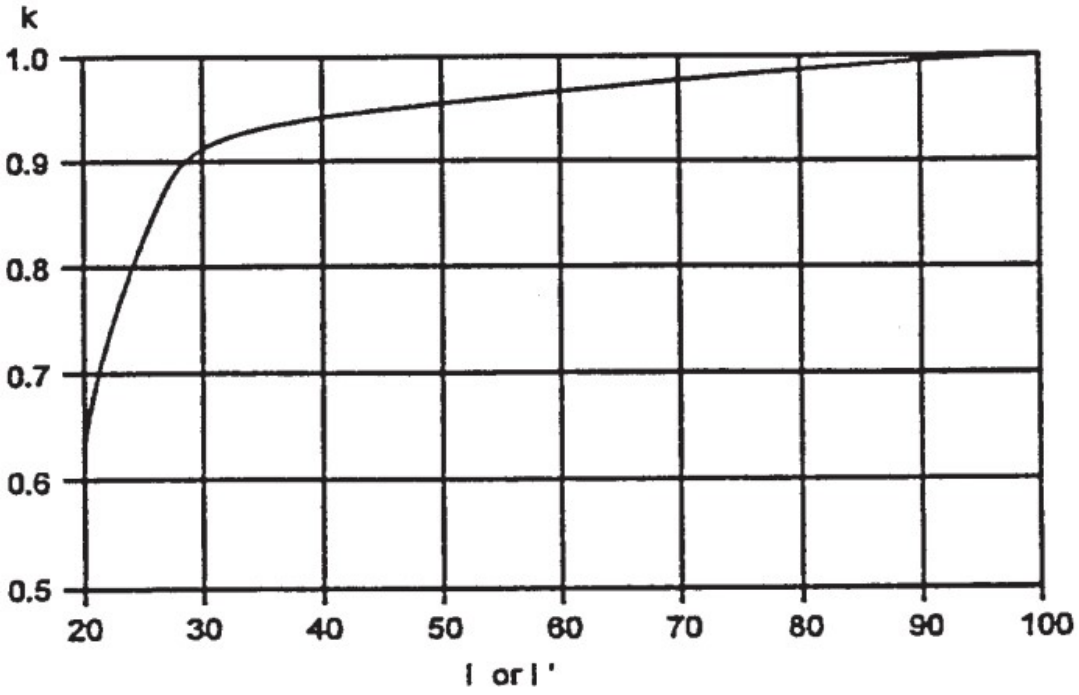

Figure 2.9 *L* or *L'* vs. modification factor k (Snowden, 1981)

- *Step 7 Modify the cantilever length* in both directions. In the long direction, the cantilever length is $k_L L$ and in the short direction $k_s L'$

- *Step 8 Calculate the number of beams* in both directions

$$N = \frac{L \text{ or } L'}{S} + 1 \tag{2.6}$$

N Number of beams
L or L' Length of the slab, in m
s Spacing from Figure 2.9, in m

- *Step 9 Assume a beam width*, calculate the sum B of all beamwidth in each direction

- *Step 10 Calculate the maximum bending moment and shearing force*

$$M_{\max} = \frac{wL'(L_c)^2}{2}$$
$$V_{\max} = wL_c L', \tag{2.7}$$

- *Step 11 Calculate the beam depth* *(note: the empirical relationship based on the imperial unit)*

$$d = \sqrt[3]{\frac{664ML_c}{B}} \left(\text{Reinforced steel}\right)$$
$$d = \sqrt[3]{\frac{553ML_c}{B}} \left(\text{Prestressed}\right) \tag{2.8}$$

d Beam depth, in inch
B Sum of all width, in inch
M Moment, in kips•ft
L_c Cantilever length modified by k, in ft

- *Step 12 Calculate the deflection for each direction*,

$$\Delta_{\max} = \frac{wL_c{}^4 L'}{4E_c I} \tag{2.9}$$

w Uniform distributed the load, in kPa
L_c Modified L_c with k_L or k_S, in m
E_c Elastic creep modulus of concrete, in kPa
I Moment inertia of section, in m^4

2.1.2.2. Guidelines from Texas ASCE (TxASCE, 2007)

From Eq. (2.7) to Eq. (2.9), the calculations involve the length of the slab in the short direction and the cantilever length. The Texas ASCE guidelines suggest the slab length be limited to 15m and that the cantilever length should be more significant than 1.8m (Clause 5.2.2.4).

2.1.3. Australian Standard AS 2870

2.1.3.1. Method Overview

The Australia Standard AS 2870 method was prepared by the Standards Australia Committee BD/25 on Residential Slab and Footings to supersede AS 2870.1-1996, and the most updated version is AS 2870.1-2011. The AS 2870 emphasis is on the design of foundations on reactive clay sites subject to significant ground movement due to moisture changes. The procedure of AS 2870 method is summarized in Figure 2.10 and detailed described as follows:

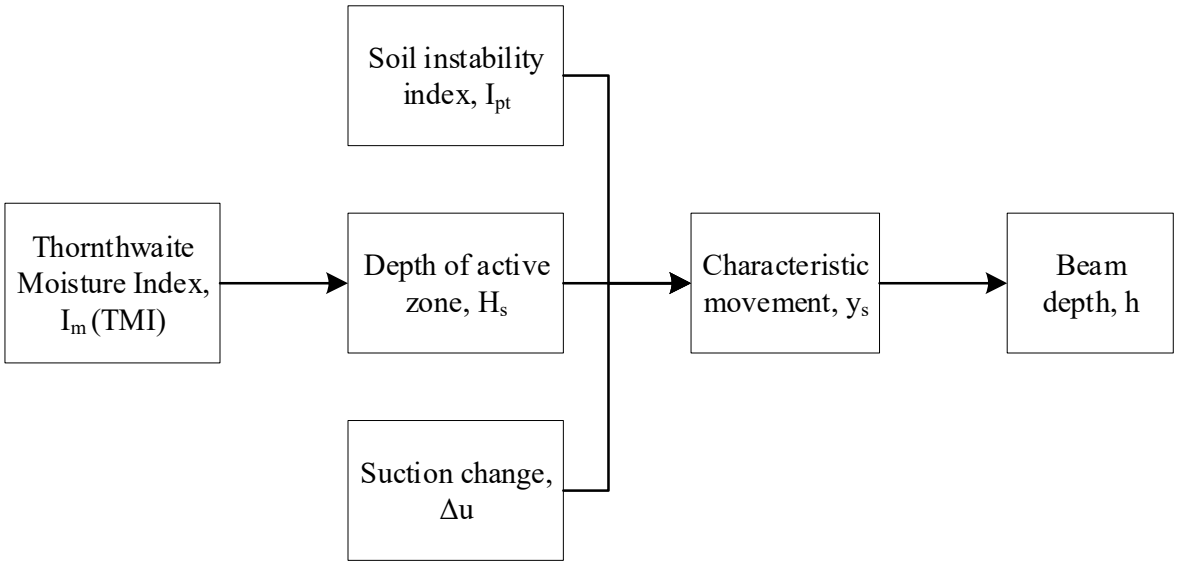

Figure 2.10 Design procedure of AS 2870 method

2.1.3.1.1. Design Steps

- *Step 1 Determine the depth of suction change H_s*. AS 2870 divides Australia into 6 climate zones and recommends the H_s value based on the Thornthwaite Moisture Index (TMI) (Table 2.2).

Table 2.2 Depth of design suction change for different climatic zones (AS 2870, 2011)

Climate Zone	TMI	H_s (m)
1	>10 to 40	1.5
2	≥ -5 to 10	1.8
3	≥ -15 to ≤ -5	2.3
4	≥ -25 to ≤ -15	3.0
5	≥ -40 to ≤ -25	4.0
6	≤40	> 4.0

- *Step 2 Determine the free shrinkage index or instability index I_{ps}*. The instability index is defined as the percentage of vertical strain per unit change in suction (in a unit of %/pF). The soil depth (usually the thickness of H_s) is divided into sublayers with similar soil properties, e.g., similar PI value.

- *Step 3 Determine the depth from the ground level to the uncracked zone* z. Typically, the thickness of the cracked zone can be estimated as

$$z \approx 0.33H_s \text{ to } 1.0H_s \tag{2.10}$$

- *Step 4 Determine the effective instability index I_{pt}*, which is the percentage of vertical strain per unit change in suction in pF, including the allowance for lateral restraint and vertical load.

$$I_{pt} = \alpha \times I_{ps} \tag{2.11}$$

α is a constant determined by the elevation of the point considered,

α=1 In the cracked zone (unrestrained)
α=2-z/5 In the uncracked zone (restrained)

- *Step 5 Determine the suction change* $\Delta\bar{u}$ at depth (z) from the surface in pF.
- *Step 6 Determine the characteristic movement y_s* (mm) by summing the movement for each layer as follows

$$y_s = \frac{1}{100}\sum_{n=1}^{N}\left(I_{pt}\Delta\bar{u}h\right)_n \tag{2.12}$$

y_s Characteristic surface movement, in mm
I_{pt} Instability index, in %/pF
N Number of soil layers within the design depth
$\Delta\bar{u}$ Soil suction change averaged over the thickness of the layer under consideration, in pF
h The thickness of the layer under consideration, in mm

- *Step 7 Determine the maximum allowable deflection* Δ based on different types of structures. AS 2870 provides the maximum permissible deflection as a function of the span length L as well as a maximum deflection value, as shown in Table 2.3

Table 2.3 Maximum design differential footing deflection for the design of footing and rafts (AS 2870, 2011)

Type of constriction	Maximum differential deflection Δ, as a function of span mm	Maximum differential deflection, Δ mm
Clad frame	L/300	40
Articulated masonry veneer	L/400	30
Masonry veneer	L/600	20
Articulated full masonry	L/800	15
Full masonry	L/2000	10

- *Step 8 Calculate the movement ratio* y_s/Δ
- *Step 9 Graphically determine the unit stiffness*

$$\log\left[\sum\left(\frac{B_w D^3}{12}\right)/W\right] \tag{2.13}$$

B_w Beamwidth, in mm
D Overall depth of the beam, in mm
W Overall width of the slab normal to the direction of the beams, in m

The stiffness is graphically determined based on the movement ratio (Figure 2.11),

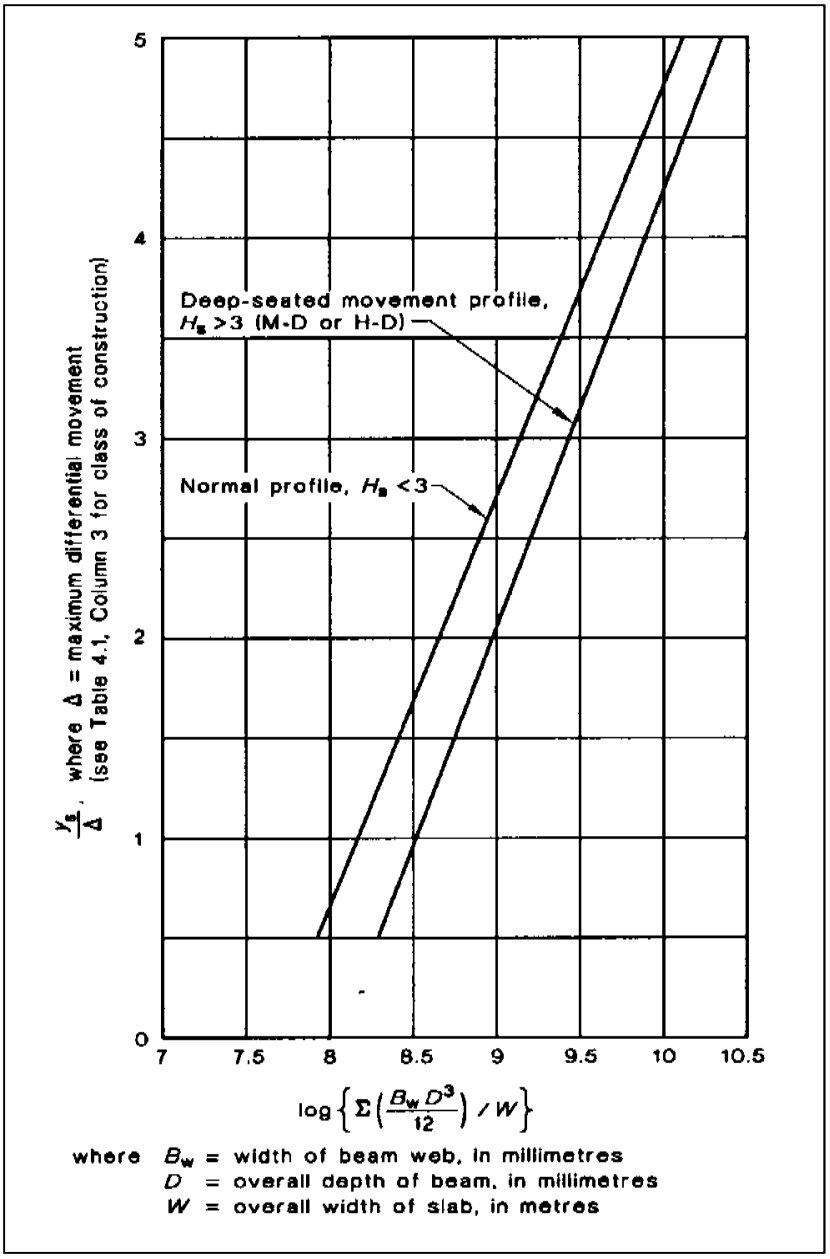

Figure 2.11 Movement ratio vs. unit stiffness (AS 2870, 2011)

- *Step 10 Calculate the beam depth*. Based on the design width of the slab and the width of the beam, calculate the depth of the beam D expressed in unit stiffness, which defined as $\log\left\{\sum\left(\frac{B_w D^3}{12}\right) / w\right\}$.

2.1.4. Post-Tensioning Institute (PTI Method) (PTI 2012)

2.1.4.1. Method Overview

The PTI method has evolved since the first version in 1980. The PTI methods of 1996 and 2004 are similar to each other. But the newest version, PTI 2012, should not be used in conjunction with any previous manual editions or standards issued by PTI.
The PTI method is based on principles of unsaturated soil mechanics for predicting support conditions. It does not address stable, compressible, or collapsible soils. The design procedure for the PTI 2012 method is summarized below.

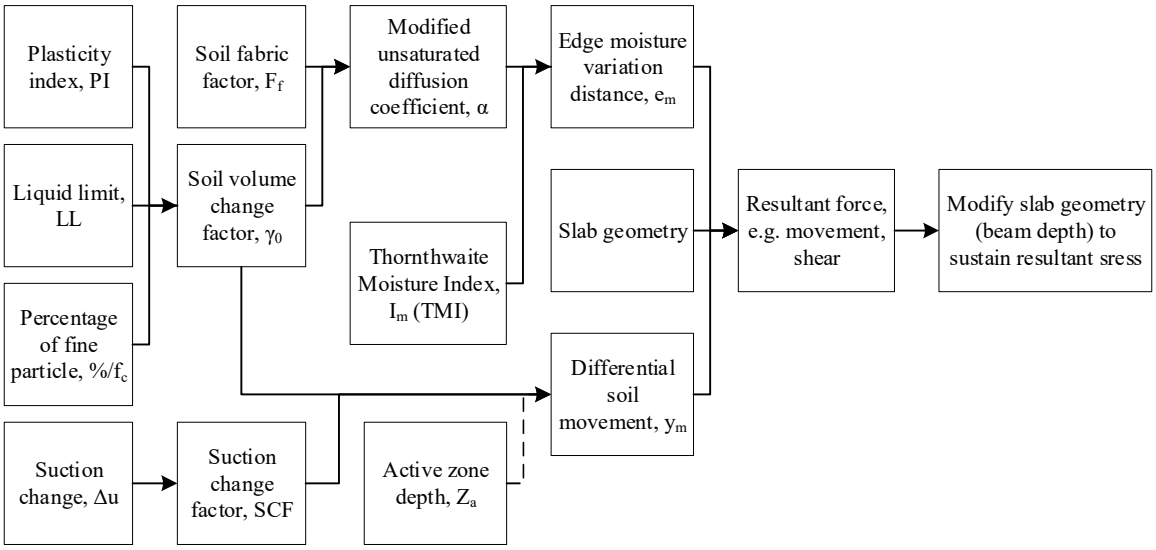

Figure 2.12 Design Procedure of PTI Method

2.1.4.1.1. Design Steps

- *Step 1 Determine the soil criterion*

Soil should satisfy the following criteria to be considered as expansive soil based on PTI (2012) method.

Criteria 1: Using a weighting procedure similar to the one described in Figure 2.2, determine the weighted plasticity index (ASTM, D4318) 1) PI≥15%; 2) more than 10% of soil particles less than 75 μm (#200 sieve) more than 10% of the soil particles less than 5 μm.

Criteria 2: Using a weighting procedure similar to the one described in Figure 2.2, determine the weighted expansion index (ASTM, D4829) EI>20, where the expansion index defined as $\Delta H / H_0 \times 1000$ in the swelling test.

- *Step 2 Determine the edge moisture variation distance e_m.*

The edge moisture variation distance is the distance beneath the edge of a shallow foundation within which the moisture will change due to the wetting or drying influence around the perimeter of the foundation. It depends on the soil suction, permeability, and cracks in the soil. The e_m value is more significant for the center lift case and smaller for the edge lift case (Figure 2.13). The details of how to obtain the edge moisture distance are detailed below.

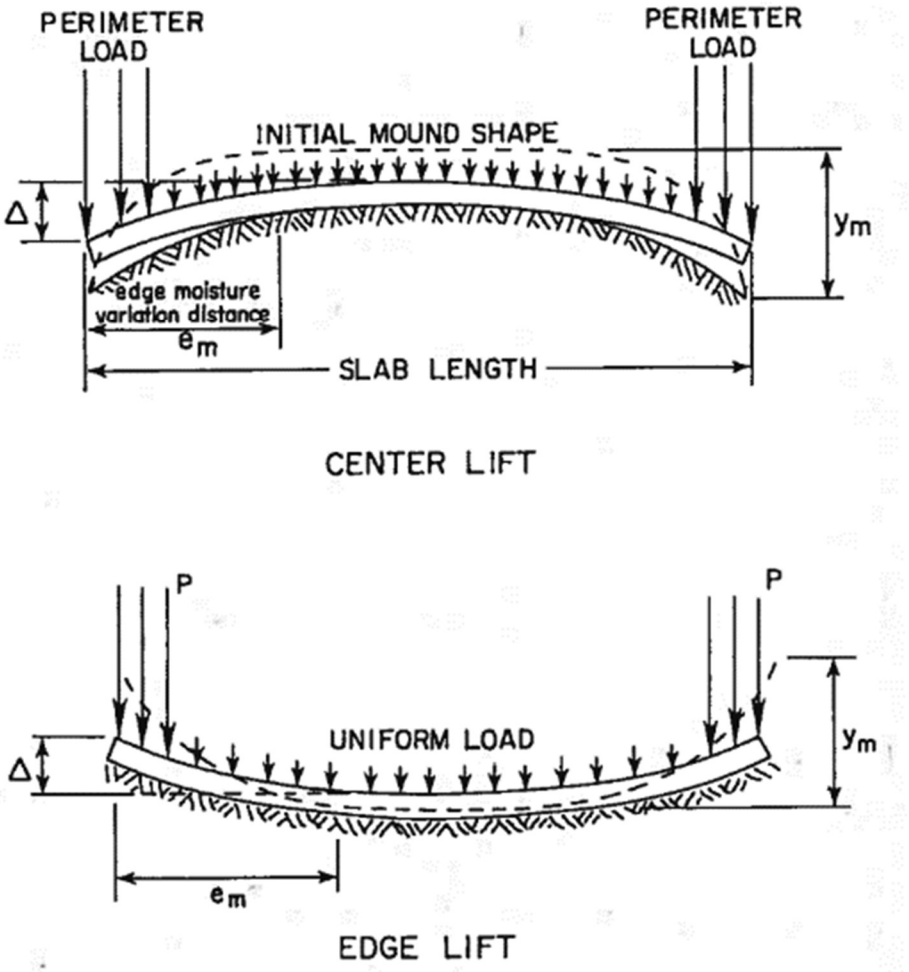

Figure 2.13 Cases of center lift and edge lift (PTI, 2012)

- *Step 2.1 Determine the moisture active zone z_m*, which is the depth below the ground surface at which the suction varies less than 0.027 pF/ft.
- *Step 2.2 Determine liquid limit* (LL), plastic limit (PL), and plastic index (PI) in accordance with ASTM D4318 for each distinct soil layer within the depth z_m.
- *Step 2.3 Determine the percentage of soil passing No. 200 (75 μm)* (%-#200), the percentage of soil finer than 2 *μm (%-2μ)* for each distinct soil layer within z_m, then calculate the percentage of fine clay as

$$\%f_c = \left(\frac{\%-2\mu}{\%-\#200}\right)\times 100\% \tag{2.14}$$

- *Step 2.4 Determine the matrix suction compression index γ_h*, which describes the change of soil volume for a unit change in suction corrected for the actual percentage of fine clay, for swelling and shrinkage in accordance with one of the following methods.

Method 1. Mineral classification and zone chart method.

M1.1 Determine the mineral classification zone in Figure 2.14 based on LL and PI.

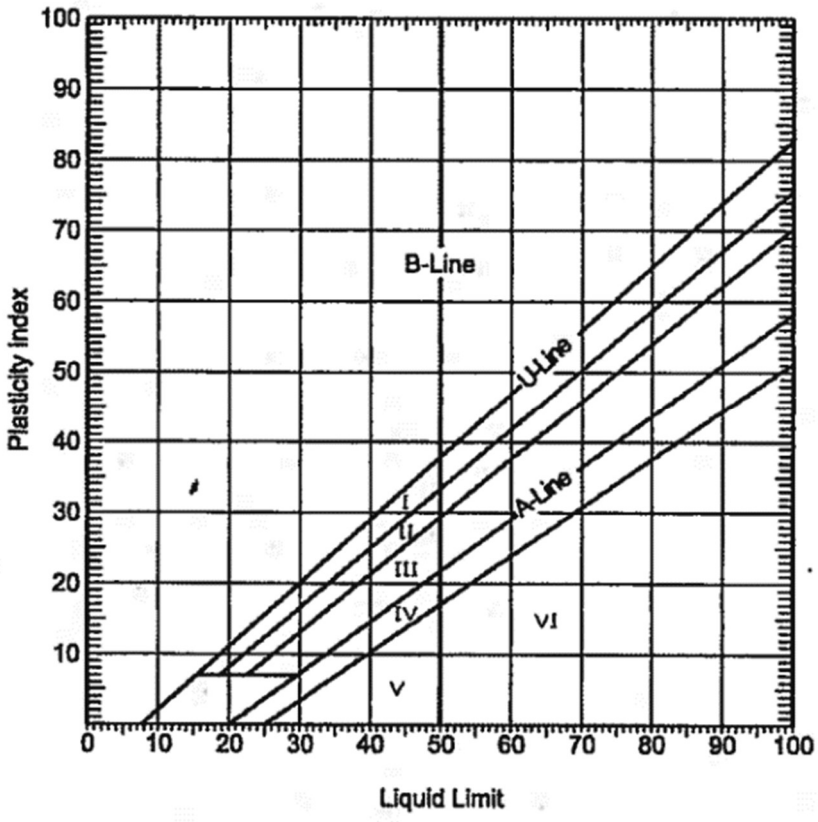

Figure 2.14 Mineral classification chart (PTI, 2012)

No values are above the U-line, and if the PI is less than 7, use γ_0=0.01, where γ_0 is the change of soil volume per unit change in suction for 100% fine clay.

M1.2 Determine the change of soil volume per unit change in suction for 100% fine clay γ_0 for five different mineral zones in the corresponding chart.

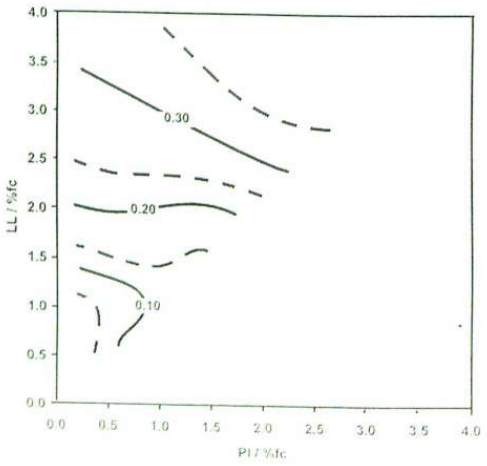

Figure 2.15 Chart for zone I (PTI, 2012)

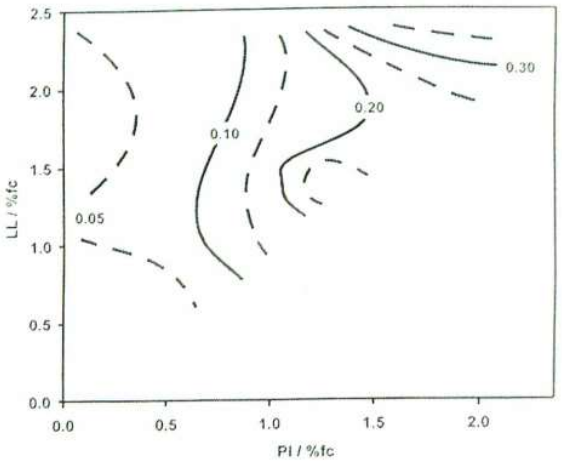

Figure 2.16 Chart for zone II (PTI, 2012)

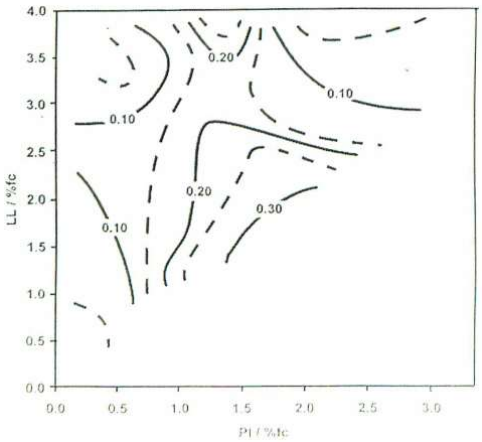

Figure 2.17 Chart for zone III (PTI, 2012)

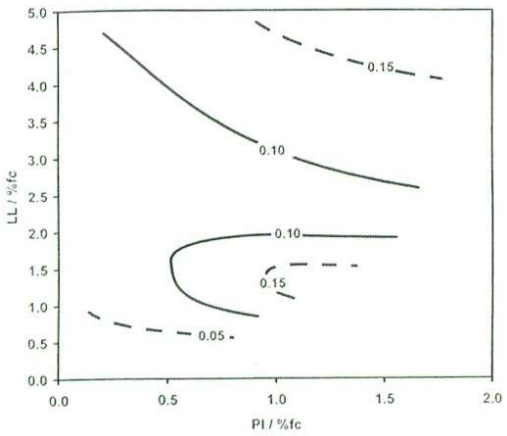

Figure 2.18 Chart for zone IV (PTI, 2012)

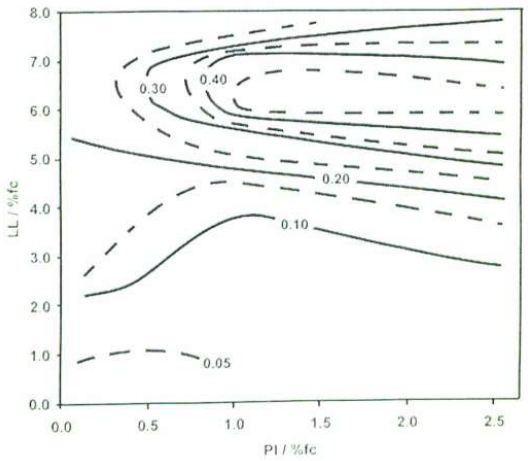

Figure 2.19 Chart for zone V (PTI, 2012)

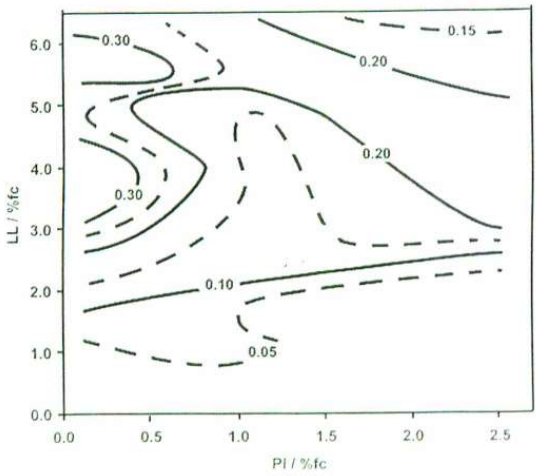

Figure 2.20 Chart for zone VI (PTI, 2012)

M1.3 Correct γ_0 for the actual percentage of fine clay

$$\gamma_h = \frac{\gamma_0 \times \%f_c}{100} \tag{2.15}$$

M1.4 Calculate $\gamma_{h\text{-swell}}$ and $\gamma_{h\text{-shrink}}$, change of soil volume per unit suction change corrected for actual percent of fine clay, for edge lift or center lift case respectively

$$\begin{aligned} \gamma_{h-swell} &= \gamma_h e^{\gamma_h} \left(Edge\ lift,\ swelling\right) \\ \gamma_{h-shrink} &= \gamma_h e^{-\gamma_h} \left(Center\ lift,\ shrinkage\right) \end{aligned} \tag{2.16}$$

Method 2 Expansion index (EI) procedure

The EI procedure uses a remolded sample approximately equivalent to the process of soil expansion (ASTM D4829). The procedure states as follows.

M2.1 Calculate the expansion index EI as ASTM D4829

$$EI = 1000 \times \frac{\left(Final\ thickness\right) - \left(Initial\ thickness\right)}{\left(Initial\ thickness\right)} \tag{2.17}$$

M2.2 Calculate the value of γ_h, but only in the swell condition,

$$\gamma_{h,swell} = \frac{EI}{1700} \tag{2.18}$$

Method 3 Consolidation-Swell Pressure Test Procedure. This method is lengthy and involves a time-consuming test, but the results are reasonably reliable (PTI, 2012). The procedures are described below.

M3.1 Obtain the following parameters by using ASTM D4546 (Figure 2.21).

$$C_s = \frac{e_1 - e_2}{\log P_2 - \log P_1} \tag{2.19}$$

$$\gamma_{h,swell} = \frac{0.7 \times C_s}{1 + e_2} \tag{2.20}$$

C_s	The slope of the rebound curve
e_1 and e_2	Void ratios
P_1 and P_2	Respective vertical effective stress

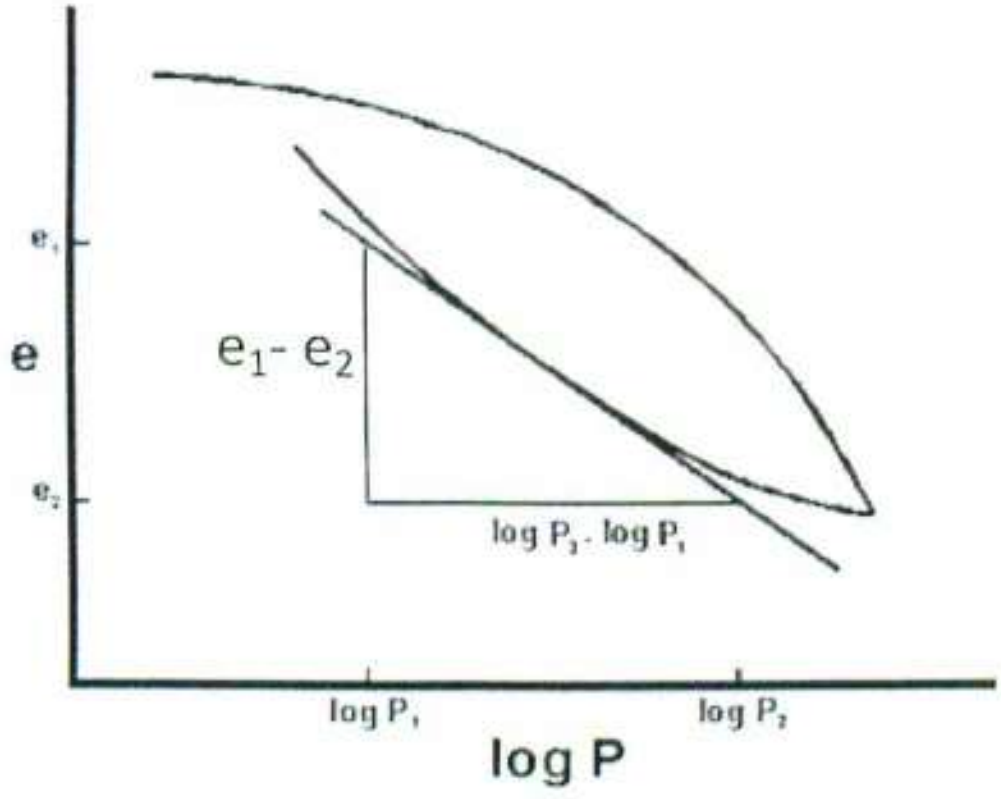

Figure 2.21 Void ratio vs. overburden pressure (PTI, 2012)

Method 4. Overburden Pressure Swell Test Procedures. This test also requires undisturbed samples and an effort approximately equivalent to the hydrometer and Atterberg limits procedures. The procedures are described below.

M4.1

$$\gamma_{h,swell} = \frac{\Delta H / H}{1.7 - \log_{10} P} \tag{2.21}$$

ΔH/H Decimal change of specimen height divided by the initial height
P Overburden effective pressure in psi

- *Step 2.5 Obtain $\gamma_{h\text{-}shrink}$*. Note that methods 2, 3, and 4 do not give $\gamma_{h,shrink}$. Thus, a converting method is provided in Figure 2.22.

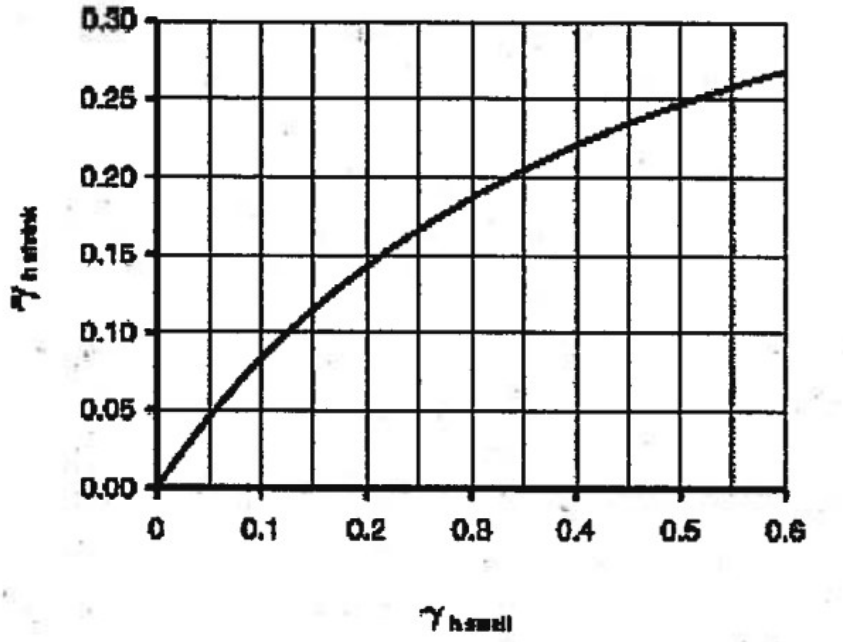

Figure 2.22 Suction compression index relationship between shrinkage and swelling (PTI, 2012)

- *Step 2.6 Determine the Modified Unsaturated Diffusion Coefficient α'*. This coefficient is calculated by using either $\gamma_{h,swell}$ or $\gamma_{h,shrink}$, which were obtained in step 2. The procedures are summarized below,

2.6.1 Determine the soil fabric factor F_f. This factor deals with the presence of horizontal and vertical moisture flow paths, such as roots, desiccation cracks, layers, fractures, and joints. It ranges from 1.0 to 1.2 (Table 2.4).

Table 2.4 Soil fabric factor F_f (PTI, 2012)

	Condition	F_f
	Non-CH Soils	1.0
CH Soils	Profile with one root, crack, sand/silt seam all ≤1/8" width/dimension in any combination	1.0
	Profile with two to four roots, cracks, sand/silt seam all >1/8" width/dimension in any combination	1.1
	Profile with more than four roots, cracks, sand/silt seam all >1/8" width/dimension in any combination	1.2

2.6.2 Calculate the slope of the suction versus volumetric water content curve S_s as follows.

$$S_s = -20.29 + 0.1555(LL) - 0.117(PI) + 0.0684(\%-\#200) \tag{2.22}$$

2.6.3 Calculate the modified unsaturated diffusion coefficient α' for edge lift (swelling), and center lift (shrinkage).
For edge lift case (swelling)

$$\alpha'_{swell} = \left(0.0029 - 0.000162S_s - 0.0122\gamma_{h,swell}\right)F_f \tag{2.23}$$

For center lift case (shrinkage)

$$\alpha'_{shrink} = \left(0.0029 - 0.000162S_s - 0.0122\gamma_{h,shrink}\right)F_f \tag{2.24}$$

- *Step 2.7 Weighted average of the parameters*. After obtaining α', $\gamma_{h,swell}$, $\gamma_{h,shrink}$ and PI, do the weighted average of all parameters as explained in Figure 2.2 except that the depth is reduced to 9 feet instead of 15 ft and the weighting factor F_i is taken as 3, 2, and 1 from the top down to the bottom.

$$(\alpha')_{weighted} = \frac{\sum F_i \times D_i \times \alpha'_i}{\sum F_i \times D_i} \tag{2.25}$$

After 2.7, all the values of α', $\gamma_{h,swell}$, $\gamma_{h,shrink,}$ and PI is the weighted average values instead of the single values for each layer.

- *Step 2.8 Determine the Thornthwaite Moisture Index* I_m based on the location of the project. This parameter describes the rainfall in excess or deficit of average evapotranspiration rates over an extended period of time (Figure 2.23). A zero value means rain equals the evapotranspiration, a negative value indicates sustained moisture less than the evapotranspiration, and a positive value implies precipitation more abundant than evapotranspiration.

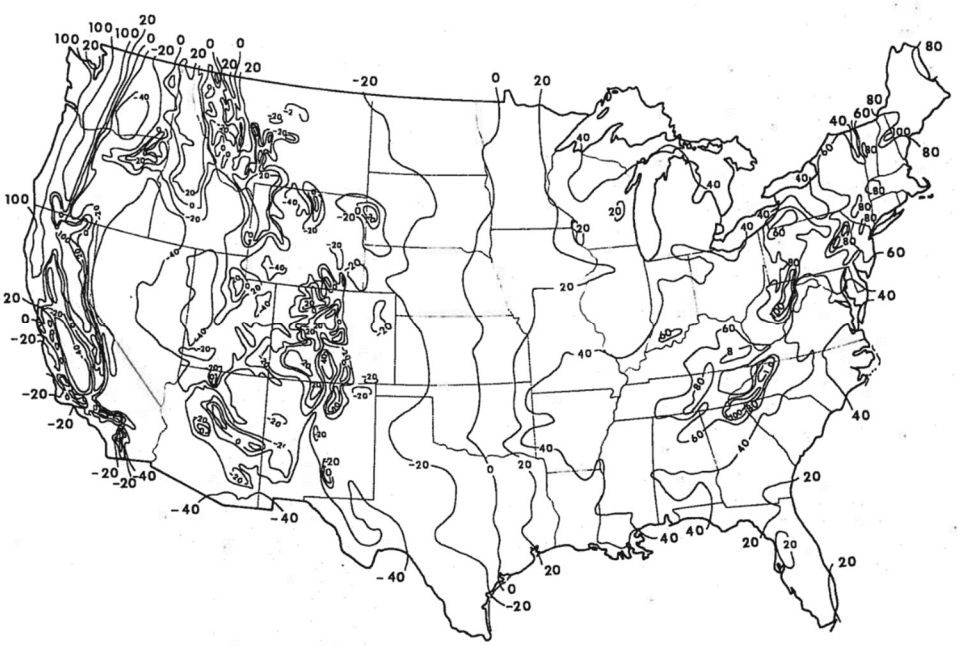

Figure 2.23 Thornthwaite Moisture Index distribution in the United States (PTI, 2012)

- *Step 2.9 Determine the value of edge moisture variation distance* e_m. This value is a distance measured inward from slab edge in which soil moisture content may vary, calculated in feet, and determine in Figure 2.24.

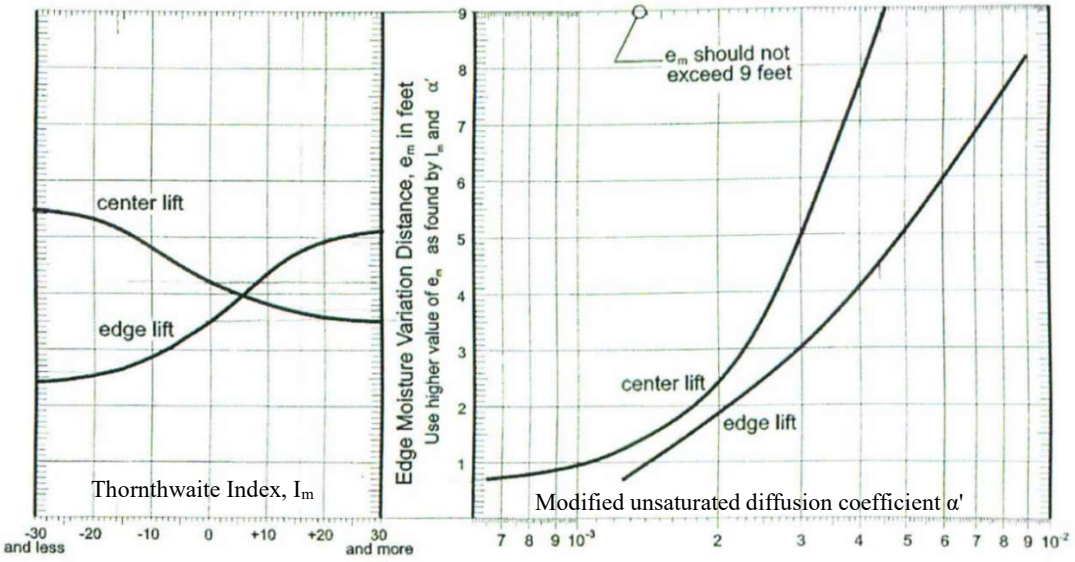

Figure 2.24 Edge moisture variation distance e_m selection chart (PTI, 2012)

For either the center lift or edge lift condition, use the I_m index to use the chart on the left side of Figure 2.24 to obtain e_m and the chart on the right side to obtain α'. Choose the maximum value of e_m as the representative value.

- *Step 3 Determine the maximum, unrestrained differential soil movement y_m in inch.*
  - *3.1 Determine the equilibrium suction* Based on the Thornthwaite Moisture Index I_m, (Figure 2.25).

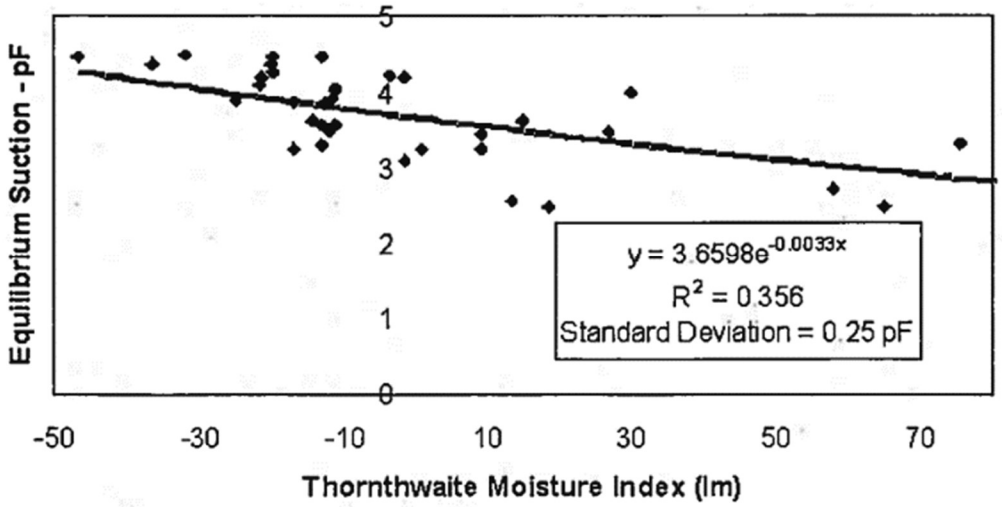

Figure 2.25 Thornthwaite Index vs. equilibrium suction (PTI, 2012)

- *3.2 Determine the suction of soil in naturally dry and wet conditions*.

- *3.3 Subdivide suction envelope* into post-equilibrium envelope and post-construction envelope. For post-equilibrium, I_m<-15 or I_m>15, and post-construction -15≤ I_m ≤15.

  - *3.4 Determine stress change factor (SCF)* based on different suction in dry and wet conditions. Use eitherTable 2.5 (Thornthwaite indexes I_m<-15 or I_m>15) or
  -
  -
  - Table 2.6 (Thornthwaite indexes -15≤ I_m ≤15).

Table 2.5 Stress change factor (SCF) for post-equilibrium case (PTI, 2012)

	Final Controlling Suction at Surface, pF						
Equilibrium Suction	2.5	2.7	3	3.5	4	4.2	4.5
2.7	3.2	0	-4.1	-13.6	-25.7	-31.3	-40
3	9.6	5.1	0	-7.5	-18.2	-23.1	-31.3
3.3	11.7	12.1	5.1	-2.6	-11.5	-15.8	-23.1
3.6	27.1	20.7	12.1	1.6	-5.7	-9.4	-15.8
3.9	38.1	30.8	20.7	7.3	-1.3	-4.1	-9.4
4.2	50.4	42.1	30.8	14.8	3.2	0	-4.1
4.5	63.6	54.7	42.1	23.9	9.6	5.1	0

Table 2.6 Stress Change Factor (SCF) for Post-Construction Case (PTI, 2012)

Suction Change, pF	1.3	1.4	1.5	1.6	1.7	1.8	1.9	2
Wetting (Swelling)	33.2	36.7	40.2	43.9	47.6	51.4	55.3	59.2
Drying (Shrinking)	-24.3	-26.7	-29.2	-31.7	-34.2	-36.7	-39.3	-41.9

For example, I_m=20, equilibrium suction = 3 pF, suction in wet weather = 4.5 pF, SCF_{wet} = -31.3

- *3.5 Determine the weighted matrix suction compression index* $\gamma_{h\ mod\ swell}$ and $\gamma_{h\ mod\ shrink}$. The weighting procedure is similar to the one in step 2.7.

- *3.6 Calculate the maximum unrestrained differential soil movement* y_m

$$y_{m\ swell} = \gamma_{h\ \mathrm{mod}\ swell} \times (SCF)$$
$$y_{m\ shrink} = \gamma_{h\ \mathrm{mod}\ shrink} \times (SCF) \quad (2.26)$$

- *Step 4 Assume the depth and width of the beam*

- *Step 5 Divide the slab into overlapping rectangles*. With long edge marked as L_L and short edge as L_S.

- *Step 6 Determine the sectional properties of the slab*.

- *Step 7 Determine the maximum bending moment and shear* based on e_m and y_m calculated previously, in both long and short directions.

- *Step 8 If the given stress condition is larger than the capacity of the slab*, increase the beam section and repeat steps 4 to 7 until the stress condition is within the tolerable limits.

2.1.4.1.2. Guidelines from the Texas ASCE (TxASCE, 2007)

Texas ASCE suggests that the moisture variation distance, e_m and differential soil movement y_m, should base on average climate values and that the analysis should take into account the added effect of trees and other environmental impacts. (Clause 5.2.2.3)

2.1.5. TAMU-SLAB Method

2.1.5.1. Method Overview

A simple method was proposed by Abdelmalak and Briaud in 2007. This simple method allows the designer to be able to carry out the design of the slab with only a spreadsheet called TAMU-SLAB. The TAMU-SLAB method is divided into the suction method and the water content method. Each method is subdivided into edge lift and edge drop portions, but the procedures for these two methods are similar.

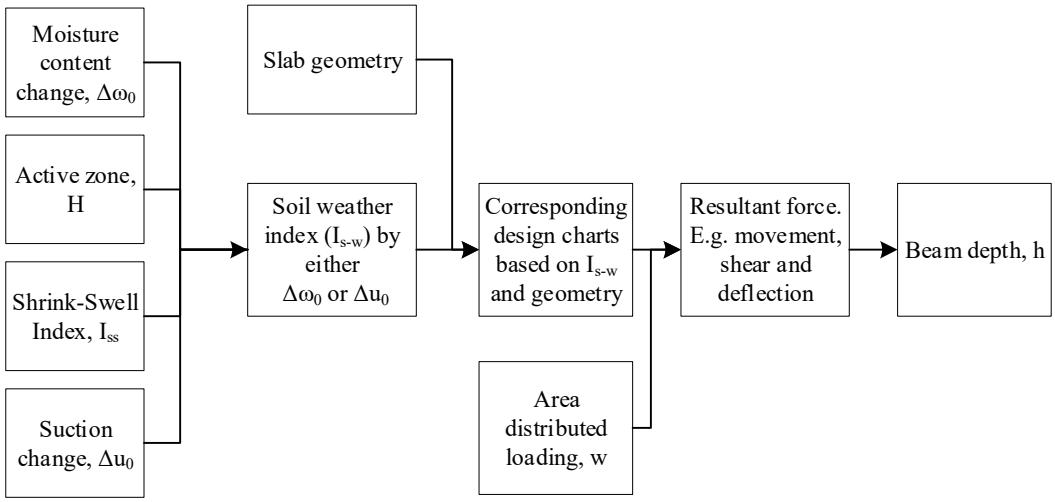

Figure 2.26 Design procedure of TAMU-SLAB method

2.1.5.2. Design Steps

- *Step 1 Determine the load on the slab*, uniformly distributed pressured (p) and uniform line distributed loading along the edge of slab (q).

- *Step 2 Determine the change in water content or change in suction in the free field* at the ground surface $\Delta\omega_0$ or Δu_0, the depth of the active moisture zone (H) and the shrink-swell index (I_{ss})

- *Step 3 change the water content or the suction to the value at the edge of the slab*:

$$\Delta\omega_{edge} = 0.5\Delta\omega_0$$
$$\Delta u_{edge} = 0.5\Delta u_0 \tag{2.27}$$

- *Step 4 Assume a beam depth and other geometric parameters*. Typically, the thickness of slab t is 4 in, the depth of beam varies from 24 to 48 in, the width of beam from 6 to 12 in and the spacing between beams varies from 9.8 to 20 ft.

- *Step 5 Calculate the equivalent depth* d_{eqv}, which represents the thickness of a flat slab which would have the same moment of inertia as the moment of inertia of the stiffened slab with a beam depth D.

$$S \times d_{eqv}^3 = b \times D^3 \tag{2.28}$$

S Beam spacing, in m
d_{eqv} Equivalent depth, in m
b Beamwidth, in m
D Beam depth, in m

- *Step 6 Calculate the soil weather index* $I_{s\text{-}w}$. The water content-based method and the suction-based method shows a difference in this step

6.1 For the suction-based method, the soil weather index is calculated as

$$I_{s-w} = I_{ss} \times H \times \log\left(\Delta U_{edge}\right) \tag{2.29}$$

6.2 For the water content-based method, the soil weather index is calculated as

$$I_{s-w} = 2 \times H \times \omega_0 \tag{2.30}$$

- *Step 7 Based on the soil-weather index* $I_{s\text{-}w}$ *and the equivalent depth* d_{eqv}, read the corresponding design charts and obtaining the design parameters.

- *Step 8 Based on the design parameters obtained in step 7, calculate the maximum deflection Δ at the end of the beam,* the maximum bending moment M_{max}, and the maximum shear force V_{max}. If the calculated distortion of the beam L/Δ is satisfactory the design is acceptable but may be optimized with a shallower beam depth. If the distortion is unacceptable the beam depth must be increased until the distortion criterion is satisfied.

2.2. Surface movement Estimation Methods

In the section 2.1, four out of five slab-on-grade design methods start with the surface movement estimation. Then based on the movement and design criterion, those methods provide additional stiffness to the foundation to reduce the damage due to the ground movement. The amount of surface movement is considered as one of the essential parameters to design the stiffened foundation. Besides the pervious methods, another two well-accepted methods that only estimate the ground surface moment is presented in this section.

2.2.1. TxDOT-124-E method (PVR method)

One of the well-accepted methods to predict the amount of swelling is the TEX-124-E from the Texas Department of Transportation. This method is mainly based on the work by McDowell and others (McDowell et al., 1956). The PVR method makes use of the plasticity index (PI), the liquid limit (LL), the design load and design curves to predict the amount of potential vertical rise (PVR) of the soil. The method is summarized as follows.

2.2.1.1. Design Steps

Step 1 Divided the soil within the active zone into sublayer based on similar LL or PI.

Step 2 For each layer, the soil is classified by comparing the current water content to the criteria set in three groups based on LL. The three groups are the wet group (0.47LL+2), the dry group (0.2LL+9), and the average group ([dry+wet]/2).

Step 3 Use Figure 15 to determine the percent volume change based on PI and the water content condition of “wet”, “dry” and “average”

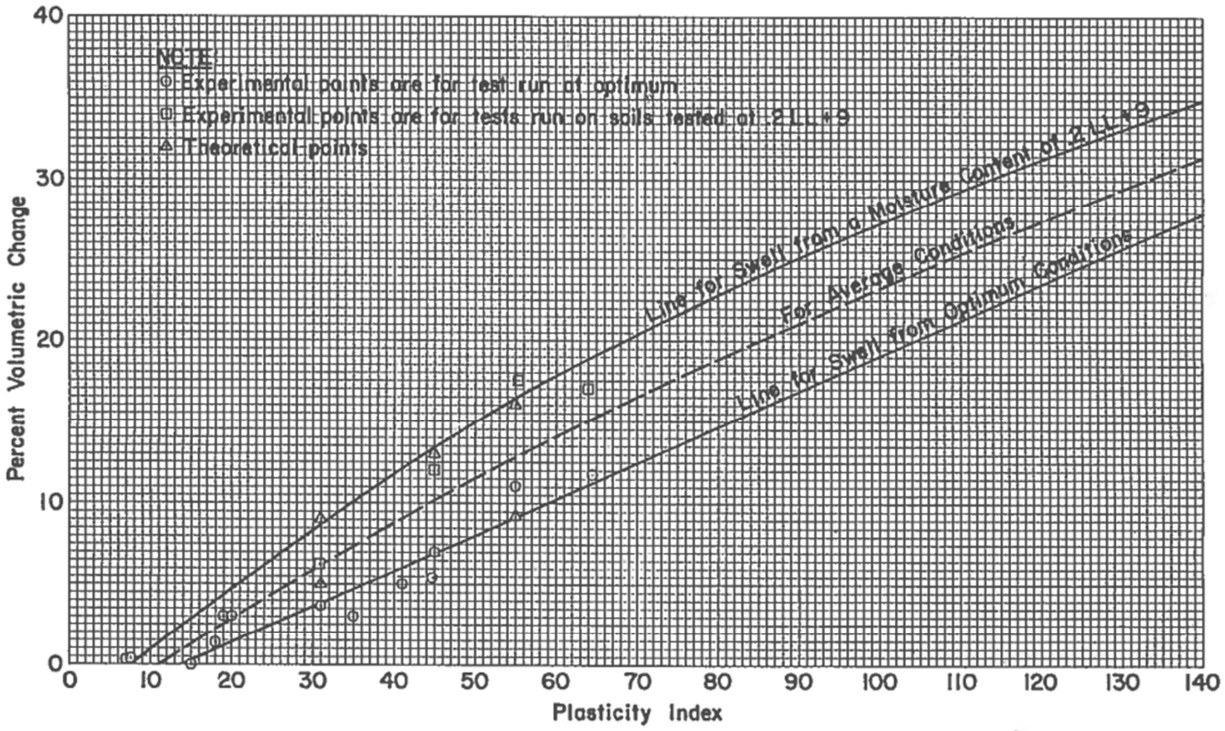

Figure 2.27 Relationship of Plasticity Index and Volume Change (TxDOT, 1995)

Step 4 As the percent of volume change from step 3 is associated with a surcharge loading of 1 psi (6.4kPa), empirically convert the percent of volume change from step 3 to the free volume change by using the equation

$$Free\ swell\ (\%) = 1.07(Vol.\ Swell\ \%) + 2.6 \tag{2.31}$$

Step 5 use Figures 17 and 18 to graphically determine the amount of swelling for each layer based on the design pressure at that depth and the amount of free swell determined in step 4. The only difference between Figure 2.28 and Figure 2.29 is the range of percent volumetric swell and the design pressure.

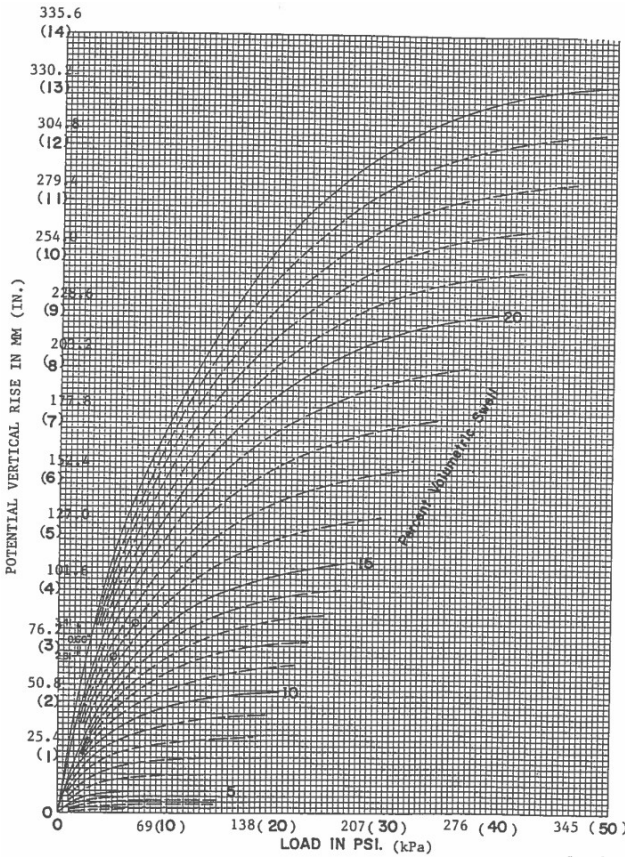

Figure 2.28 Design Load vs. Vertical Rise (TxDOT, 1995)

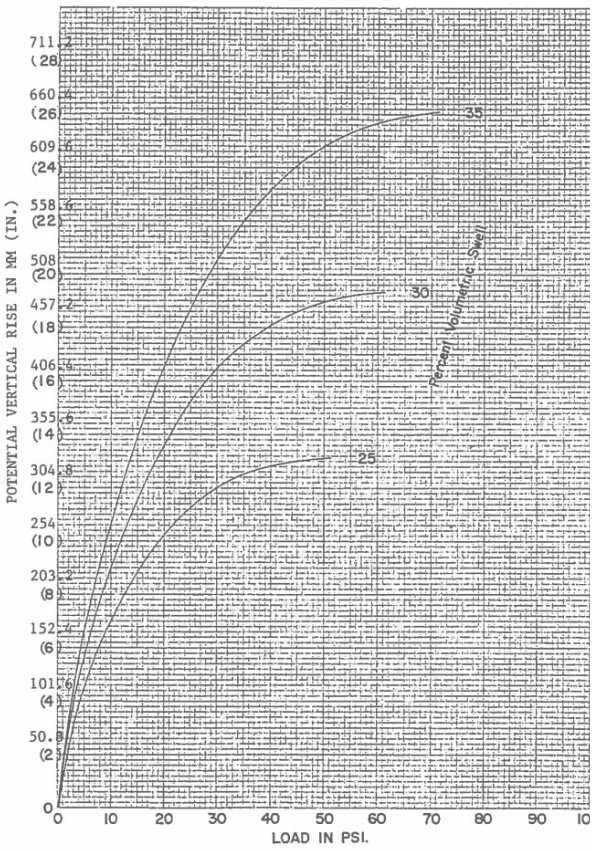

Figure 2.29 Design Load vs. Vertical Rise (TxDOT, 1995)

Step 6 Add the swelling of all layers to obtain the potential vertical rise (PVR) and modified for percent of soil finer than 425μm.

TxDOT provides a spreadsheet automating the procedure from Step 2 to 6. The design chart and empirical equation are built-in the spreadsheet.

2.2.2. Briaud, Zhang & Moon Method (Briaud et al.'s method)

After observing the shrinkage process for two clays, Briaud et al. (2003) found a relationship between the volumetric strain and the water content shown in Figure 2.30. During the shrinkage process, a linear relation between volumetric and axial strain can be observed (b), and after the water content is less than the shrinkage limit, the variation of volumetric strain becomes small (c). This is the basis for proposing to calculate the soil movement based on the water content variation.

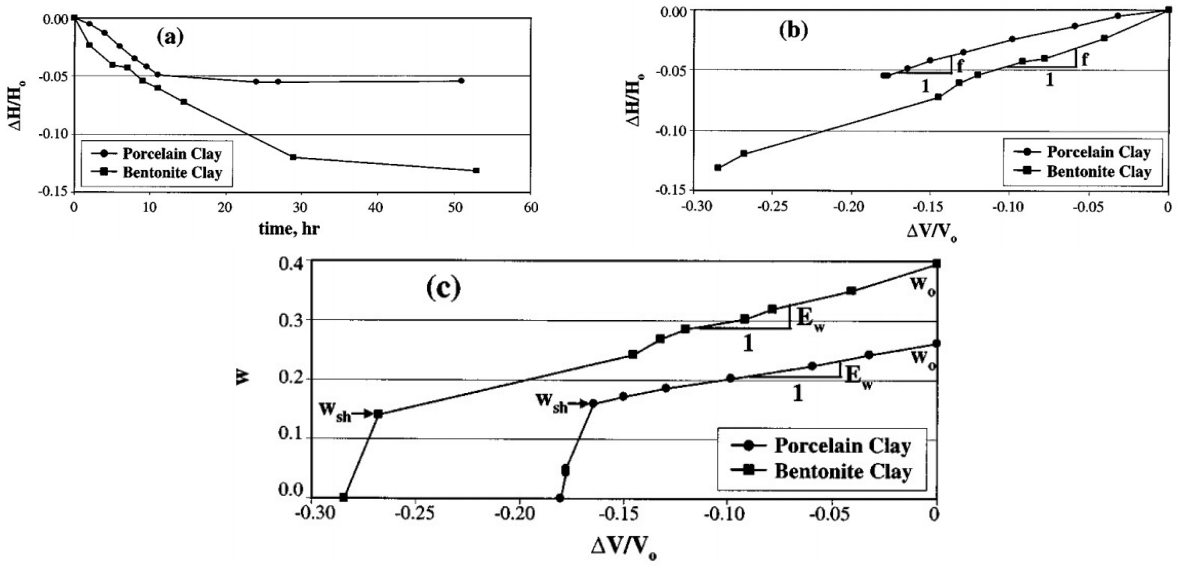

Figure 2.30 Shrink test result: (a) Axial Strain vs. time. (b) Axial strain vs. volumetric Strain. (c) Water content vs. volumetric Strain (Briaud et al., 2003)

In Figure 2.31, the natural water content of the soil can be located at any point of the line (e.g., point C in the figure). Starting at the initial water content, a free swell test can be performed to obtain line CD. A free shrink test can also be performed to obtain line CB. Points B and D correspond to water contents called the shrink limit and the swell limit respectively. The slope of

line BD is the shrink-swell modulus, E_w. However, it should be noted that, while the maximum amplitude of the water content is from B to D, the change in water content is affected by the stress level. Indeed, the higher the stress, the lower the amplitude of water content change. Measured values of the change in water content will lead to a more realistic estimate of the soil movement.

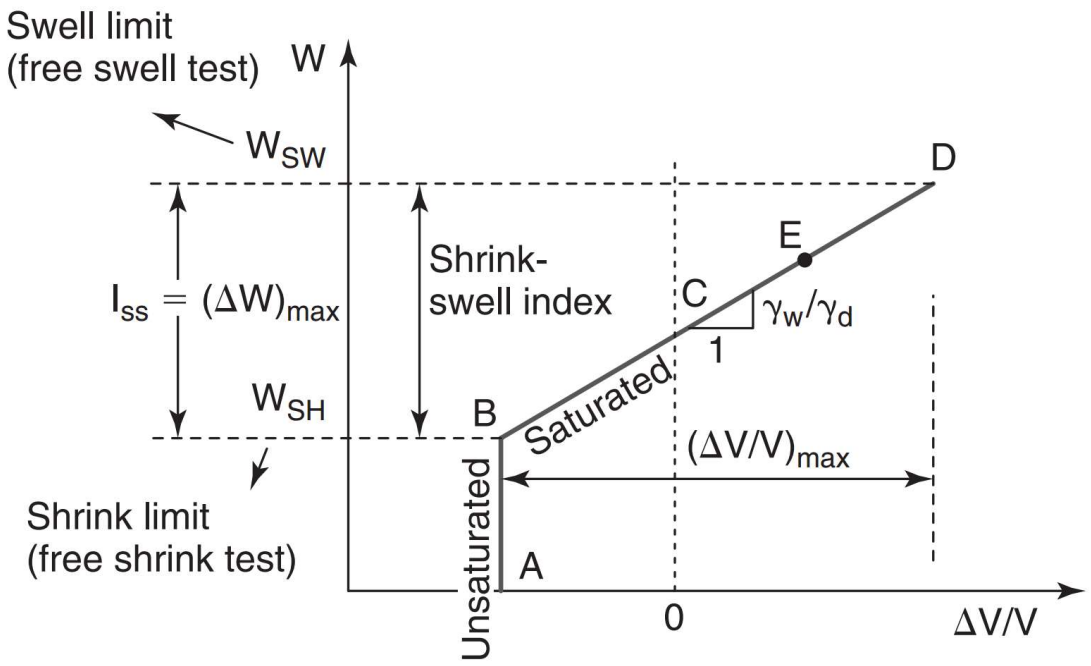

Figure 2.31 Water content vs. volumetric strain (Briaud, 2013)

The general determination of the shrink-swell modulus can be modified as

$$E_w = \left[\left(\frac{Sn}{w} \right) + \frac{0.8 \times n \times (S-1)}{(w_{sh} - w_{sw})} \right]^{-1} \tag{2.32}$$

S Degree of saturation
n Porosity
w_{sh} Shrink limit
w_{sw} Swell limit

Also, the shrink-swell index, I_{ss}, is defined as the difference between the shrink limit and the swell limit ($I_{ss} = w_{sw} - w_{sh}$) and is used to evaluate the shrink-swell potential of the soil.

When the soil is fully saturated which is the case along path BD in Figure 33, the shrink-swell modulus is calculated as

$$E_w = \frac{\Delta w}{\Delta \varepsilon_v} = \frac{\Delta M_w / M_{Dry}}{\Delta V_w / V_{Total}} = \frac{\gamma_w}{\gamma_d} \tag{2.33}$$

M_w, M_{Dry}	Mass of water and dry soil
V_w, V_{Total}	The volume of water and soil
γ_w, γ_d	Unit weight of water and dry unit weight

2.2.2.1. Design Steps

Step 1 Determine the depth of water content change based on local measurement or experience.

Step 2 Determine the shrink-swell modulus of the soil at different depth ($E_w = \gamma_w/\gamma_d$).

Step 3 Divide the depth of water content change into sublayers with similar modulus values.

Step 4 Determine the water content variation for each sublayer.

Step 5 Calculate the soil movement for each sublayer by Eq. (2.34)

$$\Delta H = \sum_{i=1}^{n} f \times \frac{\Delta w}{E_w} \times h_i \tag{2.34}$$

ΔH	Gourd surface movement, in m
i	The i^{th} layer consider
n	Total number of later considered
f	Correction factor from volumetric strain to axial strain, typically 0.33
Δw	Water content variation, in %
E_w	Shrink-swell modulus, in %
h_i	Depth of layer consider, in m

Step 5 Sum up the movement of sublayers to calculate the surface movement.

2.3. Numerical Modeling of Coupled Problems in Porous Medium

This section presents a brief introduction of the main components of the hydro-mechanical formulation and computer code adopted in this dissertation. The water flux flows within the soil mass is considering as the essential reason of the shrink swell soil problem. The soil mass is considered as a porous medium, which is defined as a medium contained multiphase matters and at least one of them is not solid (Bear, 2013). A porous medium often shows like as Figure 2.32. Such medium contains matters in three phases: 1. Solid (s), 2. Liquid (l) and 3. Gas (g); and three species: 1. Solid particles (s), 2. Water (w) and 3. Air (a). It is important to distinguish the condition of the species during the consideration, as the liquid phase contains water and dissolved air or even dissolved solid particle; the gas phase contains the evaporated water and gas. In this work, the mathematical frame work proposed by Olivella et al. (Olivella et al., 1994) is adopted. The equations can mainly divide into four groups: (1). Balance equations, (2). Constitutive equations, (3). Equilibrium restrictions and (4). Initial and boundary conditions. Due to the limitation of the content, the initial and boundary condition will not be included in this review.

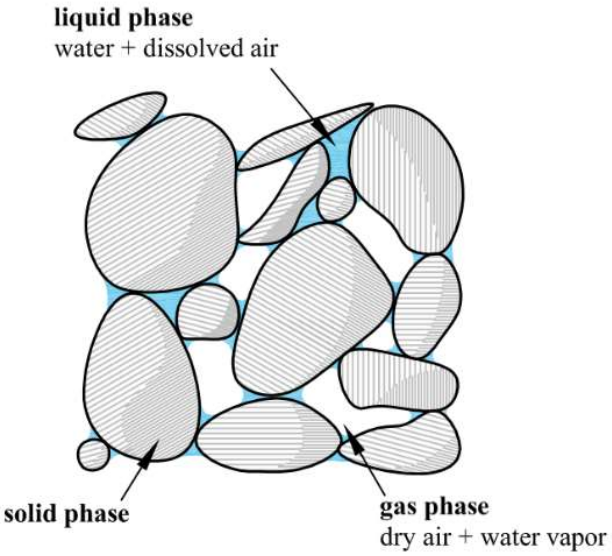

Figure 2.32 Schematic of Porous Medium (Sánchez et al., 2005)

2.3.1. Balance Equations

The balance equations describes the variation of species in different phases during mechanical changes (Panday & Corapcioglu, 1989). The equations proposed by Olivella (Olivella et al., 1994) is adopted in this work and mainly divided into four category: (1) solid mass balance equations, (2) water mass balance equation, (3) energy balance equation and (4) momentum balance equation. E.g. Figure 2.33 presents the concept of water mass balance relationship.

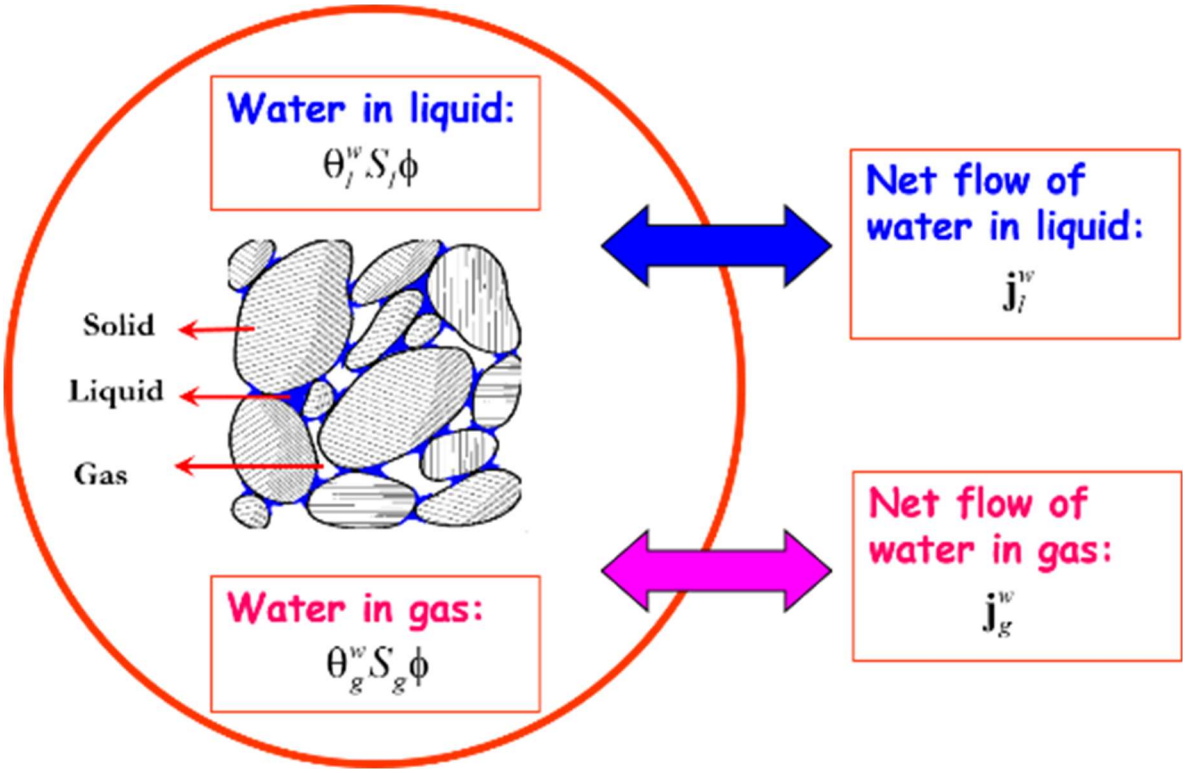

Figure 2.33 Schematic of mass balance equation of water (Sánchez et al., 2005)

2.3.1.1. Solid Mass Balance Equation

The purpose of solid mass balance equation is to calculate the porosity variation during mechanical behavior. The solid mass flow through a imaged fixed volume in the space, the inflow of the mass equals to the sum of out flow of the mass and the variation of the storage within the volume. The porosity variation is then computed as follows:

$$\frac{\partial}{\partial t}\left[\rho_s\left(1-\phi\right)\right]+\nabla\cdot\left[\rho_s\left(1-\phi\right)\dot{u}\right]=0 \tag{2.35}$$

ρ_s Solid density
ϕ The porosity of the medium
$\nabla\cdot[\bullet]$ Divergent operator
$\dot{u}$ Velocity of solid mass

It should be noticed that Eq. (2.35) follows the local description (i.e. spatial description or Eulerian description). The material time derivative operation (Eq. (2.36)) can mathematically rearrange the Eq. (2.35) to describe the variation of porosity by using global description, which present in Eq. (2.37)

$$\frac{D}{Dt}\left(\bullet\right)=\frac{\partial}{\partial t}\left(\bullet\right)+\dot{u}\cdot\nabla\left(\bullet\right) \tag{2.36}$$

$$\frac{D\phi}{Dt}=\frac{\left(1-\phi\right)}{\rho_s}\frac{D\rho_s}{Dt}+\left(1-\phi\right)\nabla\cdot\dot{u} \tag{2.37}$$

Typically, if the solid is considered as incompressible, i.e. the density variation = 0, the variation of porosity is then due to the volumetric deformation.

2.3.1.2. Water Mass Balance Equation

Water in the porous medium is usually found in both liquid and gas phases. The mass balance of water mass is expressed as:

$$\underbrace{\frac{\partial}{\partial t}\left(\theta_l^w S_l \phi + \theta_g^w S_g \phi\right)}_{\text{Storage variation}} + \underbrace{\nabla \cdot \left(\mathbf{j_l^w} + \mathbf{j_g^w}\right)}_{\text{Leave/entering}} = \underbrace{f^w}_{\text{External source}} \tag{2.38}$$

θ_l^w, θ_g^w Volumetric mass of water in liquid/gas. (Mass of water over volume of liquid/gas)

S_l, S_g Volumetric fraction of liquid/gas and voids (volume of liquid/gas over voids)

ϕ Porosity of medium

$\mathbf{j_l^w}, \mathbf{j_g^w}$ Mass flux of water in liquid/gas phases

The key point in Eq. (2.38) is to use the porosity as the single variable to describe the water mass variation. The superscript represents the species of concerned and the subscript indicates the phase which the species in correspondingly. The volumetric mass of water in liquid/gas phase is a product of mass fraction of water and liquid, ω_l^w, and the density of liquid, ρ_l. i.e.

$$\theta_l^w = \omega_l^w \rho_l = \frac{m_w}{\cancel{m_l}} \frac{\cancel{m_l}}{V_l} = \frac{m_w}{V_l} \tag{2.39}$$

The water mass flux in both liquid and gas phases can further divided into three different fluxes:

$$\begin{aligned} \mathbf{j_l^w} &= \underbrace{\mathbf{i_l^w} + \omega_l^w \rho_l \mathbf{q_l}}_{\mathbf{j'^w_l}} + \theta_l^w S_l \phi \dot{\mathbf{u}} = \mathbf{j'^w_l} + \theta_l^w S_l \phi \dot{\mathbf{u}} \\ \mathbf{j_g^w} &= \underbrace{\mathbf{i_g^w} + \omega_l^w \rho_l \mathbf{q_g}}_{\mathbf{j'^w_g}} + \theta_g^w S_g \phi \dot{\mathbf{u}} = \mathbf{j'^w_g} + \theta_g^w S_g \phi \dot{\mathbf{u}} \end{aligned} \tag{2.40}$$

In Eq. (2.40), the first term $\mathbf{i_l^w}$ is the non-advective flux; the second term $\omega_l^w \rho_l \mathbf{q_l}$ is the advective flux induced by flow motion which governed by general Darcy's law; The notation j'^w_l is the total flux of water respect to the solid phase. The third term $\theta_l^w S_l \phi \dot{\mathbf{u}}$ corresponding to the

advective flux due to solid motion. By applying Eq. (2.36), the water mass balance equation will be written as

$$\underbrace{\phi\frac{D}{Dt}\left(\theta_l^w S_l+\theta_g^w S_g\right)}_{\text{Storage variation}}+\underbrace{\left[\frac{(1-\phi)}{\rho_s}\frac{D\rho_s}{Dt}+\nabla\cdot\dot{\mathbf{u}}\right]\left(\theta_l^w S_l+\theta_g^w S_g\right)}_{\text{Storage variation due to change of density and medium skeleton}}+\overbrace{\nabla\cdot\left(\mathbf{j'^w_l}+\mathbf{j'^w_g}\right)}^{\text{Total flux of water i/o the meidum}}=f^w \quad (2.41)$$

2.3.1.3. Energy Balance Equation

The energy transfer problem in porous medium mainly has three categories: (1) thermal conduction, as the energy transfer with a contacting object; (2) advection (convection), which is the energy transfer due to the motion of a mass; (3) radiation, as the energy storage as the electromagnetic waves. The energy transferred through a porous medium can be mathematically present as:

$$\begin{aligned}&\phi\frac{D}{Dt}\left(E_l\rho_l S_l+E_g\rho_g S_g\right)+\left(E_l\rho_l S_l+E_g\rho_g S_g\right)\left[\frac{(1-\phi)}{\rho_s}\frac{D\rho_s}{Dt}+\nabla\cdot\dot{\mathbf{u}}\right]\\&+(1-\phi)\rho_s\frac{DE_s}{Dt}+\nabla\cdot\left(\mathbf{i_c}+\mathbf{j'_{El}}+\mathbf{j'_{Eg}}\right)=f^E\end{aligned} \quad (2.42)$$

E_l, E_g, E_s	Internal energy in liquid, gas and solid
ρ_l, ρ_g, ρ_s	Density of liquid, gas and solid
ϕ	Porosity of medium
$\mathbf{i_c}$	Energy conduction
$\mathbf{j'_{El}}, \mathbf{j'_{Eg}}$	External flux in liquid and gas
f^E	External energy

2.3.1.4. Momentum Balance Equation

As it can be concluded from pervious section, the variation of the porosity plays an important role in the porous medium problem. Despite the mass balance equation, the mechanical problem may induce a tremendous deformation to the medium. In general, the sum of the force acting in a medium equals to the temporal rate of change of the total momentum (Malvern, 1969). The momentum balance equation is present as follows:

$$\nabla \cdot \boldsymbol{\sigma} + \mathbf{b} = \mathbf{0} \tag{2.43}$$

$\boldsymbol{\sigma}$ Total stress tensor
$\mathbf{b}$ Body force tensor

2.3.2. Constitutive Equations & Equilibrium Restrictions

The balance equations mentioned above will be solved in conjunction with the constitutive equations and equilibrium restrictions. E.g. the hydraulic often works with Darcy's law and water retention curve theory. As the balance equations describe the mass balancing in the problem, the constitutive equations link the main unknows (e.g. liquid pressure and displacement) with dependent variable (e.g. liquid flux, suction, and stress etc.) and limited by the equilibrium restrictions. The equilibrium restriction describes the state of a species in a certain phase under certain condition.

Table 2.7 and Table 2.8 (Olivella et al., 1996; Sánchez et al., 2012) present the equations of constitutive and restriction adopted in this work. A short summary of difference between balance equations, constitutive equations and equilibrium restrictions can be draw as follows:

- Balance equation: describe the mass balancing process during a problem
- Constitutive equation: relate the unknowns to dependent variables
- Equilibrium restriction: relative the species concentration in the phases and state variable.

Table 2.7 Constitutive Equations Summary

Name	Variables	Equation	Parameter relations
Darcy's laws	Advective flux	$\mathbf{q_l} = -\frac{\mathbf{k}k_{rl}}{\mu_l}\left(\nabla P_l - \rho_l \mathbf{g}\right)$	$\mathbf{k} = \mathbf{k_0}\exp\left\{b\left(\phi - \phi_0\right)\right\}$
Relative permeability	Liquid relative permeability	$k_{rl} = \sqrt{S_e}\left[1-\left(1-S_e^{1/\lambda}\right)^{\lambda}\right]^2$	
Retention curve	Degree of saturation	$S_e = \left[1+\left(P_c/P_0\right)^{1/(1-\lambda)}\right]^{\lambda}$	$S_e = \frac{S_l - S_{lr}}{S_{ls} - S_{lr}}$ $S_l = 1 - S_g$
Mechanical constitutive model	Modified Barcelona Basic Model (BBM)	See 2.3.3	See 2.3.3
Phase density	Density of gas and liquid	$\rho_l = 1002.6\exp\left[4.5\times10^{-4}\left(P_l - 0.1\right) - 3.4\times10^{-4}T\right]$	
Phase viscosity	Viscosity of liquid	$\mu_l = 2.1\times10^{-12}\exp\left(\frac{1808.5}{273.15+T}\right)$	

$\mathbf{q_l}$	Liquid flux tensor	$\mathbf{k}$	Permeability tensor
k_{rl}	Liquid relative permeability	μ_l	Liquid dynamic viscosity
$\mathbf{k_0}$	Reference permeability tensor (ref to ϕ_0)	b	Fitting factor
ϕ	Medium porosity	ϕ_0	Reference porosity
S_e	Relative degree of saturation [0,1]	λ	Slope of retention curve
S_{lr}	Residual liquid degree of saturation [0,1)	S_{ls}	Saturated liquid degree of saturation (0,1]
S_g	Degree of saturation for gas	P_l	Pressure on liquid in MPa
T	System temperature in K	μ_l	Dynamic viscosity of liquid

Table 2.8 Equilibrium Restrictions Summary

Name	Variables	Equation	Parameter relations
Psychometric Law (Kelvin's equation)	Quantity of dissolved water in air (water vapor)	$\theta_g^w = \left(\theta_g^w\right)^0 \exp\left[-\frac{p_c M_w}{R\left(273.15+T\right)\rho_l}\right]$	$\left(\theta_g^w\right)^0 = \frac{M_w P_{v(T)}}{R\left(273.15+T\right)}$
Henry's Law	Quantity of dissolved air in liquid	$\theta_l^a = \omega_l^a \rho_l = \frac{p_a}{H}\frac{M_a}{M_w}\rho_l$	

θ_α^i	Fraction of mass of species *i* in per unit volume of phase α	p_c	Matric suction
M_w	Molar weight of water	R	Gas constant
T	Temperature in K	ω_α^i	Mass fraction of species *i* in per unit weight of phase α
p_a	Atmosphere pressure	H	Henry's constant
M_a	Molar mass of air	ρ_l	Density of liquid

With the mechanical model which will be describe later, the system of equations is fully coupled solved via Newton-Raphson algorithm (Olivella et al., 1996).

2.3.3. Modified Barcelona Basic Model (BBM)

The modified Barcelona Basic Model was proposed by Alonso (Alonso et al., 1990) and widely adopted by researchers in solving problem of unsaturated soil (Cui & Delage, 1996; Lu, 2020; Lu & Dong, 2017; Lu & Likos, 2006; McCloskey et al., 2010; Wheeler et al., 2003; Wheeler & Sivakumar, 1995). By formulating with stress and suction variables, the model has the capability to describe the mechanical behavior under different mechanical stress and suction. Typically, when the suction equals zero, the BBM is in the deviatoric plan and the yield function of BBM reduces to Modified Cam-Clay Model; while the suction is not zero, the BBM is in the isotropic plan and the yield function is called the LC yield curve (Loading-Collapse). The LC curves represent the locus where the irreversible deformations occur due to additional loading or reducing of suction (wetting). The formulation of BBM is present in the following section.

2.3.3.1. Stress-Strain Behavior in Elastic Range

The mechanical behavior of general soil may express as Figure 2.34. When normal consolidated soil subjects to saturated condition at initial stress state p^c and load to stress p^*_0, the consolidation behavior is described by the traditional consolidation theory as shown in N (0), where λ (0) is the slope of the consolidation curve and p^*_0 is the preconsolidation pressure.

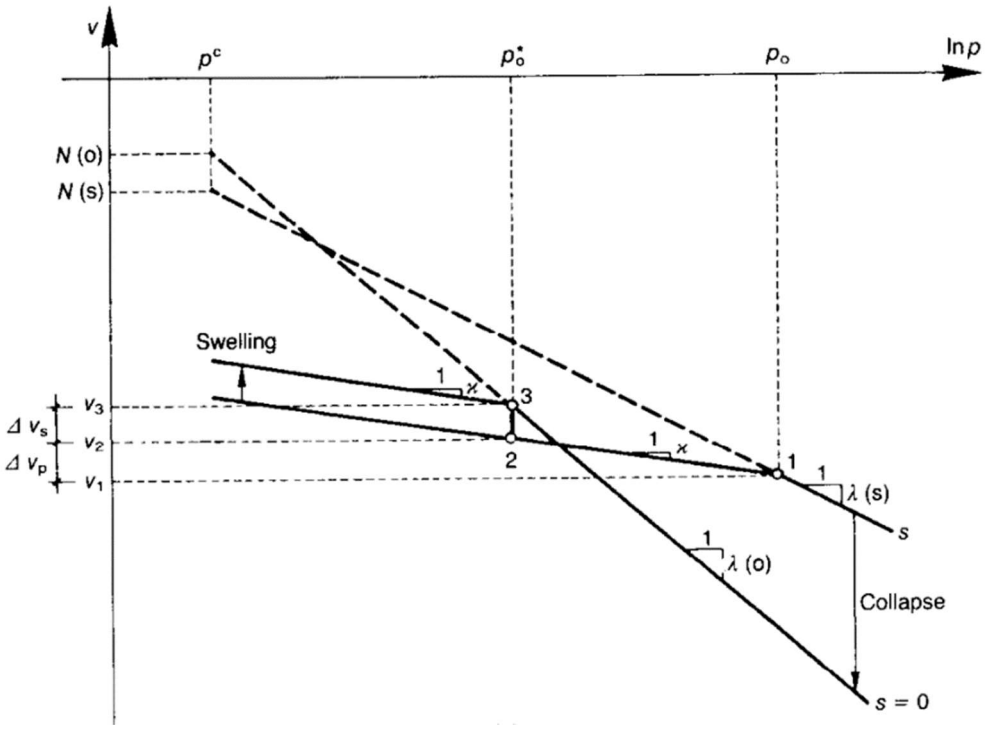

Figure 2.34 Compression Curves for Saturated and Unsaturated Soil (Alonso et al., 1990)

The formulation of elastic deformation induced by suction and stress variation is presented as Eq. (2.44)

$$d\varepsilon_v^e = \frac{k_i(s)}{1+e}\frac{dp'}{p'} + \frac{k_s(p',s)}{1+e}\frac{ds}{s+0.1} \tag{2.44}$$

Where

$$k_i(s) = k_{i0}\left(1+\alpha_i s+\alpha_{ii}\ln\left(\frac{s+0.1}{0.1}\right)\right)$$
$$k_s(p',s) = k_{s0}\left(1+\alpha_{sp}\ln\left(p'/p_{ref}\right)\right)\exp\left(\alpha_{ss}s\right) \tag{2.45}$$

ε^e_v	Elastic volumetric strain
$k_i(s)$	Elastic stiffness parameter relatives to mean stress, as the function of suction level (λ_0)
e	Void ratio
p’	Effective mean stress in MPa
$k_s(p',s)$	Elastic stiffness parameter relatives to suction, as a function of mean stress and suction (λ_s)
s	Matric suction in MPa
α_i, α_{ii}, α_{sp}, α_{ss},	Model parameters

2.3.3.2. Loading Collapse (LC) Yield Surface

The yield surface is the boundary between elastic and plastic deformation. Conjunction with Figure 2.34, when soil subjects to unsaturated condition, where the matric suction exist, the consolidation curve it then followed by curve N (S). When the load path followed by Figure 2.35, the soil is first loaded to stress p_0 with suction included, then reduce the loading only to p_0^* (from point 1 to 2), the difference of volume between V_1 and V_2 is due to the suction induced volumetric change and classified as the plastic deformation. Later, a reduction of suction, shown as point 2 to 3 in both figures, induces an elastic volumetric deformation. The line 1-3 in Figure 2.35 is so called the Loading-Collapse (LC) curve.

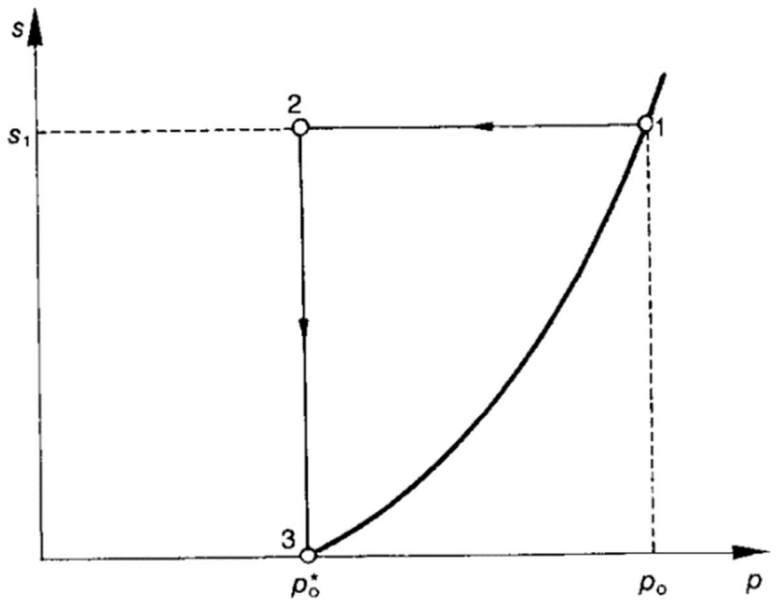

Figure 2.35 Stress Path and Yield Curve in stress-suction (p, s) plane (Alonso et al., 1990)

Alonso (Alonso et al., 1987) had detailly described the concept of LC curve. As shown in Figure 2.36, it illustrates that any variation in mean stress p or suction s within the elastic zone will

induce elastic volumetric deformation. E.g. the stress path of 2 to 3 in Figure 2.35 and volume change V_2 to V_3 in Figure 2.34.

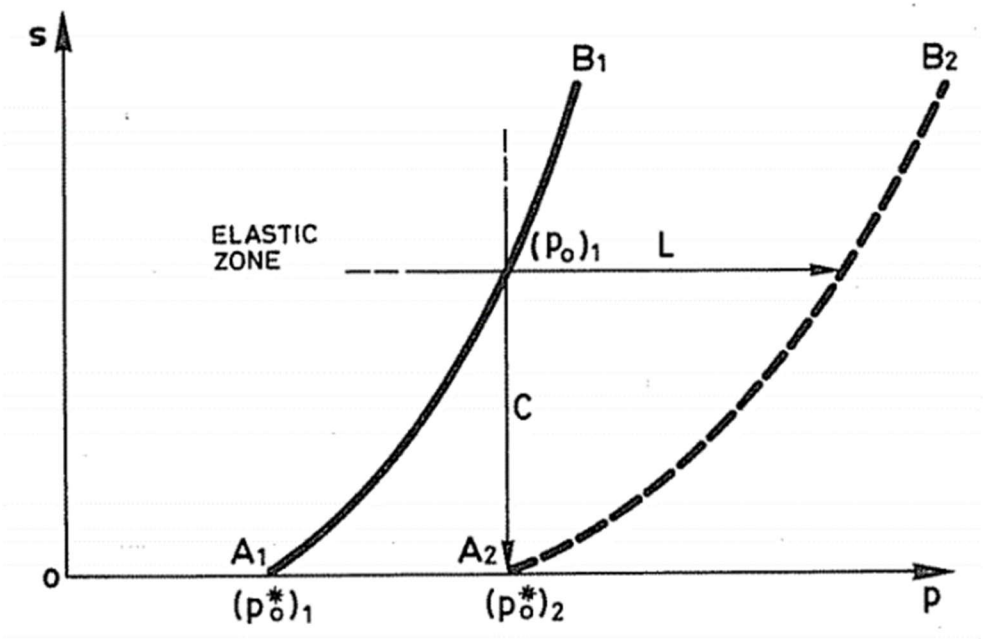

Figure 2.36 Schematic of LC Curve (Alonso et al., 1987)

As the stress path touch the yield locus, e.g. A_1B_1 in Figure 2.36, the irreversible deformation occurs and the yield locus shift to a new location i.e. A_2B_2 in Figure 2.36. Noticed that the deformation induced by stress variation, the L (pure loading) path, will be the same as the suction reduction, the C (wetting collapse) path. In a such way, the LC curve links the volumetric strain to stress condition as well as the suction condition (El Mountassir, 2011). The formulation of LC curve is presented as follows

$$p_0 = p^c \left(\frac{p_0^*}{p^c} \right)^{\lambda(0)-k_{i0} \,/\, \lambda(s)-k_{i0}} \tag{2.46}$$

Where

$$p_0^*(T) = p_0^* + 2\left(\alpha_1 \Delta T + \alpha_3 \Delta T \left|\Delta T\right|\right)$$
$$\lambda(s) = \lambda(0)\left[(1-r)\exp(-\beta s) + r\right] \tag{2.47}$$

r, β Model parameters

In Eq. (2.47), the λ(s) will decrease with suction increase, thus the r value is larger than 1(r > 1) (Alonso et al., 1990). However, Wheeler et al. (2002) observed that λ(s) may increase with suction, which implies r < 1. By the difference r value, Wheeler proposed a method to determine the reference stress p^c involved in Figure 2.34 and Eq. (2.46), as presented in Figure 2.37. (Suction $S_2 > S_1 > 0$).

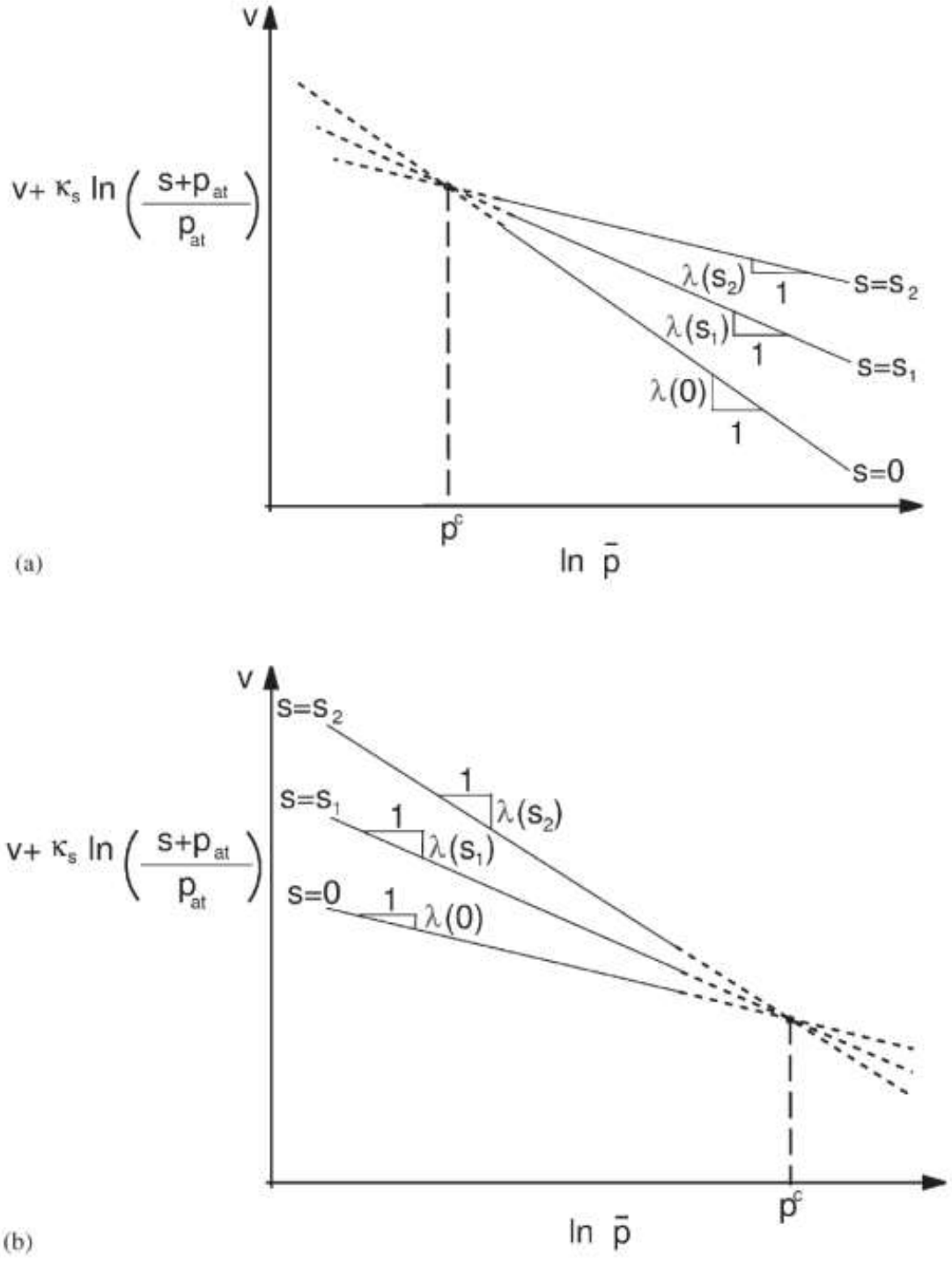

Figure 2.37 Determination for Value p^c (a) r<1, (b) r>1 (Wheeler et al., 2002)

2.3.3.3. Yield Locus Increment (Hardening Law)

The increment of the LC surface is present in Figure 2.38. The combination of stress p and suction s lies in the enclosed area of LC and SI curves will induce elastic deformation only. Analogy to the LC curve, the SI curve is the yield locus where mean stress remained constant while matric suction increase.

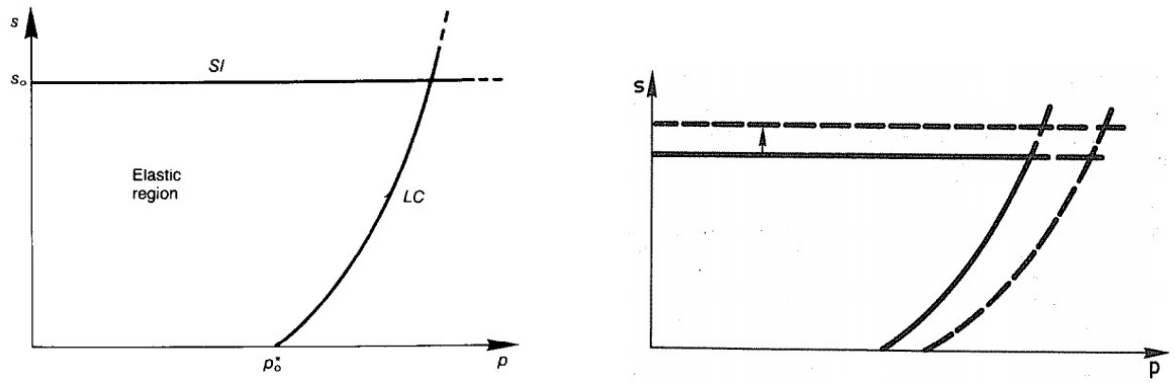

(a) (b)

Figure 2.38 (a) Loading-Collapse (LC) and Suction Increase (SI) Yield Curve. (b) The Increment of LC-SI Curve (Alonso et al., 1990)

As mentioned in 2.3.3, when soil subjects to fully saturated where the suction is zero, the BBM reduces to Modified Cam-Clay Model. Thus, on the p-q plane the yield locus is formulated as

$$q^2 - M^2\left(p + p_s\right)\left(p_0 + ks\right) = 0 \tag{2.48}$$

q Deviator stress
M Slope of Critical State Line (CSL) in MCC
k Content ratio between tensile strength and suction value

Figure 2.39 presents the yield locus in the stress (p, q) and suction (s) plane. In Figure 2.39 (a), when suction equals to 0, the ellipse is the traditional MCC yield locus, as the suction increase, the increment of tensile strength p_s proportional to the suction value in a ration of k as presented in Figure 2.39 (b). The slope of critical state line remains the same and thus the p_0 can be determined followed by Eq. (2.46).

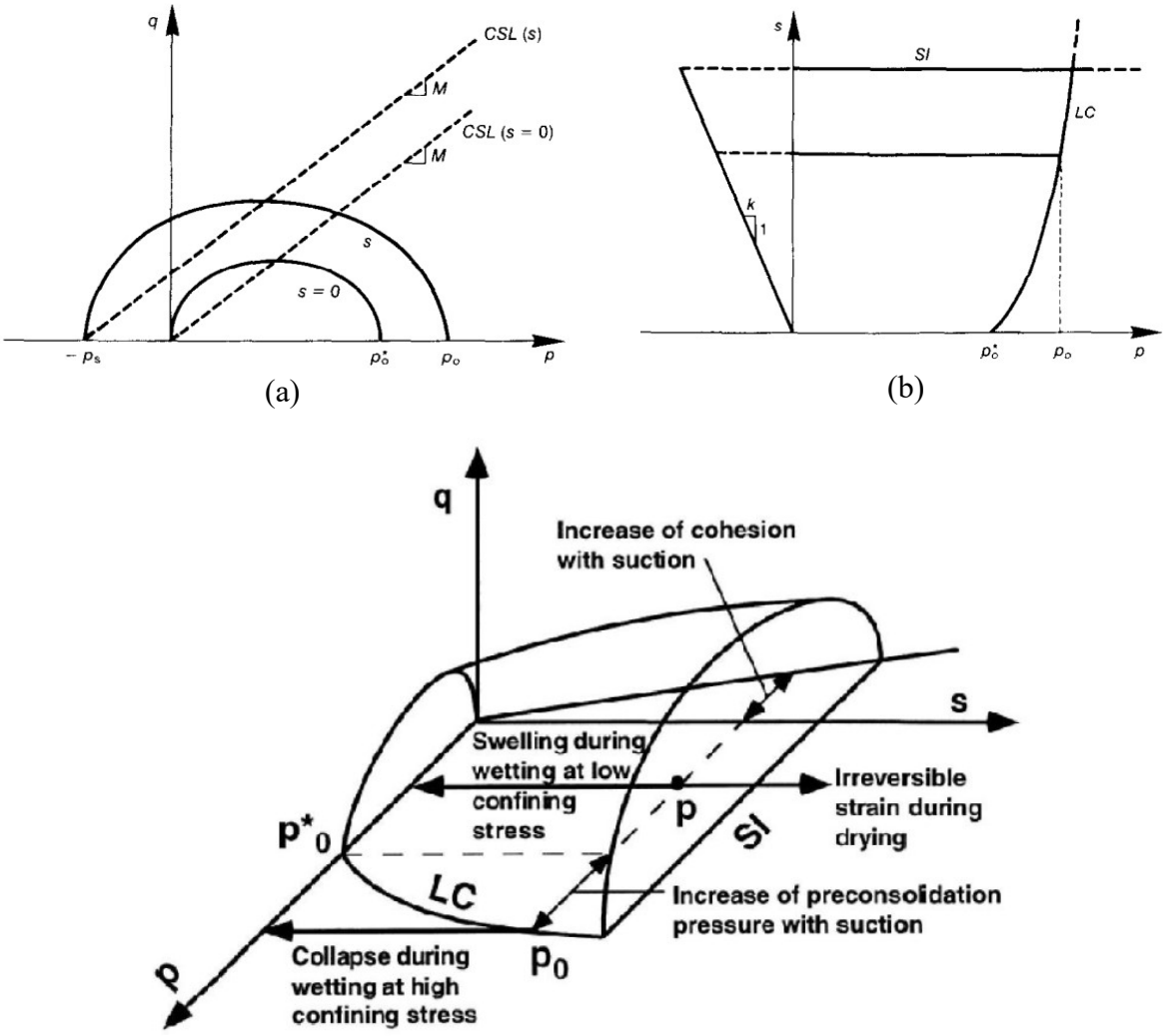

Figure 2.39 Yield Surface on (a) p-q Plane, (b) p-s Plane and (c) p-q-s Plane (Alonso et al., 1990)

3. CASE STUDIES OF PRACTICAL METHODS

3.1. Introduction

In this chapter, the practical methods mentioned previously are applied to analysis two cases history regarding to the shrink-swell soil problem. In general, the surface movement will be the first issue consider in such problem, then based on estimated movement, different design methods provide stiffen beams to strength the stiffness of the foundation to eliminate the damage of the soil.

3.2. Surface movement Estimation

3.2.1. Ellison Office Building (EOB)

The Ellison Office Building (EOB) is a 1-story building is located on Holleman Drive East, College Station, Texas (Abdelmalak & Briaud, 2017). Three boreholes were drilled to a depth from 4.5m to 9m below existing grade in 2004 and basic soil properties such as water content and Atterberg limit were obtained as shown in Figure 3.1

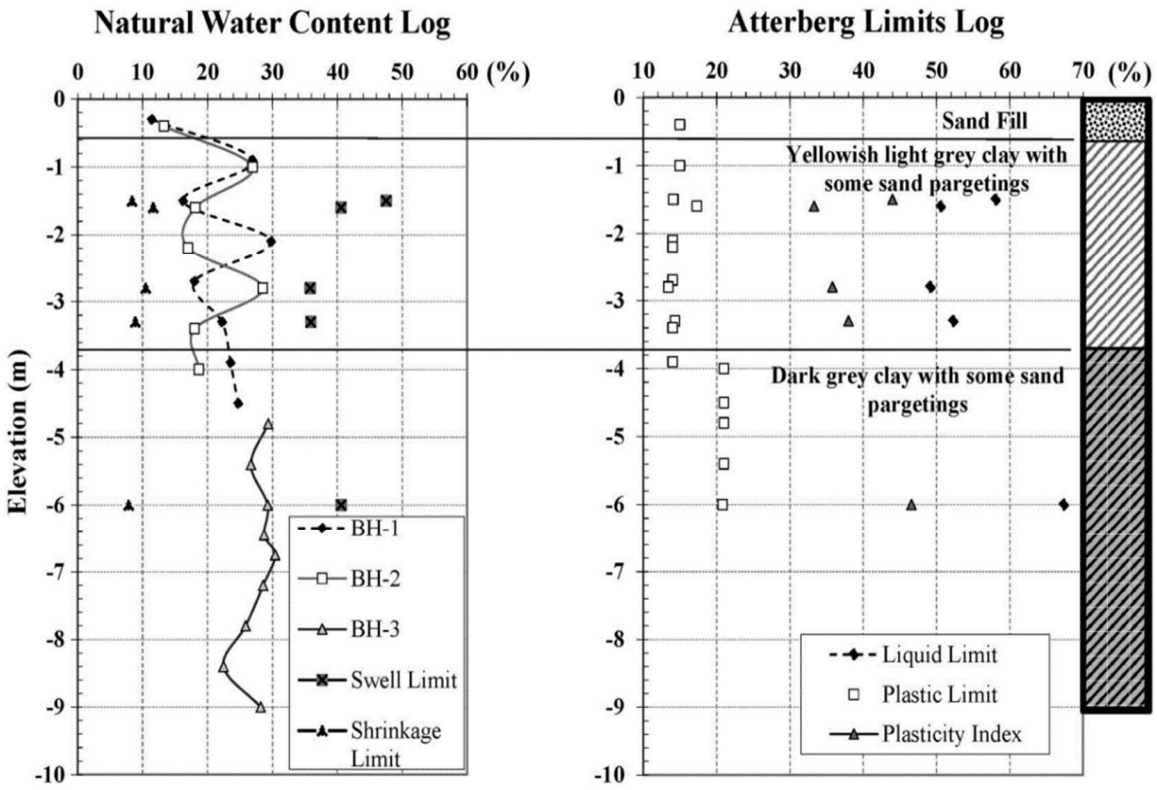

Figure 3.1 Water Content Variation and Atterberg Limit Distribution (Abdelmalak & Briaud, 2017)

The soil movement at the middle of the side of the slab and at the corner of the slab was measured for two years after construction by using vertical extensometers placed at different depths. The measurements taken as the difference between the extensometer and a 10 m deep benchmark are shown in Figure 3.2. The maximum movement of the ground surface was 48 mm and occurred at the corner of the slab.

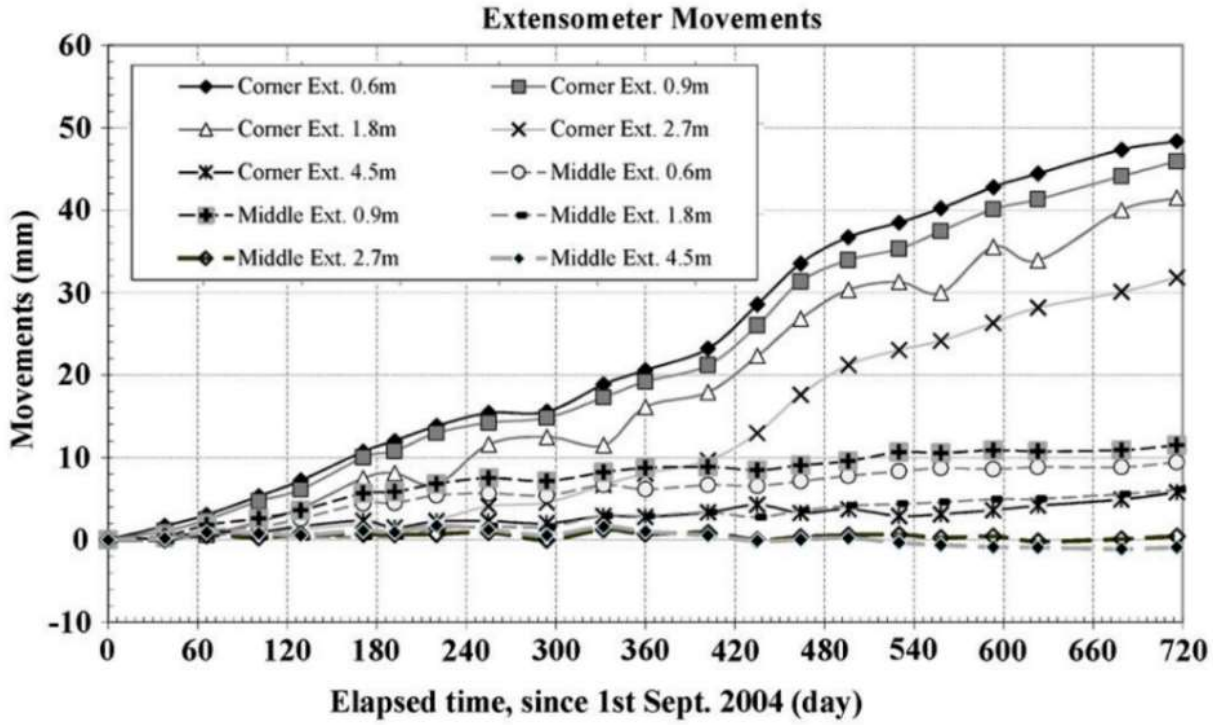

Figure 3.2 Soil Movement Measurement Distribution (Abdelmalak & Briaud, 2017)

The water content variation is not provided in the paper, however, by using such a database approach and working with Fugro and Buchanan Soil Mechanics Briaud et al (2003) created the variation of water content within about 1 m from the ground surface versus time over a two year period for Corpus Christi, San Antonio and College Station in Texas (Figure 3.3). The results indicate that the near-surface water content variation over the seasons is 5% for Corpus Christi, 8% for San Antonio and 5.5% for College Station.

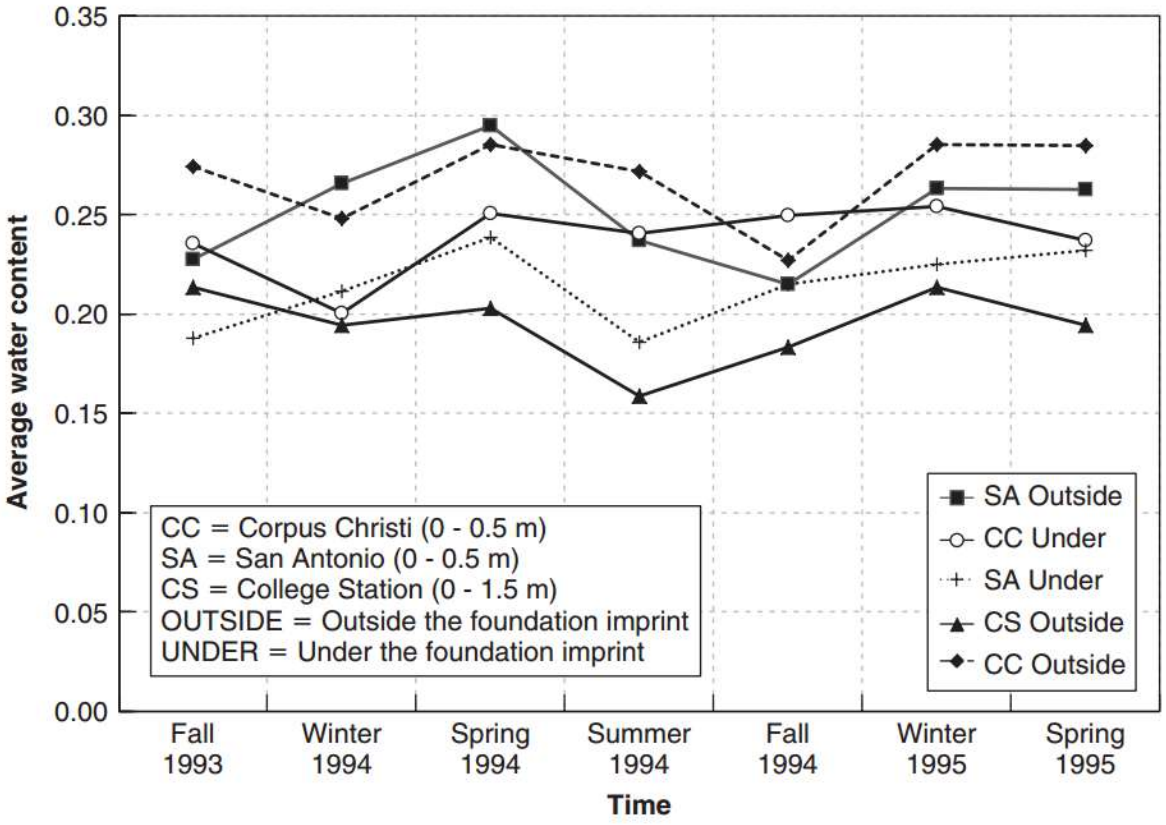

Figure 3.3 Water Content Variation in Cities in Texas (Briaud et al., 2003)

The parameters measured for the EOB case history are summarized as follow,

- PI=40%, LL=58%, PL=18%
- Natural moisture content: 26%
- Water content variation: 5.5%
- Active zone: 3m (Abdelmalak & Briaud, 2017)

Unfortunately, some of the parameters needed for the predictions were not measured during the case study, thus some assumptions were required.

A thirty-year record of relative humidity (RH) was collected to identify the high and low value of RH. Then the psychometric law was used to transform RH into a suction variation. This led to a suction variation about 1pF. Recall that the Thornthwaite moisture index is equal to 0 for

College Station, which implies that the yearly precipitation and evaporation are almost equivalent thus the suction variation can be considered as a stable value. It is also assumed that both the water content and the suction vary linearly from the ground surface down to the bottom of the active zone.

Further assumptions include:

- Bulk unit weight: 20 kN/m^3 (PVR method)
- Percentage of particle finer than No. 40 Sieve (425μm): 95 % (PVR method)
- Percentage of fine particles: 20% (PTI method)
- $\%f_c = \dfrac{\text{Percentage of soil passing } 2\mu\text{m sieve}}{\text{Percentage of soil passing } 75\mu\text{m sieve}} = 20\%$
- 1pF suction is the variation from 4pF in the dry season to 3pF in the wet season (PTI method)
- Instability index, I_{pt} = 3%/pF (AS 2870) (Fityus et. al., 2005)

A comparison between calculated and measured movements is shown in Table 3.1.

Table 3.1 Summary of Surface movement Estimation

	Site Measurement	PVR Method	PTI Method*	AS 2870 Method	Briaud et. al. Method
Surface Movement, mm	48	37.59	34.8 (Swell) 6.1 (shrink)	59.96	42.89
Diff. to Site Measured, %	N.A.	6.02	2.25	49.90	7.23

*Soil movement consider the summation of swell and shrink calculated by PTI method

Figure 3.4 shows the accumulated movement computed by different methods and compared to the result from extensometers.

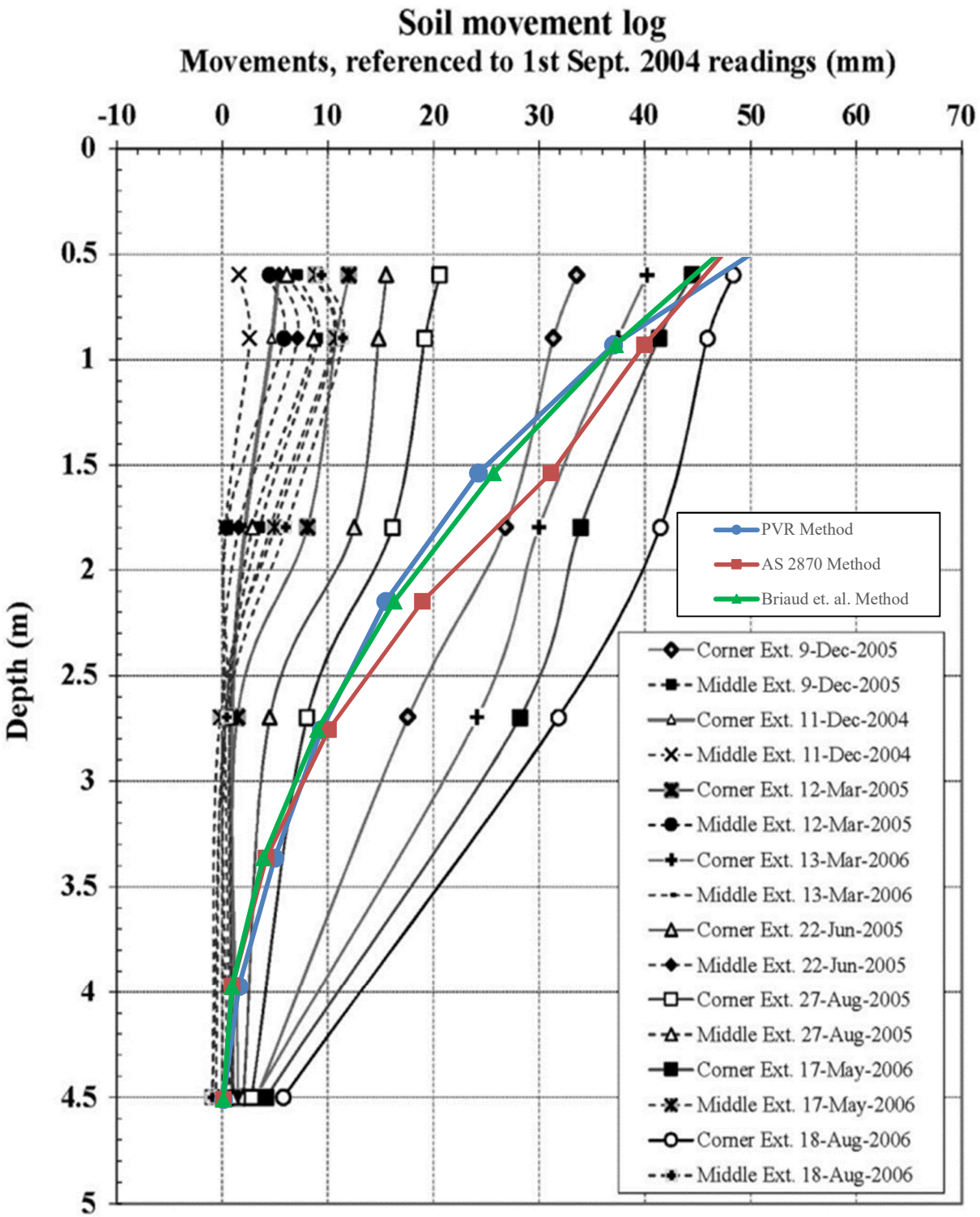

Figure 3.4 Soil Movement along the Depth into Soil Mass

3.2.2. Arlington footings case history

The Arlington site case history (Briaud et al., 2003) has 2 m by 2 m and 0.6 m thick spread footings were constructed in an open field site in Arlington. The soil was a CL and CH and the movement of the footing was observed for 2 years. The soil parameters are provided in Figure 58, and the measured surface movement is provided as a function of time for the four footings in Figure 59. The weather conditions for the period of monitoring was also monitored.

A total of 61 boreholes were drilled for 2 years to investigate the soil condition. The results from the borehole samples and site tests are summarized in Figure 3.5. The parameter E_w is the shrink-swell modulus which is then the slope of the volumetric strain versus water content line. The f value (f=0.39) is the ratio of axial strain to volumetric strain. The parameter u is the average suction measurement in the soil. The %SW is the maximum vertical strain measured in a free swell test performed according to ASTM 4546, method A.

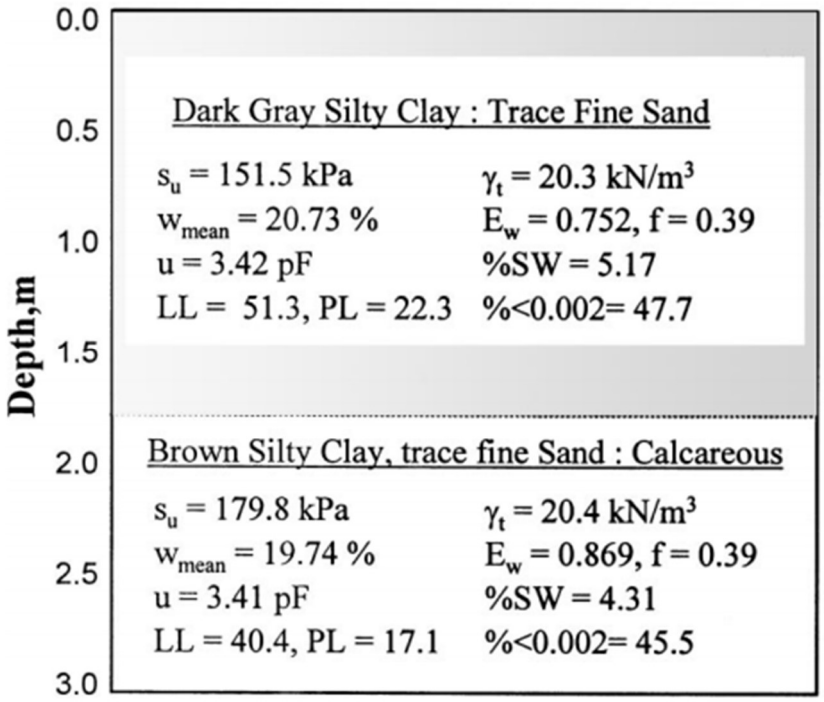

Figure 3.5 Summary of soil parameters (Briaud et al., 2003)

Because the boreholes were performed every three months for 2-years, the measurement values of water content and soil suction give the profile shown in Figure 3.6. These profiles can be used to make predictions according to the AS 2870 method and the Briaud et. al. method; indeed, these methods use either the change of water content or the suction as a function of time to estimate the surface movement.

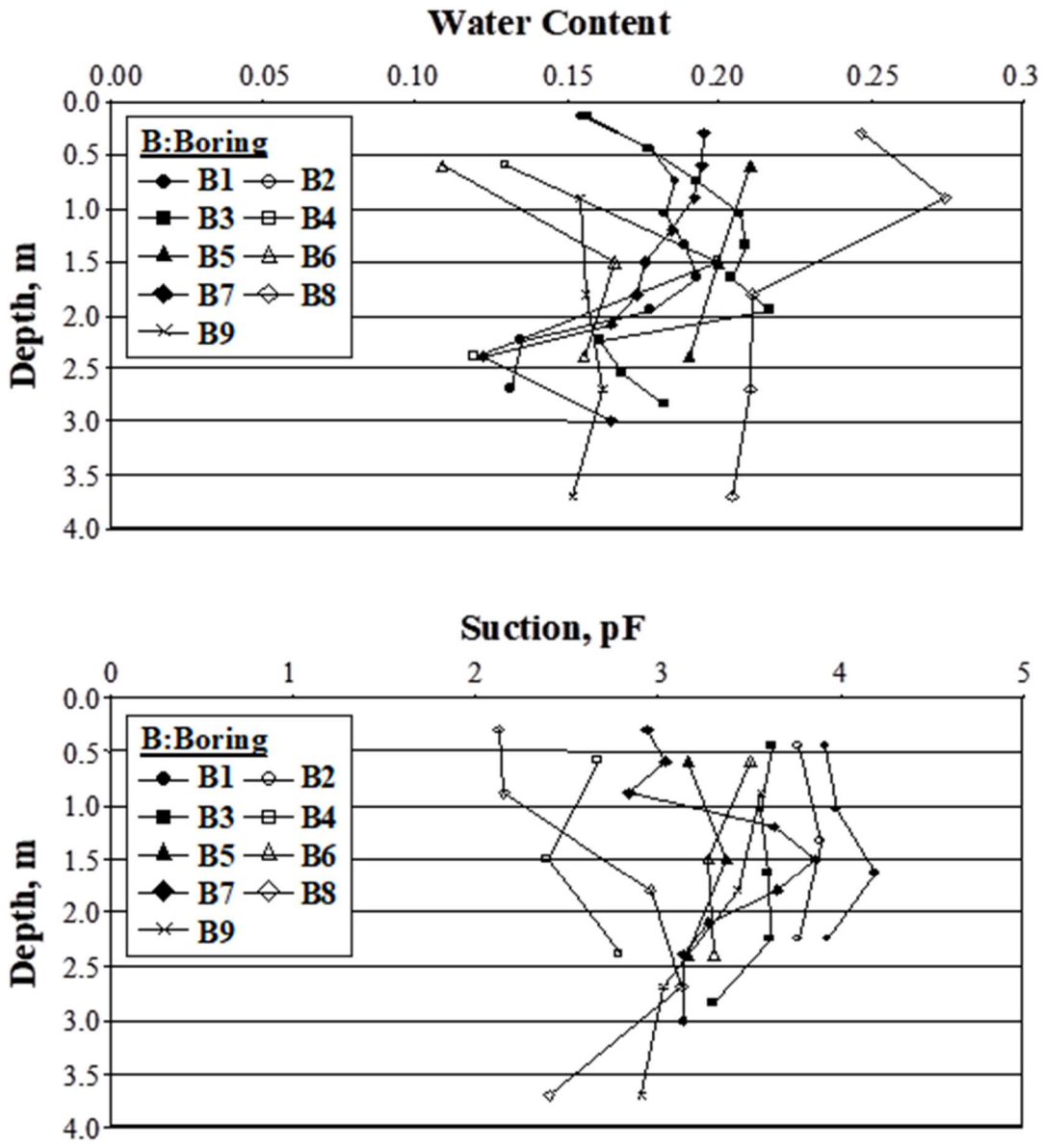

Figure 3.6 Water content and suction vs depth at a site in Arlington (Briaud et al., 2003)

The measured surface movement over two years is shown in Figure 59. Note that for footings RF1 an RF2 the soil was kept in its natural state while for footings W1 and W2 the soil was injected with water to "preswell" it.

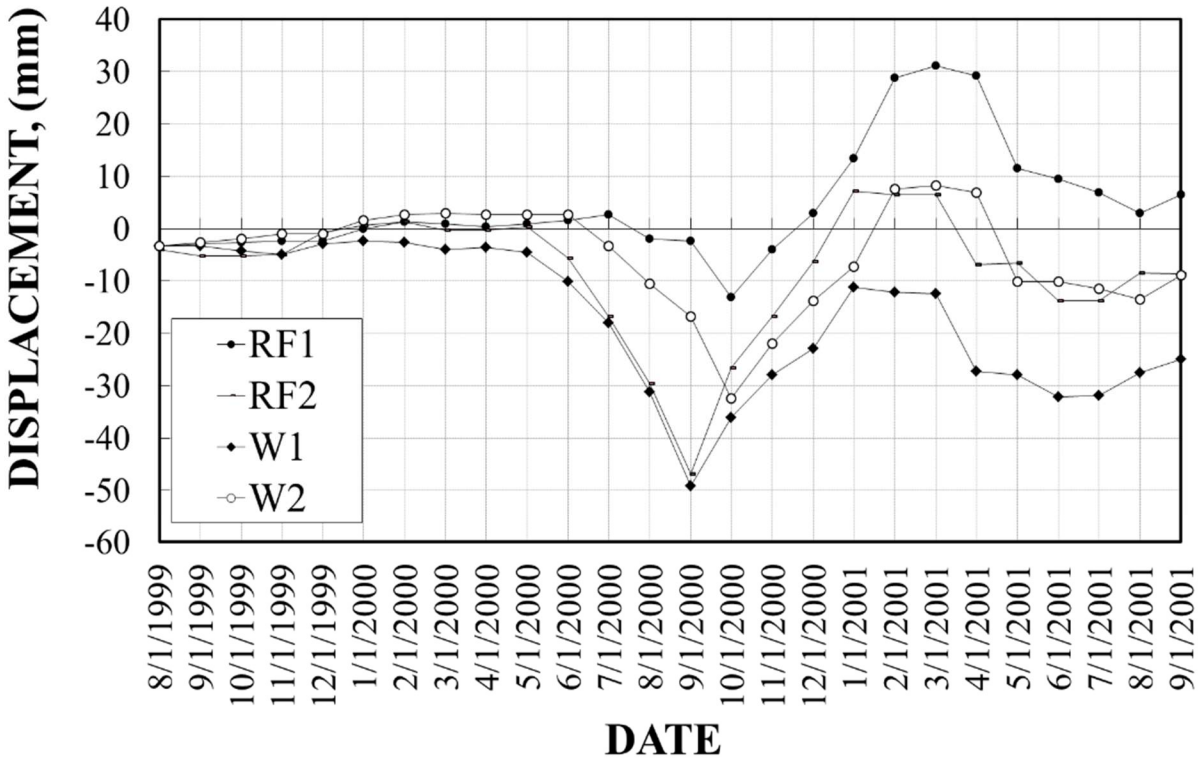

Figure 3.7 2-year continues surface movement record (Briaud et al., 2003)

The surface movement is calculated according to the PVR method by using the online spreadsheet as shown below. The predicted amount of swelling is 40.13mm (1.58in), as present in Table 3.2.

Table 3.2 Calculation result for PVR method

Depth to Bottom of Layer [ft]	Average Load [psi]	Liquid Limit (LL)	Dry 0.2LL+9	Wet 0.47LL+2	Percent Moisture	Dry Avg Wet	Percent -No.40	Plasticity Index (PI)	Percent Volume Swell	Percent Free Swell	PVR [in] Top of Layer	PVR [in] Bottom of Layer	Differential Swell [in]	Modified -No.40 Factor	Modified Density Factor	PVR in Layers [in]	Total PVR [in]
0.0	0.0	-	-	-	-	-	-	-	-	-	-	-	-	-	-	-	**1.58**
1.0	0.5	51.3	19.3	26.1	20.7	Dry	95.0	29	7.7	10.8	**0.00**	**0.00**	0.00	0.95	1.00	0.00	**1.58**
2.0	1.5	51.3	19.3	26.1	20.7	Dry	95.0	29	7.7	10.8	**0.00**	**0.46**	0.46	0.95	1.00	0.44	**1.14**
3.0	2.5	51.3	19.3	26.1	20.7	Dry	95.0	29	7.7	10.8	**0.46**	**0.84**	0.38	0.95	1.00	0.36	**0.78**
4.0	3.5	51.3	19.3	26.1	20.7	Dry	95.0	29	7.7	10.8	**0.84**	**1.15**	0.31	0.95	1.00	0.30	**0.48**
5.0	4.5	51.3	19.3	26.1	20.7	Dry	95.0	29	7.7	10.8	**1.15**	**1.41**	0.26	0.95	1.00	0.24	**0.24**
6.0	5.5	40.4	17.1	21.0	19.7	Avg	95.0	23.3	4.0	6.8	**0.73**	**0.81**	0.08	0.95	1.00	0.08	**0.16**
7.0	6.5	40.4	17.1	21.0	19.7	Avg	95.0	23.3	4.0	6.8	**0.81**	**0.87**	0.06	0.95	1.00	0.06	**0.10**
8.0	7.5	40.4	17.1	21.0	19.7	Avg	95.0	23.3	4.0	6.8	**0.87**	**0.91**	0.04	0.95	1.00	0.04	**0.06**
9.0	8.5	40.4	17.1	21.0	19.7	Avg	95.0	23.3	4.0	6.8	**0.91**	**0.95**	0.03	0.95	1.00	0.03	**0.03**
9.8	9.4	40.4	17.1	21.0	19.7	Avg	95.0	23.3	4.0	6.8	**0.95**	**0.98**	0.03	0.95	1.00	0.03	**0.00**

The key parameters to perform the PTI method calculations are the volume change factor γ_0, the Thornthwaite Moisture Index, TMI, for the location and the suction change factor based on the local suction change. The suction measurement for the Arlington site indicates an amplitude of 2pF according to Figure 3.6.

By using the Atterberg limits and the suction variation, the PTI method proceeds as follows. The surface movement is calculated as 43.43mm (1.71in).

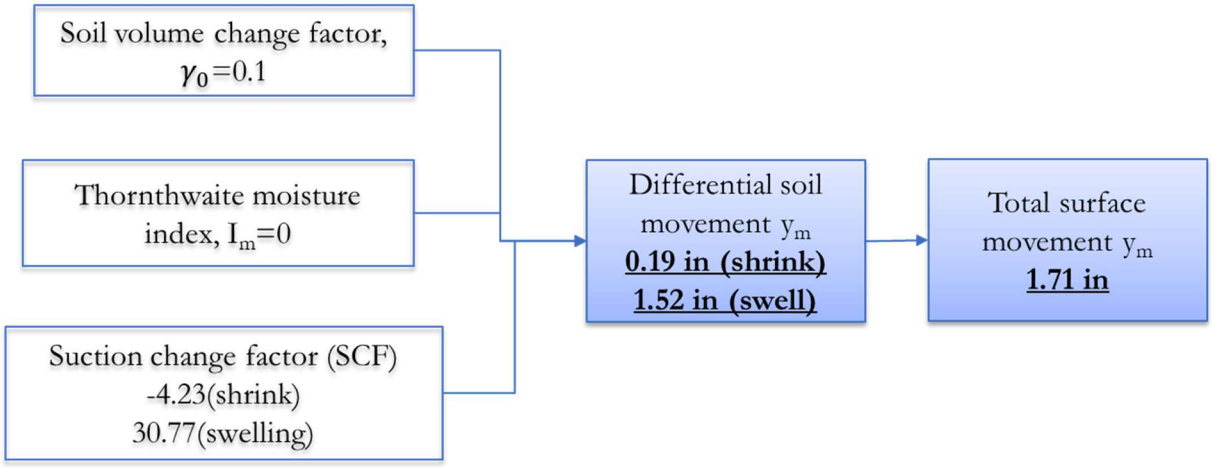

Figure 3.8 Simplify PTI estimation process

Note that the PVR and PTI method give single value predictions while the Briaud method, the AS2870 method and CODE_BRIGHT can give movement versus time. The PVR and PTI prediction are discussed here while the other three are discussed in the next section.

Table 3.3 is a summary of the measurement values and the prediction results. Figure 3.9 is a graphical representation of the results.

Table 3.3 Single value estimation result

Method	Swell	Shrinkage	Total
--	mm	mm	mm
RF1	31	-12	43
RF2	8	-48	56
W1	--	-49	-49
W2	9	-32	-41
PVR	40.13	--	40.13
PTI	38.6	-4.83	43.43

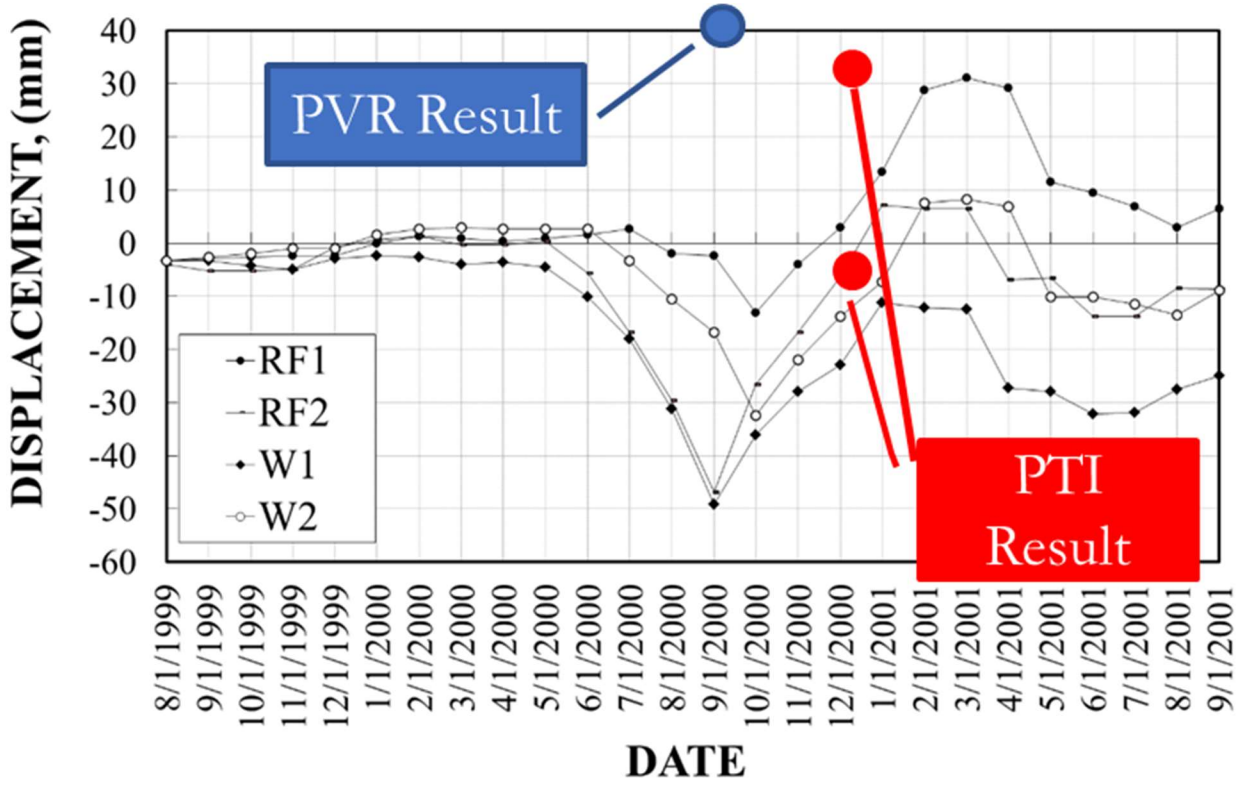

Figure 3.9 Single value estimation result on the continuous records

In Figure 3.9, the PVR result exceeds the maximum recorded swelling and thus is somewhat conservative; as is well known the PVR does not predict the shrinkage movement which in this case is comparable and sometimes exceeds the swelling movement.

The PTI method predicts both the swelling and shrinkage movement of the soil. The swelling predicted movement is slightly higher than the maximum recorded movement, while the shrinkage predicted movement is much smaller than the measured movement

The AS 2870 method requires the suction variation at different depth over time, and the Briaud et. al.'s method requires the water content variation. These two variation results were recorded at the site and are presented in Figure 3.6. The first comparison between predictions and measurements for the AS 2870 method and the Briaud et. al.'s method is presented in Figure 3.10.

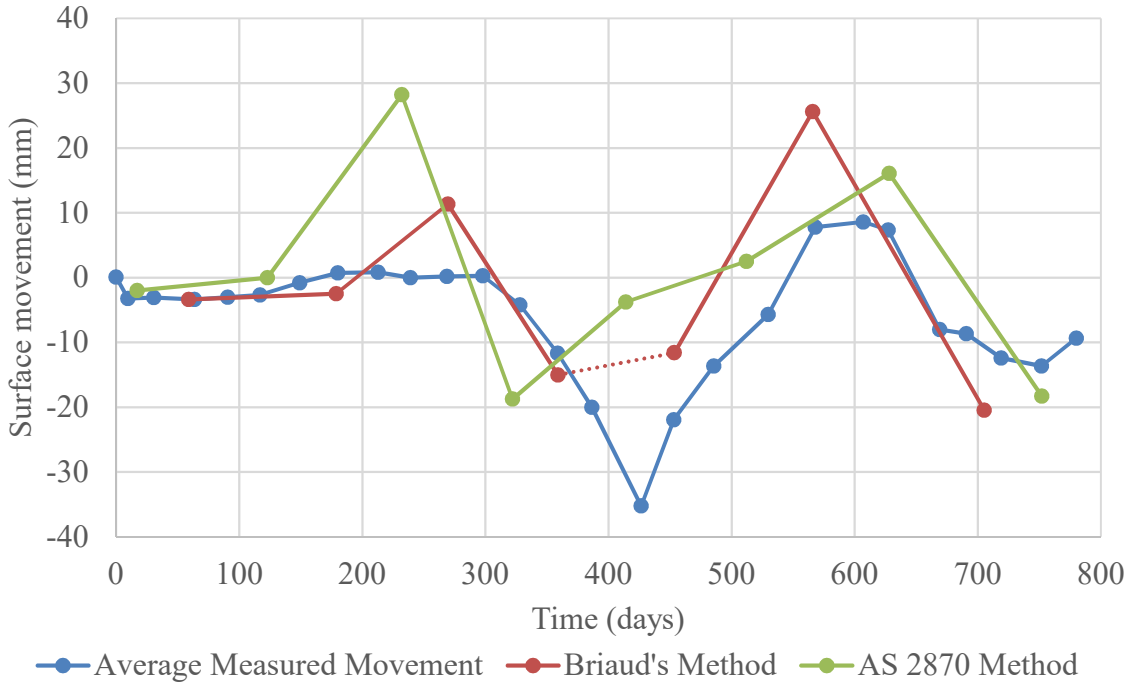

Figure 3.10 Surface movement comparison between site records, Briaud et. al.'s method and AS 2870 method

The results from Figure 3.10 indicates that both AS 2870 method and Briaud et. al.'s method can catch the movement in both the swelling and the shrinkage direction with various degree of precision.

3.3. Stiffen Beam Depth Design in Ellison Office Building (EOB)

The depth of the beams selected for the foundation beneth EOB is 1.05m with a spacing of 3m in the short direction and 3.8m in the long direction. The foundation layout is shown in Figure 3.11.

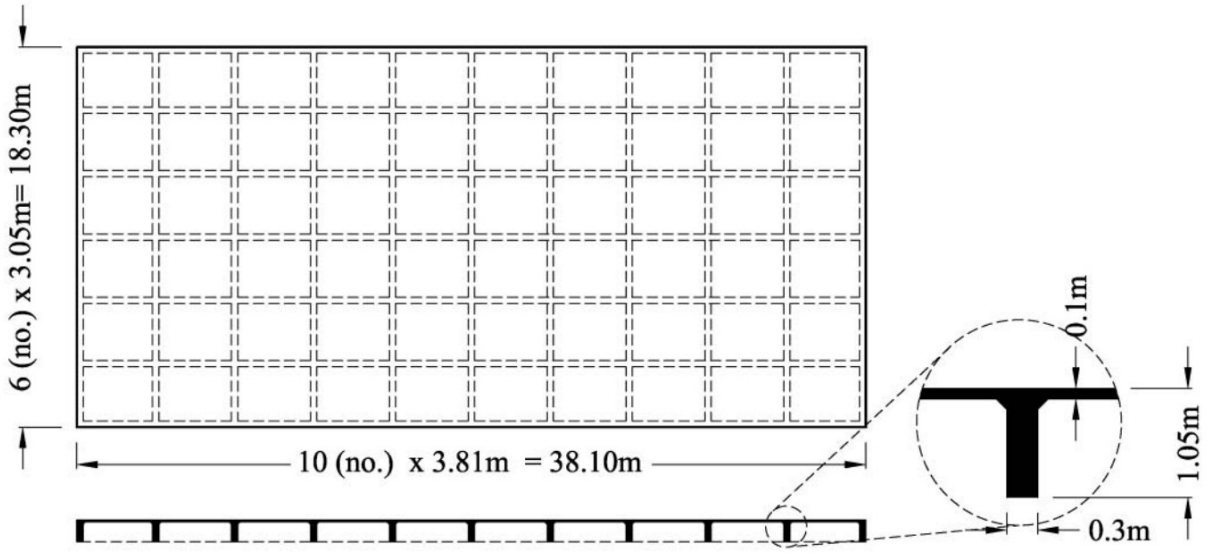

Figure 3.11 Layout of Foundation Slab on Grade with Stiffen Beams (Abdelmalak & Briaud, 2017)

The detail calculation steps are presented in Appendix B. The stiffen beam depth designed follow by individual method for the EOB case history is summarized as follows,

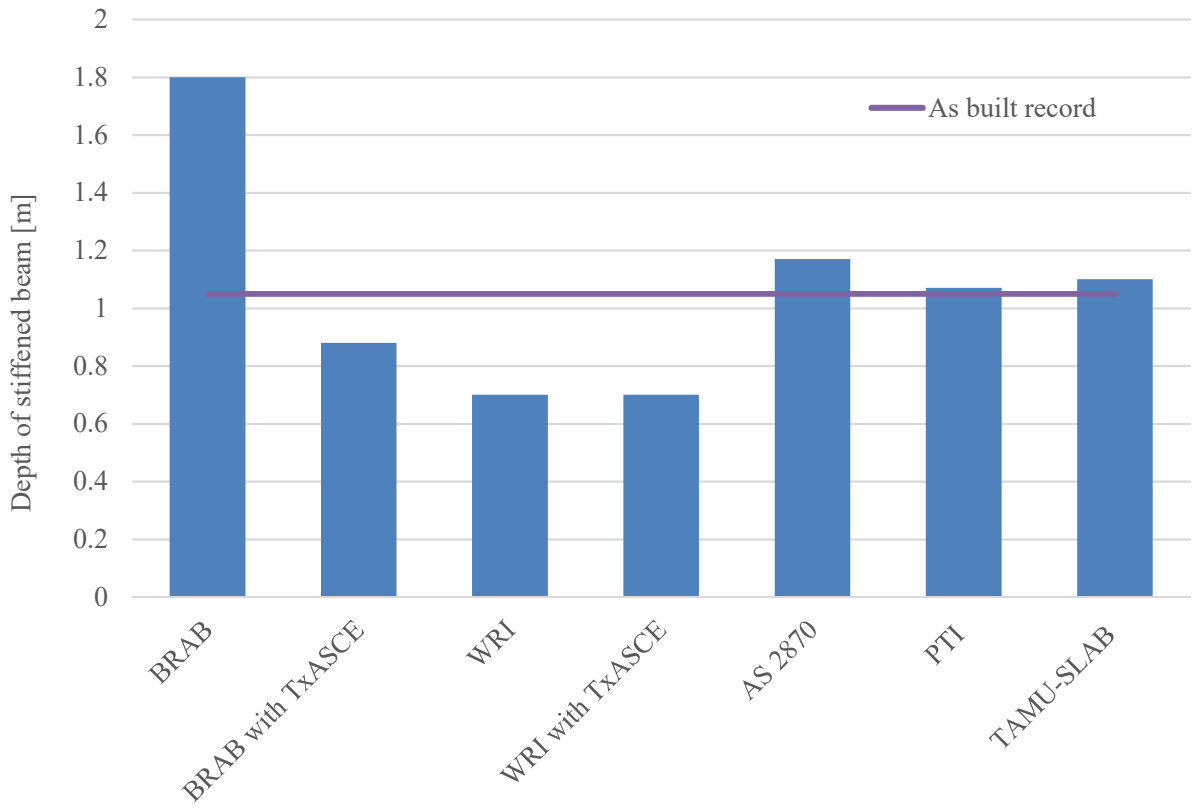

Figure 3.12 Comparison between design values and as-built record

Table 3.4 Summary of Design Depth of Beam

Method	**EOB as built**	**BRAB**	**BRAB with TxASCE**	**WRI**	**WRI with TxASCE**	**AS 2870**	**PTI method**	**TAMU-SLAB (suction based)**
Depth of beam (m)	**1.05**	1.8	0.88	0.7	0.7	1.17	1.07	1.1
Diff. in m between EOB record	**N.A.**	+0.75	-0.17	-0.35	-0.35	+0.12	+0.02	+0.05

The measured slab movement at EOB during two years after construction is shown in Figure 3.13. As can be seen on Figure 3.13, the maximum distortion is 8 mm over 6 m for an L/Δ = 750 which is very acceptable. Therefore, a beam depth of 1.05m (3.44ft) seems a good choice in this case.

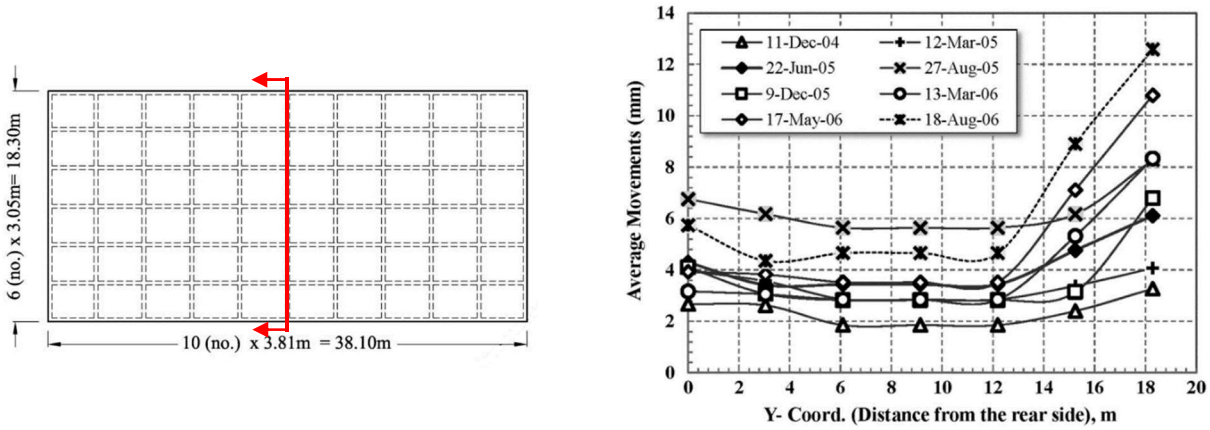

Figure 3.13 Slab Movement Record (Abdelmalak & Briaud, 2017)

3.4. Fictitious Cases Analysis

Because the number of case histories where the slab behavior and the soil have been documented in detail, it is difficult to evaluate the accuracy of the various methods. Instead it was decided to conduct an analysis of fictitious but realistic cases. A reference set of average soil and slab parameters was selected. All methods were used for this reference set. Then each parameter in the set was varied up and down from the average value. Again, all methods were used to predict the beam depth. This led to a total of 34 beam depth predictions by 8 different methods. In the end the prediction by each method in each case was compared to the average of all beam depth predictions by all methods. This will not show which method is best, but it does indicate which methods tend to be conservative and which ones tend to be optimistic.

3.4.1. Organization of the fictitious Cases

The input parameters for the fictitious cases are a combination of the input parameters for the BRAB method, the WRI method, the AS 2870 method, the PTI method and the TAMU-SLAB method. They include weather parameters, soil parameters and structural parameters as presented in Table 3.5 to Table 3.9. The values of the input parameters for the reference case are shown in Table 3.10.

Table 3.5 Input Parameters of BRAB Method

Climate Parameters	Structural Parameters	Soil Parameters
Climate Rating Index, C_w	Length of Slab, L	Plasticity Index, PI
	Thickness of Slab, t	
	Spacing of Beam, s	
	Width of Beam, b_w	
	Elastic Modulus of Concrete, E	
	Area Distributed Loading, w	

Table 3.6 Input Parameters of WRI Method

Climate Parameters	Structural Parameters	Soil Parameters
Climate Rating, C_w	Length of slab, L	Plasticity Index, PI
	Thickness of slab, t	Unconfined compression strength, q_u
	Width of beam, b_w	
	Elastic Modulus of concrete, E	
	Area distributed loading, w	
	Slope of ground, C_0	

Table 3.7 Input Parameters of AS 2870 Method

Climate Parameters	Structural Parameters	Soil Parameters
--	Length of slab, L	Soil instability index, I_{ps}
	Spacing of beam, s	Active zone, H_s
	Width of beam, b_w	Crack zone
		Suction change, Δu

Table 3.8 Input Parameters of PTI Method

Climate Parameters	Structural Parameters	Soil Parameters
Thornthwaite index, I_m	Length of slab, L	Plasticity index, PI
	Thickness of slab, t	Liquid limit, LL
	Width of beam, b_w	Percentage of fine particle, %/fc
	Spacing of beam, s	Soil fabric fraction, F_f
	Perimeter loading, p	Suction variation (constant as manual recommend)
	Creep Modulus of concrete, E	

Table 3.9 Input Parameters of TAMU-SLAB Method

Climate Parameters	Structural Parameters	Soil Parameters
--	Length of slab, L	Shrink-swell index, I_{ss}
	Spacing of beam, s	Active zone, H_s
	Width of beam, b_w	Suction change, Δu
	Area distributed loading, w	
	Elastic Modulus of concrete, E	

Table 3.10 Input Parameters Value for Reference Case

Climatic Parameters	Structural Parameters		Soil Parameters	
Climate Rating Index, C_w=21	Length of Slab, 24m×12m	Area Distributed Loading, w=10 kPa	Plasticity Index, PI=30%	Soil reactivity index, I_{ps}=4.08 %
Thornthwaite index, I_m=0	Thickness of Slab, t=0.1m	Perimeter loading, p=15kN/m	Liquid limit, LL=50%	Soil fabric factor, F_f=1.2
	Spacing of Beam, s=4.5m	Slope of ground 0 degree	Active zone, H_s=2m	Percent of fine particle, $\%f_c$ =65
	Width of Beam, b_w=0.3m		Shrink-well index, I_{ss}=22%	Elastic modulus of soil, E_s=15 MPa
	Elastic Modulus of Concrete, E=20GPa		Crack zone, z=0.5 ft	Moisture change, Δw=6%
	Creep Modulus of Concrete, E=10GPa		Unconfined compression strength, q_0=200 kPa	Suction change, Δu=1.04 pF (2.5 kPa)

3.4.2. Correlation of Input Parameters

Although the parameters in the fictitious cases are chosen arbitrarily, they should obey reasonable correlations between parameters to ensure consistency. Correlations were sought and are subdivided into methods built-in correlation and correlation developed from publicly available data.

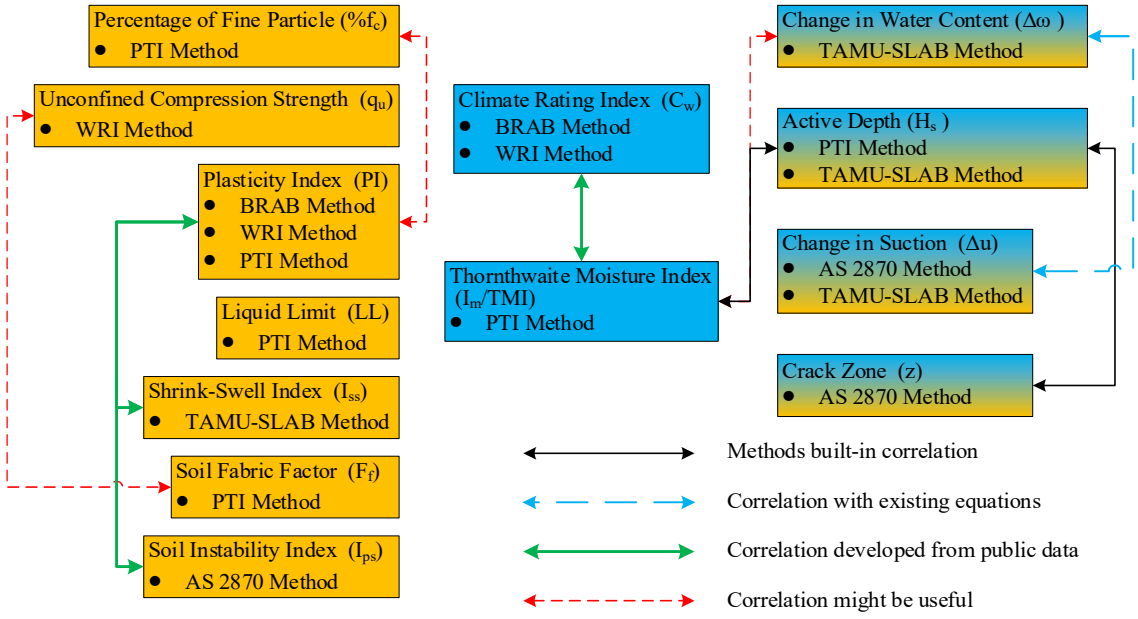

Figure 3.14 Parameters correlation overview

3.4.2.1. Methods Built-In Correlation

The AS 2870 method includes research on the correlation between the Thornthwaite Index value and the active zone, and between the active zone and the crack zone depth. The correlation details are described in section 2.1.3.

3.4.2.2. Correlation Developed from Publicly Available Data

3.4.2.2.1. Thornthwaite index I_m and climate rating index C_w

The Thornthwaite index and climate rating index have based on similar concepts. The Thornthwaite index describes the relationship between precipitation and evaporation for a period of time, and the climate rating index is a combination of precipitation and corresponding duration. Thus, five cities are chosen to evaluate the correlation (Table 3.11). A strong linear correlation is found as shown in Figure 3.15. Thus, in the fictitious cases, the Thornthwaite index and the climate index will follow this relationship.

Table 3.11 Thornthwaite Index and Climate Rating for Five Cities

City	C_w	I_m
College Station	20	0
Austin	17	-12
San Antonio	16	-15
Houston	25	18
New Orleans	35	40
Los Angeles	15	-20

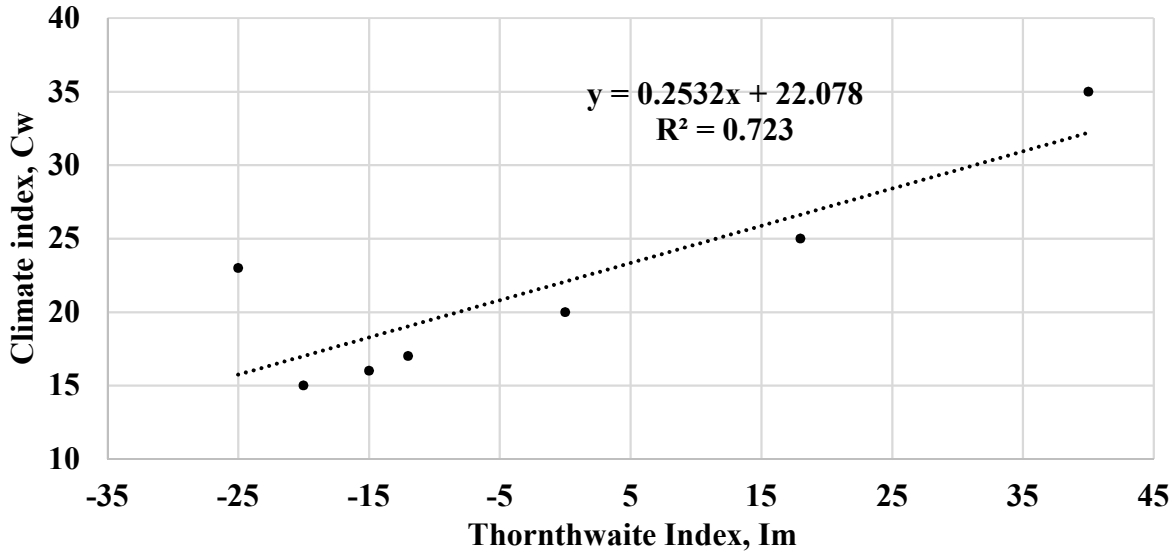

Figure 3.15 Thornthwaite Index vs. Climate Index

3.4.2.2.2. Plasticity Index and Soil Instability Index

The soil instability index is a parameter used in the AS 2870 method. It describes the volumetric strain change per unit suction in the shrinkage process. However, no comprehensive study was found relating the soil parameters to the instability index. Nevertheless, (Jayasekera & Mohajerani, 2003) provide testing data describing a relationship between the plasticity index and the shrink-swell index, where the shrink-swell index can be used to estimate the soil instability index. It should be noted that the shrink-swell index here is different from the one used in the TAMU-SLAB method. The shrink-swell index in the TAMU-SLAB method is the water content difference between the shrink limit and the swell limit, while in Jayasekera and Mohajerani the shrink-swell index I_{ss} is defined as

$$I_{ss} = \frac{\left(\varepsilon_{swell} / 2\right) + \varepsilon_{shrink}}{1.8(in\ pF)} \tag{3.1}$$

The data from Jayasekera and Mohajerani is plotted in Figure 3.16. A strong correlation is shown thus this relationship between the plasticity index and the shrink-swell index can be observed.

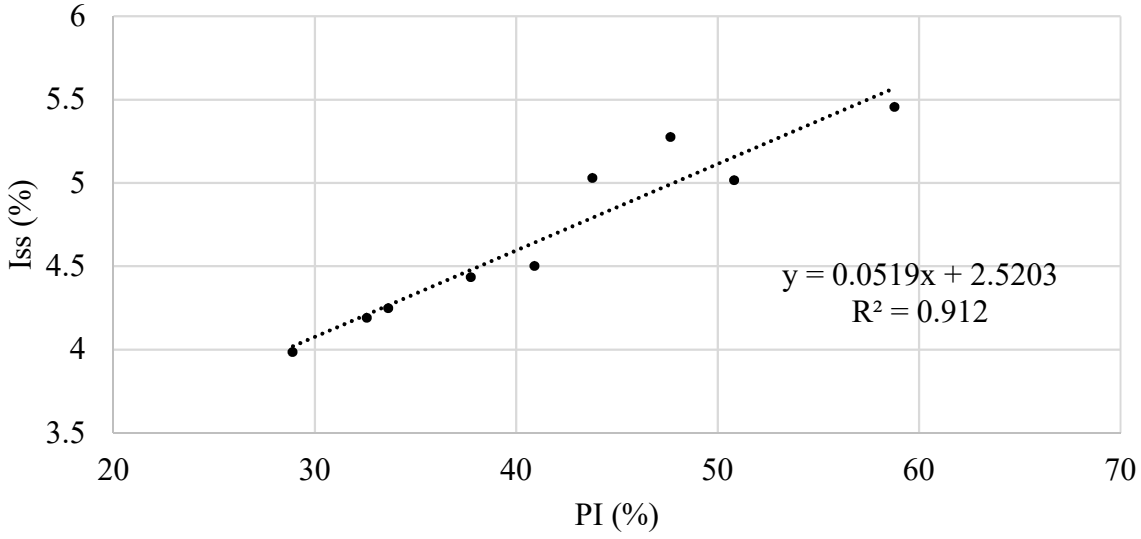

Figure 3.16 Plasticity Index vs. Shrink-Swell Index (Jayasekera, S., & Mohajerani, A., 2003).

In the AS 2870 method, the soil free shrinkage index (or called instability index) I_{ps} is required, which is defined by the percent vertical strain per unit suction change. If assuming the $\varepsilon_{swell}=2\varepsilon_{shrink}$, the free shrinkage index I_{ps} can be calculated as

$$I_{ps} = 0.9I_{ss} \tag{3.2}$$

Which is relative to the plasticity index.

3.4.2.2.3. Plasticity Index and Shrink-Swell Index

The shrink-swell index is a parameter used in the TAMU-SLAB method; it is the difference in water content between the swell limit and the shrink limit (section 2.2.2). Abdelmalak (2007) proposed a relationship between the shrink-swell index and the plasticity index, as shown in Figure 3.17.

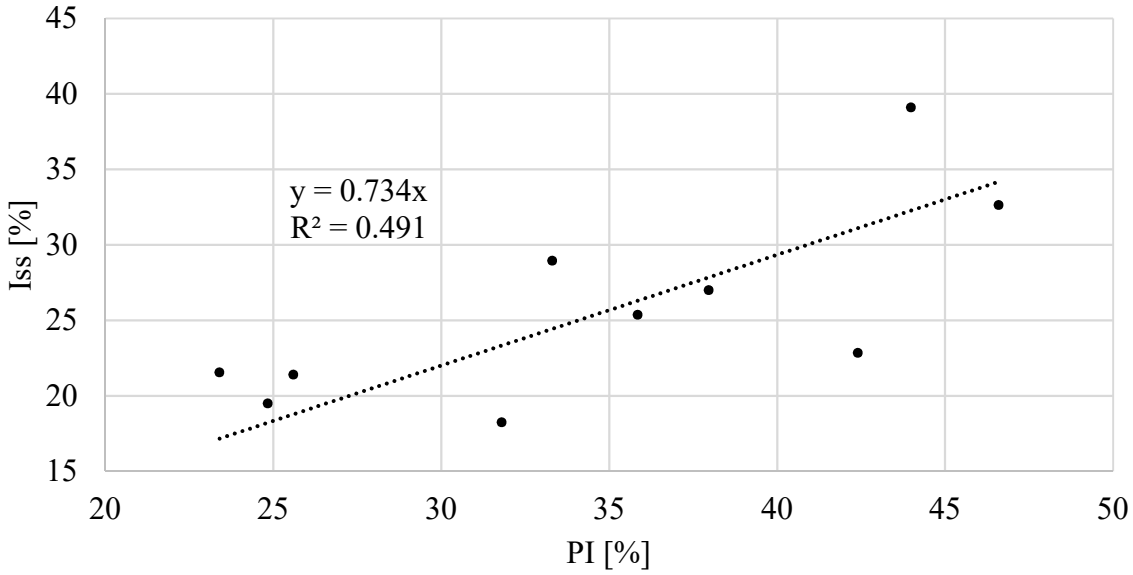

Figure 3.17 Plasticity Index and Shrink-Swell Index (Abdelmalak, 2007)

Based on the correlations mentioned above, a table of 34 fictitious cases with realistic quantities and consistent parameters is prepared in Appendix A.

3.5. Conclusion of Cases Study

Four design methods to predict the shrink-swell movement of soils are reviewed and evaluated. The PVR and Briaud et. al.'s method is based on the water content variation, and the AS 2870 method and PTI method are based on the suction variation. The PVR was developed by TxDOT and has been used for a very long time. The PTI method has also been used for a long time. The AS 2870 method is well accepted in Australia, and the Briaud et. al.'s method was proposed in 2007.The PVR method predicts the swell movement only while all other methods predict both shrink and swell movement.

Two case histories are used to evaluate the methods: The Ellison office building case history in College Station and the Arlington footings case history near Dallas. The results show that all methods predict the movement within plus or minus 30%. The PVR predicts the maximum swell movement only while the Briaud et al.'s and the AS2870 method can describe the evolution of the shrink and swell movement with time.

3.6. Conclusion of Fictitious Cases

3.6.1. Sensitivity of distributed loading

The area distributed loading involves the BRAB method, BRAB method with TxASCE guideline, WRI method, WRI method with TxASCE guideline, and TAMU-SLAB method. The loading adopted in the synthetic case was 5, 7, 10, 12 and 15 kPa (100, 150, 200, 250, and 300 psf). As expected, the depth of the stiffening beams for the slab becomes deeper when the loading increases.

As the loading increase, the stiffen beams becomes deeper in order to provide additional stiffness to the foundation. Among the result, the WRI method provides the lightest beam depth,

and the TAMU-SLAB suction method provides the deepest value. As Snowden (Snowden 1981) mentioned, the WRI is a modification to the BRAB method. The sensitivity for BRAB, WRI and corresponding methods with TxASCE guidelines are similar to each other. Because of different design curves, the result for the TAMU-SLAB suction method is different from the TAMU-SLAB water content method. The water content-based method is more sensitive compared to the suction-based method.

3.6.2. Sensitivity of climate rating index

The climate rating index adopted in BRAB, WRI method, and the corresponding modified method by TxASCE guideline. Values adopted in the synthetic case are 15, 21 25 and 30.

In general, the design beam depth becomes lighter when the weather is drier. A decreasing beam depth in dry weather implies that the methods apply additional stiffness to the foundation only against the swelling of the soil only. The BRAB and its TxASCE modification method and the WRI method have similar sensitivity to the climate rating index as the WRI method established based on the BRAB method.

Notice that the WRI method with the TxASCE guideline remains unchanged. As the guideline has limited the minimum length of cantilever involved in the calculation steps, this limitation further affects the minimum depth of the beam to a value of 0.7m.

3.6.3. Sensitivity of Thornthwaite Moisture Index

The Thornthwaite index involves in the PTI method. It is a description of precipitation, evaporation for a certain period. The value adopted in synthetic case are -20, -10, 0, 10 20. The negative value implies the evaporation larger than precipitation.

In the PTI method, the Thornthwaite index between -15 to 15 is classified as the post-construction case. In this scenario, compared to weather changing, the construction progress controls the

influence on the soil movement (swelling and shrinkage), a deeper beam depth will be calculated. When the Thornthwaite index larger than 15 or smaller than -15, as classified as post-equilibrium case, the movement is then controlled by weathering. The beam depth is lighter compared to the post-construction case.

Also, notice when the weather controls the soil movement, for a wet condition (TMI=20), the depth of the stiffened beam is lighter than in dry condition (TMI = -20). This difference implies that when the area subject to a dry condition, the soil may easily behave swelling; thus, more stiffness should be provided, while in the wet condition, the soil movement is considered relatively smaller. This conclusion follows the general logic, but detail behavior needs to be further investigated.

3.6.4. Sensitivity of plasticity index

The plasticity index involved in the BRAB method, the WRI method, and the corresponding modification method by TxASCE guideline and the PTI method. The discussion of the TAMU-SLAB method is also performed by assuming the plasticity index equals to the soil shrink-swell index I_{ss}. Only the TAMU-SLAB suction method result is present since the result of the TAMU-SLAB water content method is identical. The value adopted in the synthetic case is 25, 30, 40, 45, and 60%.

In general, a high plasticity index implies the soil has a more significant intensity to move, and thus, the foundation requires a deeper depth of the stiffened beam. The WRI method is the most sensitive one to the PI, and the TAMU-SLAB method has not significantly affected the value. The sensitivity of the BRAB method, the WRI method, and their TxASCE modified methods are similar due to the similarity of the design procedure.

It is worth to point out that the scatter results of the PTI method mainly because of the application of the plasticity index during the procedure. The PTI method adopted the PI value, conjunction with the liquid limit and the percentage of the fine particles to classify the mineral of the soil. A significantly jump at PI=40 because of the classification of soil is different. Thus, the amount of soil movement is discontinuous from the previous results.

3.6.5. Sensitivity of active zone

The active zone involves in AS 2870 method and the TAMU-SLAB method. The values adopted in the synthetic case for the active zone are 1.9m, 3m, 4.5m, and 6m (6.24, 10, 15 and 20 ft). The adoption of 3m is a typical depth of active zone in College Station, Texas, United States.

As the depth of active zone increase, with the same amount of suction/water content variation, the amount of soil movement is also increased and thus requires a deeper stiffened beam to maintain structural serviceability. Among the three methods, AS 2870 strongly sensitive to the depth of the active zone but still provides the lightest beam depth. The TAMU-SLAB suction method provides the deepest beam depth, and because of different design curves, the sensitivity of the suction method is stronger than the moisture method.

3.6.6. Sensitivity of water content and suction variation

Only the TAMU-SLAB water content method directly uses the water content variation during the design process. The BRAB method adopted the climate parameters to describe the change in water content indirectly. Thus it is not able to perform the sensitivity analysis for water content variation. The values of water content change adopted in the synthetic case are 3, 4, 10, 14 and 15%.

Suction change involves in TAMU-SLAB and AS 2870 methods. The values adopted in the synthetic case are 0.5, 1, 1.5 and 2 pF

The shape of the design curve mainly follows the sensitivity behavior of the water content in the TAMU-SLAB water content method.

Similar to water content change, the larger suction change implies more soil movement; thus the foundation requires a deeper the stiffened beam. The sensitivity of AS 2870 method is stronger than the TAMU-SLAB suction method.

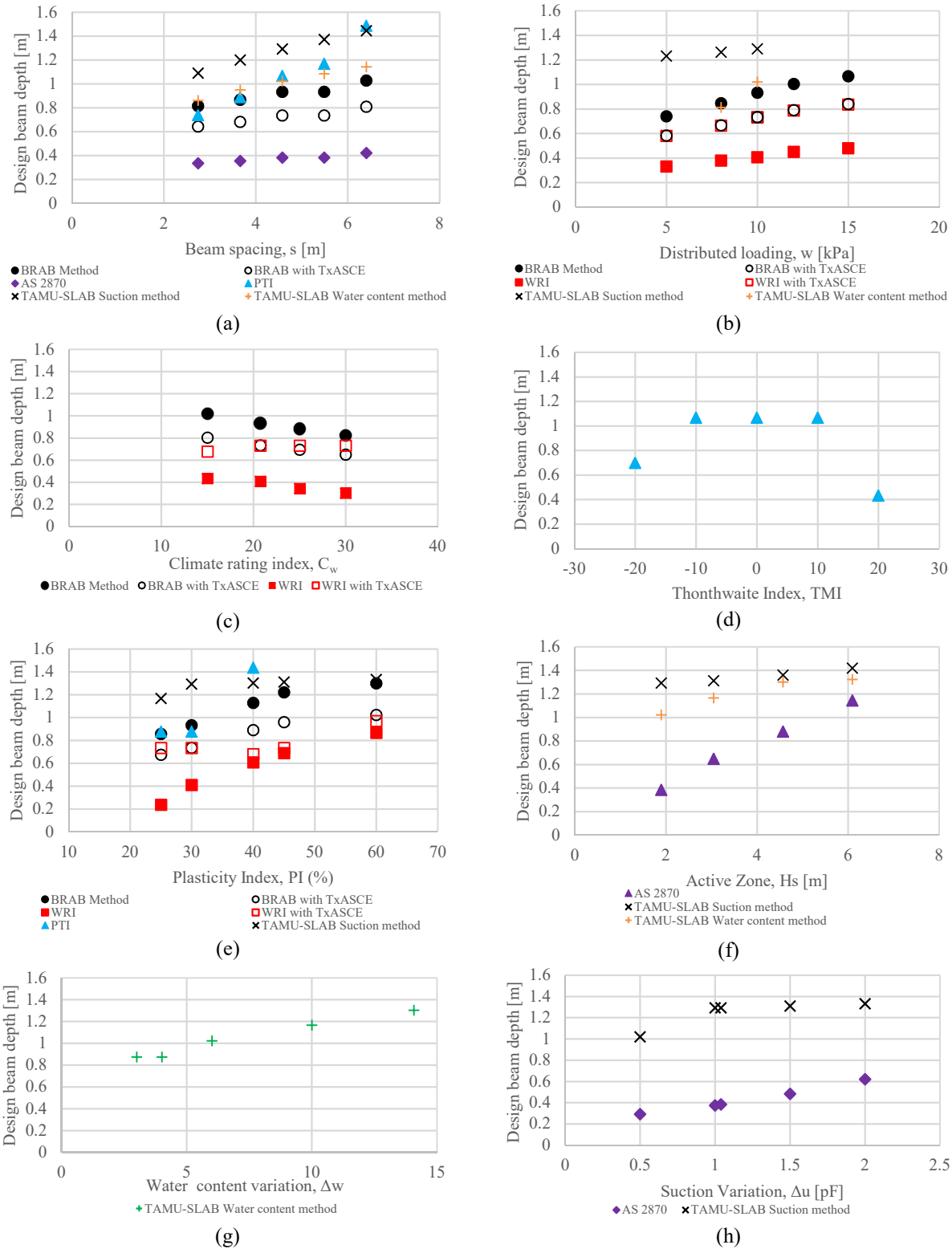

Figure 3.18 Sensitivity results of (a) beam spacing; (b) distributed loading; (c) climate rating index; (d) Thornthwaite Index; (e) Plasticity Index; (f) active zone; (g) water content variation change; (h) suction change

For each case, the calculations for all eight methods were conducted, and an average value for eight results is obtained. The same procedure for all 34 cases is calculated and plotted in Figure 3.19. This figure shows the beam depth predicted by each particular method on the vertical axis and the average prediction by all eight methods on the horizontal axis.

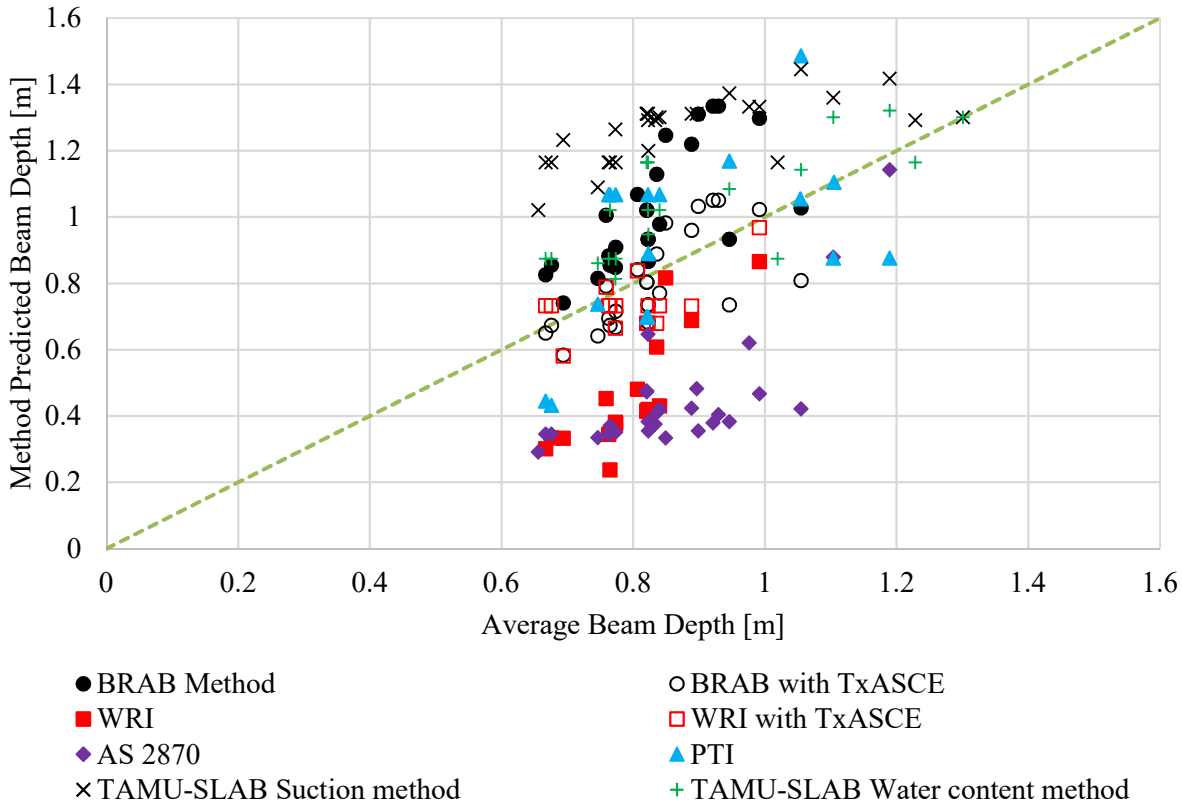

Figure 3.19 Synthetic cases calculation results

Figure 3.19 shows that the smallest beam depth is predicted by the AS 2870 method. The largest beam depth is predicted by the TAMU-SLAB suction method while the TAMU-SLAB water content method is somewhat conservative. The original BRAB method always gives beam depth that is larger than the average value, but the beam depth becomes close to the average when applying the TxASCE guidelines. The original WRI method tends to give beam depths that are smaller than the average, but the beam depth becomes closer to the average when applying the TxASCE guidelines. The beam depths calculated by the PTI method are very scattered; these scatters likely due to the complexity of the method and the potential for accumulated error with all the steps.

In general, the minimum average beam depth for all the synthetic cases is larger than 0.2m, and the maximum is 1.4m.

4. SOME COMMENTS ON THE EMPIRICAL METHODS

During the review and calculation of the empirical methods, some of the assumptions are not clearly stated. In this section, we summarized some findings during the revision of the design methods mentioned previously. Such as the original study of the design curve and other comments on the procedures.

4.1. Slab-on-Grade Methods

4.1.1. PTI method

The PTI method describes the ability of the soil to swell by using the suction compression index γ_h. This parameter is the change in volume due to a unit suction change. The concept that suction will induce volume change has been widely studied by many researchers (e.g. Alonso et al., 1990; Fredlund & Rahardjo, 1993). The PTI method relates the suction compression index value to the liquid limit and the plasticity index (Covar & Lytton, 2001), or by empirical relationships to soil swelling tests (section 2.1.4.1.1, M2, and M3). The PTI method considers that the suction compression index is different in swelling and in shrinkage as shown in Figure 4.1

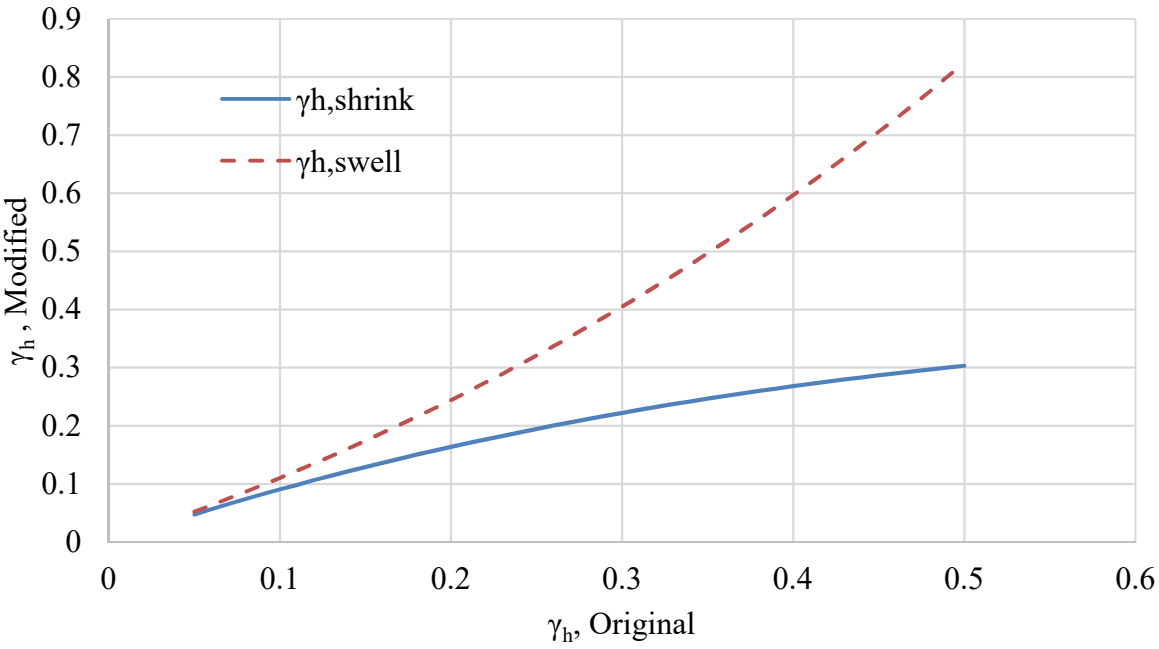

Figure 4.1 Difference between Suction Compression Indices

The PTI method also uses the unsaturated diffusion coefficient α. This coefficient is a function of the slope of the soil water retention curve, of the suction compression index and of how cracked the soil mass is. The diffusion process will occur differently during shrinkage and swelling due to hydraulic hysteresis.

Because the PTI method aims to calculate the soil movement in both shrinkage and swelling, it adopts the Thornthwaite moisture index to describe the average suction condition due to the local weather condition. The suction variation compared to the average suction indicates whether shrinkage or swelling will take place Although the original version of the Thornthwaite moisture index map was created in 1948 (Thornthwaite, 1948), a recent study (Olaiz et al., 2018) showed that there is not any significant variation of the TMI today compared to 1948. Thus, the use of the 1948 TMI map is still valid.

The PTI method calculates the soil movement (shrinkage + swelling) by using the suction change and the suction compression index. The PTI method also uses a concept called the stress change factor (SCF) to describe the difference between the highest and lowest suction and the equilibrium condition. The extreme suction value relies on on-site measurements, and the equilibrium suction is calculated by an empirical relationship (Figure 2.25). However, the low R^2 value for the correlation in Figure 31 indicates that the regression between equilibrium suction and TMI may not be very representative. The equilibrium suction, if possible, maybe replaced by site measurements over time.

4.1.2. AS 2870 method

The AS 2870 method is well accepted in Australia when dealing with the problem of shrink-swell soils. The method helps to estimate the soil movement (shrinkage + swelling) by using a parameter named the free shrinkage index or soil instability index, in volumetric strain per unit suction change (%/pF) measured by the AS 1289 method. At different depths, the instability index is used to account for the effect of cracking. Soils with cracks are considered unrestrained which leads to a lower vertical movement, while soil without cracks gives a larger movement.

The AS 2870 method also uses the Thornthwaite moisture index TMI, instead of determining the equilibrium suction as in the PTI method. The TMI value is used to estimate the depth of soil that needs to be considered (Table 2.2), also called the depth of the active zone. Because TMI describes the weather variation, a larger value of TMI indicates that the weather changes more significantly which leads to a deeper active zone.

4.2. Ground Surface Move

4.2.1. TxDOT-124-E method (PVR method)

The PVR method is mainly based on the work done by from McDowell (McDowell et al., 1956). It classifies the soil moisture condition as wet, dry and average based on empirical relationships to the liquid limit as shown in Eq. (4.1) and the empirical relationship presents in Figure 4.2

$$\begin{aligned} Wet &= 0.47LL + 2 \\ Dry &= 0.2LL + 9 \\ Average &= \left(Wet + Dry\right)/2 \end{aligned} \tag{4.1}$$

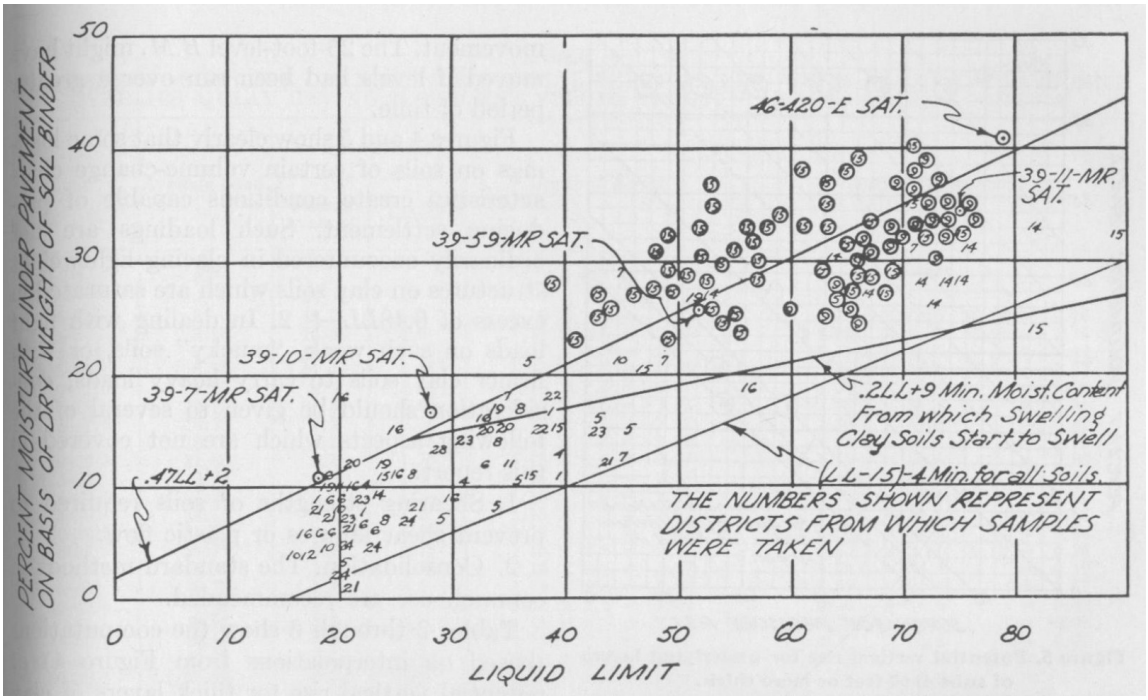

Figure 4.2 Moisture Data for Subgrade Soils under Pavement (McDowell et al., 1956)

In Figure 4.2, the dots are water content measurements for samples taken at various locations in TEXAS immediately beneath pavements. The numbers shown indicate the district in which the sample was taken. The three lines plotted in the figure are the lowest boundary line 0.4×(LL-15), start to swell line 0.2LL+9 and maximum capillary absorption line 0.47LL+2. No further information was provided in the paper on how the "start to swell" line and the "maximum capillary absorption" line were determined. The PVR method adopts the "start to swell" line (0.2LL+9) as the dry condition of the soil and the "maximum absorption" line (0.47LL+2) as the wet condition. No further explanations are given on the acceptance of these two lines and why the line 0.4×(LL-15) was not used. Furthermore, the 0.4×(LL-15) line and the 0.2LL+9 line are two lines referring to the lowest boundary of the data points, while 0.47LL+2 may be a regression line.

After the soil is classified as dry or wet, the PVR method relates the ability to swell to the plasticity index (Figure 2.27). The decision made to choose a water content classification line, as another parameter has a significant impact on the PVR result. For example, consider a soil sample with a PI = 50, the difference between the wet and the dry condition will be about 7% of percent volume change (Figure 4.3). Indeed, it is 8% for the wet condition and 15% for the dry condition. Figure 36 is a plot of the two-limiting equation for the moisture condition of the soil. The difference in water content between the wet and dry condition for the same PI of 50 is about 5% (Figure 4.4); indeed it is 19% for the dry condition and 25% for the wet condition. It is unlikely that the water content of the soil at a given site will be following these exact numbers.

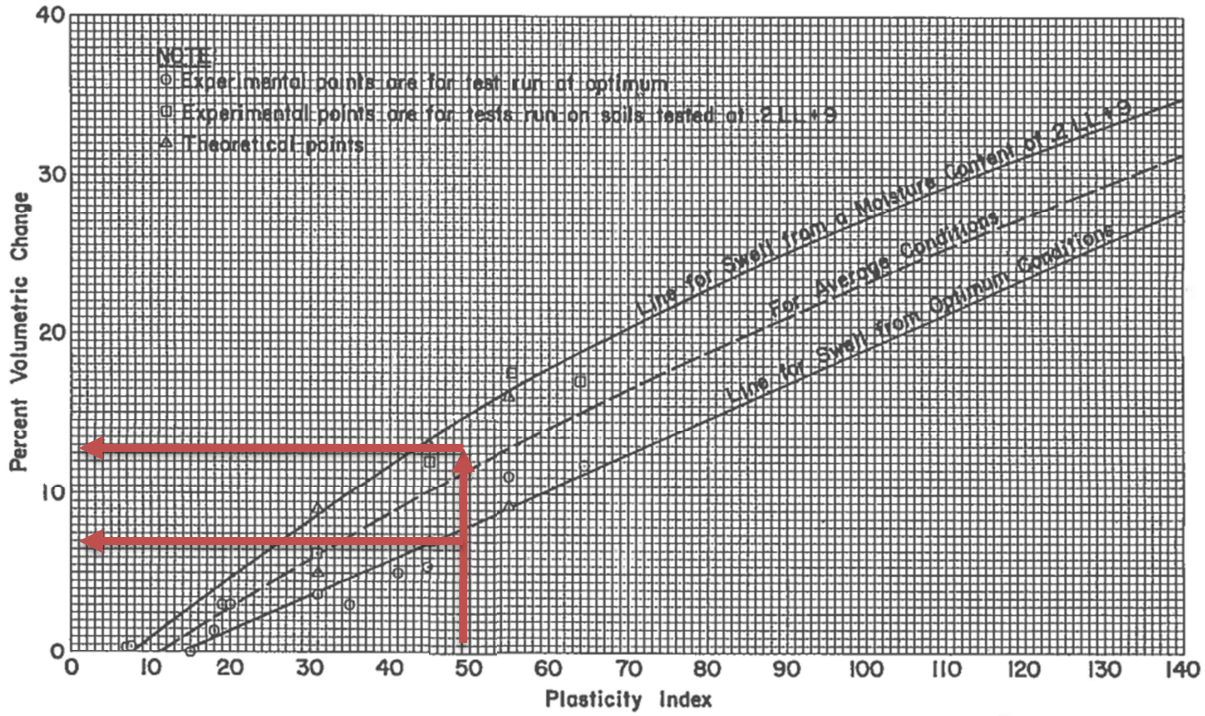

Figure 4.3 Different in Percent Volume Change for Dry or Wet Condition (TxDOT, 1995)

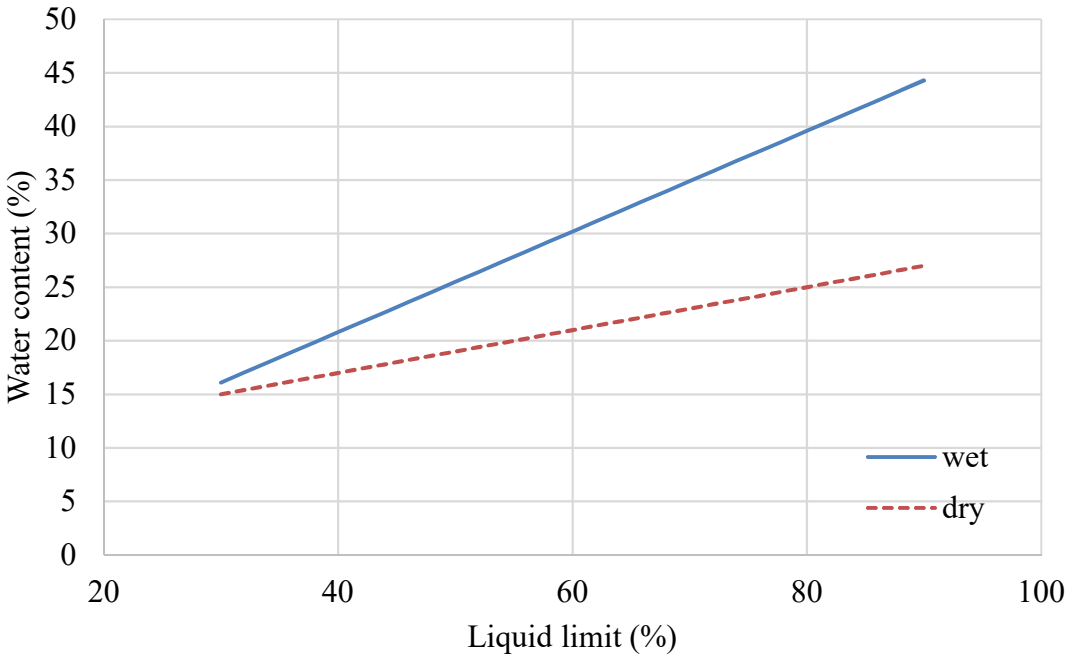

Figure 4.4 Difference between Wet and Dry Condition in Various Liquid Limit

The relationship between PI and percent volume change shown in Figure 4.3 is based on the analysis of the data shown in Figure 4.5. The data points in Figure 4.5 are from soil samples with different water content classification. Each point is determined by the PI value and the measured swell expressed as volumetric strain. The × symbols are for samples with an initial water content at "maximum capillary absorbed condition", then subjected to a swell test. The ⊗ represent samples swelling from the "dry" condition.

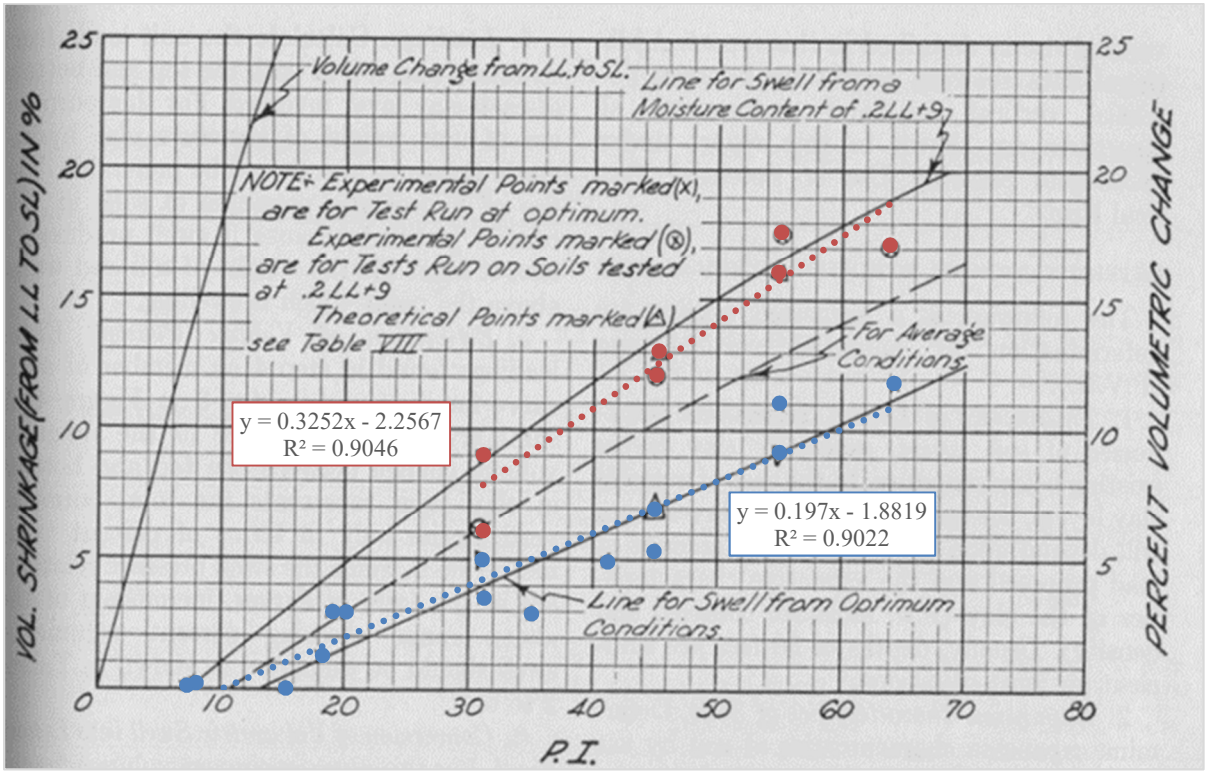

Figure 4.5 Comparison between the proposed curve and replotted curve for the Interrelationship between PI and volume change (Specimens subject to swelling under 1 psi surcharge) (McDowell et al., 1956)

Regression curves can be obtained through the orange dots in Figure 38 (wet line) and through the blue points (optimum water content in the compaction test). These regression curves can be overlapped with the curves from the paper; it shows that while the optimum water content line is close to the regression line, the wet line chosen by McDowell is somewhat conservative.

In the next step, the percent swell is corrected for the vertical stress level. Indeed, the plot in Figure 4.6 refers to free swell tests. The procedure for this correction is shown in Figure 4.7 which is based on Figure 4.6.

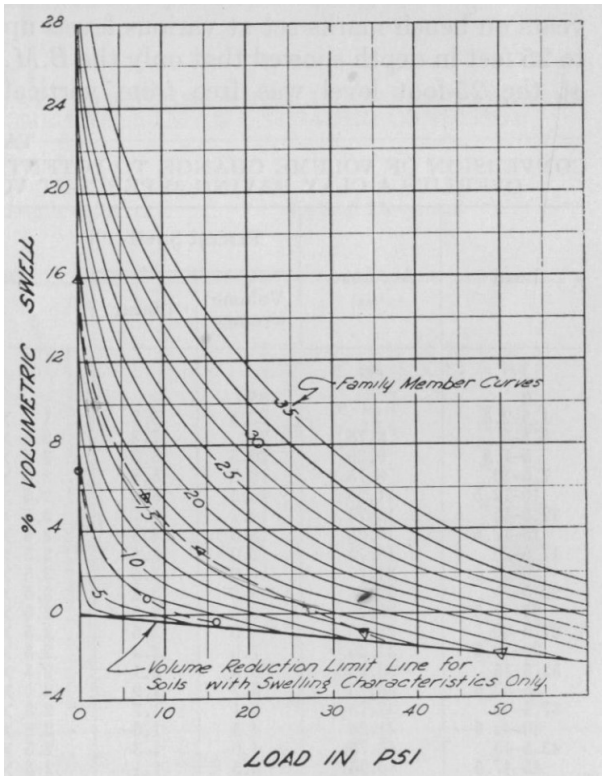

Figure 4.6 Relation of Load to Volume Change (McDowell et al., 1956)

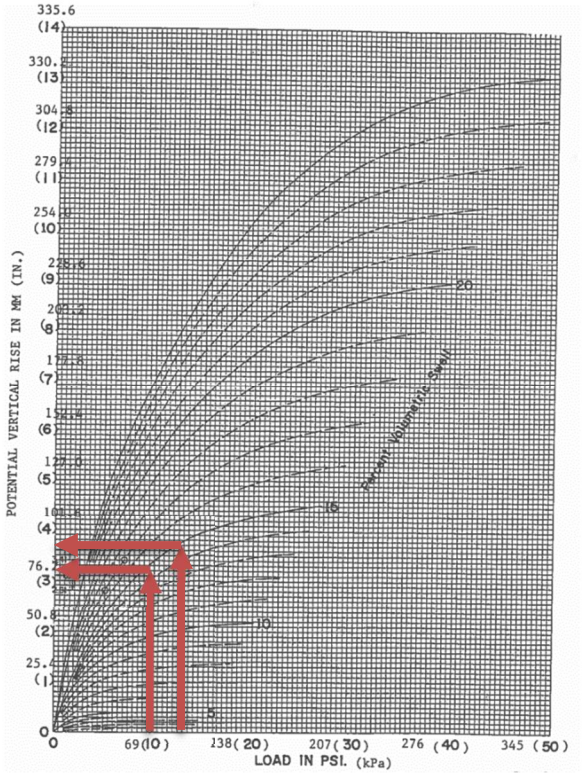

Figure 4.7 Amount of Swelling for Higher Loading (TxDOT, 1995)

Before using Figure 4.6, the amount of free swell is determined from Figure 4.5 based on the plasticity index of the soil. Then, the overburden stress is calculated and will reduce the amount of swelling. The swelling under load is found by using the "family member" curve (labeled by the percent free swell) and the corresponding overburden total stress. For example, the dashed line in Figure 39 shows the case of a sample with a free swell of 14% (volumetric strain). As mentioned previously, the soil within the depth of interested is subdivided into layers. Figure 4.7 which was prepared based on Figure 4.6 is then used to calculate the amount of swelling in millimeters and inches in parenthesis for each layer. This is done by using the vertical stress at the top and at the bottom of the layer and reading the curve as shown in Figure 4.7.

The method used to obtain Figure 4.6 is not clearly described in the original paper. Some data points are shown in the figure without a legend. This figure appears to be theoretically based; if so, the theory used is not described. This figure could also be based on consolidation tests, but this is not mentioned either.

Note that the amount of swelling is related to the percentage of particle finer than 425μm in the PVR method. The fewer particles are finer than 425μm, the less swelling there will be as confirmed by Al-Rawas and Goosen (Cojean, 2007).

4.2.2. Briaud et al's method

The Briaud et al's method is a method to estimate the soil movement based on the water content variation and it is not widely used yet. The relation between the water content variation and the volumetric strain as stated in e.q. (2.34) is an analogy to the well-known relation between stress and strain; in this way, the concept is much easier to accept by engineers.

The shrink-swell modulus proposed in this method shown in Figure 2.30 and e.q. (2.33)，and given by the ratio between the unit weight of water and the dry unit weight of the soil; it is easy to obtain and can be used to estimate the soil movement between the shrinkage limit and the swell limit This method provides a convenient and effective way to estimate the shrink-swell soil movement.

Within the depth where the soil has a low degree of saturation, the soil is below the shrinkage limit and thus theoretically does not shrink. Figure 2.31 points out that the range of water contents within which the soil can exist corresponds to the difference between the swell limit and the shrinkage limit. To obtain these two limits, a free swell test and free shrink test can be performed. The swell tests and the shrink tests can be performed under the site pressure to better simulate the realistic condition. Note that during the shrink test the soil is allowed to shrink in three directions while in the swell tests (consolidometer) the soil is laterally constrained.

5. THE DEPTH OF ACTIVE ZONE IN UNSATURATED SOIL PROBLEM

The depth of active zone is one of the critical parameters among the others in the shrink-swell soil problem, especially in the designation of foundation lying on the shrink-swell soil. Few methods have a clear definition of the depth that need to be consider, where this depth subjects to move as the environmental changing and usually refers as the depth of active zone. This section collects some of the descriptions of active zone, and based on a practical manner, a quantitatively definition of active zone is proposed.

5.1. Analogy Between Surface Movement and Settlement Problem

There is a direct analogy between calculating the settlement at the ground surface of a soil mass subjected to a mechanical load and calculating the shrink-swell movement at the ground surface of a soil mass losing and absorbing water (Figure 5.1). This analogy is presented in a two-column format with the left column being the mechanical loading procedure and the right column being the water induced movement procedure.

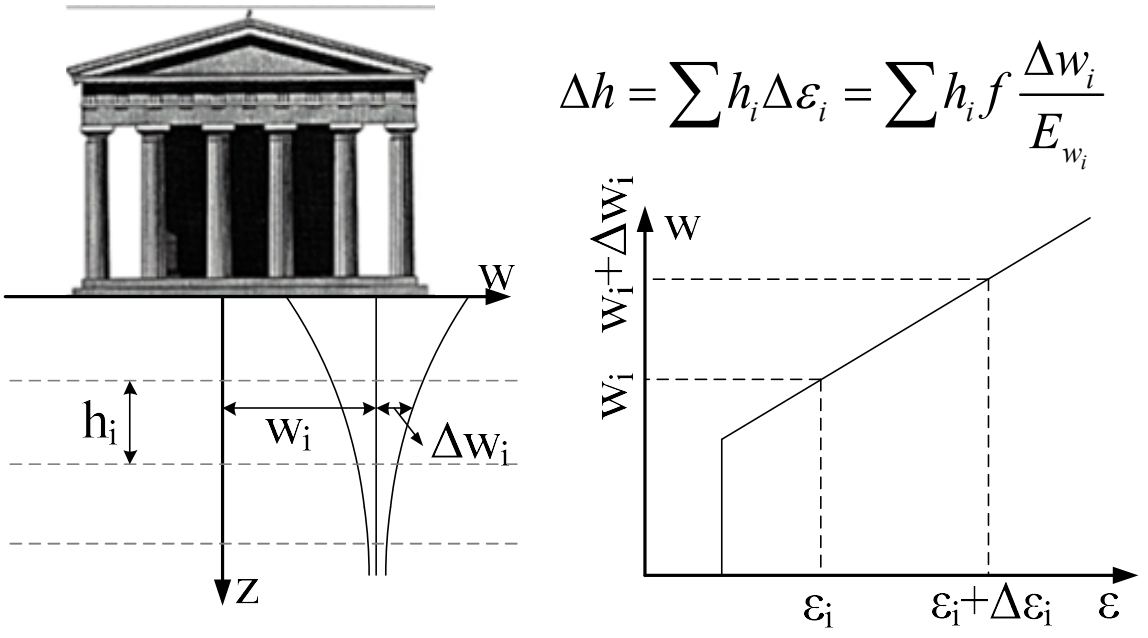

(a)

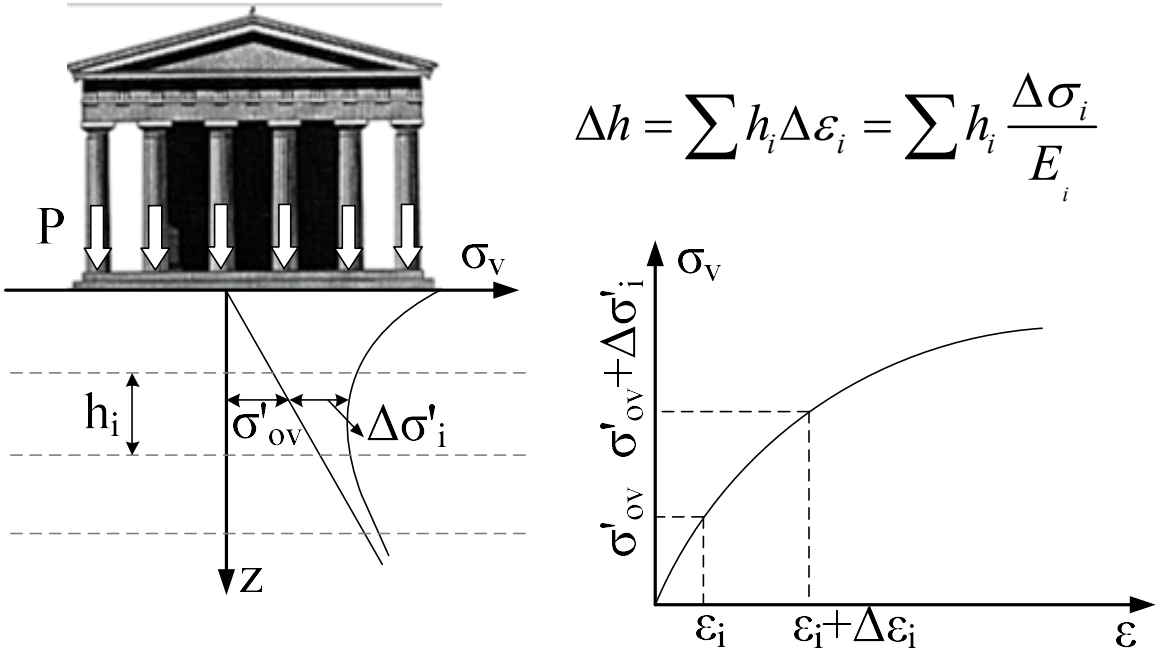

(b)

Figure 5.1 Analogy between calculating shrink-swell soil movement and calculating settlement under load (a) water content-strain method for shrink swell movement predictions (b) stress-strain method for settlement predictions (Briaud et al., 2003)

Procedure for a settlement problem

1. Determine the depth of influence, z_i (Figure 5.2)

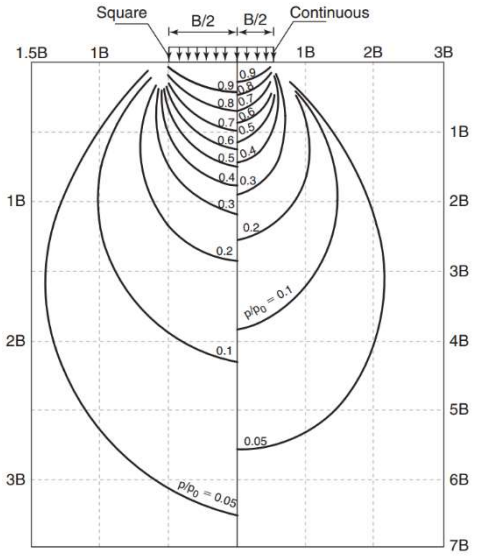

Figure 5.2 Influence Zone (Briaud, 2013)

2. Divide the depth of influence into an appropriate number of layers (n); each layer has a thickness H_i.
3. Before any load is applied, in the middle of each layer, calculate the vertical effective stress, σ'_{ovi}
4. In the middle of each layer, calculate the stress increment due to loading, $\Delta\sigma_{vi}$
5. In the middle of each layer, calculate the vertical effective stress a long time after the load has been applied, $\sigma'_{ovi} + \Delta\sigma_{vi}$
6. For each layer, select a stress-strain curve appropriate for the problem at hand (consolidation test, triaxial test, pressuremeter test, etc.)

Procedure for a shrink-swell movement problem

1. Determine the depth of the active zone, z_a (Figure 5.3)

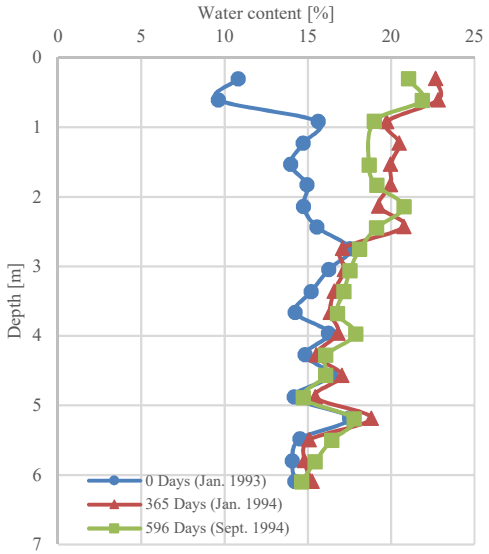

Figure 5.3 Active Zone (Nelson et al., 2001)

2. Divide the depth of the active zone into an appropriate number of layers (n): each layer has a thickness H_i.
3. Before any change in water content, obtain the water content, w_{oi} in the middle of each layer.
4. In the middle of each layer, determine the change in water content, either decrease (shrink) or increase (swell), Δw_i
5. In the middle of each layer, determine the water content after the change has occurred, $w_{oi} + \Delta w_i$
6. For each layer, select a water content-strain curve appropriate for the problem at hand (shrink test, swell test)

7. For each layer, obtain the strain ε_{bi} corresponding to the initial stress σ'_{ovi} from the stress-strain curve (e.g. Figure 5.4)

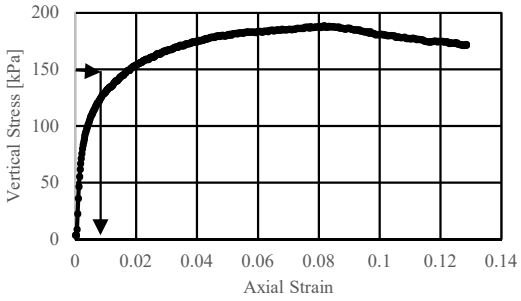

Figure 5.4 Stress-Strain Relationship of Soil

8. For each layer, obtain the strain ε_{ai} corresponding to the final stress $\sigma'_{ovi} + \Delta\sigma_{vi}$.

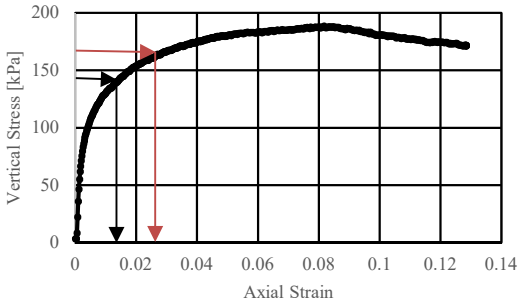

Figure 5.6 Determination of ε_{ai}

9. For each layer, calculate the compression of that layer ΔH_i, as

$$\Delta H_i = (\varepsilon_{ai} - \varepsilon_{bi}) H_i \qquad (5.1)$$

10. Calculate the settlement at the ground surface as

$$\Delta H = \sum_{i=1}^{n} \Delta H_i = \sum_{i=1}^{n} (\varepsilon_{ai} - \varepsilon_{bi}) H_i \qquad (5.3)$$

7. For each layer, obtain the strain ε_{bi} corresponding to the initial water content w_{oi} from the water content-strain curve (e.g. point E on Figure 5.5).

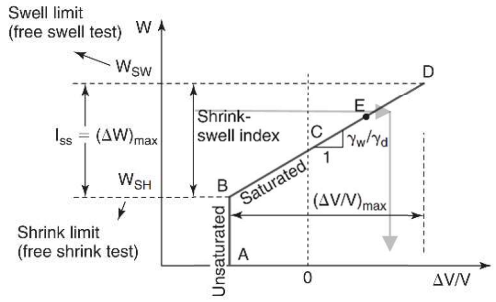

Figure 5.5 Water Content vs. Volumetric Strain (Briaud,2013)

8. For each layer, obtain the strain ε_{ai} corresponding to the final water content $w_{oi} + \Delta w_i$ from the water content-strain curve

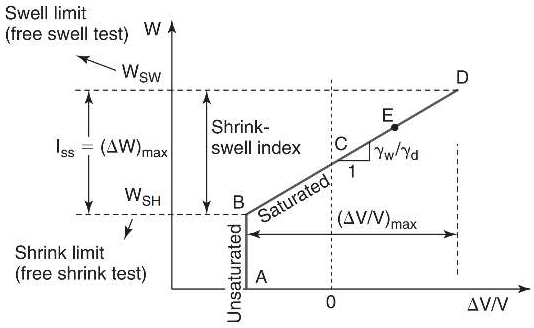

Figure 5.7 Determination of ε_{ai} (Briaud,2013)

9. For each layer, calculate the movement of that layer ΔH_i , as

$$\Delta H_i = (\varepsilon_{ai} - \varepsilon_{bi}) H_i \qquad (5.2)$$

10. Calculate the movement at the ground surface as

$$\Delta H = \sum_{i=1}^{n} \Delta H_i = \sum_{i=1}^{n} (\varepsilon_{ai} - \varepsilon_{bi}) H_i \qquad (5.4)$$

As can be seen in this comparison, the steps for both movement calculation methods are identical. The differences are listed below.

1. The depth of the zone of influence versus the depth of the active zone
2. The stress increase versus the change in water content
3. The stress-strain curve versus the water content-strain curve

The settlement calculation method is more advanced than the shrink-swell movement calculation method now. Indeed, solutions have been proposed and are well accepted for the depth of influence z_i and the stress increase with depth $\Delta\sigma_{vi}$ for the settlement method. By comparison, no well-accepted method exists to estimate the depth of the active zone z_a and the change in water content Δw_i for the shrink-swell movement calculation. The following sections aim to summarize knowledge on the depth of active zone, z_a, the water content variation, Δw_i, and the water content-strain curve. The comparison between settlement calculations and shrink-swell soil movement calculations is summarized in Figure 5.8.

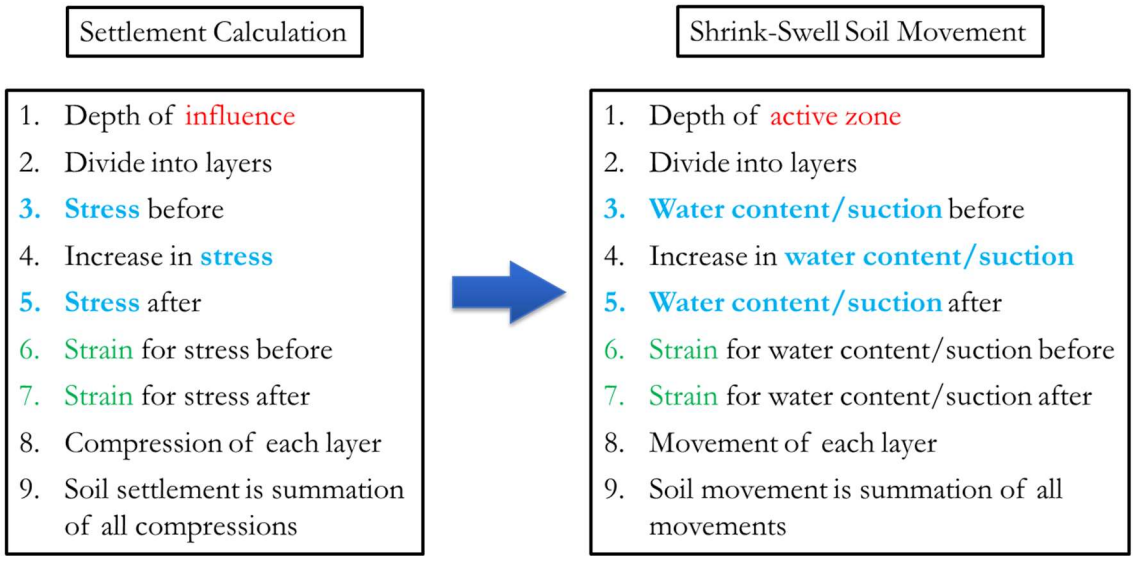

Figure 5.8 Analogy between settlement calculation and shrink-swell movement calculation

5.2. Soil Movement Calculation Relative to Analogy of Settlement Calculation

Among the four methods mentioned above, the PVR method only considers the swelling behavior, while the PTI method, AS 2870 and Briaud et. al.'s methods consider both shrinkage and swelling of the soil.

In order to quantify the soil movement, the PVR method relates it to the plasticity index, while the PTI method uses the suction compression index, the AS 2780 method uses the instability index, and the Briaud et. al.'s method uses the shrink-swell modulus.

The suction compression index is obtained by correlations to the liquid limit, plasticity index and the percentage of fine particles. The instability index adopted by AS 2870 is in %/pF; it describes the volume change vs suction change curve, which is similar to the concept of stiffness in settlement problems. The shrink-swell modulus adopted in Briaud et al's method describes the relationship between the change in water content and the associated volumetric strain. Unlike the PVR and PTI method, the soil instability index and the shrink-swell modulus are measured by laboratory testing.

The Thornthwaite moisture index (TMI) is adopted by the PTI method and AS 2870 method but plays a different role. The Thornthwaite moisture index adopted in PTI method is used to calculate the averaged/equilibrium suction condition for the region. The TMI describes the difference between precipitation and evaporation. With a positive value, the precipitation exceeds the evaporation thus implying a wet area. When TMI value is negative, there is more evaporation than precipitation, the area is much drier and has a larger average/equilibrium suction. Also, in the PTI method, the Thornthwaite moisture index is used to calculate the diffusion coefficient, leading to the edge moisture variation distance. In the design curve of Figure 2.24, the more extreme values

of the Thornthwaite index are, the more significant the change in weather conditions is between seasons, and the larger the edge moisture distance.

Similarly, the higher the diffusion coefficient, which implies that the soil can diffuse water more easily, the higher the edge moisture distance. However, PTI limits the maximum edge moisture to distance to 2.7m. There is no explanation for this limit. AS 2870 uses the Thornthwaite index empirically to determine the depth of the active zone. This relation was developed based on a study in Australia. Extrapolating to another country may be unwise.

All methods consider the depth of the active zone, but few of them provide recommendations. In the PVR method, the recommended values for the depth of the active zone from 4.5m to 6m or even the depth of the groundwater table. The PTI method also states, "calculate the suction compression index and other parameters up to 9ft." this may imply a depth of active zone of 2.7m (9ft). As for the AS 2870 method, the depth of the active zone is either measured by in situ testing or related to the weather condition through the use of the TMI. Briaud et al.'s method suggests the depth of the active zone follows the recommendation of local design experience. Typically, the depth of the active zone in College Station is 3m.

Recall Figure 5.8, the analogy provides a framework to solve the shrink-swell soil movement problem similar to the advanced problem of settlement calculation. The four methods discussed above can be grouped into the framework as they solve shrink-swell issues, as shown in follows.

5.2.1. PVR method

Procedure:

1. Does not specify the depth of active zone. Says "Sampling to a depth of 15 ft and as much as 20 ft", may imply that the depth of active zone is more than 15 ft
2. Preferable to use 2 ft thick layers to divide the active depth
3. Determine the water content, liquid limit and plasticity index for each soil layer
4. Empirically calculate dry (0.2LL+9), wet (0.47LL+2) and average ([dry+wet]/2) moisture content of the soil. Compare the natural moisture content to dry, wet, and average condition to decide which one applies.

Shrink-Swell Soil Movement

1. Depth of active zone
2. Break into layers
3. **Water content/~~suction~~** before
4. Increase in **water content/~~suction~~**
5. **Water content/~~suction~~** after
6. Strain for water content/suction before
7. Strain for water content/suction after
8. Movement of each layer
9. Soil movement is summation of all movements

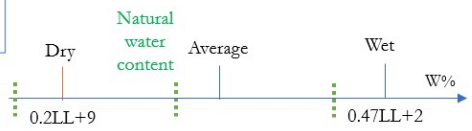

PVR approach

5. Graphically determine the percent volume change based on the PI and the chosen water content condition (wet/dry/average from previous step). This % volume change is the free swell maximum value.

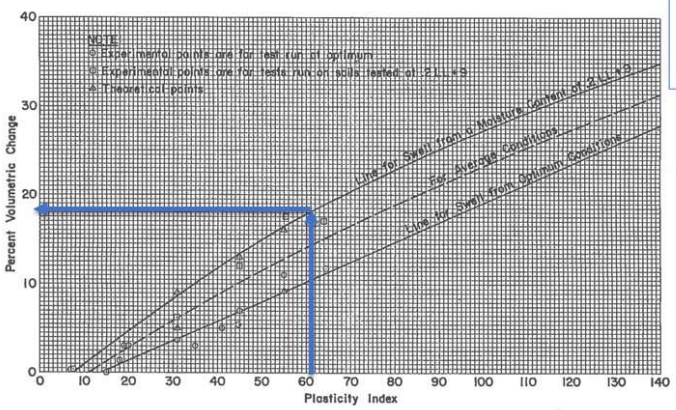

Shrink-Swell Soil Movement

1. Depth of active zone
2. Break into layers
3. **Water content/~~suction~~** before
4. Increase in **water content/~~suction~~**
5. **Water content/~~suction~~** after
6. Strain for water content/suction before
7. Strain for water content/suction after
8. Movement of each layer
9. Soil movement is summation of all movements

5.2.2. PTI method

Procedure:

1. No recommendations for depth of active zone. It says "Calculate the averaged suction compression index and other parameters down to 9 ft or more".
2. Divide total soil profile into top, middle and bottom.
3. Use Thornthwaite index to determine the equilibrium suction for the location
4. Determine the suction variation. Typically from 2.5pF to 4.5pF
5. Determine suction compression index, γ_h by Atterberg limits, particle distribution or other recommended methods
6. Determine stress change factor (SCF) based on equilibrium suction and suction variation

Shrink-Swell Soil Movement

1. Depth of active zone
2. Break into layers
3. ~~Water content/~~suction before
4. Increase in ~~water content/~~suction
5. ~~Water content/~~suction after
6. Strain for water content/suction before
7. Strain for water content/suction after
8. Movement of each layer
9. Soil movement is summation of all movements

7. No calculations made for each layer. By assuming that a constant suction is reached at a depth of 9 ft and a suction compression index variation of no more than 10%, the soil movement is directly calculated based on the γ_h and SCF values from the previous step as

$$y_m = SCF \times \gamma_h$$

Otherwise software VOLFLO is required

Shrink-Swell Soil Movement

1. Depth of active zone
2. Break into layers
3. ~~Water content/~~suction before
4. Increase in ~~water content/~~suction
5. ~~Water content/~~suction after
6. Strain for water content/suction before
7. Strain for water content/suction after
8. Movement of each layer
9. Soil movement is summation of all movements

y_m	Ground surface movement, in inch
SCF	Stress change factor
γ_h	Suction compression index

5.2.3. AS 2870 method

Procedure:

1. Determination of active zone is correlated with the Thornthwaite index (TMI)

TMI	H_s (m)
10 to 40	1.5
-5 to 10	1.8
-15 to -5	2.3
-25 to -15	3.0
-40 to -25	4.0
40	> 4.0

Shrink-Swell Soil Movement

1. Depth of active zone
2. Break into layers
3. Water content/suction before
4. Increase in water content/suction
5. Water content/suction after
6. Strain for water content/suction before
7. Strain for water content/suction after
8. Movement of each layer
9. Soil movement is summation of all movements

2. Divide soil into sublayers, 1m or 1ft is preferred
3. No recommendation. Determine the suction variation for each sublayer
4. Determine the soil instability index I_{pt} by swelling test for each sublayer
5. Calculate the soil movement in each layer ΔH in mm or in

$$\Delta H = \frac{1}{100}\int_0^{H_s} I_{pt}\Delta u \Delta h$$

ΔH	Ground surface movement, mm
H_s	The depth of interested, also refers as depth of active zone, mm
I_{pt}	Instability index of soil, %/pF
Δu	Suction change at certain depth, pF
Δh	Thickness of interested, mm

Shrink-Swell Soil Movement

1. Depth of active zone
2. Break into layers
3. ~~Water content~~/suction before
4. Increase in ~~water content~~/suction
5. ~~Water content~~/suction after
6. Strain for water content/suction before
7. Strain for water content/suction after
8. Movement of each layer
9. Soil movement is summation of all movements

6. Summation of soil movement of each soil element

5.2.4. Briaud et. al.'s method

Procedure:

1. Determine the depth of active zone by local data based or other methods
2. Divide the soil profile into layers
3. Determine the initial water content

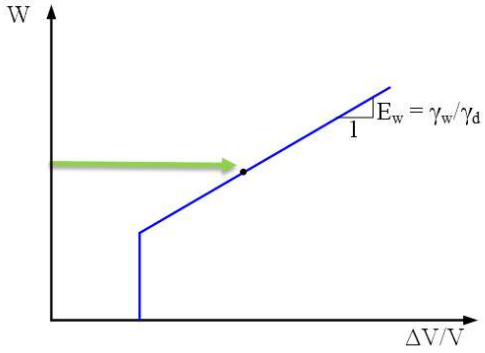

Shrink-Swell Soil Movement

1. Depth of active zone
2. Break into layers
3. **Water content/~~suction~~** before
4. Increase in **water content/~~suction~~**
5. **Water content/~~suction~~** after
6. Strain for water content/suction before
7. Strain for water content/suction after
8. Movement of each layer
9. Soil movement is summation of all movements

4. Determine the water content variation, e.g. $\Delta w_{1,2}$
5. Determine the strain variation based on water content variation
6. Movement for each layer is calculated

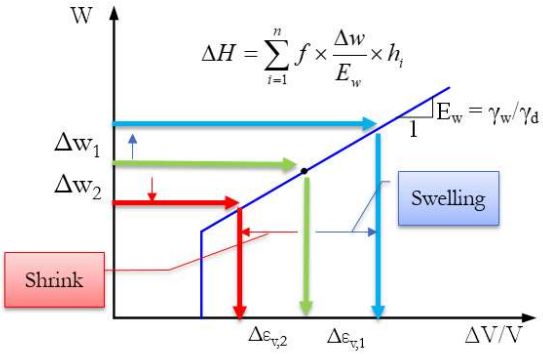

Shrink-Swell Soil Movement

1. Depth of active zone
2. Break into layers
3. **Water content/~~suction~~** before
4. Increase in **water content/~~suction~~**
5. **Water content/~~suction~~** after
6. Strain for water content/suction before
7. Strain for water content/suction after
8. Movement of each layer
9. Soil movement is summation of all movements

7. Sum the soil movement of all layers

5.3. Definition of The Depth of The Active Zone

Numerous definitions of the depth of the active zone (DAZ) have been discussed in past decades. Nelson (Nelson et al., 1994) points out that the active zone is a depth that will vary with time. He further defines the active zone as the depth within which the vertical stress is equal or smaller than the swelling pressure (Nelson et al., 1998). This definition only considers the effect of swelling. In 2001, Nelson (Nelson et al., 2001) described some of the relative concepts of different types of the active zone. (1) active zone is the zone of soil contribute to the soil heaving at any time. (2) zone of seasonal moisture fluctuation is the zone where water content changes due to weather conditions. (3) depth of wetting is the zone of soil will be wetting by human factors. (4) depth of potential heave is the depth where the swelling pressure of soil equals to the overburden pressure. Others point out that the potential for swelling or shrinkage depends on the current water content (Briaud et al., 2003) or suction in the soil (Alonso et al., 1990). In conclusion, the active zone defined by the amount of movement (movement active zone) is the depth of soil directly contributing to the swelling or shrinkage of the ground surface (Figure 5.9). It should be emphasized that the soil movement will behave both swelling and shrinking. Definition on the movement active zone solely considering swelling only requires more attention.

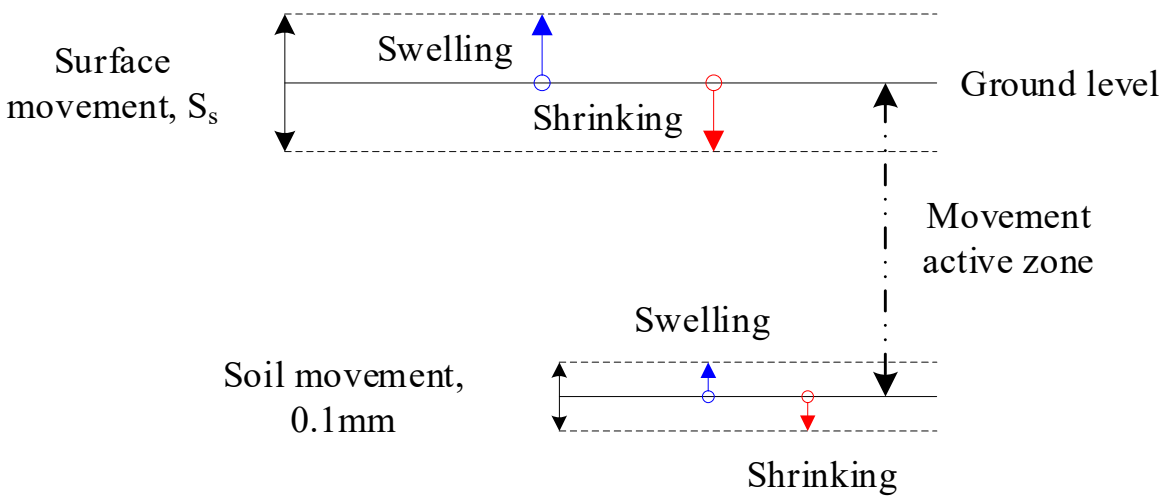

Figure 5.9 Schematic of movement active zone

Durkee (Durkee, 2000) discussed the depth of seasonal moisture fluctuation defined as the depth within which the water content changes due to the climatic conditions. Nelson mentions the depth of water content variation due to an external source such as irrigation, seepage from ponding or ditches, or even broken water pipe. In general, there is three types of active zone in the real problem: 1) the potential active zone, 2) the design active zone and 3) The actual active zone.

The potential active zone is the deepest active zone among three concepts. The potential active zone is the depth where the water content or suction has a tremendously small variation. As the environment of soil interested soil had changed, e.g. sunny to rainy or inversely, and because the soil is a porous medium, the variation of the water content or the suction induced by environmental changing will penetrate into the soil. Such variation will potentially induce the soil movement. Thus, the depth where will potentially move is defined as the potential active zone.

The actual active zone is similar to the potential active zone but limited by certain conditions such as the depth of phreatic level, leaking pipeline, underground structures (tunnel). Such conditions physically limit the penetration of the water content/suction penetrates the soil to reach the depth of potential active zone. The actual active zone describes the limits of water content/suction variation under in-situ condition.

The design active zone is not deeper than the actual active zone. The design active zone, as it described, is the depth where the soil water content/suction or movement meet a certain criterion required by design process. For example, if a typical foundation focus on the movement not larger than 10mm and such movement variation is measured at a depth of 10m, while the depth of real active zone may reach to a depth of 20m and the potential active zone may as deep as 30m, soil improvement only needs to consider the depth of the first 10m to eliminate the damage of the shrink-swell soil.

All three types of active zone can be defined by three criterion, water content variation, suction variation and the movement variation. The depth considering water content variation within the soil mass called the **water content active zone** Figure 5.10 presents a typical potential water content active zone. The suction within the soil is correlated with the water content by using the soil water retention curve (van Genuchten, 1980). The **suction active zone** is not as popular as the water content active zone because of the difficulty in suction measurement compared to water content measurements. However, because the suction value correlates with the stress state directly, it is more popular among the academic area.

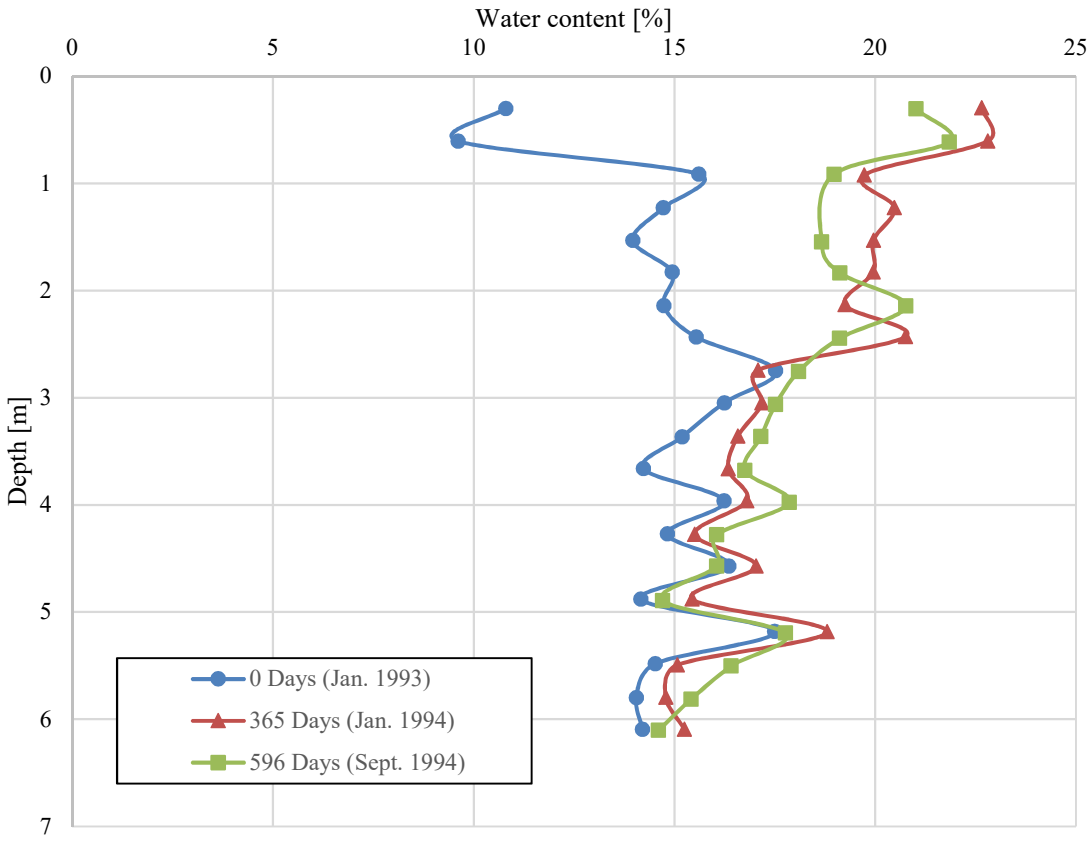

Figure 5.10 Water content active zone (Nelson et al., 2001)

In the settlement calculation problem, the zone of influence is related to the stress increment due to surcharge loading versus depth. It is defined as the depth where the increase in stress is equal to 10% of the increase in stress at the foundation level. In the shrink-swell soil movement problem, the **movement active zone** is the depth over which the soil movement, including both swelling and shrinking, meets a certain criterion. The estimation of movement active zone is not as advance as the depth of the zone of influence and not as straight forward as the water content/suction variation criterion. The development of the movement active zone will be discussed in following sections. Figure 5.11 presents a summary of different types of active

zone. In this work, we will mainly discuss the potential suction active zone and design movement active zone.

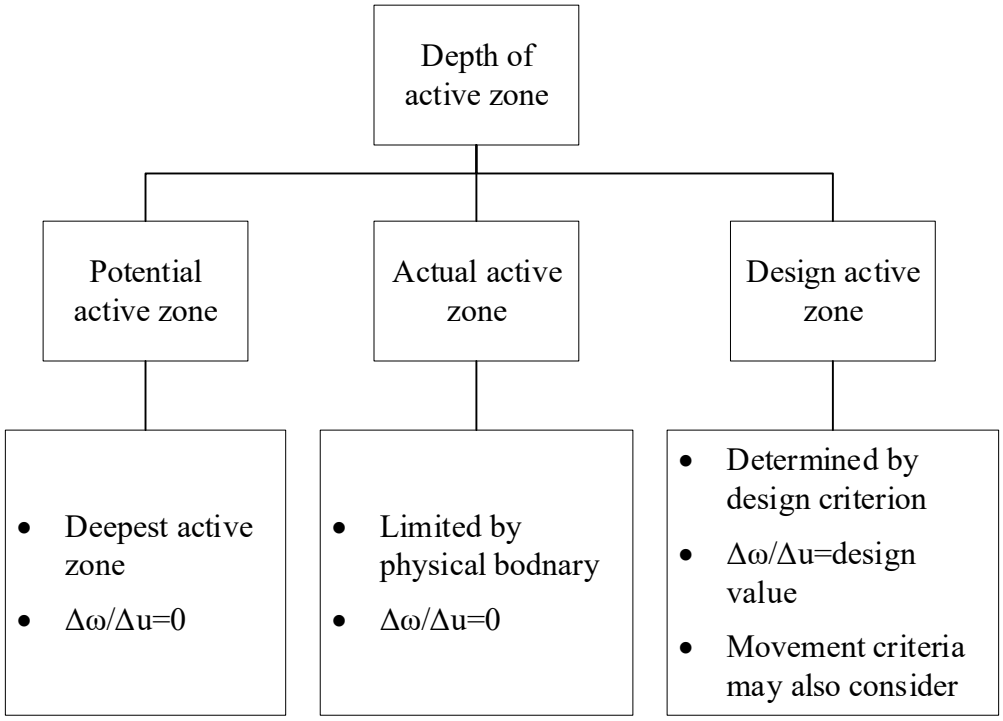

Figure 5.11 Different types of active zone

The most common way to determine the water content active zone z_a has been through the local experience with values often ranging between 3 and 6m (10 and 20 ft). However, the depth z_a can be much deeper than that, in some cases, with reported values as deep as 30m (100 ft) (Blight, 1997; Nelson et al., 2001). Some factors to consider in determining z_a include the depth of the water table (upper bound), the depth to which samples retrieved in the summer months are fissured (lower bound), and the stratigraphy. Lytton (Lytton, 1994) also suggests considering z_a as the depth 2 ft below the deepest recorded root fibers, as well as the depth where the suction

becomes equal to the equilibrium suction (PTI, 2004) according to the weather conditions (Thornthwaite Moisture Index, TMI). Determining the depth of the active zone is a problem involving several soil properties such as permeability, shrink-swell modulus or instability index, and the weather conditions.

The quantitatively definition of the active zone is also important during the discussion and in the particle manner as well. As the depth of active zone is determined by the measurement devices during the SI process, the accuracy of measurement devices can be used as an important reference for the criterion.

The WP4 and tensiometer are two major devices that use to measure the suction in the soil body. Typically, the WP4 has an error of around 100 kPa (Decagon Devices, 2007). The tensiometer, based on different brand and quality, has an error range from 10~1000 kPa. Thus, reasonable value to quantitatively define the active zone based on a suction criterion is a variation of 10kPa. Meanwhile, the soil movement at different depth is measured by extensometer. According to ISO 18674-3 (ISO, 2017), the error for the extensometer should be within 0.1mm. Thus, the depth of active zone based on soil movement is defined as the depth where soil movement variation is 0.1 mm.

Another criterion often adopted in the industry is considering a certain amount of the movement compared to the surface. In this work, by refereeing the zone of influence, the depth where the shrink-swell soil movement equals to 10% of the surface movement considered as the depth of active zone. The advantage of this criterion will be discussed in the following section, as it normalizes the amount of the surface movement. Table 5.1 summarizes the criteria for the active zone determination adopted in this work. However, the values can be modified in the future accordingly.

Table 5.1 Criterion to define the depth of the active zone

Active zone based	Characteristic value
Suction	10 kPa
$Movement_{-0.1mm\ based}$	0.1mm
$Movement_{-10\%\ based}$	10% of surface movement

6. EMPIRICAL METHOD TO THE SHRINK-SWELL SOIL

The swelling potential (SP) and swelling pressure (P_s) are two key factors in the shrink-swell soil problem. The swelling potential was found to correlate with the type of clay mineral, Atterberg limits, dry density, solid practical distribution (Nelson & Miller, 1997; Schneider & Poor, 1974; Seed et al., 1962; Vijayvergiya & Ghazzaly, 1973). among all influence parameters, the mineral of clay believes to be the most significant one (Komornik & David, 1969). As for the swelling pressure, researchers also correlate the pressure value with the physical parameters mentioned above (Komornik & David, 1969). Estimation methods help the designer to evaluate the amount of soil movement and how strong the soil will push by using fundamental soil parameters. However, the dataset adopted to establish the correlation between the swelling potential/pressure usually concentrate in one region. Thus, a regional effect of the regression may happen and the estimation method may not be applied in other region.

By collecting swelling test data worldwide, we proposed an empirical equation to estimate the swelling pressure with physical soil properties. The proposed equation eliminates the regional effect by adopting no constant. We also used the collected dataset to evaluate some of the current classification methods and try to figure out the bias behind the methods.

6.1. Dataset Organization

We collected 454 pairs of shrink-swell soil testing results from the literature to organize the dataset. The test results covered the region of Ankara, Turkey (Kayabali & Yaldiz, 2014), Barranquilla, Colombia (Cantillo et al., 2017), Texas, USA (Viyayvergiya & Sullivan, 1973; Wang et al., 2016), and a wide range of the Middle East (Komornik & David, 1969). As the Atterberg limit and the dry unit weight are two main factors in literature that relative to the swelling pressure,

Figure 6.1 presents the distribution of swelling pressure along with dry unit weight and plasticity index. This figure points out that the swelling pressure is positively correlative in an exponential way with the dry unit weight and plasticity index. Figure 6.2 presents the swelling pressure distribution overlapping by the Atterberg limit curves, which shows the data are mostly located in MH/OH zone, and especially, the high swelling pressure data are in the MH zone.

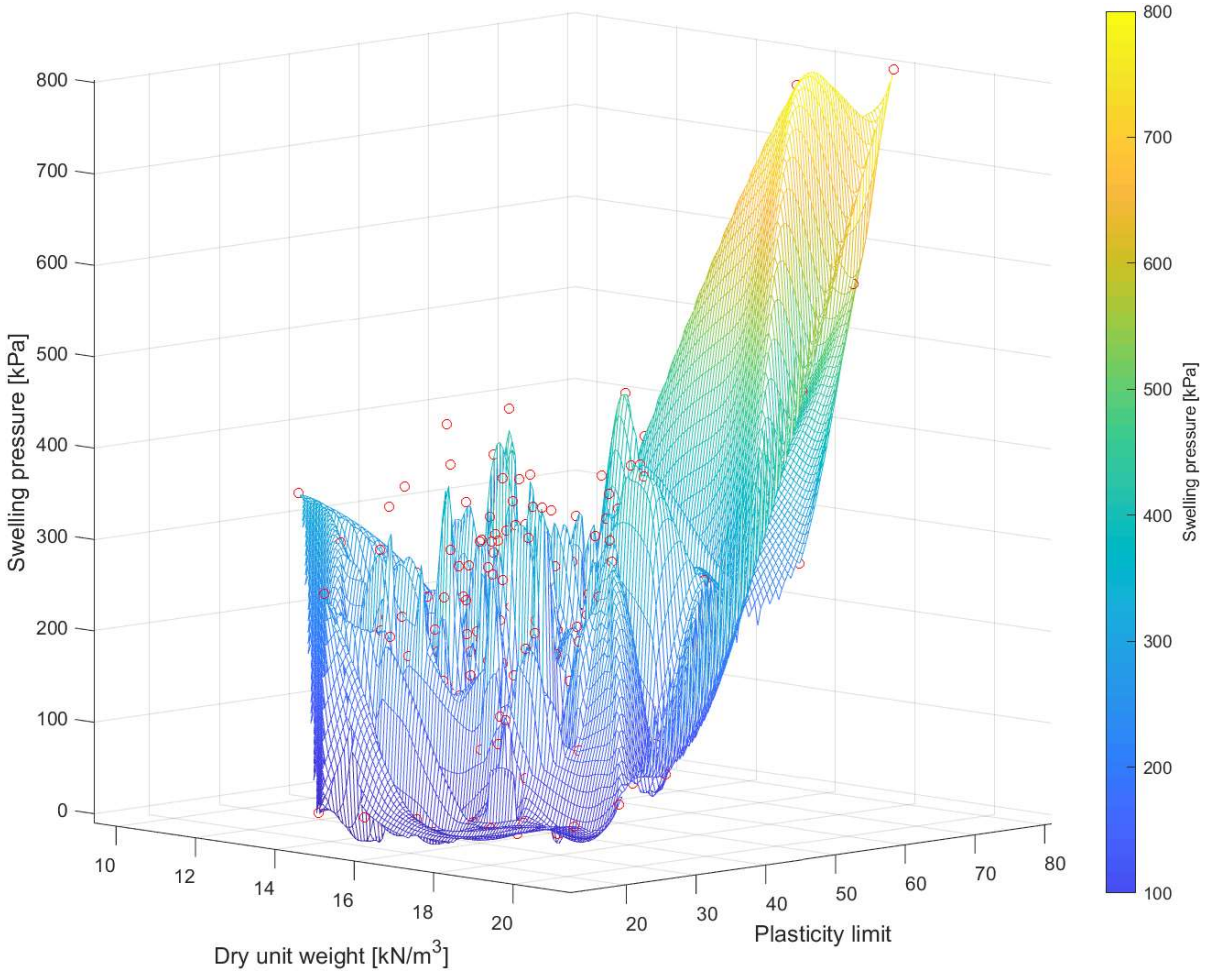

Figure 6.1 Swelling pressure vs. dry unit weight and plasticity index

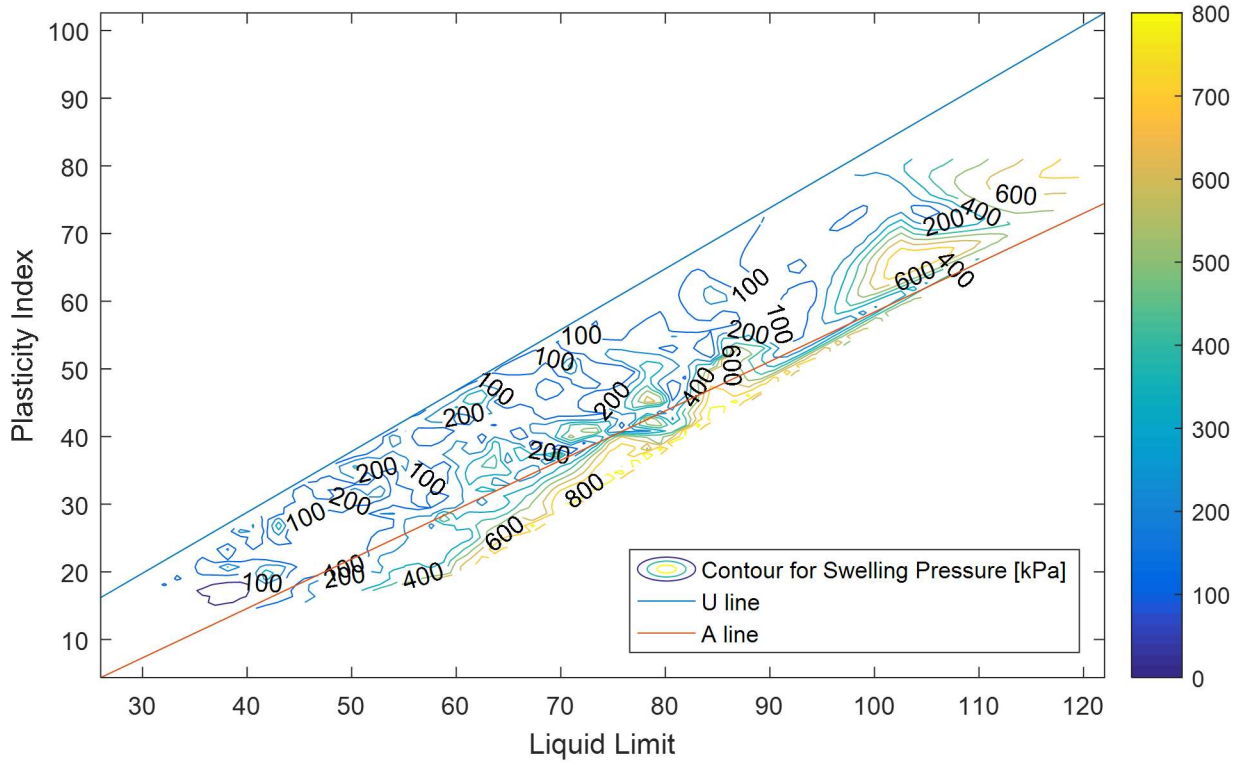

Figure 6.2 Swelling pressure contour based on Atterberg limit chart

As a proper estimation of the swelling pressure and potential can greatly benefit the industry, researchers had been working on the empirical correlation between the swelling potential/swelling pressure and the engineering parameters (Çimen et al., 2012; Tu & Vanapalli, 2016). The swelling potential and swelling pressure can analogize the elongation and the force of the spring. Even though the reaction force of spring needs to consider the type of metal used, there is a direct relationship between the strain and force. Among the dataset collected, 163 pairs of data provide the value for both swelling pressure and swelling potential. These data are presented in Figure 6.3, which implies a clear linear relationship between the swelling potential and the

swelling pressure. Although the simple correlation does not consider the different component of soil, it provides a rough estimation for the designer to have a primary judgement.

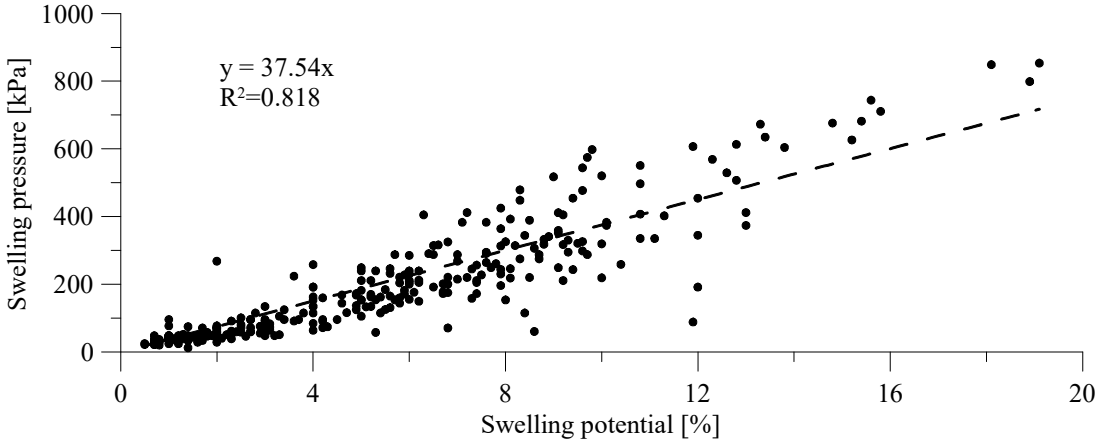

Figure 6.3 Relationship between swelling potential and swelling pressure

As the 454 pairs of data contain the measurement of swelling pressure, in the following section, we will reevaluate some of the empirical methods estimating the swelling pressure and propose a new empirical method with physical meaning to predict the swelling pressure.

6.2. A New Empirical Method to Estimate Swelling Pressure

Not only how much soil will move the foundation, but also how strong it will push upward is vital during the foundation design. Thus, the swelling pressure is also an essential factor that needs to consider in the shrink-swell soil problem. Some of the researchers' analogy the swelling pressure to the preconsolidation pressure in the settlement problem (Fredlund et al., 2012) and use the ratio between overlaying pressure and swelling pressure to estimate the soil movement. Also, the swelling pressure is essential in predicting the depth of movement active zone. Shuai (Shuai,

1998) summarized there are two categories of testing for the swelling pressure: 1) the constant stress test, such as Chinese standard and ASTM D4546, where the swelling pressure defined as the stress required to compress a free swell soil to its original shape in an odometer. 2) the constant volume test includes a constant volume odometer and strain control test, and the swelling pressure defined as the stable pressure measured. Shuai recommended the constant volume test between these two as which does not affect by volume change and easy to operate.

As the test to obtain the swelling pressure is time-consuming. Researchers had spent a great effort to develop a simple method to estimate the swelling pressure (P_s) by practical engineering parameters. Such parameters as but not limit to initial water content, Atterberg limits, dry density. Some of the well-accepted methods are summarized in Table 6.1. In the table, it can be seen that the empirical methods are usually in a linear format, which is different from the dataset collected. And the coefficients of the parameters are difficult to explain in a physical manner.]

Table 6.1 Empirical methods found in the literature

No.	Equation	Note	Author
1	$\log(P_s)=-2.1+0.021LL+0.00067r_d-0.027\omega_i$	P_s in kgf/cm^2 ρ_d in kg/m^3	(Komornik & David, 1969)
2	$\text{Log } P_s=2.55(\gamma_d/\gamma_w)-1.705$	P_s in kPa	(Dedier, 1973)
3	$P_s=2.39LL-108.04$	P_s in kPa	(Abiddin Erguler & Ulusay, 2003)
4	$P_s=-3.72+0.0111PI+2.077\ \rho_{dry}+0.244$ logs ($P_s<=100$kPa) $P_s=-16.31+0.033PI+8.253\ \rho_{dry}+0.829$ logs ($100<P_s<=3500$kPa)	γ_d in g/cm^3 s is suction in bar	(Erzin, 2004; Erzin & Erol, 2007)
5	$P_s=-30.8\omega_i+1025\rho_d+6.35LL+42.4PL-2208$	P_s in kPa ρ_d in kg/m^3	(Kayabali & Yaldiz, 2014)
6	$\ln(P_s)=7.77-0.12w+0.0054PI$	P_s in kPa	(Cantillo et al., 2017)

By reviewing the swelling test data Figure 6.1, the relationship between the swelling pressure, plasticity index, and dry unit weight may be described exponentially. We propose a new empirical equation to estimate the value of swelling pressure based on the reviewed dataset as e.q.(6.1)

$$P_s = \exp\left(\frac{\gamma_{dry}}{\gamma_{water}}\right) \times PI^{\frac{LL-\omega_i}{PI}} \tag{6.1}$$

By comparing the proposed empirical equation with other methods found in literature, the primary benefit is that the new equation has a much clearer physical meaning behind. The dry density and the plasticity index are positively correlated to the swelling pressure. The term (LL-ω_i/PI) describes the ratio of the soil water content from the current value to the liquid limit, which is the range of water content that can help to develop the full swelling pressure. This term can also be described as 1-I_L, where I_L is the liquidity index.

$$P_s = \exp\left(\frac{\gamma_{dry}}{\gamma_{water}}\right) \times PI^{\frac{1-I_L}{PI}} \tag{6.2}$$

The activity A_c is a factor that usually use to describe the shrink-swell soil (Seed et al., 1962) and estimate the swelling pressure or swelling potential (Skempton, 1953; Van Der Merwe, 1964). By definition, the activity is defined as PI over percent finer than 2μm, and a higher activity soil implies a more significant movement. In general, a soil with high PI values usually means high shrink-swell behavior. On the other hand, a smaller percentage of fine particle also increase the value of activity. As a smaller particle has a larger specific surface area compared to large particle, samples consist with small particles trend to have stronger attraction with water, and thus will behave a stronger movement compare to samples with large particles. This conclusion may

conflict with the general description of activity to the shrink-swell soil, though we do not consider the activity in the correlation equation.

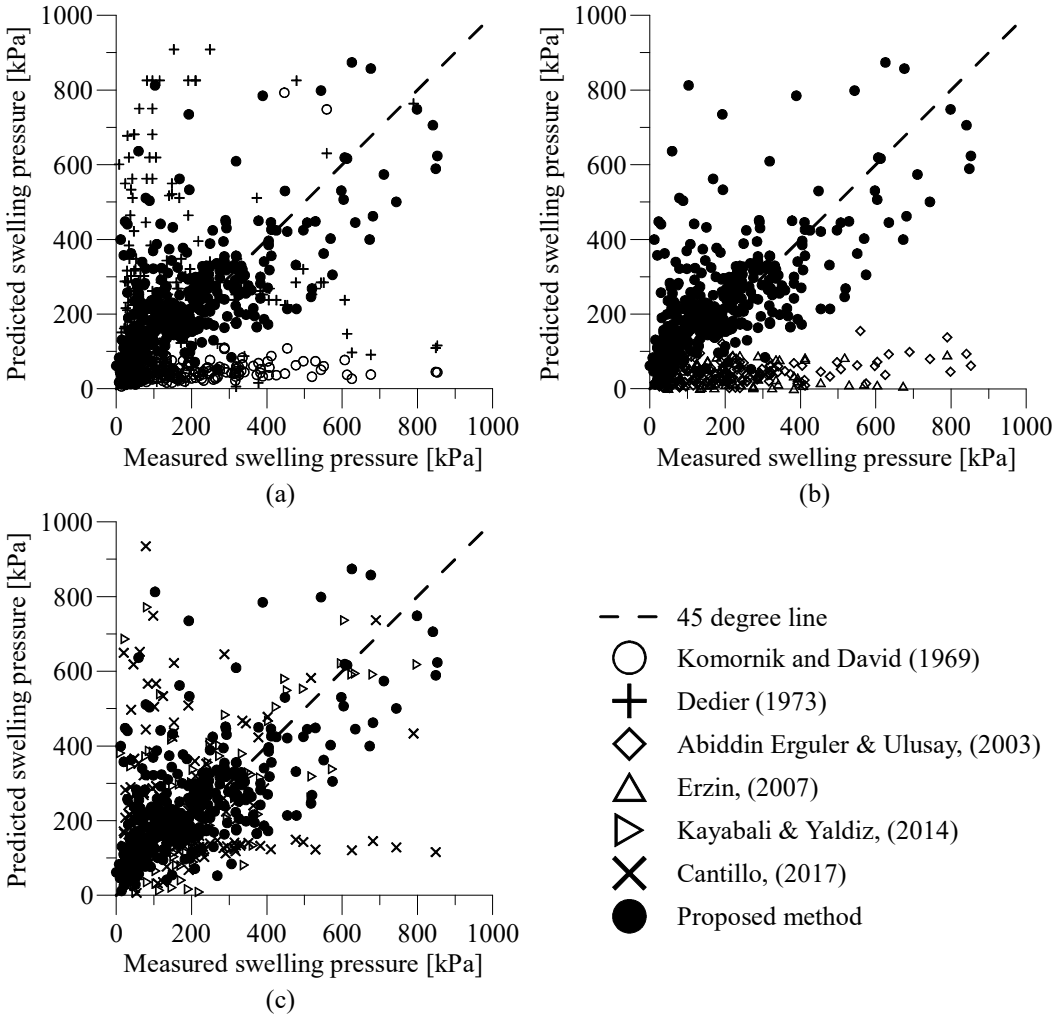

Figure 6.4 Proposed estimated method vs. methods in the literature

Figure 6.4 presents the comparison between swelling pressure predicted by the proposed methods and methods found in the literature. Figure 6.4 (a) is the comparison among the proposed method, Komornik & David's method (Komornik & David, 1969), and Dedier's method (Dedier,

1973). Both two literature methods failed to have a good estimation when swelling pressure reach to a high value, i.e., 300kPa. Similarly, Figure 6.4 (b) points out that the Erzin's method (Erzin & Erol, 2007) predicts well in the low range of swelling pressure and Abiddin Erguler & Ulusay's method (Abiddin Erguler & Ulusay, 2003) underestimates the pressure. In Figure 6.4 (c), both Kayabali & Yaldiz's method (Kayabali & Yaldiz, 2014) and Cantillo's method (Cantillo et al., 2017) predicts swelling pressure well agreed with the measured values but the Cantillo's method has larger variation compared to Kayabali & Yaldiz's method. To quantifiably describe the accuracy of the prediction, the statistical loss function defined as e.q.(6.3) is adopted. Methods with a smaller loss value represent a better. The results of the methods mentioned above are presented in Table 6.2. It should be pointed out that Kayabali & Yaldiz's method will predict negative swelling pressure value; thus, the accuracy is significantly reduced. According to the result, the proposed method provides a relatively good estimation among all empirical equations.

$$L = \frac{\sum \sqrt{\left(\text{Predicted value-Measured value}\right)^2}}{No.\ case} \tag{6.3}$$

A prediction method with a smaller loss value implies a more accuracy prediction than others. The results of loss for the methods mentioned above are presented in Table 6.2. Referring to Figure 6.4, the Dedier's method gives tremendous variation compared to the testing result, while the Komomik & David method generally underestimate the swelling pressure but gives a relatively better estimation of the results. The result from Abiddin Erguler & Ulusay's method is similar to the ones from Komornik & David's method. the Kaybali & Yaldiz's and Cantillo's methods follow the trend of the measurement for the swelling pressure under 400kPa. However, as the swelling pressure increased, the predictions have larger diversity from the measured values. At this point, the proposed method catches the 45-degree line, with the minimum loss value among the methods.

Table 6.2 Comparison of loss between different models

Methods	Loss
Komornik & David's method	133.4
Dedier's method	394.7
Abiddin Erguler & Ulusay's method	147.6
Erzin's method	169.3
Kayabali & Yaldiz's method	177.6
Cantillo's method	178.7
The proposed method $_{(min)}$	**93.00**

6.3. A Review of Classification method of Shrink-Swell Soil

A Proper classification can enhance the estimation of the behavior of the shrink-swell soil. Typically, the swelling potential alone is always adopted as a criterion for classification, while some methods use the Atterberg limits as classification criteria to simplify the process. However, these two different based classification methods categorize the shrink-swell soil into the same levels, which sometimes will bring misunderstanding in stating the behavior of the soil behavior. Meanwhile, the swelling pressure sometimes also needs to be considered during a design process, but very few of the classification mentioned how to classify the soil with swelling pressure. In this section, we will compare and discuss the relationship between some of the well-adopted classification methods.

6.3.1. Swelling potential criterion

The first swelling potential test may date back to 1957 (Jennings & Knight, 1957), where swelling potential clearly defines as the percentage of swell under 1-psi surcharge for a sample compacted at optimum water content in standard compaction test (Seed et al., 1962). Such tests usually conducted in an odometer cell to observe the 1-D movement behavior by controlling the environmental conditions, which are the environmental humidity (sample suction is essential) (e.g. (Dhowian, 1992; Lawrence D. Johnson, 1977; Lawrence D. Johnson & McAnear, 1973; McKeen & Nielsen, 1978)); or water content in a sample (e.g. (Briaud et al., 2003)). Detail testing procedure may refer to the literature correspondingly.

Based on the results of the test mentioned above, the soil is then classified into different categories. Seed (Seed et al., 1962) classifies the soil into low, medium, high, and very high swelling potential, as shown in Table 6.3. The Bureau of Reclamation, United States Department of the Interior (USBR), had proposed a similar category but with a different amount in swelling, as shown in Table 6.4. The ASTM D4829 (ASTM, 2019) also has a similar way of classification but using the expansion index (EI) as e.q.(6.4), where ΔH in mm is the change in height in a swelling test, and H_i in mm is the initial sample height, the category is presented as Table 6.5. Because the EI value is the 1000 times of the axial strain, where usually 100 time is adopted, the modified EI value, which is defined as 1/10 of the EI value, describes the amount of swelling in percentage is adopted and then the ASTM method can be compared to others. Chen (Chen, 1975) has proposed a classification based on practical experience shown in Table 6.6. Typically, the overlapping in medium and high categories indicates the uncertainty in practical estimation.

$$EI = \frac{\Delta H}{H_i} \times 1000 \tag{6.4}$$

Table 6.3 Seed's classification (Seed et al., 1962)

Degree of expansion	Swelling potential [%]
Low	0 to 1.5
Medium	1.5 to 5
High	5 to 25
Very high	>25

Table 6.4 USBR's classification (USBR, 1998)

Degree of expansion	Total swelling [%] From air dry to saturated condition
Low	0 to 10
Medium	10 to 20
High	20 to 35
Very high	>35

Table 6.5 ASTM's classification (ASTM, 2019)

Potential Expansion	Expansion index, EI	EI modified
Very low	0 to 20	0 to 2
Low	21 to 50	2.1 to 5
Medium	51 to 90	5.1 to 9
High	91 to 130	9.1 to 13
Very high	>130	>13

Table 6.6 Chen's classification (Chen, 1975)

Degree of expansion	Probable expansion, percent total volume change
Low	<10
Medium	10 to 30
High	20 to 30
Very high	>30

Besides the difference in the amount of swelling potential, different restrictions are adopted on the initial condition of the sample, which has some disagreement from the definition by Seed, where the OMC of the sample is required (Seed et al., 1962). The USBR classification restricts the

initial and final condition of the sample as a possible driest and fully saturated state. Such a limitation can cover the maximum movement of the testing sample. Similarly, the ASTM method considers the sample movement from 50% of saturation to fully saturated. Although Chen's classifications do not specify the initial condition, it is worth believing that the samples are subjected to be in the in-situ state before testing. The Seed's classification method defines the soil in different degrees of expansion in an exponential incremental way such that the very high category covers a larger range than its low category. As the USBR classification are measuring the full range of soil movement; however, considering the soil, the total swelling reaches 35% classified as "high." In contrast, other methods, e.g., ASTM method, for initial saturation of 50% to fully saturated with 13% swelling classified high potential, the USBR method value is considered optimistic to the soil movement behavior. Compare to the division value of the category, the Seed's method, the USBR method are both in an exponential distribution.

In contrast, the ASTM method has a much more linear gradient compared to these two methods, and Chen's method does not behave a clear relationship due to its conservative purpose. However, the ASTM method is also optimistic about the soil movement estimation, similar to the USBR method compared to Seed's method. As for Chen's classification, a wide range of "very high" expansion implies the conservative consideration from a practical aspect.

6.3.2. Soil properties criterion

As the swelling test is time-consuming to classify the shrink-swell soil, an alternative option to conduct such work by using the results from the traditional tests, e.g., Atterberg limit test. Briaud (Briaud, 2013) adopts the shrink-swell index I_{ss}, which is the water content difference between maximum swelling and shrinking states of the soil (Figure 6.5), and the range is stated in Table 6.7. Chen (Chen, 1975) also proposed the classification by laboratory results and in-situ test factors in Table 6.8

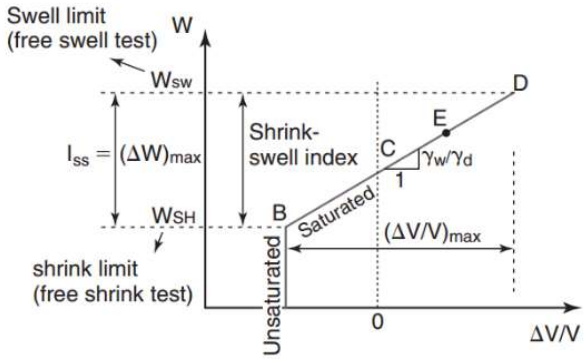

Figure 6.5 Definition of the shrink-swell index (Briaud, 2013)

Table 6.7 Briaud's classification (Briaud, 2013)

Potential Expansion	I_{ss}
Low	<20%
Moderate	20 to 40
High	40 to 60
Very High	>60%

Table 6.8 Chen's classification (PI and LL) (Chen, 1975)

Degree of expansion	Laboratory and field data			
	Plasticity index	Percentage passing No. 200 sieve	Liquid limit, percent	Standard penetration resistance, blows/ft
Low	0 to 15	<30	<30	<10
Medium	10 to 35	30 to 60	30 to 40	10 to 20
High	20 to 55	60 to 95	40 to 60	20 to 30
Very high	35 and above	>95	>60	>30

It needs to point out that although Briaud's method uses the value relative to soil movement, the value of the shrink-swell index is defined by the difference between two water content, and its value is closed to the plasticity index of soil. Thus, this classification method belongs to the group based on soil properties criterion.

As the classification method classify the shrink-swell soil into same category but by various criterion, it still worth to evaluate the agreement among the methods. In the following section, by using the dataset collected, we investigate the consistency of the classification methods mentioned above.

We apply the classification methods on the dataset collected and the result is presented in Table 6.9.

Table 6.9 Classification result based on methods found in the literature

	Seed	USBR	ASTM	Chen (SP)	Briaud	Chen (LL&PI)
Low	0	358	213	358	24	3
Medium	213	94	122	94	267	53
High	241	2	79	2	145	223
Extreme high	0	0	40	0	18	175

In Table 6.9, although all methods classified the shrink-swell soil into swelling potential as the same categories, i.e. low, medium high and extreme high, the result of classification has significantly different among methods due to the different criteria. In another word, if a site is classified as medium by ASTM method, the SSS might have a swelling potential up to 9%. If report this ASTM classification result to the designer who uses the USBR method, the design then subjected to a swelling potential up to 20%.

By comparing some of the well-adopted classification methods, it is concluded that there is a large difference among the classification results, and one of the important reasons is that there is not a comprehensive description of the swelling behavior of the shrink-swell soil. A standard classification method, such as the Unified soil classification system (USCS), can provide some basic information, such as the percentage of clay or sand particles, the range of Atterberg limit, when a soil sample had been classified. Because the shrink-swell soil problem is a worldwide challenge, it would be a tremendous contribution to have a representative method to deliver the swelling potential and swelling pressure information when it presents a classification result. However, such a method required a standardized testing procedure and data contribution worldwide. We will reserve this idea for future studies.

7. ACTIVE ZONE DETERMINATION VIA NUMERICAL METHOD

By adopting the numerical tools, it is then possible to investigate the influence of soil parameters on the entire soil behavior, to explore the shrink-swell soil behavior under different scenarios consist of other environmental condition; and to study the remedial solution of the shrink-swell soil problem in a long term behavior.

Based on the discussion in the previous section, it is evident that the shrink-swell soil problem, especially the determination of the depth of the active zone is important and complex as the mechanical and hydraulic problems are strongly coupling. In this section, the hydro-mechanical coupling numerical model is adopted to determine the depth of the active zone and further discuss one of the remedial solutions of the shrink-swell soil problem. In the following part, we will present the numerical process to determine the depth of the active zone. We then will show how the numerical tool assists in providing a remedial solution to reduce the shrink-swell soil movement.

It should be noticed that in the dry and hot environment, cracks may form on the light depth of soil mass and increase the depth of active zone significantly. However, in this work, the influence of crack is not considered. As the simulation of the formation of the cracks requires other special numerical methods.

7.1. Primary Sensitivity analysis

As mentioned in section 2, the empirical methods are interested in the environmental conditions, typically the precipitation for the region, the soil permeability of the soil, and other factors. Further, Lytton (Lytton, 1999) mentioned the groundwater level would also affect the determination of active zone. In this work, the sensitivity analysis in this work will focus on the weather condition and the permeability. The impact of the water table will be discussed in later sections.

7.1.1. Soil properties calibration

As the shrink-swell soil damage is one of the critical engineering problems in Texas, the soil properties in a study conducted in College Station, Texas (Wang et al., 2016), is chosen as the benchmark for calibration. Wang's research included the basic soil parameters and properties of the retention curve (Figure 7.1). The swelling pressure equals to 200 kPa with the initial water content of 21%. The van Genuchten model (van Genuchten, 1980) is adopted to describe the relationship between the degree of saturation and the corresponding suction and well match with the laboratory measurement, as shown in Figure 7.1.

To calibrate the parameters, a model simulating the unit cell developed swelling pressure is established. The swelling pressure development is presented in Figure 7.2, which allows the swelling pressure to be fully developed in nearly two days. The final calibrated parameters are shown in Table 7.1.

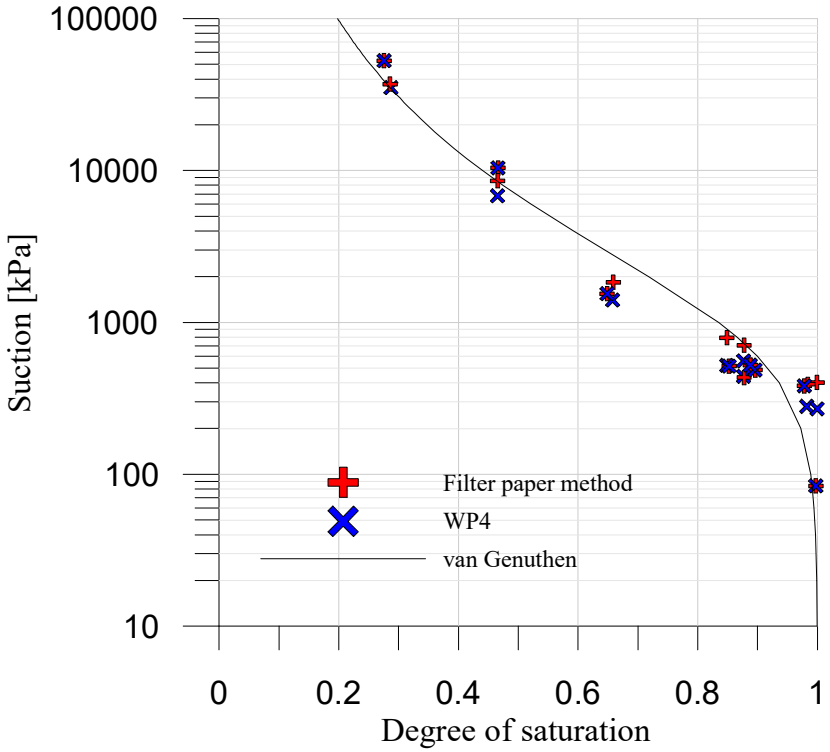

Figure 7.1 Determination of retention curve

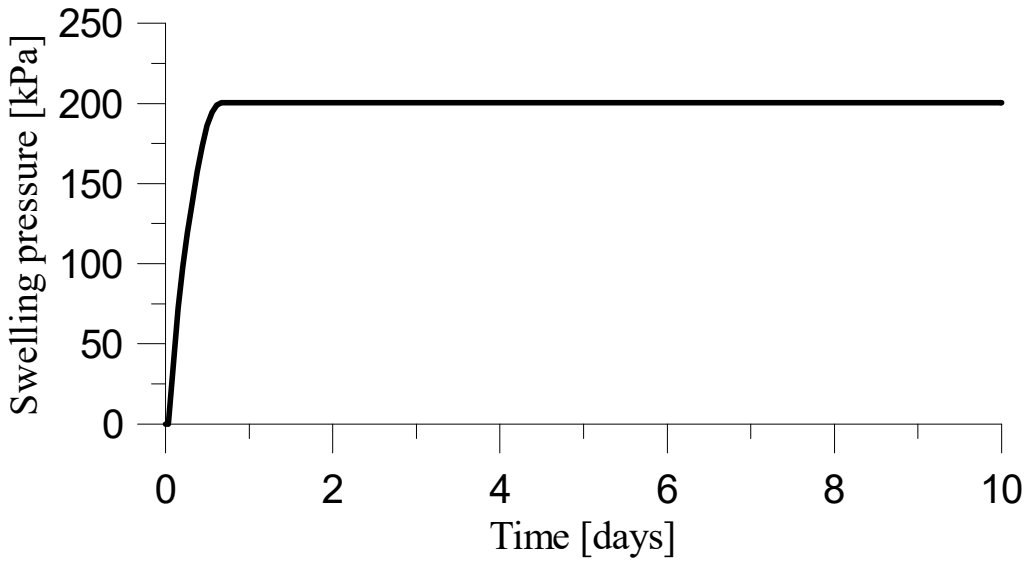

Figure 7.2 Swelling test data

Table 7.1 Calibrated soil parameters

	Parameter	Value
Basic parameters	Porosity	0.435
	Permeability [m/s]	7.34×10^{-10}
	Liquid limit	65
	Plasticity index	42
Retention curve (van Genuchten)	Air entry value [kPa]	1000
	Slope of the retention curve	0.26
BBM parameters	κ_{i0}	0.3
	κ_{s0}	0.1
	α_{ss}	0.88

7.1.2. Model establishment for sensitivity analysis

Figure 7.3 is a 50m by 25m model mesh for the sensitivity analysis of the active zone with a capillary effect presented. According to the information from the city of College Station, the water table varies between 3m to 12m (10 ft to 40 ft), and the average value will be about 16 ft (5m). Mechanical boundaries for two sides of the model allows the vertical movement and fully restrained at the bottom. At the top of the model is the flux boundary, where the suction from the atmosphere is applied. With the different values of suction, the hydraulic gradient will change the flow of water (flux) within soil mass and the permeability is the key parameter during this process. Meanwhile, the mechanical behavior also varies due to the changing of the suction follow by the constitutive model and the formulation is presented in

Table 2.7. As the permeability will be updated during each time step during the simulation, Figure 7.4 presents the schematic of the permeability calculation loop.

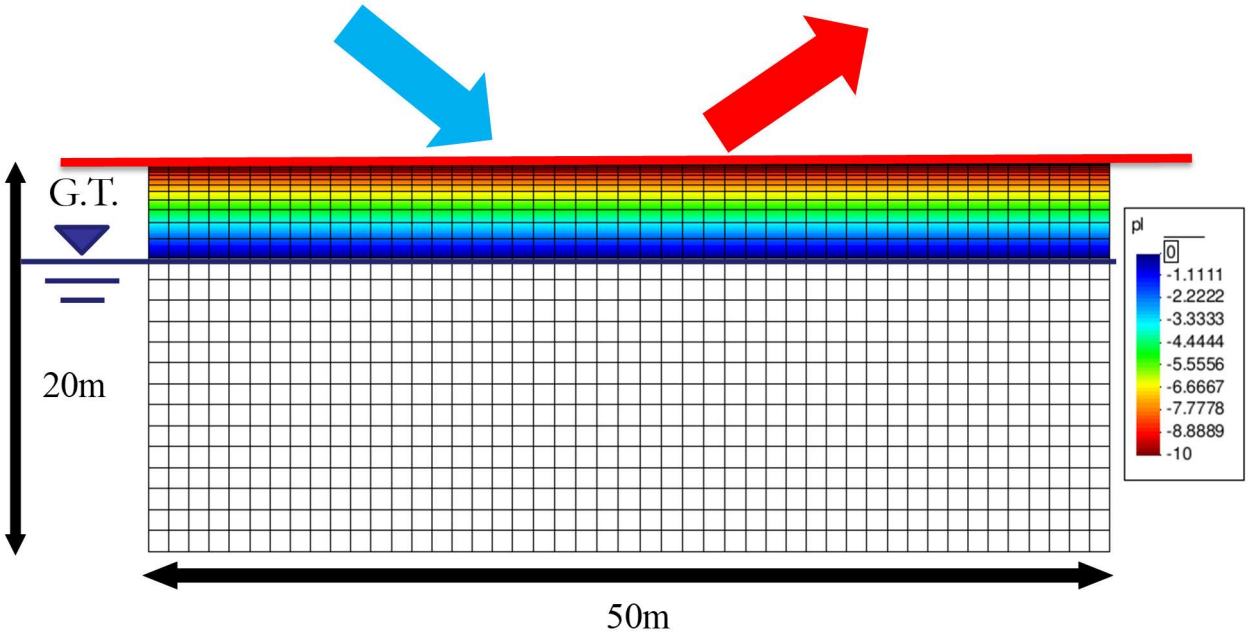

Figure 7.3 Mesh of sensitivity analysis (pl = suction in MPa)

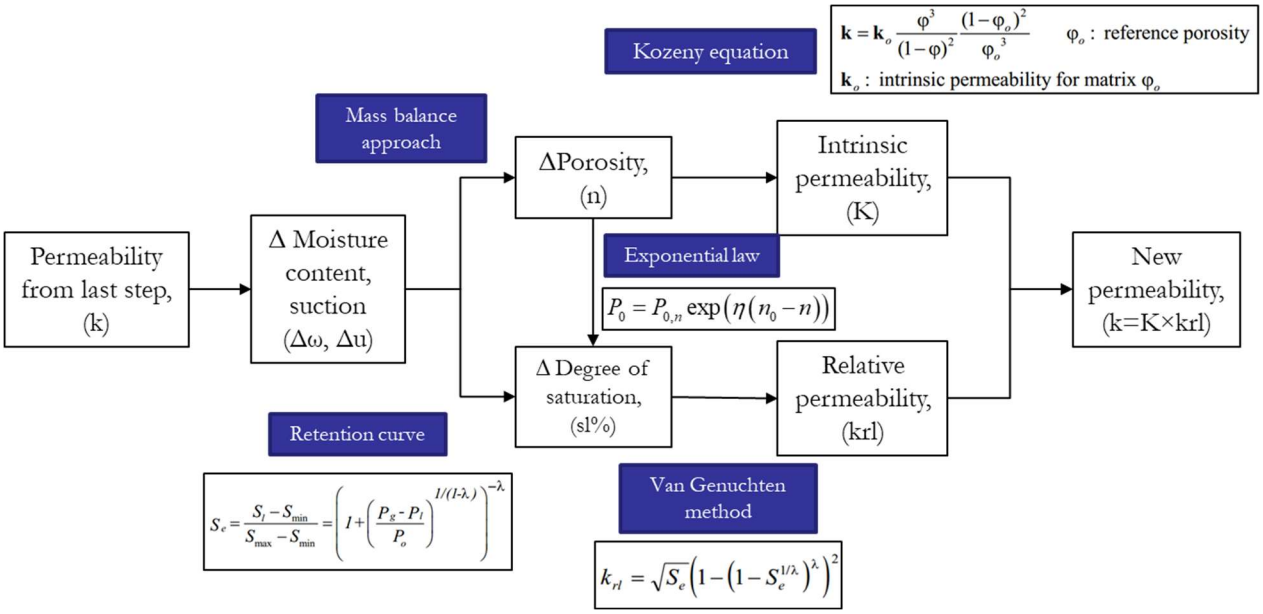

Figure 7.4 Permeability calculation loop in the CODE_BRIGHT

7.1.3. Initial condition and modeling sequence

As mentioned previously, the depth of the water level is 5 meters, while the top of soil equilibriums with the atmosphere. Soil above the water level subjects to unsaturated condition due to the capillary effect and followed by the description of the retention curve from the depth of the water table. Based on the literature, the top suction may assume to be 5pF (10MPa). Figure 7.3 presents the suction profile above the water table, the suction varies from 0 MPa to 10 MPa as described previously.

The relative humidity is adopted to describe the rainy and sunny weather conditions. It is assumed that only when rainy days the relative humidity (RH) equals 100%. This atmosphere suction corresponding to 100% RH is 0 MPa based on the Psychometric Law. Meanwhile, the relative humidity equals to 84% corresponding to 10 MPa atmospheric suction.

To describe a rainy period commonly occurs in the city of College Station, due to the personal experience, the period of rainy is assumed to be 5 days. The weather combination is describing a 5-day rainy followed by a 5-day sunny. Between two events, there is a 1-day ponding period, which allows the suction change from 0 MPa to 10 MPa for both numerical and realistic purpose. The simulation sequence of the relative permeability is shown in Figure 7.5. Typically, the period of the rainy subject to change for sensitivity analysis.

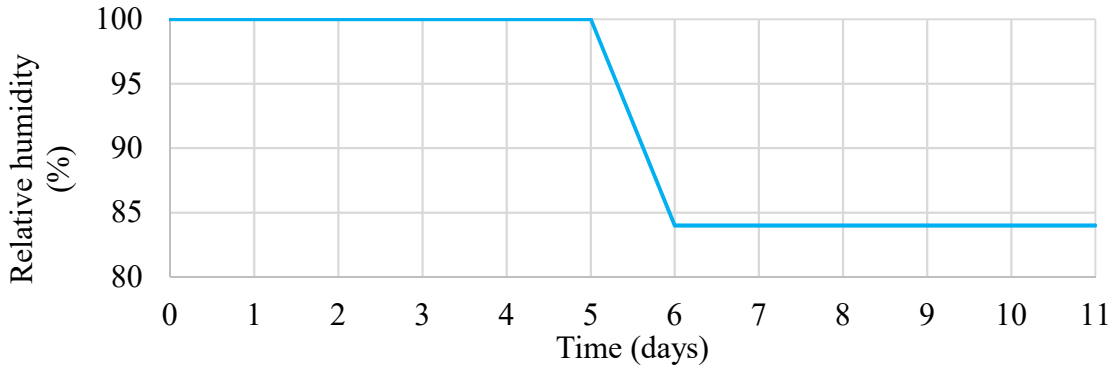

Figure 7.5 Relative humidity variation for the given condition

7.1.4. Modeling results

Using the model and parameters mentioned previously, Figure 7.6 presents a series results after 5-day rainy to demonstrate the permeability calculation procedure in Figure 7.4. The solid blue line represents the initial condition, and the dashed line is the condition after 5-day wetting.

Figure 7.6 (a) is the water content profile for the initial condition and after 5-day rainy. The initial condition of the model is considered exposed under dry conditions. Thus, the water content in the shallow region of the soil is smaller than the deeper area. For the initial condition of the model, we assume the soil is homogeneous. Thus, the water content below the water table is constant as they are fully saturated. After 5-day rainy, water from the top of the soil begins to penetrate soil mass. The water content begins to increase in the shallow region of the soil because of the increase of degree of saturation.

As the water content increase, the degree of saturation then switches from the unsaturated condition to fully saturated. The solid blue line in Figure 7.6 (b) indicates the unsaturated condition for the soil above the water table. Then the dash line, which is very closed to 1, points about that the soil becomes fully saturated after the rainy.

Because of the characteristic of shrink-swell soil (SSS), soil always subject to swelling when it subject to wet. In Figure 7.6 (c), the profile indicates that the porosity has a significant increase after the rainy period. The increment of porosity implies the larger volume of the soil mass and surface movement behaves heaving under this condition.

Figure 7.6 (d) is the increment of the intrinsic permeability. The intrinsic permeability is a permeability of the soil, which only relatives to the porosity of the soil under given condition. As the soil behaves swelling after the rainy period, the increment of porosity leads to a larger intrinsic permeability.

However, the actual permeability presented in Figure 7.6 (f) is the product of the intrinsic permeability (Figure 7.6 (d)) and the relative permeability (Figure 7.6 (e)). The relative permeability, instead of a parameter describing the rate of flux, describes the ratio between the true permeability of the soil and the intrinsic permeability due to the degree of saturation. The range of the relative permeability is 0 to 1. The relative permeability is very sensitive to the degree of saturation, where fully saturated corresponding to relative permeability equals to 1. The detailed formulation is described in Table 2.7. Thus, when soil subjects to fully saturated condition, the relative permeability equals to 1 at the very top, then the actual permeability equals to the intrinsic permeability as the value of porosity increased. While the degree of saturation reduces as the depth increase, the relative permeability significantly decreases. Thus, the actual permeability decreases tremendously as well. When the depth approach to the water level, because of the capillary effect, the degree of saturation is again increased, and the permeability then equals to the intrinsic permeability.

After 5-day rainy, the model continues to simulate the condition after 1-day ponding and 5-day sunny. The results are present in Figure 7.7

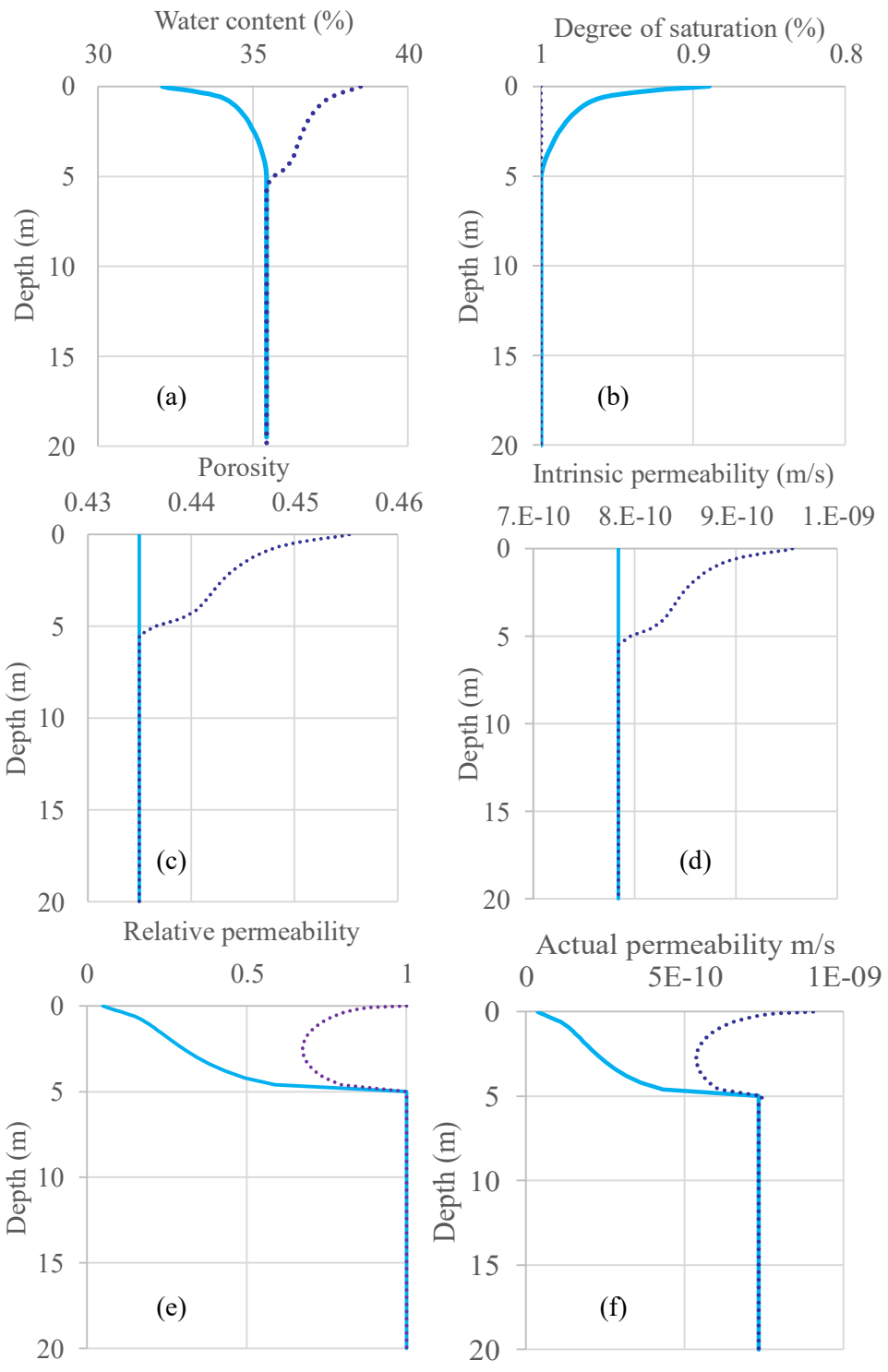

Figure 7.6 Simulation results profile after 5 days rainy (a) water content (b) degree of saturation (c) porosity (d) intrinsic permeability (e) relative permeability and (f) actual permeability

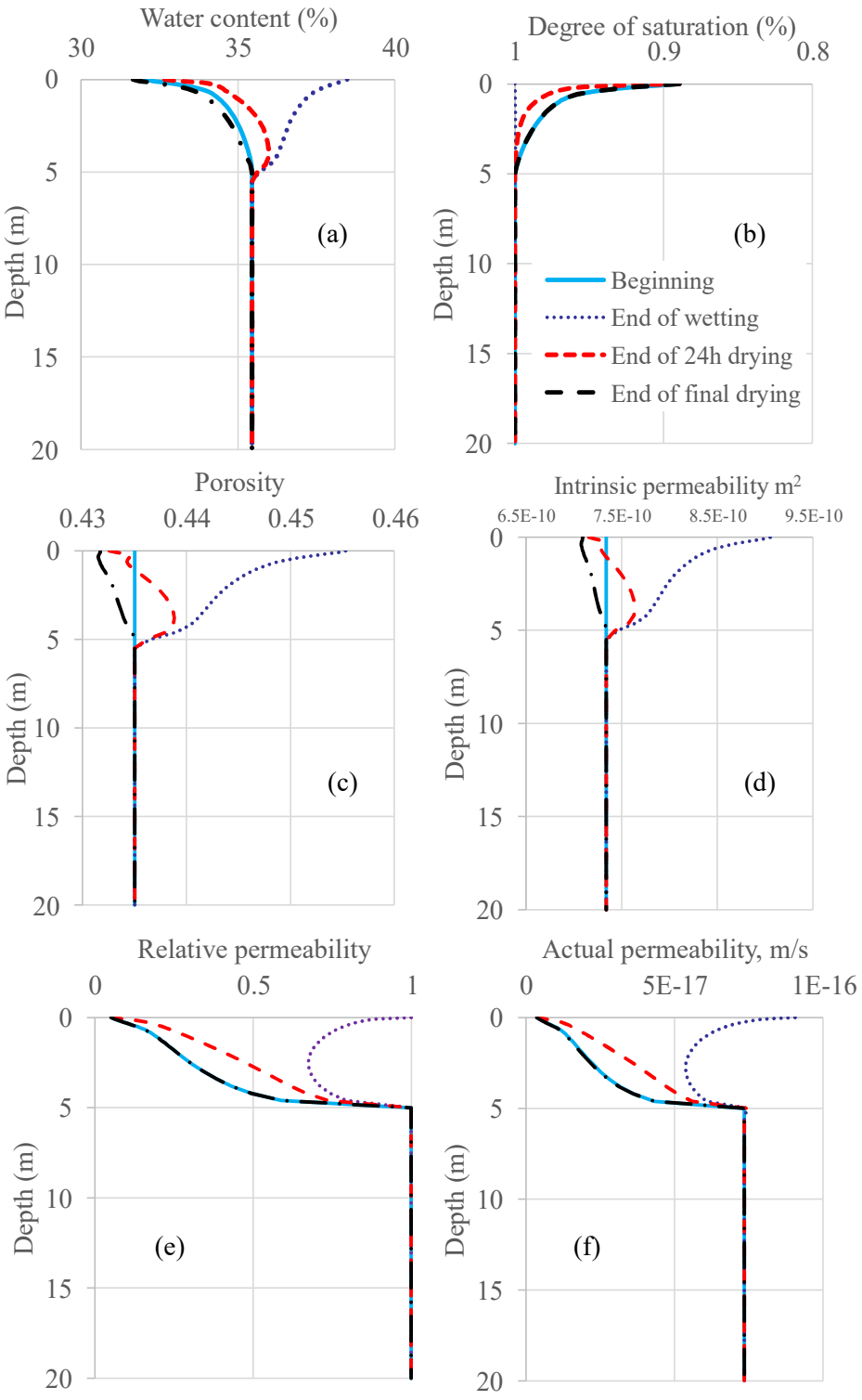

Figure 7.7 Simulation results profile throughout the simulation process (a) water content (b) degree of saturation (c) porosity (d) intrinsic permeability (e) relative permeability (f) actual permeability

By using the model mentioned previously and changing the value of permeability and the period of rainy (ponding), the results are presented as follows:

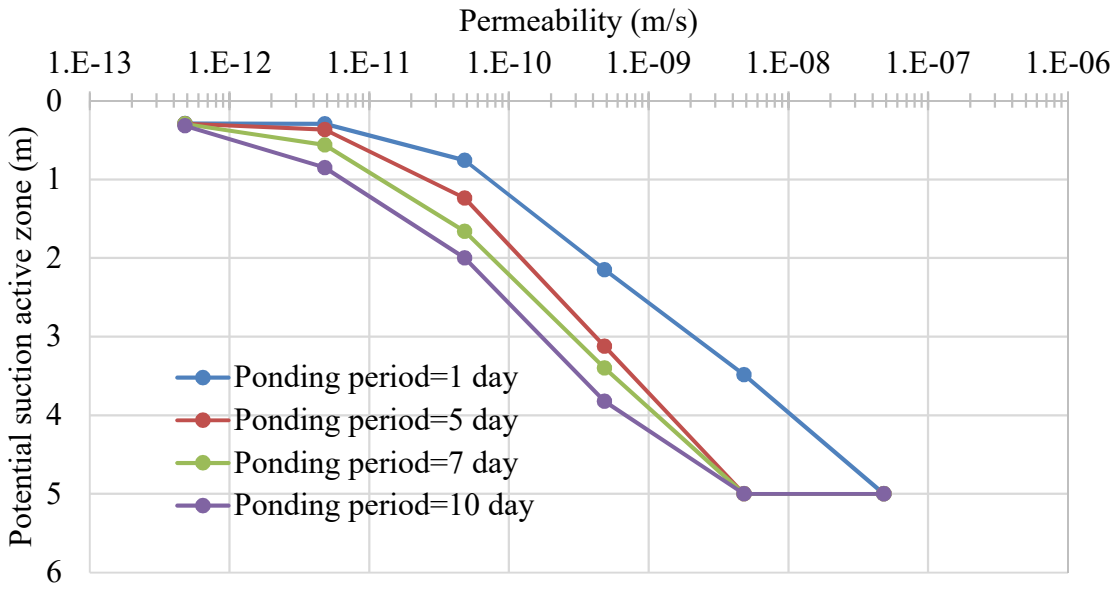

Figure 7.8 Relationship between permeability and active zone for different ponding period with water table of 5m

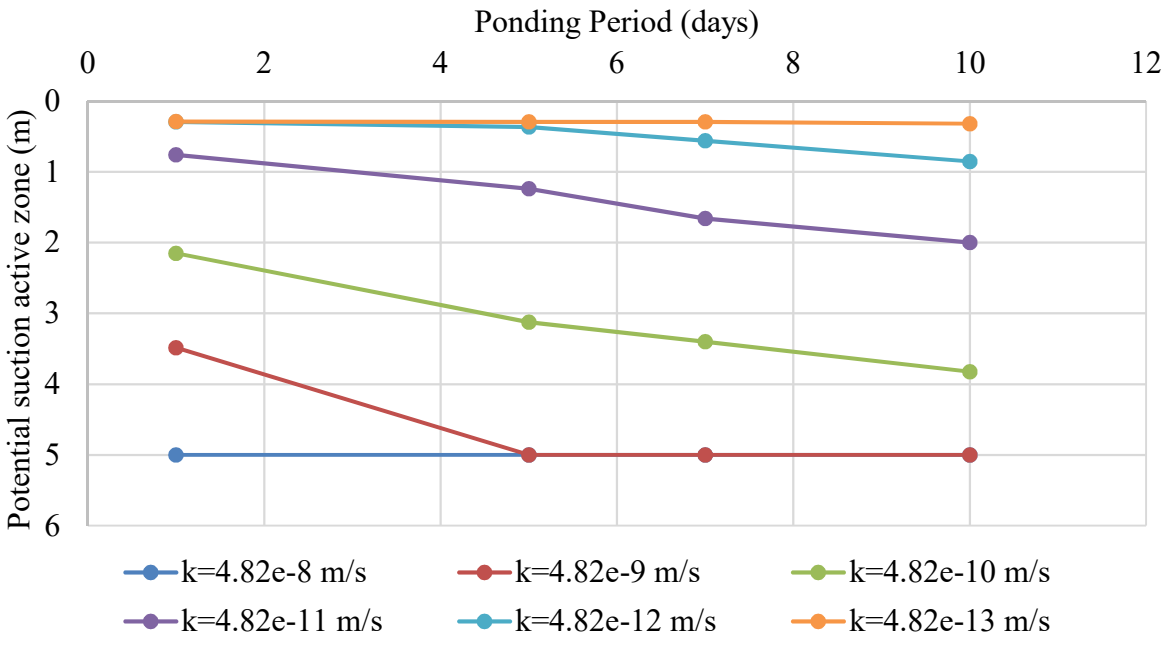

Figure 7.9 Relationship between ponding period and active zone for different permeability with water table of 5m

In Figure 7.8 and Figure 7.9, the depth of the water table is assumed to be 5m at a constant value. The permeability varies from 4.82×10^{-8}m/s to 4.82×10^{-13}m/s where 4.82×10^{-11}m/s is a reference value founded in the literature (Wang et al., 2018). The rainy period is assumed to be 1, 5, 7 and 10 days continuously.

From the result, the first conclusion is that there is not a simple relationship can be used to describe the connection between the permeability and the depth of the active zone. Because the curve does not an algebra function, the best way to describe the relationship may be a design curve for a particular location with the variation of the permeability. For the same period of rainy, a higher permeable soil will develop a deeper active zone until it reaches to the water table. The water table is considered as the physical boundary condition in this problem. Meanwhile, with a longer period of wetting, a deeper depth of active zone is observed. Because the soil body is exposed in a wet environment, both the intrinsic permeability and the relative permeability both increases. Thus, a larger actual permeability is occurred and the water flux can penetrate the soil body much easier.

Figure 7.9 points out that if the soil with extremely small permeability, the active zone may not be a problem since the DAZ is constantly shallow regardless of wetting period. A similar situation is that if the permeability is high enough, the depth of active zone yields to the depth of water table. Also, there is not a simple model that can be used to describe the relationship between ponding period and the depth of active zone.

7.2. The critical weather condition determination

The period of rainy is very sensitive to the depth of active zone as stated in the previous section. Thus, a representative/critical weather condition is very important in the estimation of active zone problems.

The weather condition in this work simply considers as only sunny and rainy days. To investigate the most critical impact on the soil mass and formation of the deepest active zone, the longest sunny and rainy period need to be determined. For simplicity, daily precipitation equals to 0 is considered as a sunny day, and larger than 0 is considered as rainy day. Figure 7.10 presents the precipitation record in College Station from NOAA. These data will be used in later calculation.

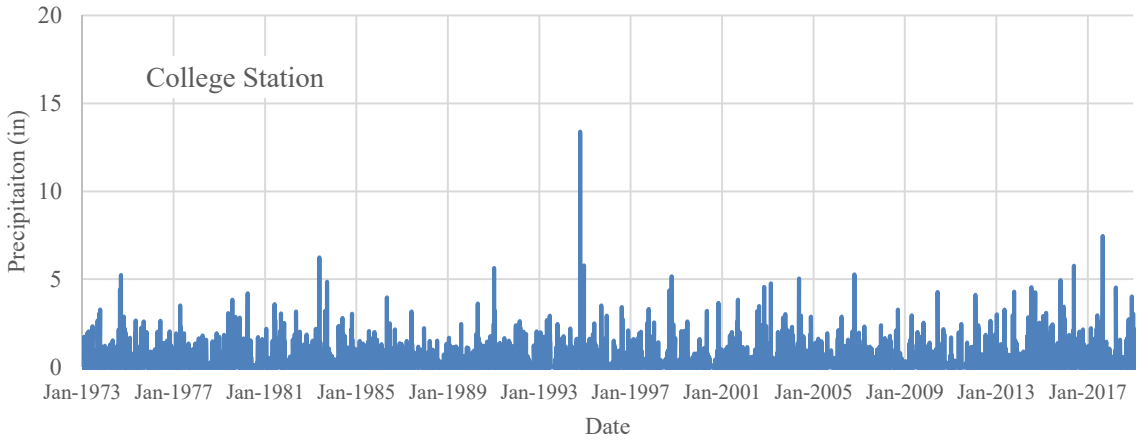

Figure 7.10 Precipitation record in College Station, Texas (NOAA, 2019)

A return period is a common way to describe the critical condition to a problem. As the DAZ determination involved the combination of the sunny and rainy period, the design event is the continuant period for both sunny and rainy, or the combination of two event.

The return period is described by the probability of exceedance, which means the percentage that a certain event may being equaled or exceeded in any year. The relationship between the return period T and the probability of exceedance P under period of L is described as e.q.(7.1). In this work, we adopt the return period of 100-year event in every year, where T=100 (years) and L=1 (per year), thus the P=0.01.

$$P = 1 - \left(1 - \frac{1}{T}\right)^{L} \tag{7.1}$$

Notice that the P=0.01 is the probability of the 100-year event, the probability of exceedance is determined as e.q.(7.2), where the m is the rank of inflow value, and n is the total number of the event.

$$Probability\ of\ exceedance = 100\% \times \frac{m}{n+1} \tag{7.2}$$

Figure 7.11 presents the general steps to obtain the probability of exceedance. By collecting the precipitation record from year 1970 to 2018 and record the sunny day with precipitation of 0 and rainy days with non-zero precipitation, we tracked the longest continues rainy period in a certain year. E.g. in the year of 1970, the longest continues rainy period was 6 days. Then we rearranged and ranked the length of rainy period from longest to shortest. By using e.q.(7.2), the frequency curve for both rainy and sunny period are presented as Figure 7.12 and Figure 7.13. The trend line in both figures help to calculate the 100-year design event, for P=0.01=1%. e.g. for rainy event, the continues rainy period for 100-yeasr returned value is calculated as e.q.(7.3). Similar procedure is applied for the sunny event.

$$-1.368 \times \ln(1\%) + 11.072 = 11.072\ days\ (use\ 11\ days) \tag{7.3}$$

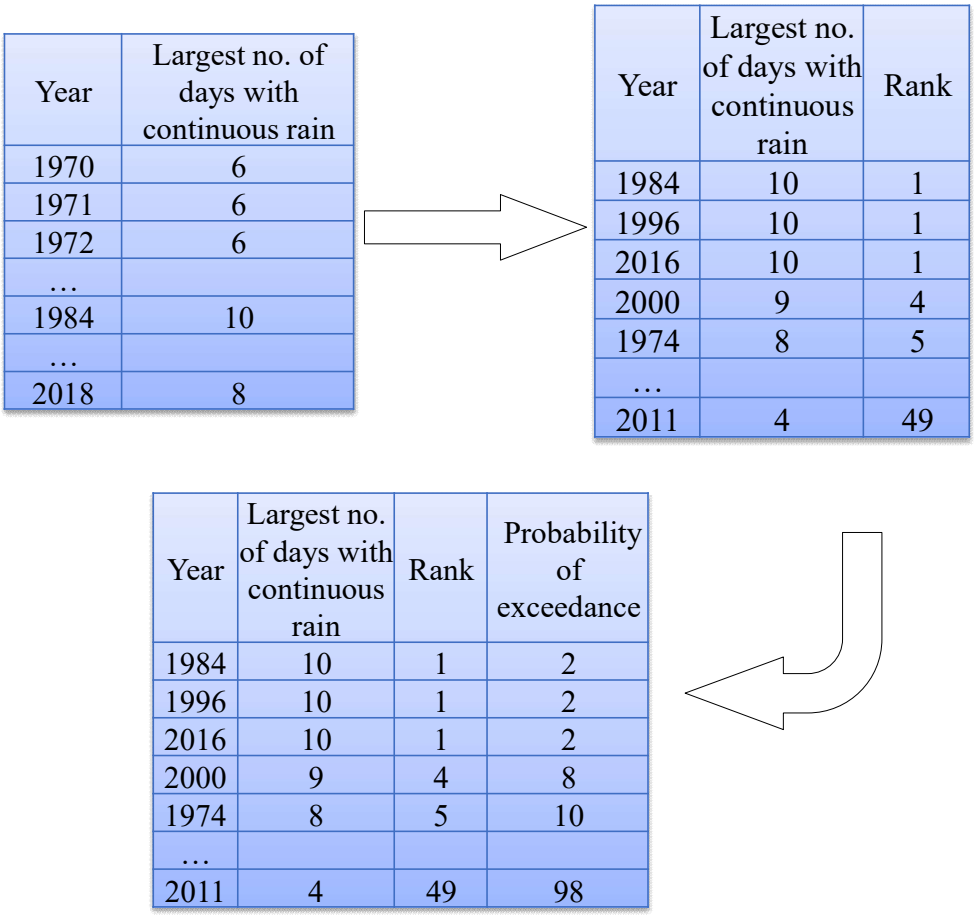

Figure 7.11 Schematic of determination of probability of exceedance for rainy event

However, as the simulation is considering the combination of rainy and sunny period, the total probability of exceedance should be considered. As the combined probability is 0.01, the product of the probability of rainy and sunny period should be 0.01. Thus, the combined event for 100-year return period is presented in Table 7.2

Table 7.2 Combined event for 100-year returned period

No.	Continuous rainy		Continuous sunny		Total probability of exceedance
	Probability of exceedance	Continuous rainy period	Probability of exceedance	Continuous sunny period	--
1	1	5	0.01	66	0.01
2	0.1	8	0.1	41	0.01
3	0.01	11	1	16	0.01

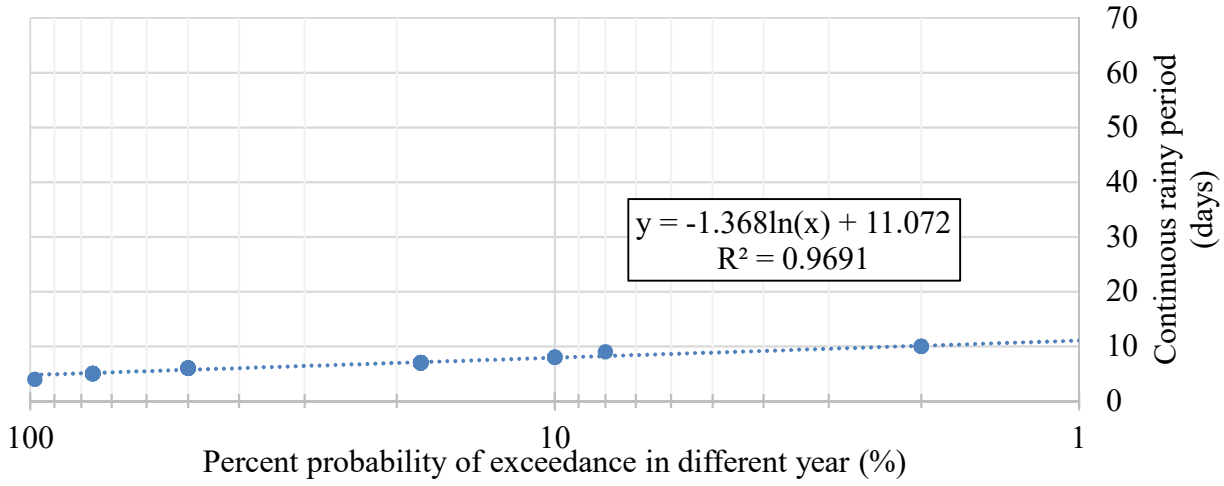

Figure 7.12 Rainy frequency curve obtained from precipitation record analysis

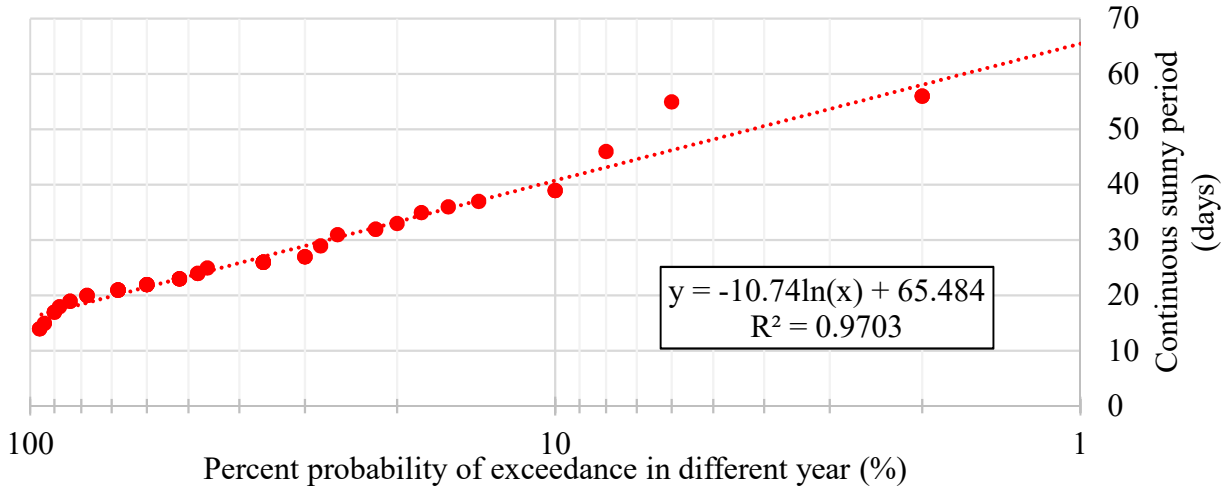

Figure 7.13 Sunny frequency curve obtained from precipitation record analysis

Although Table 7.2 lists out 3 types of combination for the 100-year design event and theoretically there will be infinite combinations, the analysis should consider the actual weather history in College Station. Based on the revision of design method, the TMI value in College Station is about 0, which indicates that the amount of precipitation (rainy) is approximately equals to the evaporation (sunny). In this case, the case No.3 with 11 continuous rainy and followed by 16 days continuous sunny will be considered as a critical weather combination for the simulation. By using the mesh and the boundary indicates in pervious section, the result of the simulation is shown as follows.

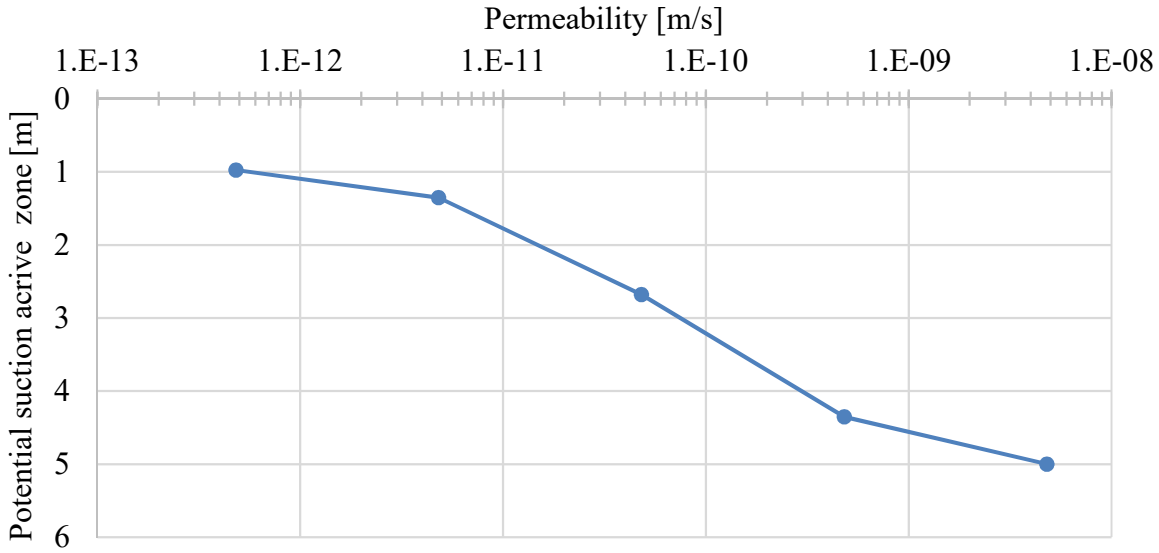

Figure 7.14 Design curve for the depth of active zone of permeability under critical weather combination

Comparing Figure 7.8 and Figure 7.14, the design curve between the permeability and the depth of active zone is generally deeper in Figure 7.14. Noticed that the period of ponding actually increases from 10 days to 11 days. An assumption is that is the rainy period plays a more important role in the active zone problem than the sunny period. This assumption will be discussed in the following section. Also, based on the Figure 7.14, as the permeability in College Station is in a scale of 1×10^{-10}m/s, the active zone thus estimates to be around 3m, which is agreed with the experience value.

7.3. Depth of Active Zone Development with Site Conditions

The pervious section demonstrates the DAZ development under primary assumed conditions. The results turn out that the permeability, the period of rainy and the depth of water table strongly affect the development of DAZ. This section presents a more detailed simulation result with more site conditions involved.

7.3.1. Simulation process

A bigger and finer mesh is adopted to conduct a more detailed analysis. The simulation is conducted by assuming plane strain condition with a mesh of size 50m by 50m, 8450 quadrilateral elements, as presented in Figure 7.15. The mechanical boundary CD is fixed; AD and BC are constrained in the x-direction, thus allows the movement in a vertical direction. Line AB is the flux boundary. The water can flow in or out from the boundary by assigning different suction values simulating the suction in the atmosphere. At the top of the model, different colors in the mesh representing the shrink-swell soil will be replaced by non-shrink-swell soil in later analysis.

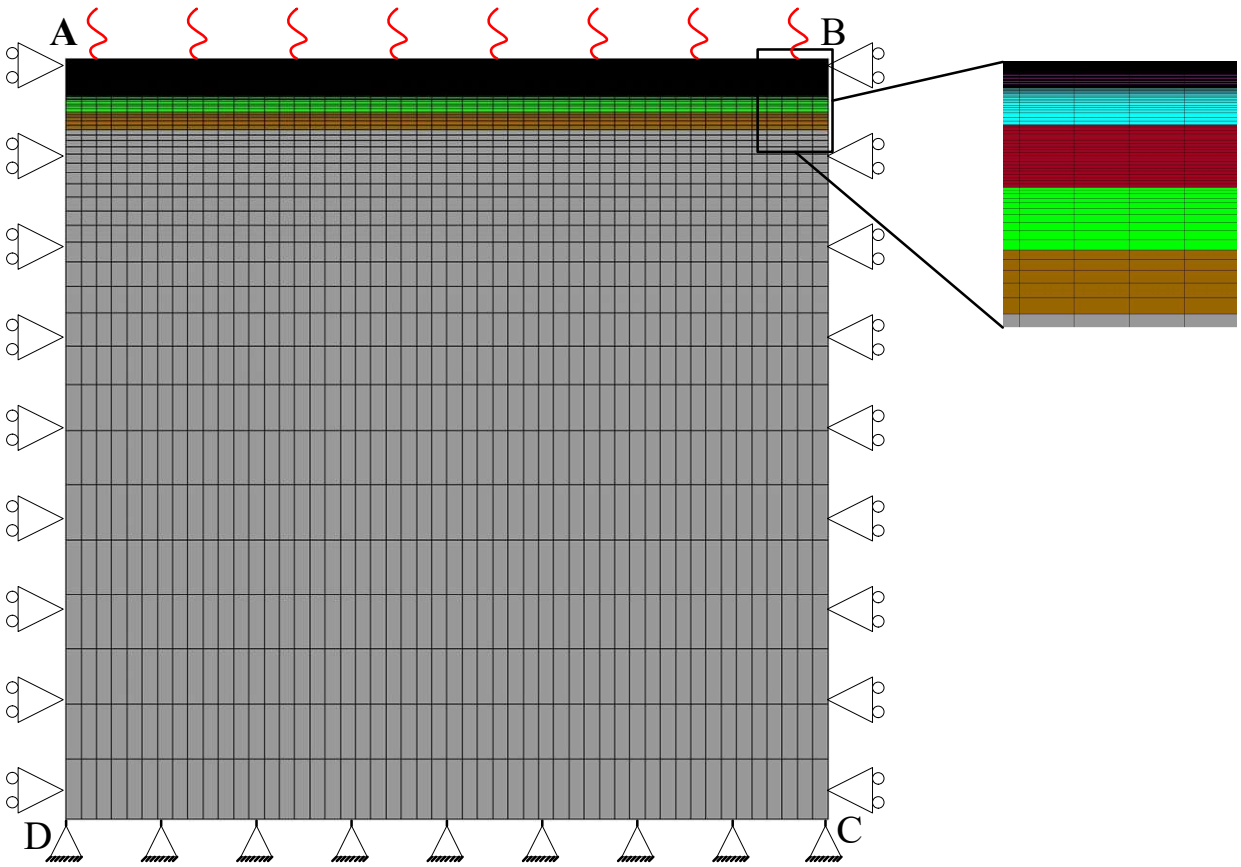

Figure 7.15 Mesh of simulation

The analytical method proposed by Mitchell (Mitchell, 1979) is adopted in this work to describe the suction envelope. In the analytical approach, the suction at the ground surface can be described as a sinusoidal function $u(0,t)=u_e+u_0\cos(2\pi tn)$, where u_e is the equilibrium suction correlative with the weather condition, i.e., Thornthwaite Moisture Index (TMI) (Covar & Lytton, 2001; Lytton, 1994), u_0 is the amplitude of the suction variation at the ground surface, n is the frequency of the suction cycle. The formulation of suction within soil mass as a function of depth and time described by using Laplace transform analysis is present in e.q.(7.4), where α is the diffusion coefficient and z is the depth into soil mass.

$$u(z,t) = u_e + u_0 \exp\left(-\sqrt{\pi z^2 n/\alpha}\right)\cos\left(2\pi tn - \sqrt{\pi z^2 n/\alpha}\right) \quad (7.4)$$

As e.q.(7.4) describes the suction oscillation controls purely with atmosphere suction, to adequately apply this equation the water table needs to be deeper than about 10m in a practical manner (Aubeny & Long, 2007; Lytton, 1997; McKeen & Johnson, 1990), which had been satisfied in this study. Further, considering the envelope described by e.q.(7.4), the sinusoidal part can simply as ±1. E.q. (7.4) is then also modified as e.q. (7.5).

$$u(z,t) = u_e \pm u_0 \exp\left(-\sqrt{\pi z^2 n/\alpha}\right) \quad (7.5)$$

To apply e.q. (7.5) in this study, the equilibrium suction u_e equals 3.6 pF (398kPa) determined by the relationship between TMI, which is 0 in College Station (Wray, 1978). The value of u_0, is back calculated after assessing the range of suction at the soil surface. The practical method proposed by Post Tension Institute (PTI, 2012) suggest the dry surface suction shall be 4.5 pF, Briaud (Briaud et al., 2003), recorded the ground surface suction equals to 4pF, Wray (Wray, 1989) measured the ground surface suction may go up to 5pF. Thus, 4.5pF (3162kPa) is adopted as the suction value for the dry weather. Similarly, the PTI method suggests suction in a wet season equals 3pF, Briaud's measurement for the wet season may lower to 2pF, and Wray's record is around 3.4pF. Also, considering the axisymmetric of e.q.(7.5), the ground surface suction equals to 2.7pF (50kPa) for wet weather is adopted.

The suction frequency n describes the return period of suction in a unit of time. Aubeny (Aubeny & Long, 2007) adopted n=1 year, Briaud's weather studying (Briaud, 2013) also implies the return of high suction will be around 1 year. Thus n=1 year is adopted.

The unsaturated diffusion coefficient α is an analogy to the permeability but under unsaturated condition. Extensive work on measuring the diffusion coefficient among different

locations in Texas. Aubeny (Aubeny & Long, 2007) had summarized the values in Table 7.3. As the amount of α will directly determine the depth of suction active zone, this value should lead the envelope to a proper DAZ. Lytton and Nelson (Lytton, 1997; Nelson et al., 2012) suggested the active zone depth may various between 9.39 ft (286.2cm) to 21ft (640.1cm). Information provided by the City of College Station that the depth of the active zone may no less than 3m. Abdelmalak (Abdelmalak & Briaud, 2017) records the active zone in College Station is 4.5m. Wray records (Wray, 1989) the depth of active zone can up to 4.6m. Based on the limited records of the depth of the active zone collected, the unsaturated diffusion coefficient adopted in the analysis is 2.55m^2/year, which located in the range of field estimated data in Table 7.3. Figure 7.16 (a) presents the envelope determined by e.q.(7.5) with parameters described previously.

Table 7.3 Unsaturated diffusion coefficient found in the literature (C. Aubeny & Long, 2007)

Category	Location	Value [m^2/year]	Reference
Laboratory results	Fort Worth, Texas	0.18±0.12	(Lytton et al., 2006)
	Austin, Texas	0.20±0.10	(Lytton et al., 2006)
	Austin. Texas	0.19±0.10	(Lytton et al., 2006)
	Waco, Texas	0.085±0.045	(Aubeny & Lytton, 2004)
	Australia	0.11-0.14	(Mitchell, 1979)
Field estimated data	N.A.	3.2-13	(McKeen & Johnson, 1990)
	N.A.	0.33	(Mitchell, 1979)
	N.A.	4.5	(McKeen & Johnson, 1990)
	N.A.	1.9	(Mitchell, 1979)

An agreement on the suction profile between the numerical model and the analytical solution plays a vital role in the validation process. In e.q.(7.5), the suction varies from the equilibrium as a function of depth. Thus, in the numerical model, the simulation also starts from the equilibrium suction. The atmosphere suction for both wet and dry season is assigned as the boundary at the top of the model (edge AB in Figure 7.15). Based on the weather record in Figure 3.3, the suction cycle is determined as n = 1 year, the period to develop the envelope then equals to 90 days from the equilibrium condition to each side of the suction profile

$$i.e.\ \ dry \xrightarrow{90\ \text{days}} equilibrium \xrightarrow{90\ \text{days}} wet \xrightarrow{90\ \text{days}} equilibrium \xrightarrow{90\ \text{days}} dry$$
$$\underbrace{\qquad\qquad\qquad\qquad\qquad\qquad\qquad\qquad\qquad\qquad}_{360\ \text{days}}$$

By starting the suction profile develops from equilibrium condition to dry or wet season in 90 days, the simulation results versus the analytical value present in Figure 7.16 (a) which shows the simulation result well agrees with the analytical value. Thus, the model is considered adequate for simulating the problem.

As the analytical value presented in Figure 7.16 (a) represents the envelope of the suction variation for the region, the envelope is considered as the “extreme” initial condition. Meanwhile, a profile with more common appearance will also be interested to investigated as the “ordinary” initial condition. Based on literatures, atmosphere suction equals to 3pF (100kPa), and 4pF (1000kPa) is most commonly measured. Thus, besides starting from the envelope, two initial profile apart from the boundary, which presented in Figure 7.16 (b) and (c) are the ordinary wet and dry initial profile represent the initial condition that might more commonly occurs.

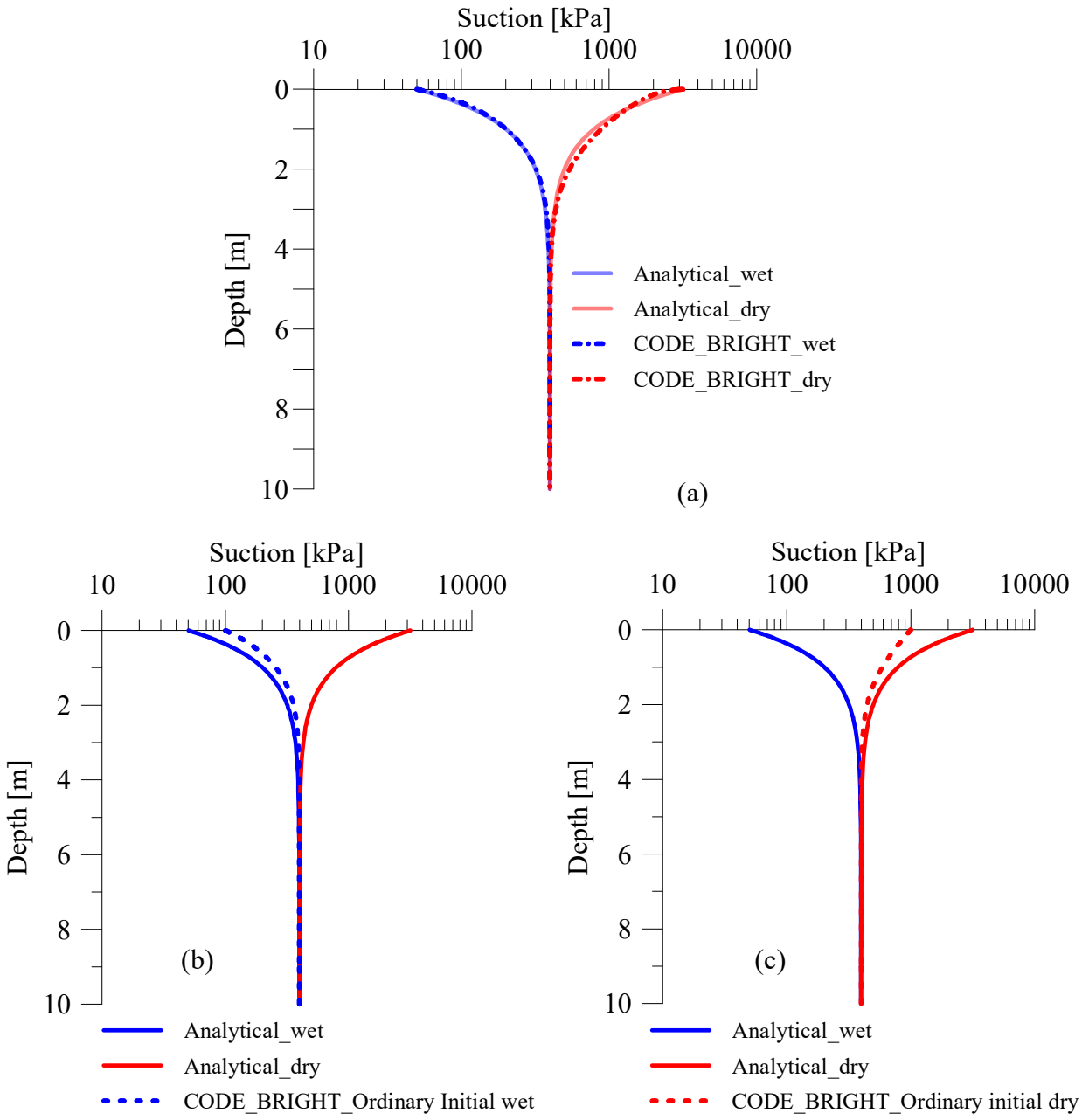

Figure 7.16 Initial condition for wet and dry season (a) extreme initial condition for both wet and dry season (b) ordinary initial condition for wet season (c) ordinary initial condition for dry season

Start from the either wet or dry initial profile, the code will conduct simulation by imposing atmospherical suction as the flux boundary at the top of model and calculate the suction oscillation within soil simultaneously with the soil body movement for given period. For conservative purposes, the suction imposed at the top will only consider the value at extreme condition, e.g., when the initial top suction equals to ordinary or extreme wet conditions (50kPa or 100kPa/2.7pF or 3pF), the imposed suction for simulation will equal to extreme dry condition (3126kPa/4.5pF) only.

Based on the result in Table 7.2, instead of the combination event, the longest period of drying is 66 days. To analyze the longest influence of the drying/wetting period, the lasting time designs to be 1, 5, 10, 15, 20, 30, 40, 50 and 60 days. The narrow spacing at the beginning will imply the immediately changing due to the suction change. Furthermore, the long-last period aims to show the result after a long-term effect if the soil body meets a critical weather condition. The following section will present the simulation results from both extreme and ordinary initial conditions in the either wet or dry season of the development of the depth of active zone and the soil movement.

7.3.2. Modeling results

This section presents the suction variations and soil movement behavior under the wetting and drying combination mentioned previously. Also, based on the definition of suction active zone and movement active zone proposed in this work, the variation of active zones due to the weather influence will be shown as well.

7.3.2.1. Suction variation and active zone determination

Figure 7.17 presents the suction profile oscillation from either ordinary or extreme initial condition in dry or wet season subject to swell or shrink with infinite depth of water table.

Among four figures, (a) and (b) present the results start from initial condition in dry season. The light blue and red represent the suction envelope determined by the analytical method. The solid red line represents the initial condition and the blue lines with different capacities are the suction profile at different time during wetting. In the ordinary dry initial case Figure 7.17 (a), 1 day of wetting swift the suction at shallow layer to the wet side significantly then gradually approach to wet envelope as the wetting period increasing. The shifting of suction profile also implies that the depth of active zone increases tremendously for the first 10 days then gradually reducing the rate of development. At the end of 60-day wetting, the suction profile is closed to the wet envelope. This points out that the depth of the suction active zone is lighter than the value determined by the analytical method. Moreover, a 60-day wetting period is rarely found in the weather history in Texas. A designation considering the effect of the suction active zone also needs to visit the history of wetting as it might be lighter than expected based on analytical analysis.

Similarly, Figure 7.17 (b) presents the suction distribution started from extreme initial dry condition. The extreme initial dry condition is overlapping on the envelope. By definition, it is the driest condition for the given location. Compare (b) to (a), the depth of active zone of 1-day wetting

from extreme dry initial condition seems to be lighter than that from ordinary one. However, an important issue regarding the figure is that the suction value is plotted in log scale, a small virtual variation in different portion of x-axis will stand for very different value. In this case, the 10kPa, as the criteria to determine the suction active zone appears in a deeper depth in the extreme initial dry condition compare to the ordinary initial dry condition.

Figure 7.17 (c) and (d) present the cases where the initial profile start in dry season at either ordinary or extreme condition. Between (c) and (d), the depths of suction active zone at the same period of drying period are closed to each other. At the end of 60 days of drying, the suction profile almost overlapping on the drying envelope, which implies that the suction closed to fully develop in dry season.

At the end of 60 days of weather changing, the suction profile started from wet season get closed to the envelope, while the ones started from dry season the developed profile still away from the wet envelope. The reason behind the difference is that the relative permeability significantly affects the real permeability and the real permeability then becomes extreme small in dry season compared to wet season. The real permeability which describes how much water can flow through the soil within a given time in reality, is the product of the intrinsic permeability and the relative permeability. The intrinsic permeability is the physical property of the soil media determined by the opening of the porous, and the relative permeability is a factor between 0 and 1 depend on the degree of saturation (Gilman & Kazemi, 1983; Kazemi & Gilman, 1993; Rossen & Kumar, 1992; Thomas et al., 1983; van Golf-Racht, 1982). With a higher value of suction, the low degree of saturation leads to a low value of the relative permeability thus tremendously decrease the real permeability. In this case, the water is more difficult to flow in dry season than in the wet season.

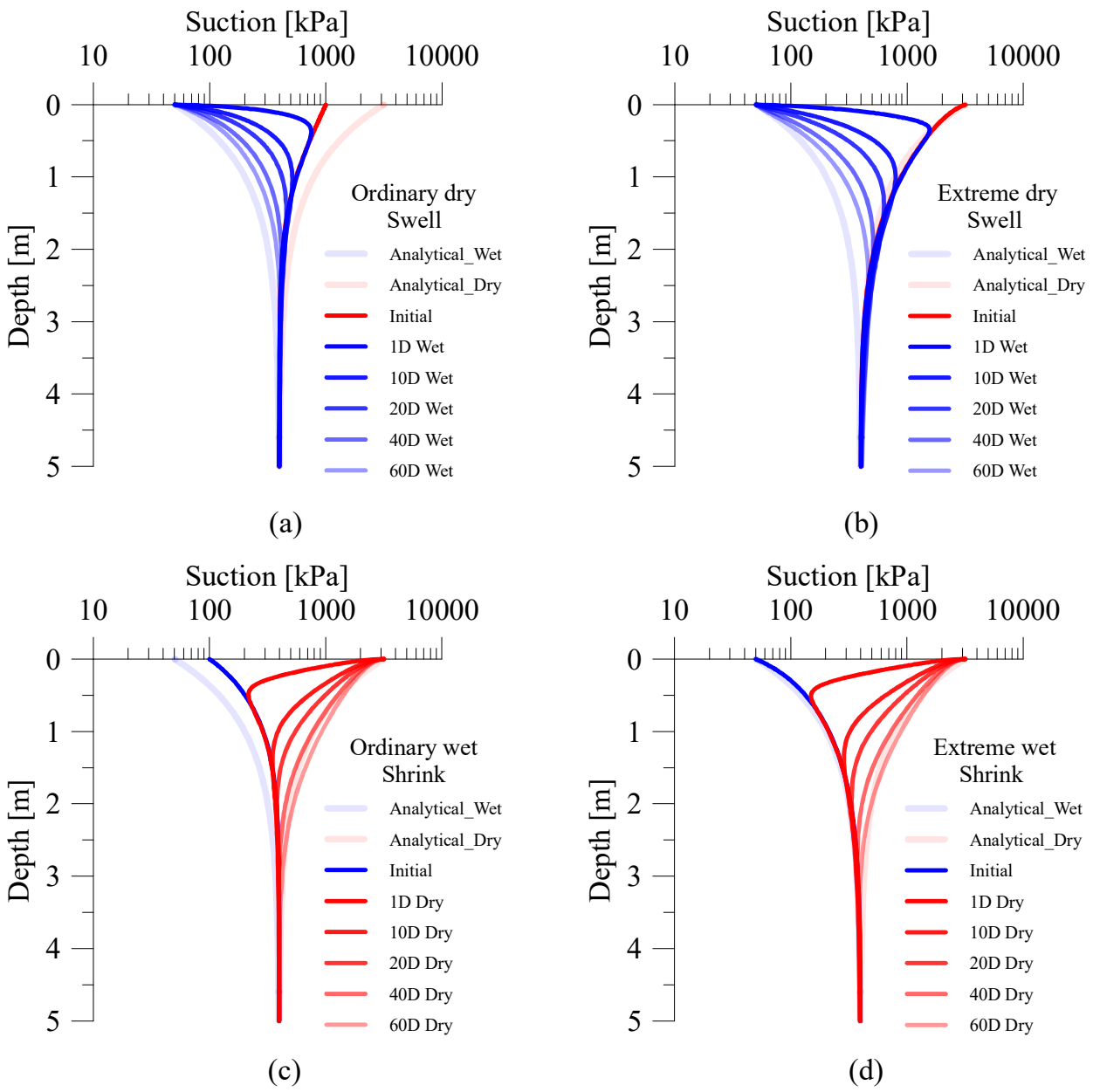

Figure 7.17 Suction profile variation for infinite water table (a) start from ordinary dry initial condition (b) start from extreme dry initial condition (c) start from ordinary wet initial condition (d) start from extreme wet initial condition

Figure 7.18 presents the summary for the suction active zone for the infinite depth of water table condition. The depth of suction active zone for the given case is about 3.5m, which

determined by the started from wet season case. In another point of view, the development of active zone is more depended on the high permeable initial condition, which means a higher permeability plays an important role for suction oscillation. Also, the ordinary or extreme initial case does not cause significant difference of suction active zone. Also noticed that at the end of long period, the suction active zone for both start-from-dry and start-from-wet season is deeper in the ordinary cases than in the extreme case. Typically, for the start-from-dry case, the suction at the deeper depth for the ordinary case is smaller than extreme case, which turns to have a higher permeability for the water flow and then it has a slightly deeper suction active zone than in extreme case. For the start-from-wet case, the degree of saturation for extreme case is higher than the normal case. After a long period, the reduction of the permeability for the extreme case is more significant than the ordinary case. The suction active zone then becomes shallower.

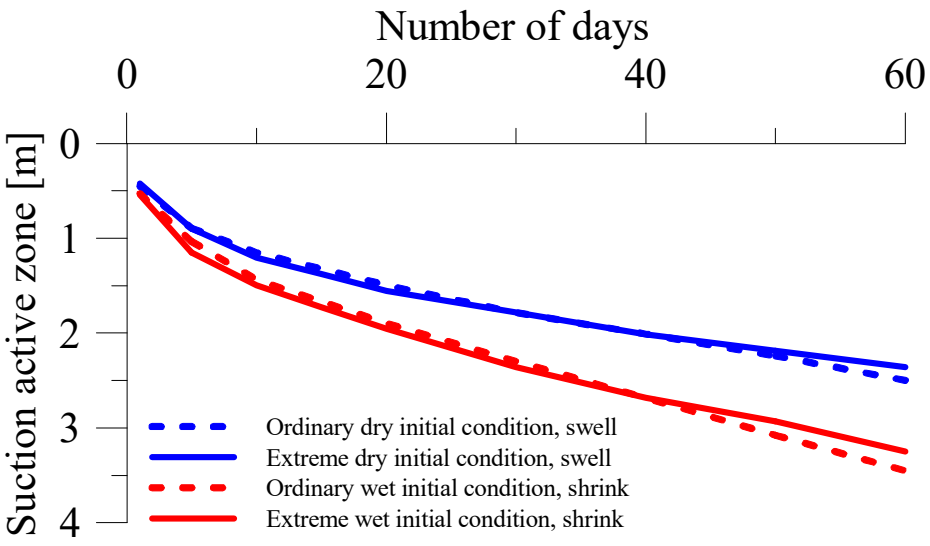

Figure 7.18 Summary of suction active zone for infinite water table

Figure 7.19 presents the suction active zone development for different water table conditions.

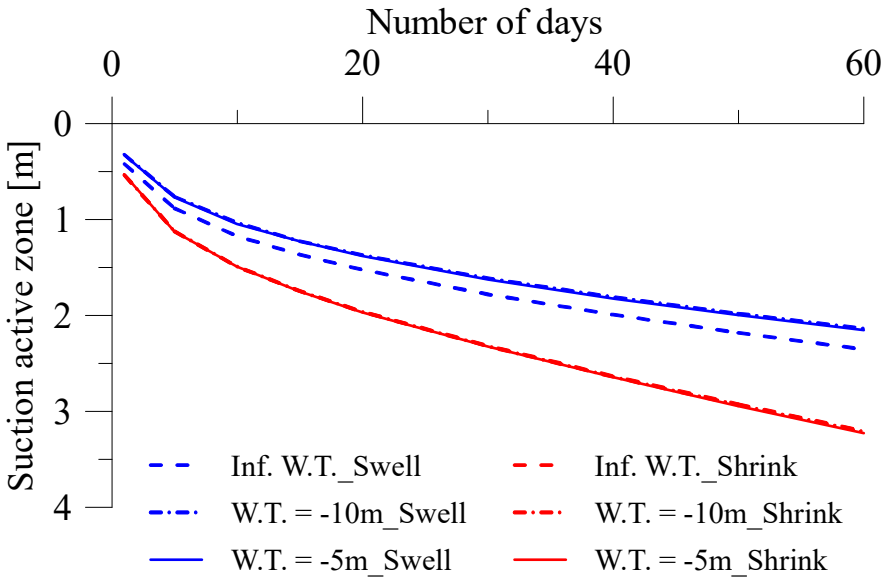

Figure 7.19 Summary for suction active zone for different depth of water table

As shown in red, the suction active zone for started-from-wet season cases is deeper than the other condition. It is because the soil has a relatively high value of permeability as discussed previously. With the low suction value at initial condition, soil subject to have a high degree of saturation thus has higher value of relative permeability. Meanwhile, it is also because the soil was at swelling state initially. Which further increase the value of intrinsic permeability. Compared to the cases start-from-dry season and soil body subject to swell and shown in blue, the cases start-from-dry season has a shallower depth of suction active zone. The reason is the small permeability at initial state induced by high value of suction prevents the dissipation of the suction. Besides, the depth of suction active zone for the cases started in wet season has very similar value among

different water table conditions, while the cases started in the dry season, the infinite depth of water table has the deepest active zone. When the water table rose to 10m or 5m, the active zone depth is lighter than the case with infinite water table. This conclusion shows that with low permeable soil, the depth of water table will also affect the depth of suction active zone.

However, it is also important to mention that the depth of suction active zone in this analysis is based on the criterion proposed in this work, where the suction variation is 10kPa, as 10% of some well-adopted sensor. It is clearly that with a smaller variation, e.g. 1kPa, the depth of suction action will be deeper, or in another way, with a larger variation will obtain a lighter active zone. We will not discuss the sensitivity of the criterion as it is a strongly experience based value and may be adjusted in the future

7.3.2.2. Movement variation and active zone analysis

Similar to Figure 7.17, Figure 7.20 presents the vertical movement profile for cases with initial condition stared in wet or dry season. Typically, Figure 7.20 (a) and (b) present the results of cases started from dry season. Because of the amount of soil movement directly relative to the suction variation (Alonso et al., 1990; Olivella et al., 1996), the case with extreme dry initial condition subject to higher swelling than the cases started with ordinary initial condition. And thus, the depth of soil movement active zone is deeper for the extreme case than the ordinary case. For the cases start-from-wet season, the movement of shrinking is similar to each other. It is because the extreme and ordinary initial cases is actually closed to each other, where the extreme wet initial case equals to 50kPa (2.7pF) while the ordinary condition is 100kPa (3pF). Thus, the surface movement value has a slightly difference between the ordinary and extreme initial cases. Figure 7.21 presents the summary for the surface movement of infinite depth of water table for different initial conditions.

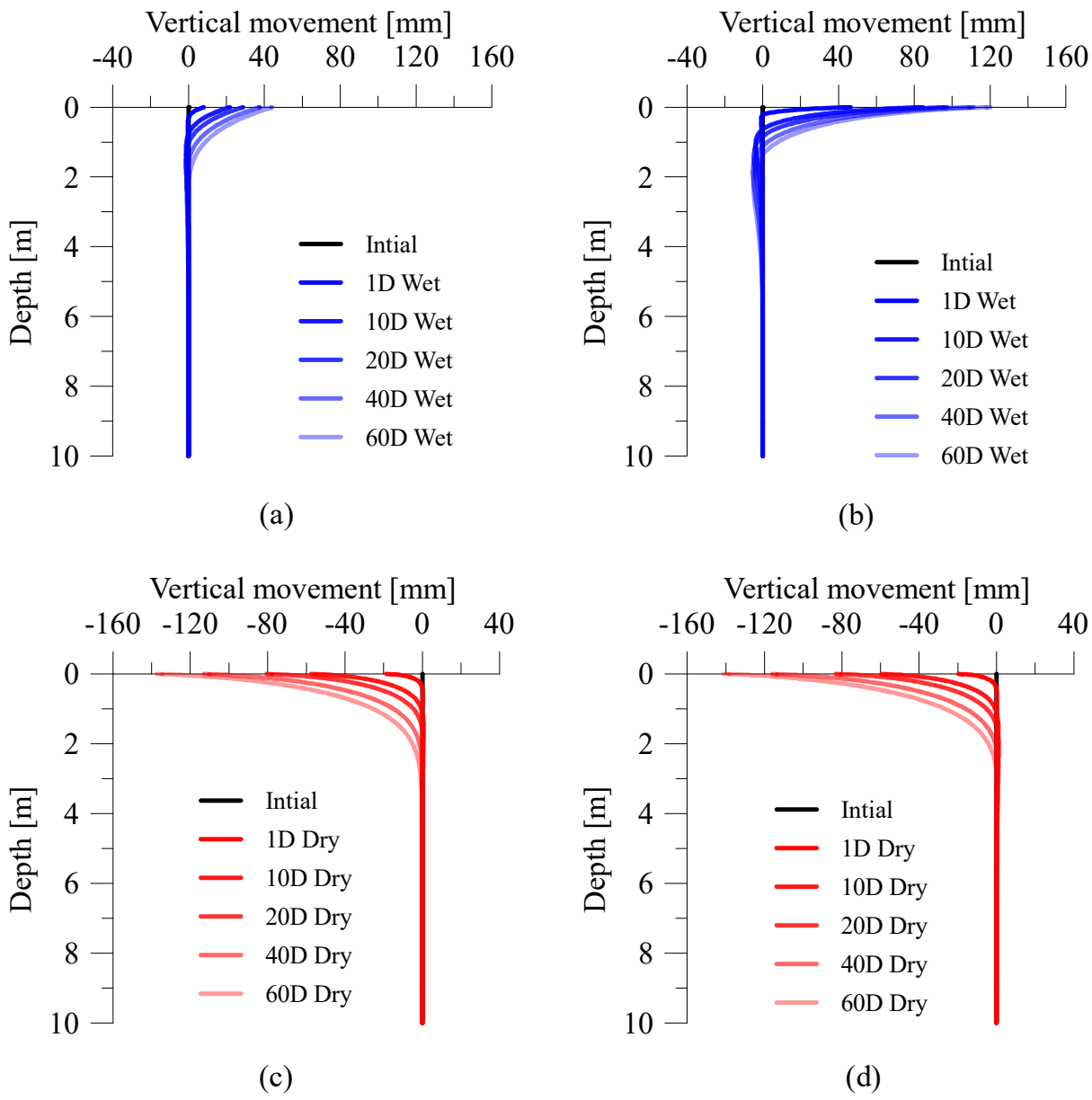

Figure 7.20 Movement profile variation (a) start from ordinary dry initial condition (b) start from extreme dry initial condition (c) start ordinary wet initial condition (d) start extreme wet initial condition

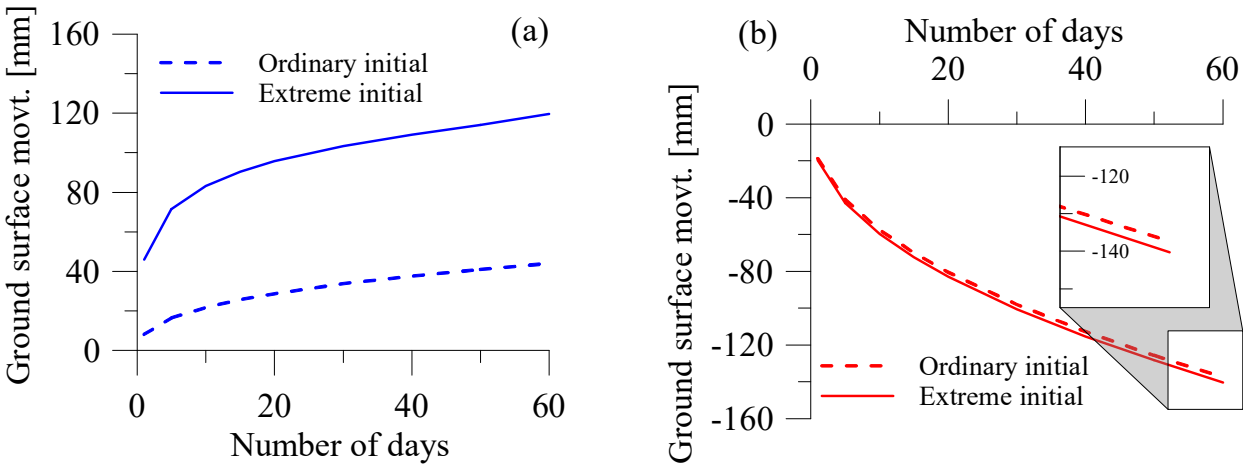

Figure 7.21 Surface movement for infinite water table (a) start from dry initial condition (b) start from wet initial condition

Later, Figure 7.22 presents the movement active zone development for the infinite water table case. In general, the movement active zone determined by the criterion listed in Table 5.1 (0.1mm) gradually increases as the period of wetting/drying lasting. Among four conditions, the rank of active zone is started with extreme dry initial condition subject to swelling (E.D.) > started with extreme wet initial condition subject to shrink (E.W.) > started with ordinary dry initial condition subject to swelling (O.D.) > started with ordinary wet initial condition subject to shrink (O.W.).

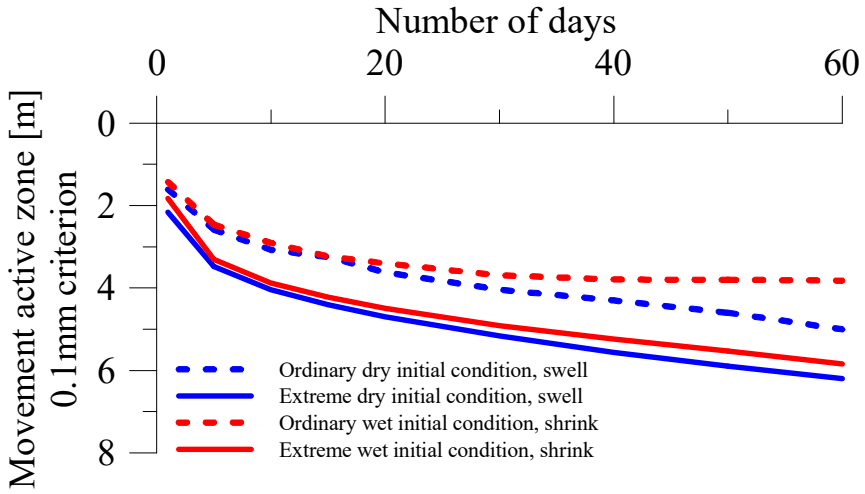

Figure 7.22 Movement active zone with 0.1mm movement criterion for infinite water table

By adopting the movement criterion of 10% movement of the surface, the active zone development significantly changes as presented in Figure 7.23. With the wet initial condition, the movement can be fully developed among soil mass. And because of the adoption of the 10% criterion, it eliminates the influence of the suction variation. The development of the active zone with different time interval is similar for both extreme initial condition and ordinary condition.

On the other hand, again, because of the 10% criterion, the active zone determination is no longer affect by the suction variation at the soil surface. For the initial dry weather condition, the ordinary initial condition has deeper active zone compares to the extreme dry initial condition. This concludes that the initial condition with higher degree of saturation trends to have deeper active zone determined by the 10% surface movement criterion.

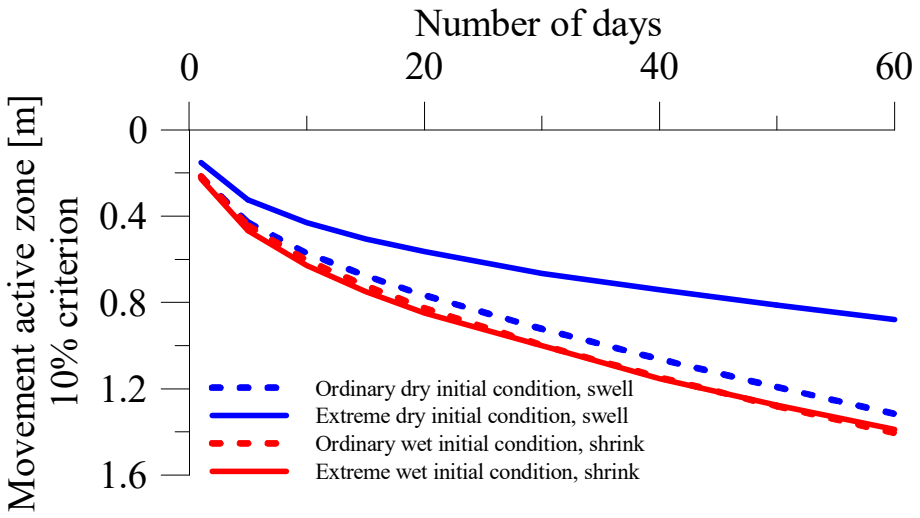

Figure 7.23 Movement active zone with 10% movement criterion for infinite water table

As indicate by Figure 7.22, the movement for cases started from extreme wet/dry initial condition is much larger than ordinary initial cases. Thus, the variation of water table analysis will focus on the extreme wet/dry initial cases, as presented in Figure 7.24. The cases started in dry season and subject to swell for different depth of water table reach a similar swelling value, which is around 120mm. Typically, the case with infinite depth water table has the maximum swelling value, while the case with water table with 5m has the smallest value. For the cases started in wet season and subject to shrink for different depth of water table reaches a similar shrinking value, which closed to 140mm. Similar to the swelling behavior, the infinite depth of water table has the relatively maximum movement while the 5m-depth water table case has the smallest shrinkage.

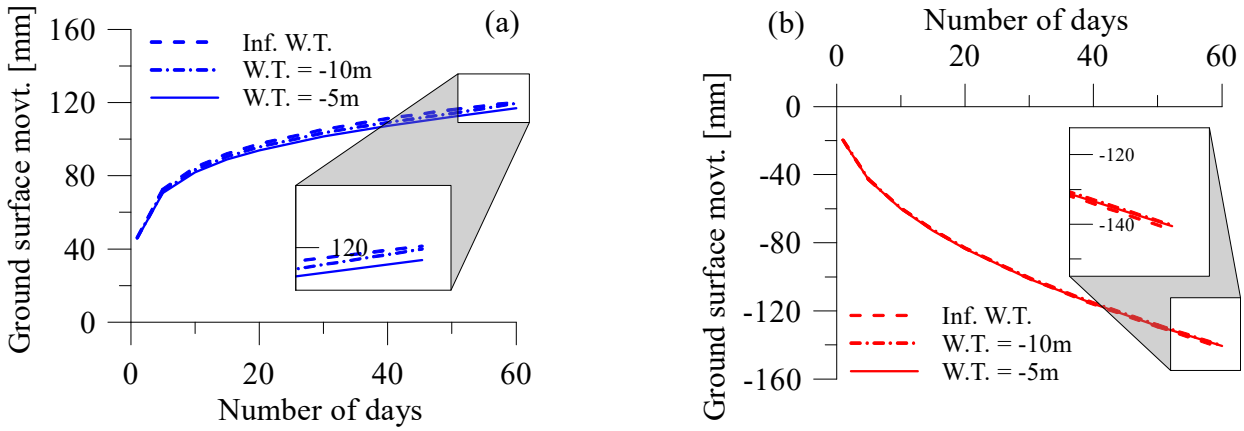

Figure 7.24 Summary of surface movement (a) start from dry initial condition (b) start from wet initial condition

Figure 7.25 presents the summary of the movement active zone for different water table cases started from extreme dry/wet initial condition. The most deeper movement active zone among cases discussed is the case started from dry initial condition with 10m water table, following by dry initial condition with infinite water table. Then the active zone of wet initial case with 10m water table and infinite water table are the third and fourth depth value. When the water table rises to 5m, the case stared from dry initial condition has deeper value than the case stared from wet initial condition.

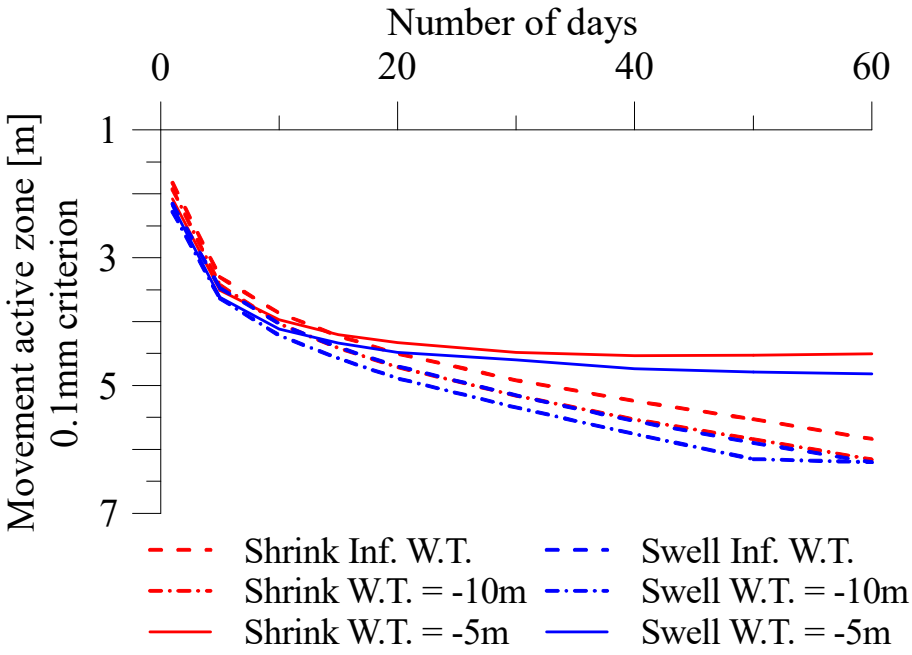

Figure 7.25 Summary for movement active zone with 0.1mm criterion for different depth of water table

For the development of movement active zone, the case with infinite depth of water table has deeper value than 5m water able follows by the common sense. When water table rises to 10m, the capillary effect from water table is strong enough to affect the determination of active zone thus the movement active zone becomes deeper than infinite water table case. However, it should also consider the criterion adopted to determine the movement active zone, if the criterion of movement variation is large enough, the movement active zone of infinite water table may deeper than any shallower water table. A clear trend of limitation of 5m water table case and 10m water table started from dry season indicate the boundary effect induced by the level of water table.

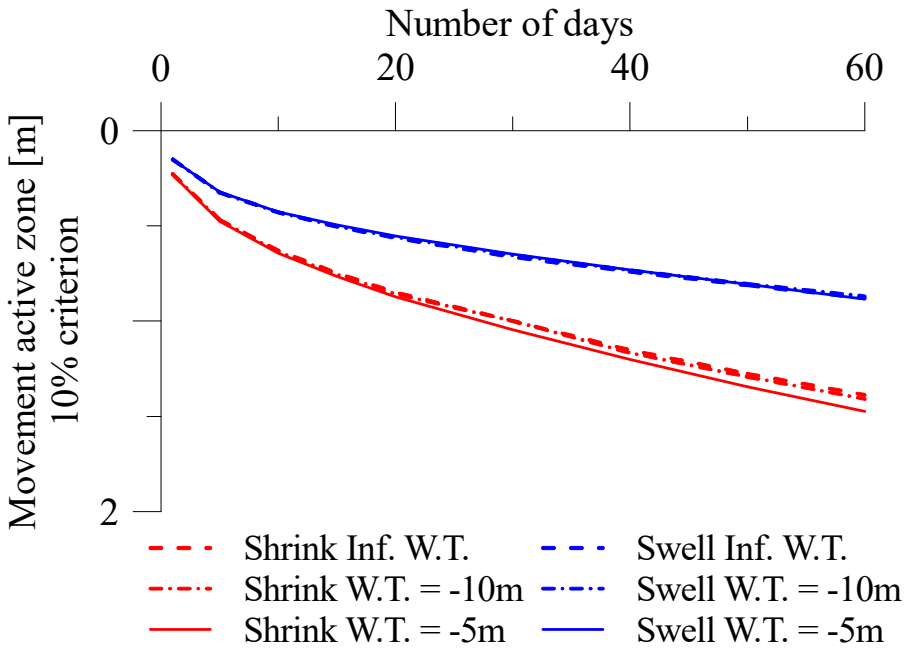

Figure 7.26 Summary for movement active zone with 10% criterion for different depth of water table

Figure 7.26 presents the active zone determined by the 10% movement criterion. In general the depth of active zone is lighter than Figure 7.25. Typically, the initial condition with low degree of saturation, i.e. the dry initial condition trend to swelling in the blue color, has very similar active zone development with different water able conditions. While for high degree of saturation initial condition, which are the red color in the figure, shows slightly difference after long period of simulation. In general, the active zone development for high degree of saturation at initial condition is deeper than the low degree of saturation cases. Further, if the active zone development is closed to the water table, the movement trends to influence by the capillary effect of the active zone. Thus, the active zone with 5m water table depth is deeper than other conditions.

7.3.3. Summary

In this section, by using the well-adopted analytical solution as the initial conditions and the result from the critical weather combination from pervious section, the numerical code CODE_BRIGHT calculates the suction and movement profile at certain time. Further, by using the criterion proposed in this work, the simulated profile determines the depth of suction active zone and movement active zone. The simulation firstly divided into start from wet season and start from dry season. And in each case, the initial profile will start either overlapping on the analytical envelope, refers to the extreme initial condition, or between the extreme and equilibrium, refers as the ordinary initial condition. Later, the simulation will proceed by changing the weather to the other season, i.e. the suction profile assumed to be in the dry season and the simulation will goes to wet condition. As we had discussed the influence of the permeability in the previous section, this section mainly focusing on the influence of period and the depth of water table.

For the suction active zone, the duration of weather positive associated with the development of the DAZ. There is not a significant difference between weather the initial profile started from ordinary initial condition or extreme initial condition. When the suction profile starts from dry season, the overall soil movement is swelling. And there is a positive correlation between the depth of water table and the DAZ. For the suction profile starts from wet season, the overall soil movement turns to shrink and the suction active zone is deeper than the cases started from dry season. There is no significant different of the suction active zone with different depth of water table.

For the movement active zone. Because the movement associated with the amount of suction variation, the movement for initial profile started from extreme condition is always larger than it for the started from ordinary condition. However, the cases started from dry initial condition have deeper movement active zone than the cases started from wet initial condition. The reason behind the result is that as the wetting process keeps opening the porous of the soil mass, the movement at deeper depth may gradually develop. By using the relatively smaller movement criteria compared to the 10 kPa suction criteria, a deeper active zone is determined. Under the extreme initial condition, the movement active zone yields to a depth above the water table. With the depth of water table increase, the movement active zone also becomes deeper. However, as the water table becomes deeper, where the capillary effect may not affect the soil movement, the active zone gradually increase but shallower than the same period with a lighter water table, which is the 10m in this case.

However, the difference in the active zone determination points out that the criteria adopted in this work may be further modified. Although we adopted a fixed value as the criteria with practical meaning, the movement active zone determined to be deeper than the suction active zone.

The first conclusion is that the suction active zone is more sensitive to the initial wet/dry condition, in another word, is sensitive to the permeability at the initial state. The movement active zone is more sensitive to the permeability development with time. Because of the suction and movement criteria for active zone determination adopted in this work consider the accuracy of the measurement device, there is no directly correlation between them. To eliminate this effect, the movement criterion may adopted a certain portion of the surface movement measurement e.g. 10% movement of the surface movement as shown in Figure 7.27. Such that the amount of movement is associated with the variation of suction, but will be difficult to determine during practice.

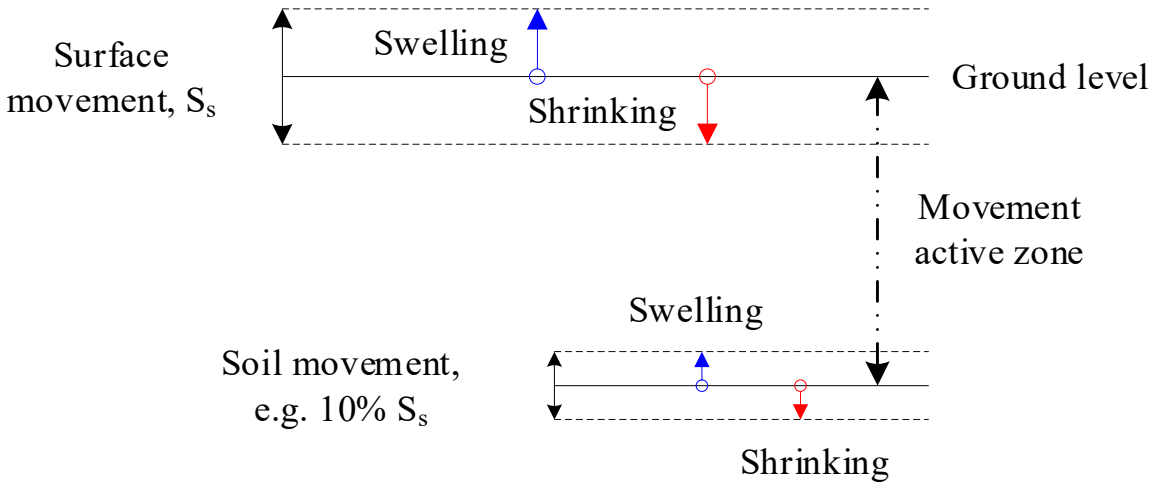

Figure 7.27 Alternation of movement active zone definition

7.4. An Application of the Simulation: A Remedial Solution, the Replacement Curve

With the assistance of numerical tools, it is possible to investigate the systematical influence due to the different material parameters to explore the surface movement under various scenarios, such as different weather conditions. It is also possible to study the remedial solution caused by the SSS movement. There are varies methods can help to eliminate the damage of SSS movement such as foundation with additional stiffness (Figure 7.28), chemical method, geosynthetic, or a replacement the SSS with non-expansive soil. In this section, by using the numerical tools, we investigated the relationship between the replacement depth vs. the surface movement. By the criterion of the design, such relationship can provide the most economical solution to the replacement depth, which refers to the optimum replacement depth.

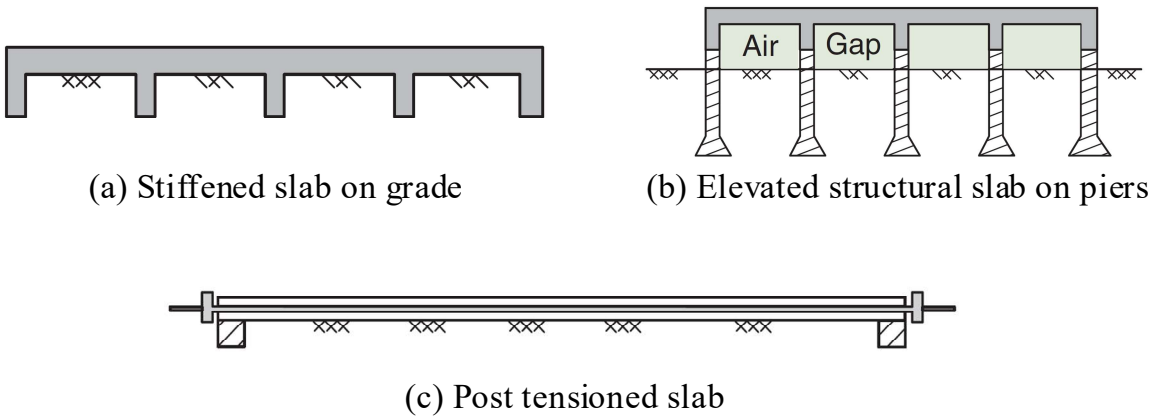

Figure 7.28 Types of foundations used on shrink-swell soils (After Briaud, 2013)

The simulation procedure follows the initial condition discussed in 7.3.1 As discussed previously, the weather combination with start of wet season, with a period of rainy then followed by sunny days will provide a deeper active zone. For conservative purpose, the soil mass subjected to experience 7-day wetting period, following by 1-day ramping, then 25-day drying period.

In Figure 7.29, (a) presents the soil movement with identical shrink-swell soil calibrate throughout entire soil profile. (b) presents the soil movement with the first 0 to 0.23m replaced by non-expansive soil. The reason adopted 0.23m here is the deepest suction active zone determined by analytical profile is 4.6m, and 0.23m is 5% of maximum active zone. And to see how the movement varies as different replacement, (c) to (g) are vertical movement with the replacement of 0.46m (10% of the maximum active zone), 1.15m (25%), 2.3m (50%), 3.45m (75%) and 4.6m (entirely replaced). Also, it should be noticed that the scales on the figures are not identical to catch enough information for small variation.

In Figure 7.29 (a), as the wetting process happened after wet profile, the soil swells a tiny amount compared with later methods, as presented in the blue color. Later, the surface suction increase to the value of dry weather. The movement does not have time to fully develop but turns to shrink. In this step, it can be observed that soil experiencing both shrinkage and swelling simultaneously, mainly because some of the flux from the wet cycle still penetrates the soil leading a swelling behavior, while the flux within the shallow zone is forced to leave due to the dry period and causing a shrinking behavior. Such profile present in green color in the figure.

The red line in the figure represents the movement profile after 25-day dry, which shows a significant shrink at the end of the dry period. Some of the practical methods designing slab-on-grade, e.g. (BRAB, 1968), consider only swelling behavior of the soil and foundation design is

based on resisting upward movement of soil. Others methods e.g. (Standards Association of Australia, 2011), consider the total movement consider the gross movement. More attentions are needed as the foundation behavior on shrinking or swelling are different. The gross movement for the full shrink-swell soil case is 13.94mm.

Figure 7.29 (b) present the results with first 5% shrink-swell soil replaced by non-shrink-swell soil. The swelling behavior due to further wetting procedure is further smaller compared to Figure 7.29 (a) and so as the ramping movement behavior. A significantly movement reduction is observed from the 0 to 0.23m. This implies the replacement of the top surface soil tremendously improves the soil condition. Figure 7.29 (c) and (d) are in similar condition with 10% and 25% of shrink-swell soil within suction active zone being replaced thus the behavior is not described repeatedly.

Begin with Figure 7.29 (e) and follows, at the end of dry weather the overall movement behaves swell. As the replacement depth becomes deeper, suction variation at ground surface has less impact to the deeper soil. However, the soil mass still responding to the initial wet period and the permeability is low but maintain constant. Thus, the soil mass behaves an overall swelling at this point. The replacement depth that isolate the soil from ground surface suction variation may be a practical value to reduce the damage of shrink-swell soil, however, the soil will still move due to the weather behavior at the beginning. Similar results are observed for (f) and (g) thus not going to repeatedly describe.

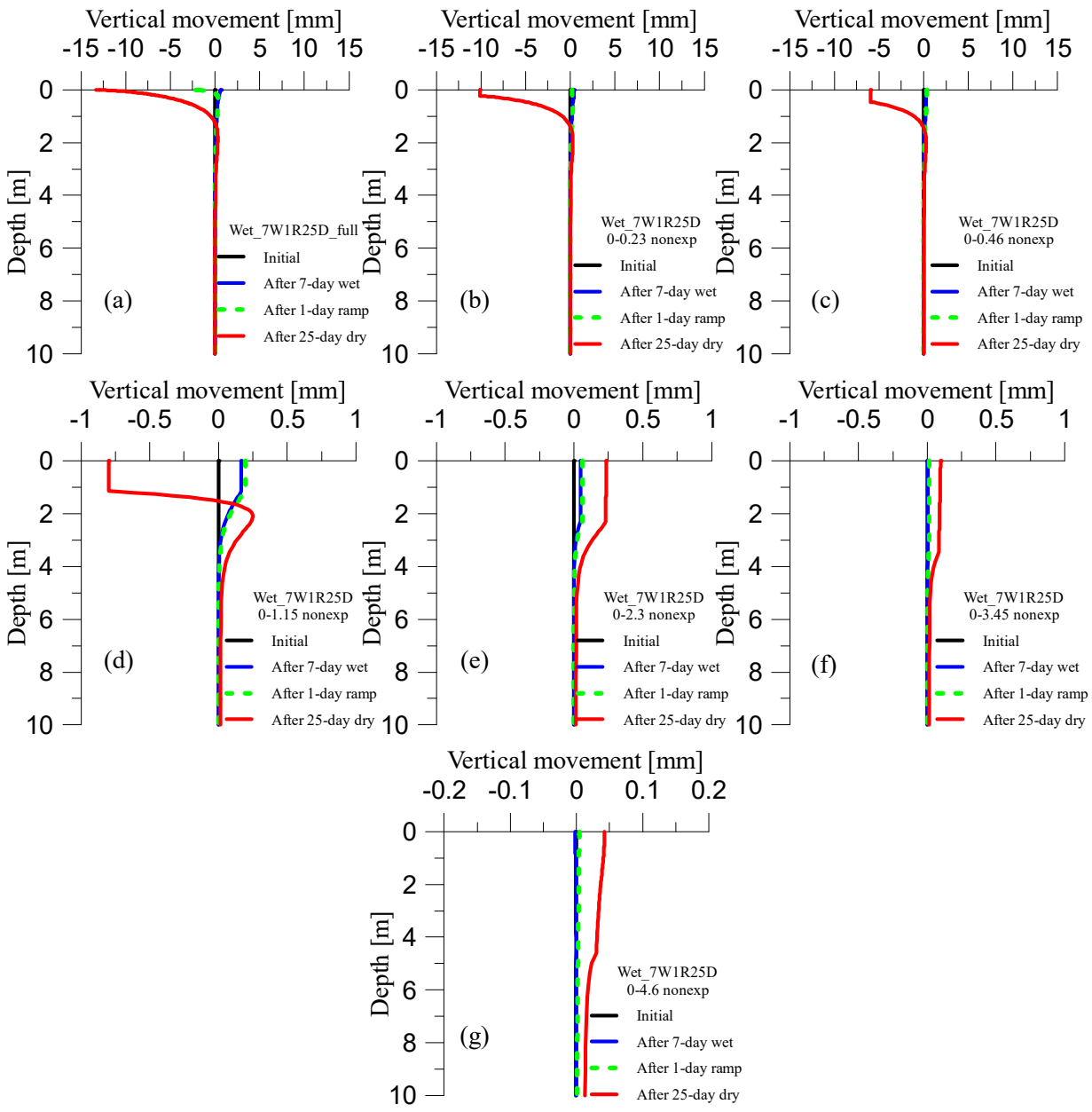

Figure 7.29 Movement variation under different wet-dry combinations starting from wet weather. (a) soil body with full shrink-swell soil. (b) 0-0.23m soil replaced (c) 0-0.46m soil replaced (d) 0-1.15m soil replaced (e) 0-2.3m soil (f) 0-3.45m soil replaced (g) 0-4.6m soil replaced

Similarly, Figure 7.30 presents the result of movement profile start from dry weather. Compared Figure 7.29 (a) and Figure 7.30 (a), the swelling movement is much more significant in later as the initial condition is dry instead of wet; the movement in the shrinking direction is smaller in later as the soil mass need to neutralize the amount of swelling from in pervious steps. Start from (b), top shrink-swell soil is replaced by non-shrink-swell soil. The surface movement is significantly reduced.

A significantly difference in (g) between case start from wet and dry is observed. In the case start from wet, the permeability is higher than the start from dry case. Thus, the movement profile is more sensitive to the suction variation in the start from wet condition to the start from dry condition. However, the swelling behavior at the end of 7-day wet is not significant in the start from wet case but obviously in the start from dry case under the same scale. It is because the suction change from start from wet condition to wet season is much smaller than start from dry condition. Finally, because of the permeability for start from dry condition is significantly smaller than start from wet condition, the suction was “trapped” in the middle of the soil mass and thus the delay of suction distribution leads to the non-uniform pattern.

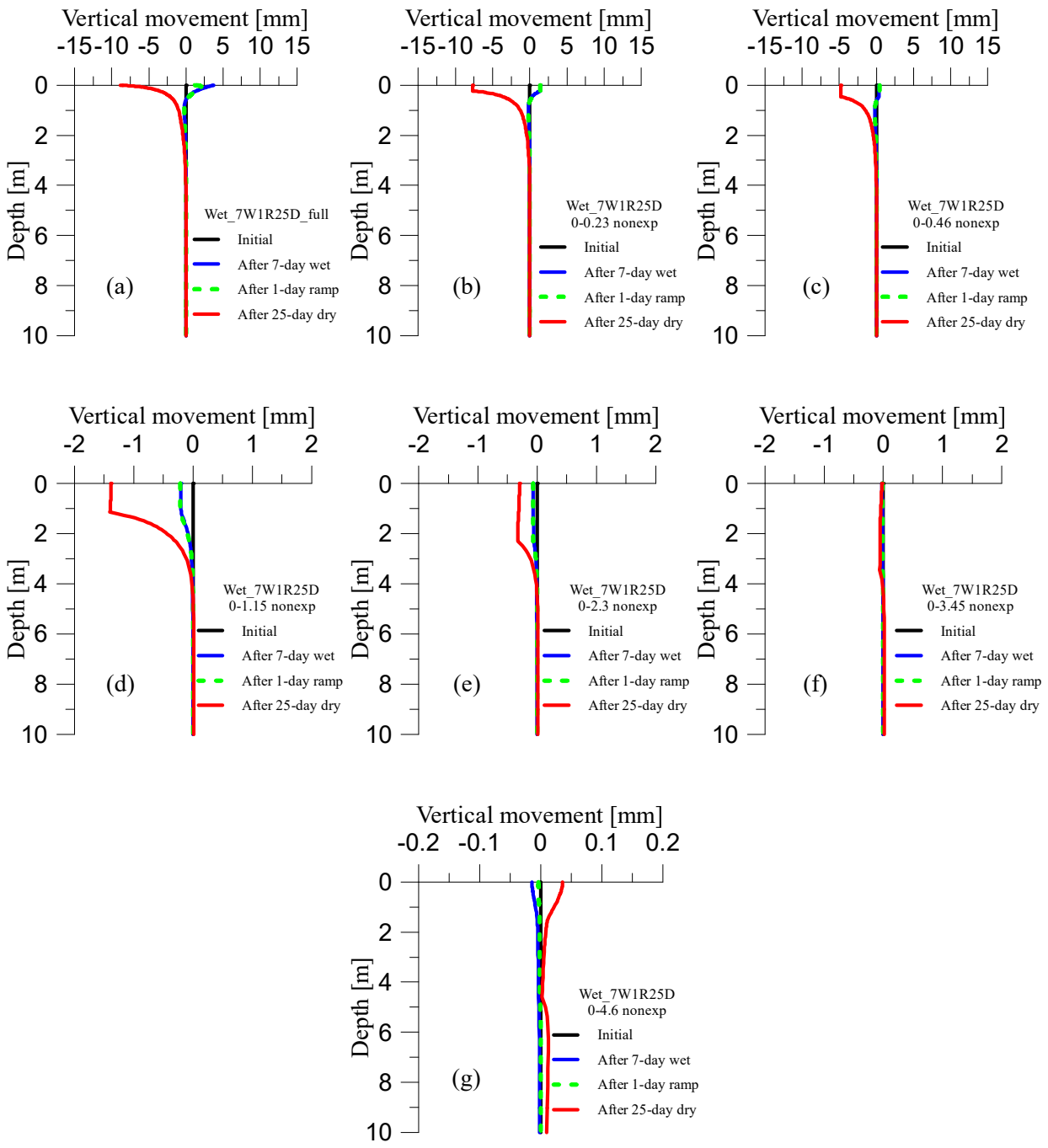

Figure 7.30 Movement variation under different wet-dry combinations starting from dry weather (a) soil body with full shrink-swell soil. (b) 0-0.23m soil replaced (c) 0-0.46m soil replaced (d) 0-1.15m soil replaced (e) 0-2.3m soil (f) 0-3.45m soil replaced (g) 0-4.6m soil replaced

The relation between the surface movement and soil replacement depth is presented in Figure 7.31. (a) is the surface movement vs. the corresponding shrink-swell soil replaced by non-shrink-swell soil and (b) is the surface movement normalized by the movement when no soil being replaced. Due to the high permeability, the surface movement in the case start from wet is higher than the case starts from dry weather. When normalized the surface movement, a similar relationship between surface movement and replacement depth is observed for both start from wet and dry condition. At this point, it can be concluded that it is possible to establish a direct relationship between the surface movement and replacement depth to obtain an optimized replacement zone for a practical case regardless of the influence of initial condition.

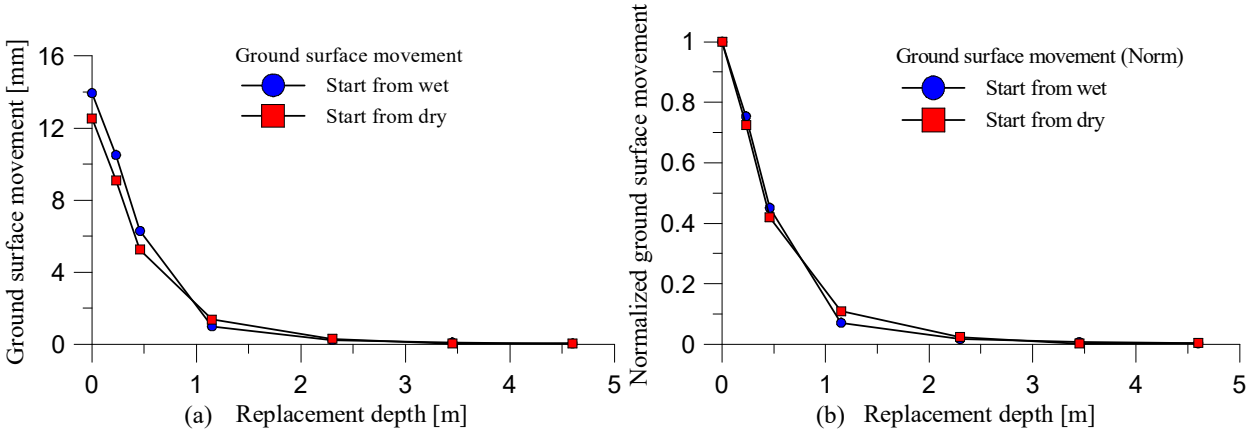

Figure 7.31 Summary of surface movement vs. replacement depth (a) surface movement with replacement depth. (b) surface movement normalized by 0 replacement vs. replacement depth

8. ACTIVE ZONE DETERMINATION VIA EMPIRICAL METHOD

8.1. Introduction

Because of the significant damage to the lightweight structure, the geotechnical industry conducted extensive efforts to deal with the shrink-swell soil movement problem. In the meantime, engineers gained a lot of experience. In this section, the experience of active zone determination within Texas is collected among the member of CERGEP (Consortium for Education and Research in Geo-Engineering Practice) at Texas A&M University, who are experienced Geotechnical consultant companies. The result of the collection will imply the first assumption for the design value of the depth of active zone.

8.2. Survey Design and Results

To collect the most updated data, the top 40 most populated cities are selected as the target cities included in the survey distributed to the members. The location of the towns presents in Figure 8.1.

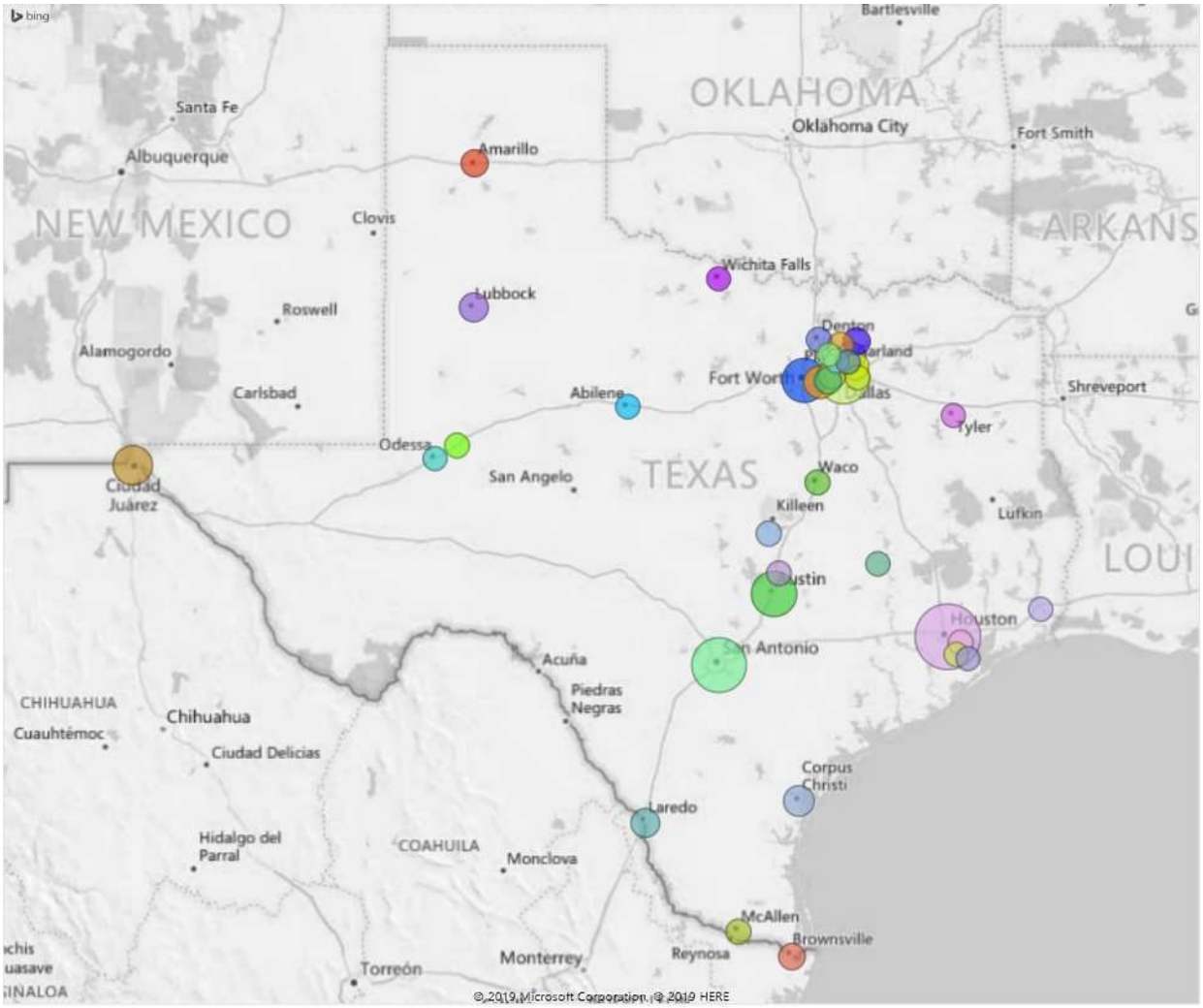

Figure 8.1 Population among 40 cities in Texas

The results of the survey are presented in Table 8.1 with cities listed in alphabetical order. Nine companies (Com in the Table) replied to the survey. The depth of active zone quoted by the respondents was given either according to water content variation measurement over a period (marked in orange in Table 1) and according to local experience (marked in gray in Table 1. The range and averaged value for each city are also presented in Table 8.1.

Table 8.1 Result of anonymous survey of the depth of active zone [m]

Cities	Com.1	Com.2	Com.3	Com.4	Com.5	Com.6	Com.7	Com.8	Com.9	Range [m]	Avg. [m]
Abilene				9.1						9.1	9.1
Allen				4.6	3.0			3.0		3.0 to 4.6	3.6
Amarillo				9.1						9.1	9.1
Arlington				4.6	3.0	4.6	3.7	3.7	3.0	3.0 to 4.6	3.8
Austin	3.0			4.6			3.7		4.6	3.0 to 4.6	4.0
Beaumont		2.1	3.7	2.1			2.4	2.4	2.1	2.1 to 3.6	2.5
Brownsville	1.5			4.6					2.4	1.5 to 2.4	2.8
Carrollton				4.6	6.1	6.1		3.7	3.0	3.0 to 6.1	4.7
College Station	3.0			4.6			3.7		4.6	3.0 to 4.5	4.0
Conroe		2.4		2.1			2.4		3.0	2.4 to 3.0	2.5
Corpus Christi	2.1		3.7	3.7			3.0		2.4	2.1 to 3.7	3.0
Dallas	2.4			4.6	6.1	4.6	3.7	3.7	3.0	2.4 to 6.1	4.0
Denton				4.6			3.7	3.0	3.0	3.0 to 4.6	3.6
El Paso				9.1					4.6	4.6 to 9.1	6.9
Fort Worth	2.4			4.6	3.0	4.6	3.7	3.7	3.0	2.4 to 4.6	3.6
Frisco				4.6	6.1		3.7	4.6	3.0	3.0 to 6.1	4.4
Garland				4.6	3.0		3.7	3.7	3.0	3.0 to 4.6	3.6
Grand Prairie				4.6	3.0	6.1	3.7	3.0	3.0	3.0 to 6.1	3.9
Houston	3.0	2.4	3.7	2.1			2.4	3.7	3.0	2.1 to 3.7	2.9
Irving				4.6	6.1	7.6	3.7	4.6	3.0	3.0 to 7.6	4.9
Killeen				4.6			3.7		4.6	3.7 to 4.6	4.3
Laredo				3.7					3.0	3.0 to 3.7	3.4
League City	3.0	2.1	3.7	2.1			2.4		2.1	2.1 to 3.7	2.6
Lewisville				4.6	3.0	4.6	3.7	3.7	3.0	3.0 to 4.6	3.8
Lubbock				9.1			3.7		4.6	3.7 to 9.1	5.8
McAllen				3.7					2.4	2.4 to 3.7	3.0
McKinney				4.6	3.0		3.7		4.6	3.0 to 4.6	4.0
Mesquite				4.6	4.6	4.6	3.7	3.7		3.7 to 4.6	4.2
Midland				9.1					4.6	4.6 to 9.1	6.9
Odessa				9.1					4.6	4.6 to 9.1	6.9
Pasadena		2.1	3.7	2.1			2.4	2.4	2.1	2.1 to 3.7	2.5
Pearland		2.1	3.7	2.1			2.4		2.1	2.1 to 3.7	2.5
Plano				4.6	2.4		3.7	4.6	3.0	2.4 to 4.6	3.7
Richardson				4.6	2.4		3.7	3.7	3.0	2.4 to 4.6	3.5
Round Rock				4.6		4.6	3.7		4.6	3.7 to 4.6	4.3
San Angelo				9.1					4.6	4.6 to 9.1	6.9
San Antonio	4.6			9.1		6.1	3.7		4.6	3.7 to 9.1	5.6
Tyler				2.1			2.4			2.1 to 2.4	2.3
Waco				4.6			3.7			3.7 to 4.6	4.1
Wichita Falls				4.6						4.6	4.6

Variation of water content

Local experience

As can be seen, most of the responses are based on local experience. Company 1 and 9 provided their responses based on water content measurement, and these depths of active zone turn out to have shallower values compared to the values based on experience with an average value of 2.8m. Company 4 provides the most conservative estimates, with an average value of 5m. In general, the average value of the depth of the active zone in Texas is 4.6m, and the distribution of the active zone is shown in Figure 8.2

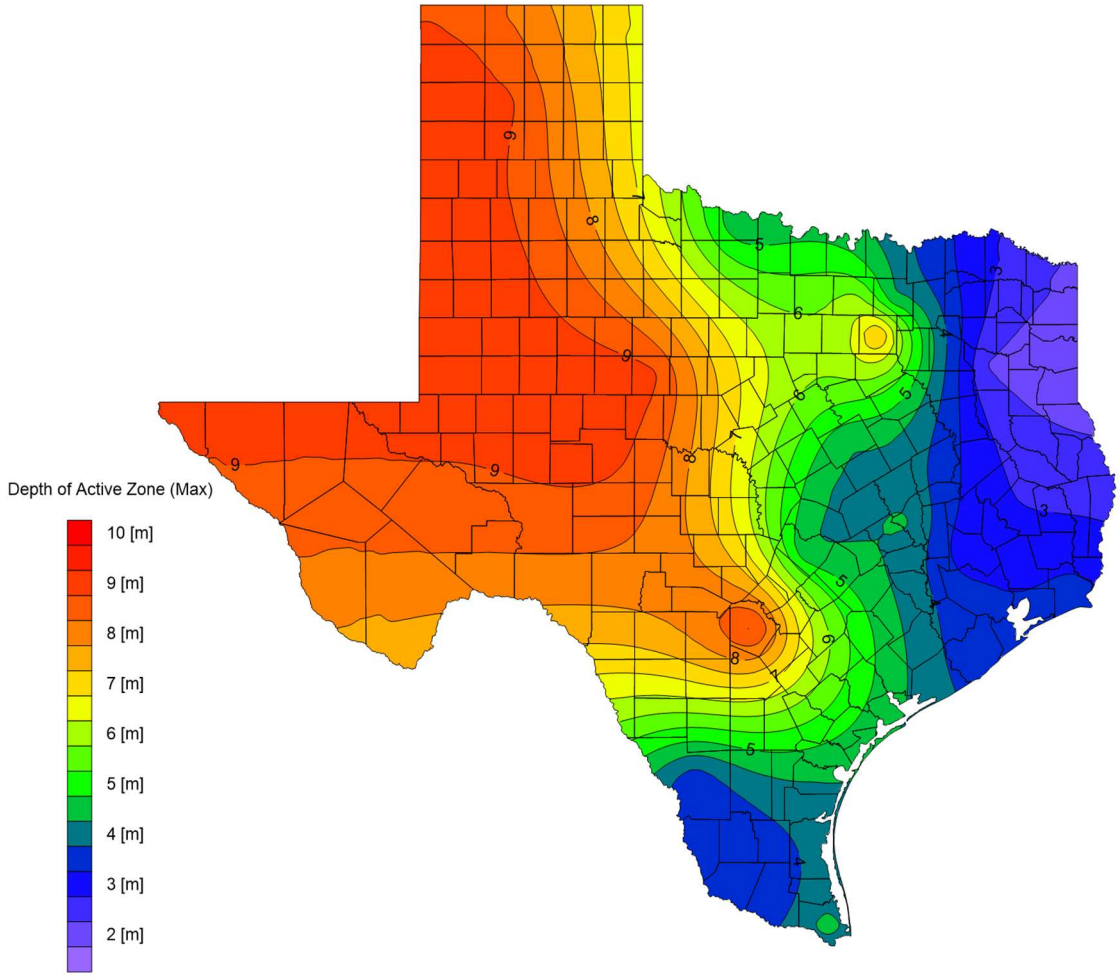

(a)

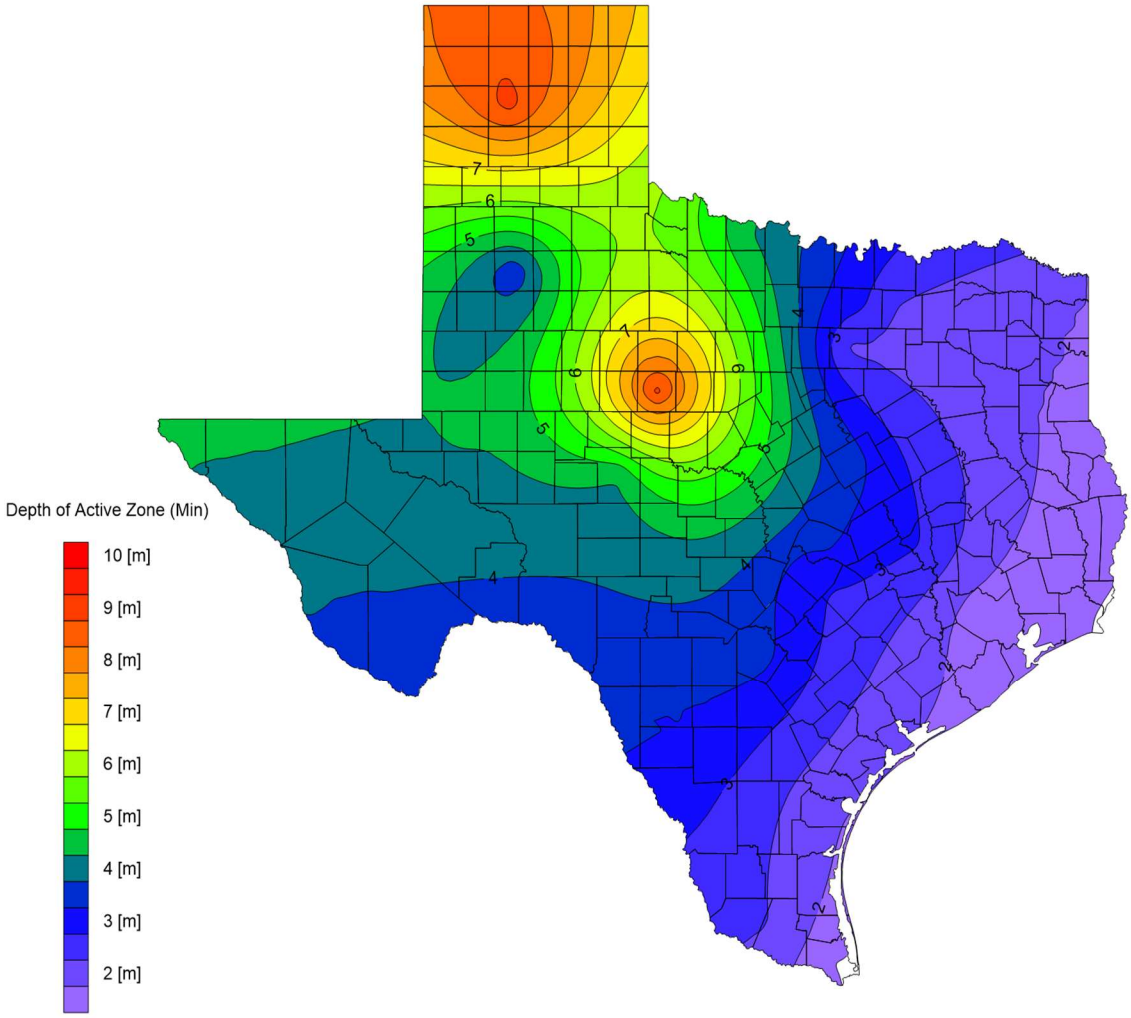

(b)

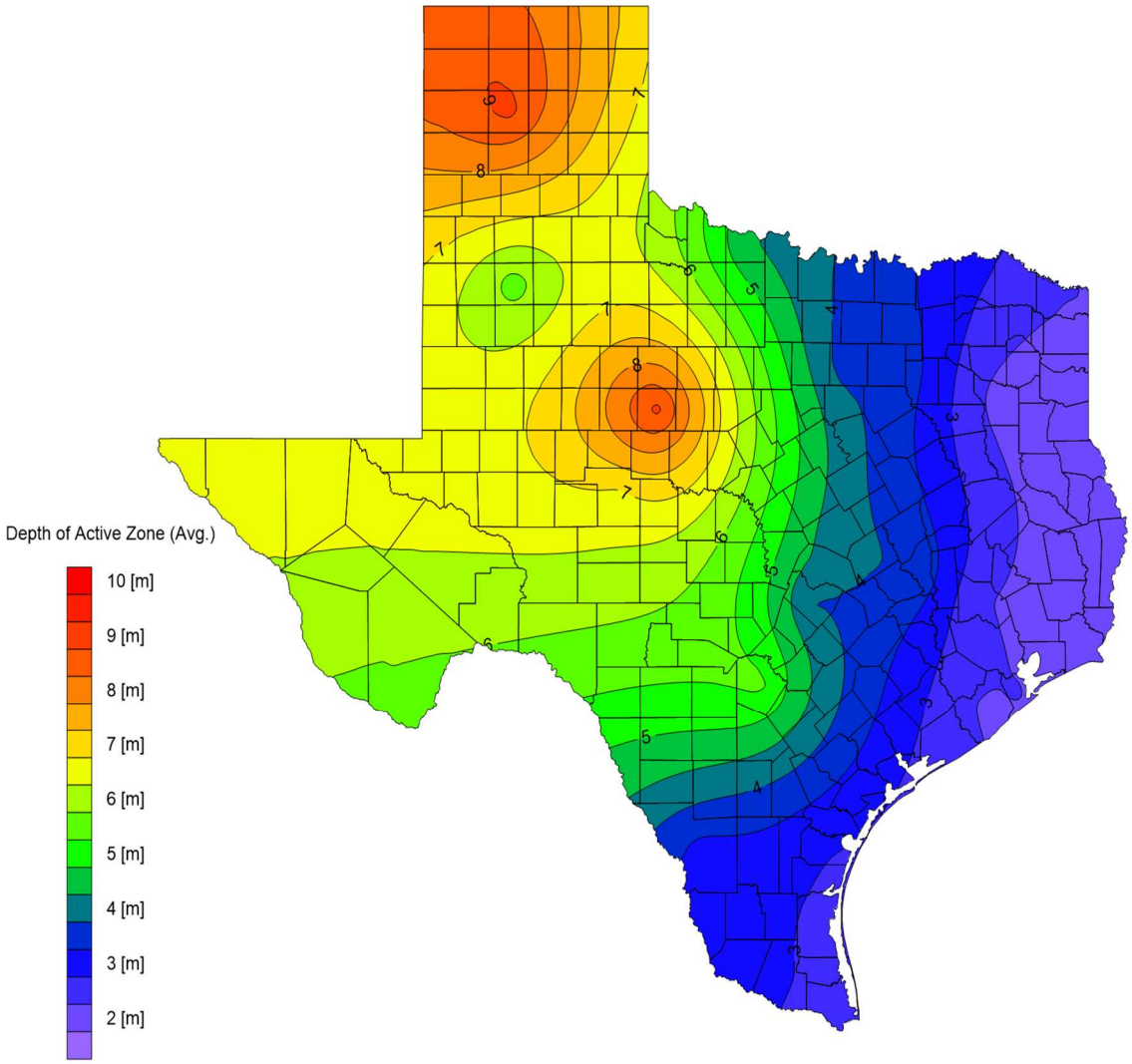

(c)

Figure 8.2 Distribution of depth of active zone in Texas (a) Maximum replied value. (B) Minimum replied value. (c) Averaged replied value

The distribution tends to increase from east to west and from coastline to land. When superposing Figure 8.2 on top of the Thornthwaite moisture index (TMI) of Texas (PTI, 2004) in Figure 8.3, the areas considered as wet (TMI>0) have a shallower depth of active zone. On the

contrary, the areas considered dry (TMI<0) have deeper depth of active zone. A possible explanation for this difference is that the dry areas have the ability to form much deeper cracks thereby allowing for the deep and rapid infiltration of water to penetrate the soil mass.

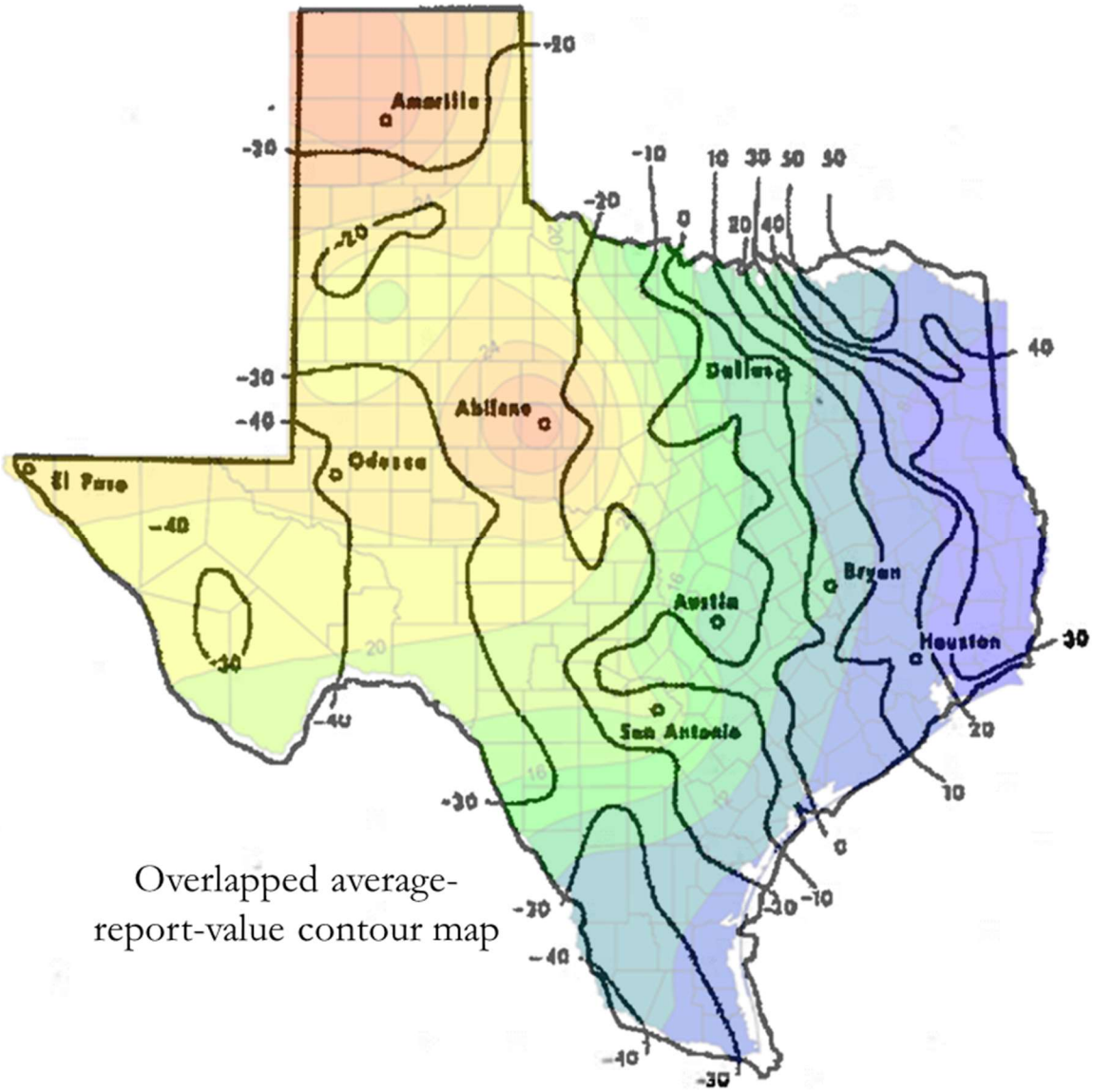

Figure 8.3 Distribution of active zone and TMI (overlapping)

The Australian method proposes to relate the Thornthwaite Moisture Index (TMI) to the depth of the active zone. The TMI is an index representing the difference between the precipitation and the evaporation at a site. A TMI value of -40 implies that the precipitation is much lower than the evaporation, in which the soil mass is very dry and likely with cracks. In this weather condition, precipitation may induce a deep-water content variation within the soil and lead to a deep active zone. This conclusion agrees with the result in Figure 8.3. A comparison between the AS 2870 recommendation for the depth of active zone relative to the TMI value and the value obtained from Figure 8.3 are listed in Table 8.2.

Table 8.2 Comparison between recommended depths of active zone by Australian method and survey results

TMI	**AS 2870**	**Survey Value**
--	H_s [m]	Z_a [m]
10 to 40	1.5	2.7
-5 to 10	1.8	3.0
-15 to -5	2.4	4.0
-25 to -15	3.0	6.1
-40 to -25	4.0	9.1
≤ -40	> 4.0	> 9.1

Table 8.2 implies that the active zone consideration in Texas is deeper than the correction results in Australia. Thus, the estimation of the active zone needs to be more careful with both conservative and economic purposes.

9. CONCLUSIONS

Because of the significant damage related to the shrink-swell soils movements, numerous works have been conducted to seek an advanced understanding of such problems. The depth of active zone is found to be an important factor for the SSS problem but without a clear way to be determined. The importance of the active zone is similar to the zone of influence, which indicates the depth of soil subjected to move under certain conditions. A well determined active zone benefits a better-estimated surface movement and further provide a more economical solution to the foundation design.

This work quantitatively defines the depth of active zone by refereeing to the accuracy of the measurement instrument. Such a definition provides a practical solution to describe the depth of active zone either during the in-situ condition or in the simulation process later in this work. However, the criterion proposed in this work subjected to be modified in the future, as the sensitivity might be too high for a practical project.

The permeability, the history of weather and the depth of water table are three parameters we are interested in the DAZ development. The determination of the weather history provides a 100-year designed event for the DAZ development. And the variation of the permeability and the water table helps to establish the design curve to correlative the corresponding value versus the DAZ.

The adoption of the FEM code CODE_BRIGHT provides the fully coupled analysis of the hydraulically and mechanical behavior of the SSS problem and to estimate the development of the DAZ. In conjunction with the weather history, the simulation result agrees with the value of local experience. The agreement implies that by providing the proper soil properties and estimation of the weather history, the numerical tools can provide a good estimation of the DAZ. Such a result may improve the design of the foundation against the SSS movement during the design steps and help provide a reference value for the remedial solution, such as a depth of SSS replacement to reduce the SSS movement.

REFERENCES

Abdelmalak, R. (2007). *Soil Structure Interaction for Shrink-Swell Soils " A New Design Procedure for Foundation Slabs on Shrink-Swell Soils"* (Issue December). College Station, Texas, Texas A&M University, 2007.

Abdelmalak, R., & Briaud, J.-L. (2017). Performance of stiffened slab-on-grade foundation on shrink-swell soils: Case study of the Ellison Office Building, College Station, Texas. *Journal of Performance of Constructed Facilities*. https://doi.org/10.1061/(ASCE)CF.1943-5509.0000978

Abiddin Erguler, Z., & Ulusay, R. (2003). A simple test and predictive models for assessing swell potential of Ankara (Turkey) Clay. *Engineering Geology*. https://doi.org/10.1016/S0013-7952(02)00205-3

Adem, H., & Vanapalli, S. (2016). Soil–environment interactions modelling for expansive soils. *Environmental Geotechnics*. https://doi.org/10.1680/envgeo.13.00089

Aitchison, G. D., & Martin, R. (1973). The Quantitative Description of the Stress-Deformation Behaviour of Expansive Soils; 2: A Membrane Oedometer for Complex Stress-Path Studies in Expansive Clays. *Proceedings of the 3rd International Conference on Expansive Soils, Haifa*, Vol.2, pp. 83–88.

Alonso, E. E., Gens, A., & Hight, D. (1987). Special problem soils. General report. *9th European Conf. on Soil Mechanics and Foundation Engineering*, 1087–1146.

Alonso, E. E., Gens, A., & Josa, A. (1990). A constitutive model for partially saturated soils. *Géotechnique*, *40*(3), 405–430.

ASTM. (2017). *Standard Test Methods for Liquid Limit, Plastic Limit, and Plasticity Index of Soils* (No. D4318-17e1). https://doi.org/https://doi.org/10.1520/D4318-17E01

ASTM. (2019). *Standard Test Method for Expansion Index of Soils* (No. D4829-19; D4829-19). https://doi.org/10.1520/D4829-19

Aubeny, C. P., & Long, X. (2007). Moisture diffusion in shallow clay masses. *Journal of Geotechnical and Geoenvironmental Engineering*. https://doi.org/10.1061/(ASCE)1090-0241(2007)133:10(1241)

Aubeny, C. P., & Lytton, R. L. (2004). Shallow slides in compacted high plasticity clay slopes. *Journal of Geotechnical and Geoenvironmental Engineering*. https://doi.org/10.1061/(ASCE)1090-0241(2004)130:7(717)

Bear, J. (2013). *Dynamics of fluids in porous media*. Courier Corporation.

Blight, G. E. (1997). Interactions between the atmosphere and the earth. *Géotechnique*, *47*(4), 715–767.

BRAB, B. R. A. B. (1968). Criteria for Selection and Design of Residential Slabs-on-Ground. In National Research Council (U.S.). Building Research Advisory Board (Ed.), *Criteria for Selection and Design of Residential Slabs-on-Ground*. National Academy of Sciences. https://doi.org/10.17226/9804

Briaud, J.-L. (2013). Geotechnical Engineering: Unsaturated and Saturated Soils. In *Geotechnical Engineering* (pp. 46–62). John Wiley & Sons. https://doi.org/10.1002/9781118686195

Briaud, J.-L., Zhang, X., & Moon, S. (2003). Shrink test-water content method for shrink and swell predictions. *Journal of Geotechnical and Geoenvironmental Engineering*, *129*(7), 590–600. https://doi.org/10.1061/(ASCE)1090-0241(2003)129:7(590)

Cantillo, V., Mercado, V., & Pájaro, C. (2017). Empirical Correlations for the Swelling Pressure of Expansive Clays in the City of Barranquilla, Colombia. *Earth Sciences Research Journal*. https://doi.org/10.15446/esrj.v21n1.60226

Chen, F. H. (1975). Foundations on Expansive Soils. In F. H. CHEN (Ed.), *Foundations on Expansive Soils* (12th ed., Vol. 12). Elsevier. https://doi.org/https://doi.org/10.1016/B978-0-444-41393-2.50002-8

Chiu, C. F., & Ng, C. W. W. (2003). A state-dependent elasto-plastic model for saturated and unsaturated soils. *Geotechnique*. https://doi.org/10.1680/geot.2003.53.9.809

Çimen, Ö., Keskin, S. N., & Yıldırım, H. (2012). Prediction of Swelling Potential and Pressure in Compacted Clay. *Arabian Journal for Science and Engineering*. https://doi.org/10.1007/s13369-012-0268-4

Cojean, R. (2007). Amer Ali Al-Rawas and Mattheus F. A. Goosen (eds.): Expansive soils. Recent advances in characterization and treatment. *Bulletin of Engineering Geology and the Environment*, *66*(4), 505–505. https://doi.org/10.1007/s10064-007-0102-5

Covar, A. P., & Lytton, R. L. (2001). Estimating soil swelling behavior using soil classification properties. In *Expansive Clay Soils and Vegetative Influence on Shallow Foundations* (pp. 44–63).

Cui, Y. J., & Delage, P. (1996). Yielding and plastic behaviour of an unsaturated compacted silt. *Geotechnique*. https://doi.org/10.1680/geot.1996.46.2.291

Decagon Devices, I. (2007). *WP4 Dewpoint PotentiaMeter Iperator's Manual* (5th ed.). http://www.ictinternational.com/content/uploads/2017/04/WP4-Operators-Manual.pdf

Dedier, G. (1973). Prediction of potential and swelling pressure of soils. *Proceeding of 8th International Society for Soil Mechanics and Foundation Engineering*, *22*, 1–20.

Dhowian, A. W. (1992). Soil Suction-Potential Model. *Journal of Geotechnical Engineering*, *118*(4), 521–539.

Driscoll, R. M. C., & Crilly, M. S. (2000). *Subsidence damage to domestic buildings: Lessons learned and questions remaining*. CRC.

Durkee, D. B. (2000). *Active zone and edge moisture variation distance in expansive soils*. Dissertation submitted in partial requirement for the Ph. D. Degree ….

El Mountassir, G. (2011). *Behaviour of a collapsible structured unsaturated fill material*. University of Strathclyde.

Erzin, Y. (2004). Correlations for quick prediction of swell pressures. *Electronic Journal of Geotechnical Engineering*.

Erzin, Y., & Erol, O. (2007). Swell pressure prediction by suction methods. *Engineering Geology*. https://doi.org/10.1016/j.enggeo.2007.04.002

Fityus, S. G., & Smith, D. W. (1998). A simple model for the prediction of free surface movements in swelling clay profiles. *The 2nd International Conferene on Unsaturated Soils*, 473–478.

Fredlund, D. G. (1983). Prediction of ground movements in swelling clays. In *Annual Soil Mechanics and Foundation Engineering Conference*.

Fredlund, D. G., Hasan, J. U., & Filson, H. L. (1980). The prediction of total heave. *The 4th International Conference on Expansive Soils*, 1–11.

Fredlund, D. G., & Rahardjo, H. (1993). Soil Mechanics for Unsaturated Soils. In *Soil Mechanics for Unsaturated Soils*. https://doi.org/10.1002/9780470172759

Fredlund, D. G., Rahardjo, H., & Fredlund, M. D. (2012). Unsaturated Soil Mechanics in Engineering Practice. In *Unsaturated Soil Mechanics in Engineering Practice*. https://doi.org/10.1002/9781118280492

Gilman, J. R., & Kazemi, H. (1983). Improvements in simulation of naturally fractured reservoirs. *Society of Petroleum Engineers Journal*, *23*(04), 695–707.

Houston, W. N., & Nelson, J. D. (2012). The state of the practice in foundation engineering on expansive and collapsible soils. *Geotechnical Special Publication*. https://doi.org/10.1061/9780784412138.0023

ISO. (2017). *18674-3: Geotechnical investigation and testing — Geotechnical monitoring by field instrumentation — Part 2: Measurement of displacements along a line: Extensometers*.

Jayasekera, S., & Mohajerani, A. (2003). Some relationships between shrink-swell index, liquid limit, plasticity index, activity and free swell index. *Australian Geomechanics Journal*, *38*(2), 53–58.

Jennings, J. E., & Knight, K. (1957). The prediction of total heave from the double oedometer test. *Transactions of the South African Institution of Civil Engineers*, *7*(9), 285–291.

Johnson, L D. (1973). Influence of suction on heave of expansive soils, Miscellaneous paper S-73-17. *US Army Engineers Waterways Exp. Station, Vicksburg, MS, USA*.

Johnson, Lawrence D. (1977). EVALUATION OF LABORATORY SUCTION TESTS FOR PREDICTION OF HEAVE IN FOUNDATION SOILS. *Tech Rep US Army Eng Waterw Exp Stn S-77-7*.

Johnson, Lawrence D., & McAnear, C. L. (1973). Controlled field tests of expansive soils. *Publication of: Wyoming University*, *1*(Workshop Proceedings).

Jones Jr, D., & Holtz, W. (1973). Expansive soils - The hidden disaster. *Civil Engineering*, *43*(8), 49–51.

Jones, L. D., & Jefferson, I. (2012). *Expansive soils*.

Kayabali, K., & Yaldiz, Ö. (2014). Estimation of swelling pressure using simple soil indices. *Bulletin of the Mineral Research and Exploration*. https://doi.org/10.19111/bmre.83986

Kazemi, H., & Gilman, J. R. (1993). Multiphase flow in fractured petroleum reservoirs. *Flow and Contaminant Transport in Fractured Rock*, 267–323.

Komornik, A., & David, D. (1969). Prediction of swelling pressure of clays. *J. Soil Mech. Found. Div., Am. Soc. Civ. Eng.;(United States)*, *95*.

Lu, N. (2020). Unsaturated Soil Mechanics: Fundamental Challenges, Breakthroughs, and Opportunities. *Journal of Geotechnical and Geoenvironmental Engineering*, *146*(5), 2520001.

Lu, N., & Dong, Y. (2017). Correlation between soil-shrinkage curve and water-retention characteristics. *Journal of Geotechnical and Geoenvironmental Engineering*. https://doi.org/10.1061/(ASCE)GT.1943-5606.0001741

Lu, N., & Likos, W. J. (2006). Suction stress characteristic curve for unsaturated soil. *Journal of Geotechnical and Geoenvironmental Engineering*. https://doi.org/10.1061/(ASCE)1090-0241(2006)132:2(131)

Lytton, R. L. (1999). Expansive Soils Problems and Practice in Foundation and Pavement Engineering John D. Nelson and Debora J. Miller, Wiley, New York, 1992, 259 pp. *International Journal for Numerical and Analytical Methods in Geomechanics*. https://doi.org/10.1002/(sici)1096-9853(19990825)23:10<1067::aid-nag994>3.0.co;2-e

Lytton, R. L. (1997). Engineering structures in expansive soils. *Proc., 3rd Int. Symp. on Unsaturated Soils*, 333–354.

Lytton, R. L. (1994). Prediction of movement in expansive clays. *Geotechnical Special Publication*, *2*(40), 1827–1845.

Lytton, R. L., Bulut, R., Aubeny, C. P., Sood, E., & Thakur, A. (2006). *Evaluation of a Diffusion Coefficient for Design of Pavements on Expansive Soils*.

Malvern, L. E. (1969). *Introduction to the Mechanics of a Continuous Medium* (Issue Monograph).

McCloskey, G., Sánchez, M., & Romero, E. (2010). Characterisation, mechanical and microstructural behaviour of an unsaturated silt. *Unsaturated Soils: Theoretical and Numerical Advances in Unsaturated Soil Mechanics - Proceedings of the 4th Asia Pacific Conference on Unsaturated Soils*.

McDowell, C., Herner, R. C., & Wooltorton, F. L. (1956). Interrelationship of Load, Volume Change, and Layer Thicknesses of Soils to the Behavior of Engineering Structures. *Highway Research Board Proceedings*, *35*.

McKeen, R. G., & Johnson, L. D. (1990). Climate-controlled soil design parameters for mat foundations. *Journal of Geotechnical Engineering*. https://doi.org/10.1061/(ASCE)0733-9410(1990)116:7(1073)

McKeen, R. G., & Nielsen, J. P. (1978). *Characterization of Expansive Soils for Airport Pavement Design.* NEW MEXICO UNIV ALBUQUERQUE ERIC H WANG CIVIL ENGINEERING RESEARCH FACILITY.

Mitchell, P. W. (1979). The structural analysis of footings on expansive soil. *Expansive Soils*, 438–447.

Nelson, J. D., Durkee, D. B., & Bonner, J. P. (1998). Prediction of free field heave using oedometer test data. *Proc. 46th Annual Geotechnical Engineering Conference, University of Minnesota, St. Paul, MN. February*, *2*.

Nelson, J. D., Durkee, D. B., Reichler, J. D., & Miller, D. J. (1994). Moisture Movement and Heave Beneath Simulated Foundation Slabs on Expansive Soils. *Prepared for US Army Corps of Engrs. by Civil Engr. Dept., Colorado State University*.

Nelson, J. D., & Miller, D. J. (1997). *Expansive soils: problems and practice in foundation and pavement engineering*. John Wiley & Sons.

Nelson, J. D., Overton, D. D., & Durkee, D. B. (2001). Depth of wetting and the active zone. In *Expansive clay soils and vegetative influence on shallow foundations* (pp. 95–109).

Nelson, J. D., Thompson, E. G., Schaut, R. W., Chao, K. C., Overton, D. D., & Dunham-Friel, J. S. (2012). Design procedure and considerations for piers in expansive soils. *Journal of Geotechnical and Geoenvironmental Engineering*. https://doi.org/10.1061/(ASCE)GT.1943-5606.0000647

Ng, C. W. W., Zhan, L. T., Bao, C. G., Fredlund, D. G., & Gong, B. W. (2003). Performance of an unsaturated expansive soil slope subjected to artificial rainfall infiltration. *Geotechnique*, *53*(2), 143–157.

NOAA. (2019). *Daily Summaries Station Details in College Station*. https://www.ncdc.noaa.gov/cdo-web/datasets/GHCND/stations/GHCND:USW00003904/detail

Olaiz, A. H., Singhar, S. H., Vann, J. D., & Houston, S. L. (2018). Comparison and Applications of the Thornthwaite Moisture Index Using GIS. *Geotechnical Special Publication*, *2017-Novem*(GSP 302), 280–289. https://doi.org/10.1061/9780784481691.028

Olive, W. W., Chleborad, A. F., Frahme, C. W., Schlocker, J., Schneider, R. R., & Schuster, R. L. (1989). *Swelling clays Map of the Conterminous Unitedm States*.

Olivella, S., Carrera, J., Gens, A., & Alonso, E. E. (1994). Nonisothermal multiphase flow of brine and gas through saline media. *Transport in Porous Media*. https://doi.org/10.1007/BF00613282

Olivella, S., Gens, A., Carrera, J., & Alonso, E. E. (1996). Numerical formulation for a simulator (CODE_BRIGHT) for the coupled analysis of saline media. *Engineering Computations (Swansea, Wales)*. https://doi.org/10.1108/02644409610151575

Osman, N. Y., McManus, K. J., & Ng, A. W. M. (2005). Management and analysis of data for damage of light structures on expansive soils in Victoria, Australia. *Proceedings of the 1st International Conference on Structural Condition Assessment, Monitoring and Improvement: 12-14 December 2005, Perth, Western Australia*.

Panday, S., & Corapcioglu, M. Y. (1989). Reservoir transport equations by compositional approach. *Transport in Porous Media*, *4*(4), 369–393. https://doi.org/10.1007/BF00165780

Pedarla, A., Puppala, A. J., Hoyos, L. R., & Chittoori, B. (2016). Evaluation of swell behavior of expansive clays from internal specific surface and pore size distribution. *Journal of Geotechnical and Geoenvironmental Engineering*. https://doi.org/10.1061/(ASCE)GT.1943-5606.0001412

PTI. (2012). *Standard requirements for design and analysis of shallow post-tensioned concrete foundations on expansive soils* (Post-Tensioning Institute (Ed.)).

Rossen, W. R., & Kumar, A. T. A. (1992). Single-and two-phase flow in natural fractures. *SPE Annual Technical Conference and Exhibition*.

Sánchez, M., Gens, A., do Nascimento Guimarães, L., & Olivella, S. (2005). A double structure generalized plasticity model for expansive materials. *International Journal for Numerical and Analytical Methods in Geomechanics*, *29*(8), 751–787. https://doi.org/10.1002/nag.434

Sánchez, M., Gens, A., & Guimarães, L. J. N. (2012). Thermal-hydraulic-mechanical (THM) behaviour of a large-scale in situ heating experiment during cooling and dismantling. *Canadian Geotechnical Journal*. https://doi.org/10.1139/T2012-076

Schneider, G. L., & Poor, A. R. (1974). *The prediction of soil heave and swell pressures developed*

by an expansive clay. University of Texas.

Seed, H. B., Lundgren, R., Woodward, J., & Lundgren, R. (1962). Prediction of swelling potential for compacted clays. *Journal of the Soil Mechanics and Foundations Division*, *88*(3), 53–87.

Shuai, F. (1998). *Simulation of swelling pressure measurements on expansive soils.*

Skempton, A. W. (1953). The colloidal activity of clays. *Selected Papers on Soil Mechanics*, 106–118.

Snowden, W. L. (1981a). *Design of Slab-on-Ground Foundation* (Issue August). Wire Reinforcement Institute.

Snowden, W. L. (1981b). DESIGN OF SLAB-ON-GROUND FOUNDATIONS. In *Wire Reinforcement Institute* (Issue August).

Snowden, W. L. (1996). *Design of Slab-On-Ground Foundations: An UpdateDESIGN OF SLAB-ON-GROUND FOUNDATIONS: An Update* (p. 8). Wire Reinforcement Institute.

Standards Association of Australia (Ed.). (2011). *Residential slabs and footings.* Sydney, N.S.W. : Standards Australia.

Thomas, L. K., Dixon, T. N., & Pierson, R. G. (1983). FRACTURED RESERVOIR SIMULATION. *Society of Petroleum Engineers Journal*. https://doi.org/10.2118/9305-PA

Thornthwaite, C. W. (1948). An Approach toward a Rational Classification of Climate. *Geographical Review*, *38*(1), 55. https://doi.org/10.2307/210739

Tu, H., & Vanapalli, S. K. (2016). Prediction of the variation of swelling pressure and one-dimensional heave of expansive soils with respect to suction using the soil-water retention curve as a tool. *Canadian Geotechnical Journal*. https://doi.org/10.1139/cgj-2015-0222

TxDOT. (1995). Determination of Potential Veritcal Rise. In *Manual of Testing Procedrures*.

USBR, U. S. B. of R. (1998). *Earth Manual*. US Department of the Interior, Bureau of Reclamation.

Van Der Merwe, D. H. (1964). The prediction of heave from the plasticity index and percentage clay fractions of soils. *Civil Engineer in South Africa*, *6*, 103–107.

van Genuchten, M. T. (1980). CLOSED-FORM EQUATION FOR PREDICTING THE HYDRAULIC CONDUCTIVITY OF UNSATURATED SOILS. *Soil Science Society of America Journal*, *44*(5), 892–898. https://doi.org/10.2136/sssaj1980.03615995004400050002x

van Golf-Racht, T. D. (1982). *Fundamentals of fractured reservoir engineering*. Elsevier.

Vanapalli, S. K., Lu, L., & Oh, W. . (2010). Comparison between the measured and the estimated 1-D heave of expansive soils for seven case studies results using a simple technique. *63rd Canadian Geotechnical Conference & 6th Canadian Permafrost Conference*.

Vijayvergiya, V. N., & Ghazzaly, O. I. (1973). Prediction of swelling potential for natural clays. *Proceedings of the 3rd International Conference on Expansive Soils, Haifa, Israel*, *1*, 227–236.

Viyayvergiya, V. N., & Sullivan, R. A. (1973). Simple technique for identifying heave potential. *Proceedings of the Workshop on Expansive Clays and Shales in Highway Design and Construction, University of Wyoming, Laramie*, *1*, 275–294.

Vu, H. Q., & Fredlund, D. G. (2004). The prediction of one-, two-, and three-dimensional heave in expansive soils. *Canadian Geotechnical Journal*. https://doi.org/10.1139/T04-023

Wang, D., Sánchez, M., & Briaud, J.-L. (2016). Behavior of railroads on shrink-swell soils [Texas A&M University]. In *E3S Web of Conferences* (Vol. 9). https://doi.org/10.1051/e3sconf/20160920007

Wang, D., Sánchez, M., & Briaud, J.-L. (2018). Existing railroads on shrink-swell soils: Field monitoring, laboratory tests, and numerical simulation. *ICRT 2017: Railway Development, Operations, and Maintenance - Proceedings of the 1st International Conference on Rail Transportation 2017*, *2017-July*, 1080–1089. https://doi.org/10.1061/9780784481257.108

Wheeler, S. J., Gallipoli, D., & Karstunen, M. (2002). Comments on use of the Barcelona Basic Model for unsaturated soils. *International Journal for Numerical and Analytical Methods in Geomechanics*. https://doi.org/10.1002/nag.259

Wheeler, S. J., Sharma, R. S., & Buisson, M. S. R. (2003). Coupling of hydraulic hysteresis and stress-strain behaviour in unsaturated soils. *Geotechnique*. https://doi.org/10.1680/geot.2003.53.1.41

Wheeler, S. J., & Sivakumar, V. (1995). An elasto-plastic critical state framework for unsaturated soil. *Geotechnique*. https://doi.org/10.1680/geot.1995.45.1.35

Wray, W. K. (1978). *Development of a Design Procedure For Residential and Light Commercial Slabs-on-Ground Constructed Over Expansive Soils*. Texas A&M University.

Wray, W. K. (1989). *Mitigation of Damage to Structures Supported on Expansive Soils*. US Department of Commerce, National Technical Information Service.

Wray, W. K., El-Garhy, B. M., & Youssef, A. A. (2005). Three-dimensional model for moisture and volume changes prediction in expansive soils. *Journal of Geotechnical and Geoenvironmental Engineering*. https://doi.org/10.1061/(ASCE)1090-0241(2005)131:3(311)

Zhang, J., Little, D. N., Hariharan, N., & Kim, Y. R. (2019). Prediction of climate specific vertical

movement of pavements with expansive soils based on long-term 2D numerical simulation of rainwater infiltration. *Computers and Geotechnics*. https://doi.org/10.1016/j.compgeo.2019.103172

Zhang, X., & Briaud, J.-L. (2010). Coupled water content method for shrink and swell predictions. *International Journal of Pavement Engineering*, *11*(1), 13–23. https://doi.org/10.1080/10298430802394154

APPENDIX A

Summary of Findings

Table A.1 Comparison between recommended depths of active zone by Australian method and survey results

TMI	**AS 2870**	**Survey Value**
--	H_s [m]	Z_a [m]
10 to 40	1.5	2.7
-5 to 10	1.8	3.0
-15 to -5	2.4	4.0
-25 to -15	3.0	6.1
-40 to -25	4.0	9.1
≤ -40	> 4.0	> 9.1

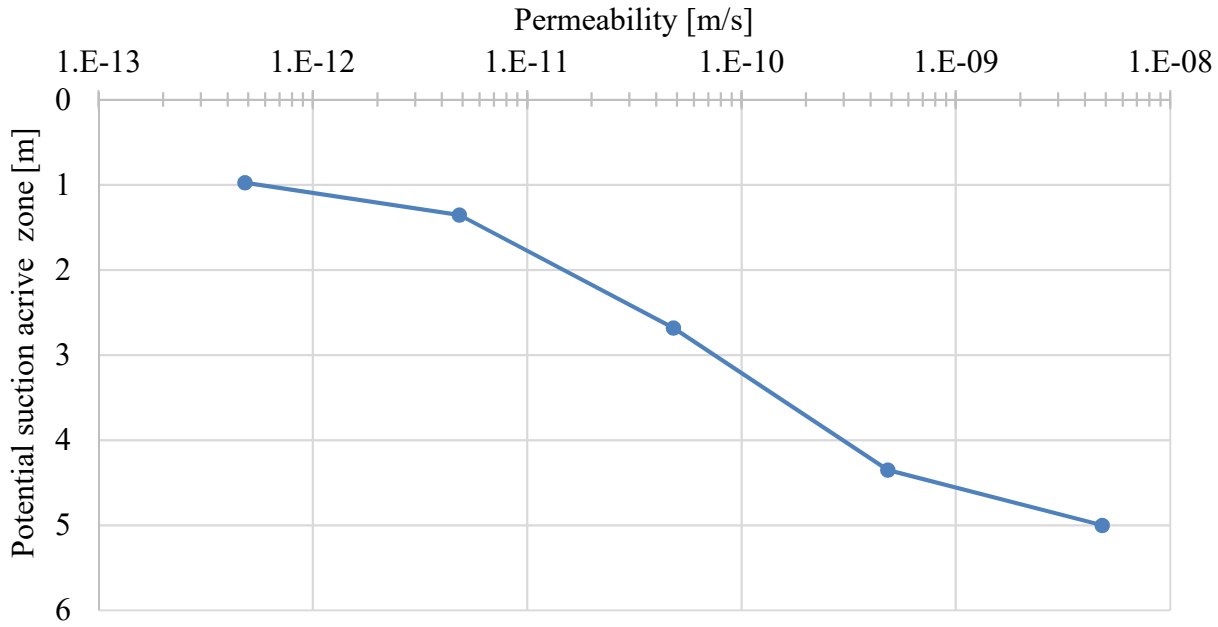

Figure A.9.1 Active zone curve for the depth of active zone of permeability under critical weather combination

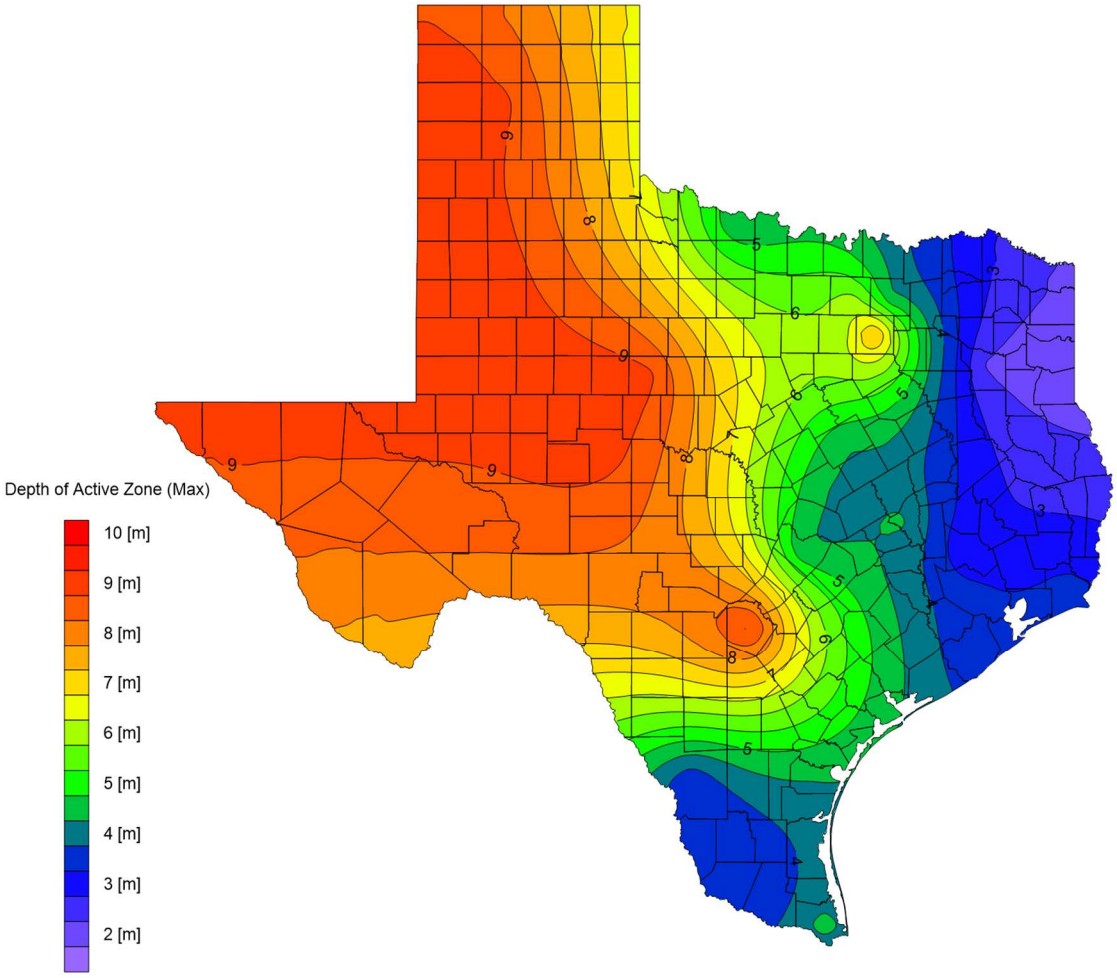

Figure A.9.2 Distribution of depth of active zone in Texas Maximum replied value

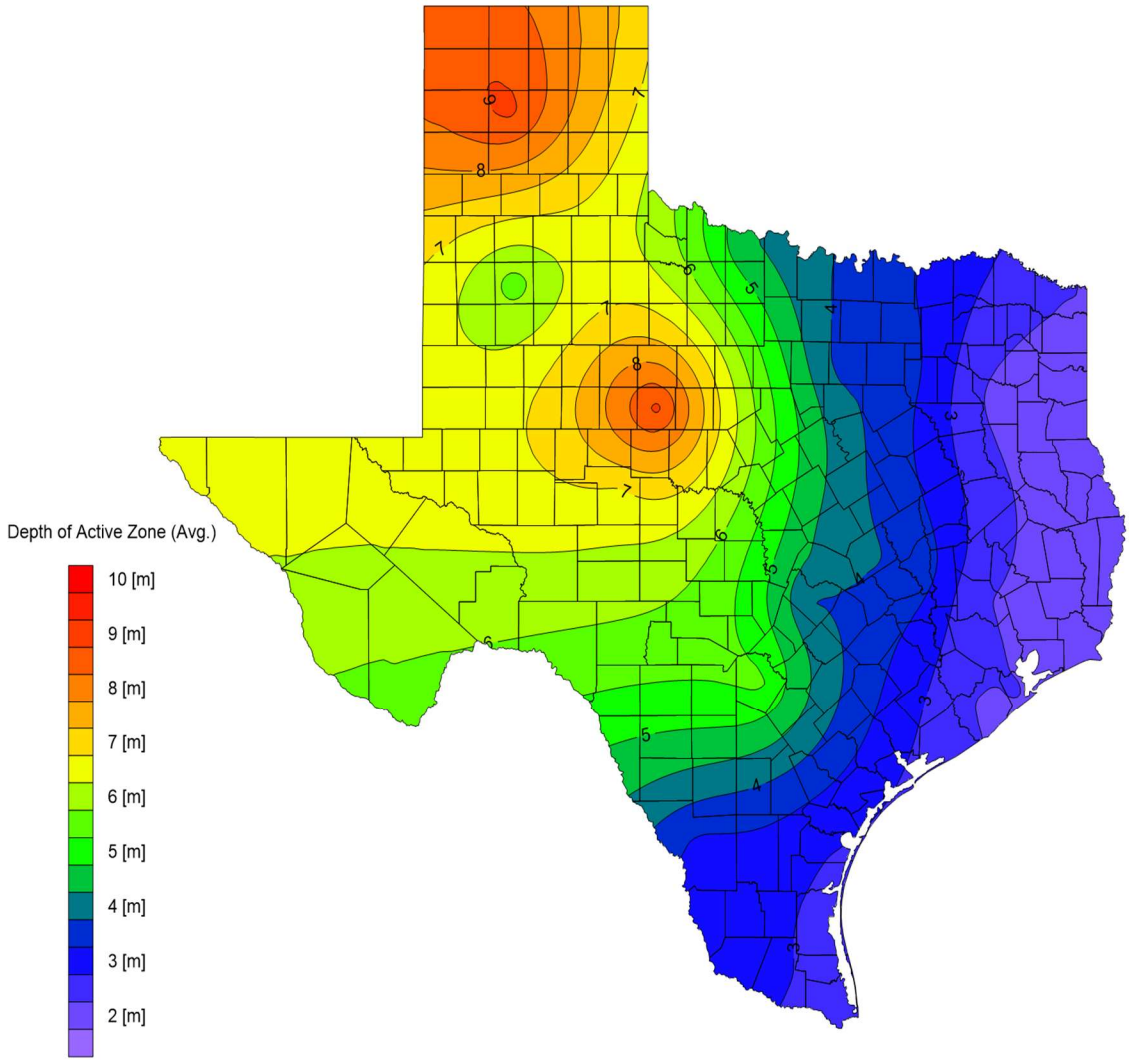

Figure A.9.3 Distribution of depth of active zone in Texas Averaged replied value

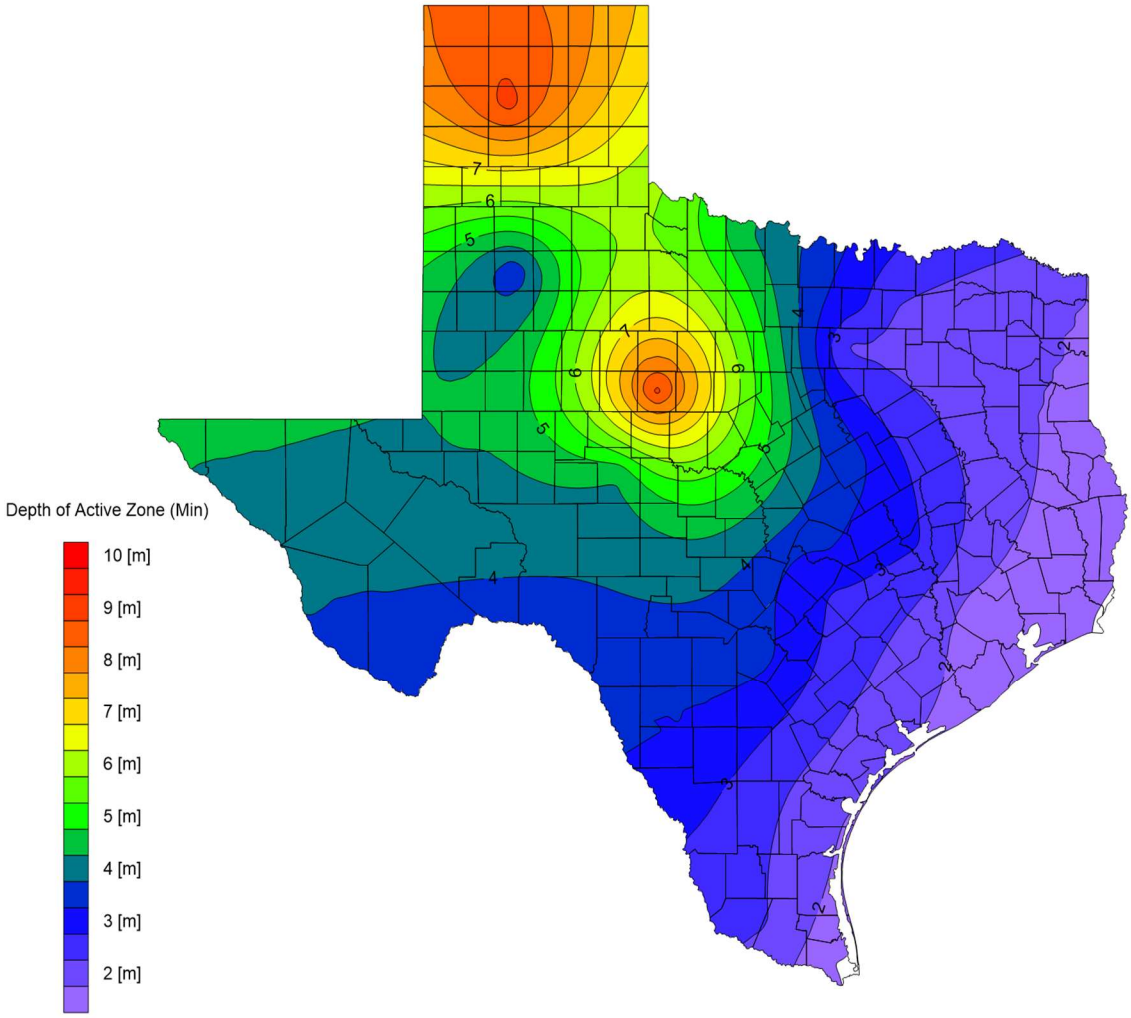

Figure A.9.4 Distribution of depth of active zone in Texas Minimum replied value

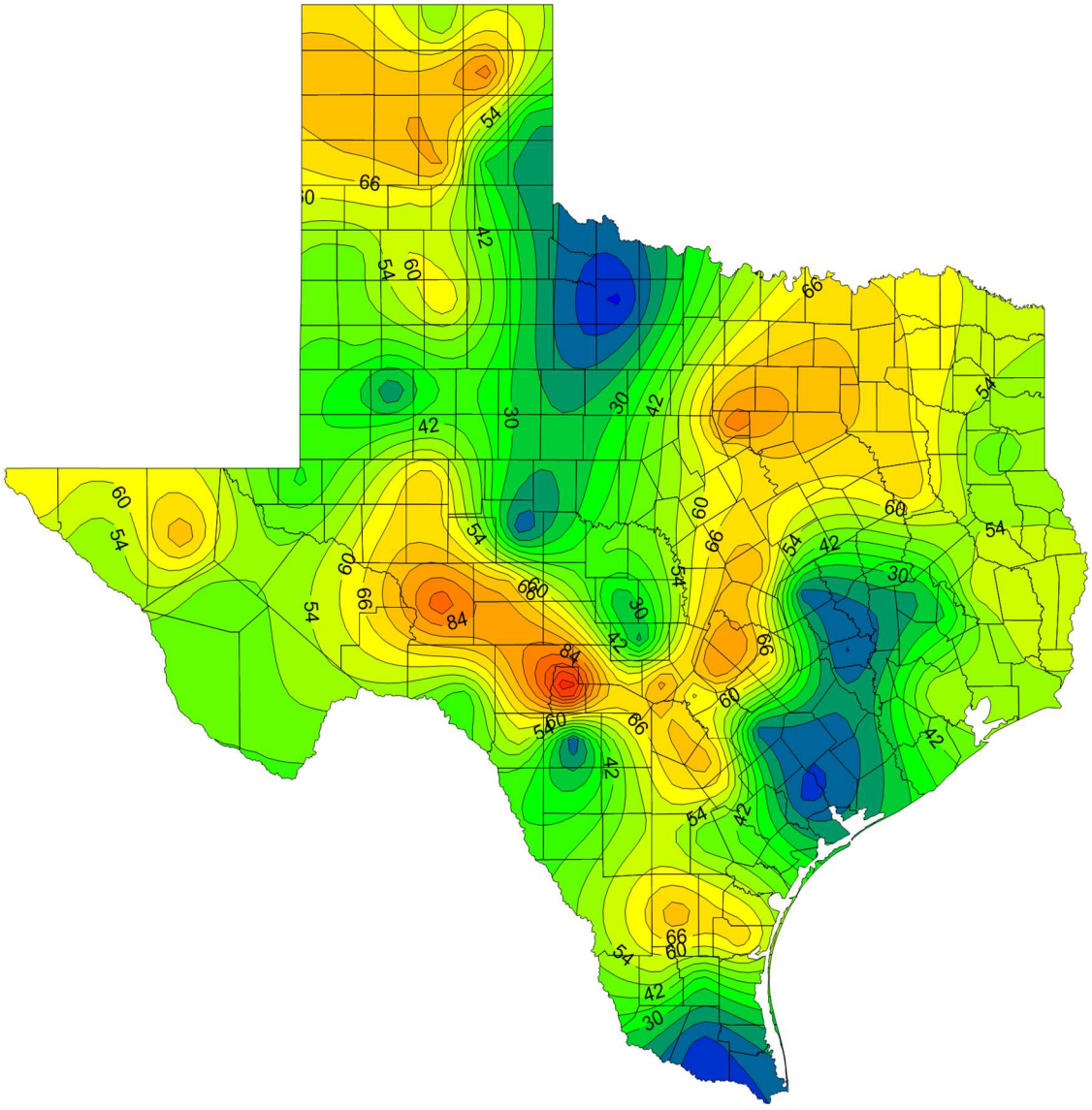

Figure A.9.5 Distribution of water table in Texas (Data accessed on Oct 12.2020 from https://waterdatafortexas.org/groundwater)

APPENDIX B

Organization of Fictitious Case

	Weather Parameters		Structural Parameters								Soil Parameters												
	Thornthwaite Index	Climate Rating Index	Slab size	Slab size	Thickness of slab	Width of beam	Spacing of beam	Area distributed loading	Perimeter loading	Ground slope	Plasticity Index	Active zone	Shrink-Swell Index	Crack zone	Unconfined compression strength	Soil reactivity	Soil fabric factor	Percent of fine particle	Elastic modulus of soil	Surface suction in wet weather	Surface suction in dry weather	Moisture change	Suction change
	Im	Cw	L(long)	L'(short)	t	bw	s	w	p	C0	PI	Hs	Iss	z	qu	Ips	Ff	%fc	Es	--	--	Δw	Δu
	--	--	m	m	m	m	m	kPa	kPa	kPa	kN/m	Degree	%	%	m	%	m	kPa	%/pF	--	%	kPa	pF
Method		BRAB	BRAB	BRAB	BRAB	BRAB	BRAB	BRAB			BRAB												
		WRI	WRI	WRI	WRI	WRI		WRI		WRI	WRI				WRI								
			AS 2870	AS 2870		AS 2870	AS 2870					AS 2870		AS 2870		AS 2870							AS 2870
	PTI		PTI	PTI	PTI	PTI	PTI		PTI		PTI						PTI	PTI	PTI	PTI	PTI		
						TAMU-SLAB	TAMU-SLAB	TAMU-SLAB				TAMU-SLAB	TAMU-SLAB							TAMU-SLAB	TAMU-SLAB	TAMU-SLAB	TAMU-SLAB
1=Refer	0	21	24	12	0.1	0.3	4.6	2E+07	1E+07	10	15	0	30	50	2	22	1	200	4.08	1.2	65	1E+04	3
2	-10	17	24	12	0.1	0.3	4.6	2E+07	1E+07	10	15	0	30	50	2	22	1	200	4.08	1.2	65	1E+04	3
3	-20	14	24	12	0.1	0.3	4.6	2E+07	1E+07	10	15	0	30	50	3	22	1	200	4.08	1.2	65	1E+04	3
4	10	24	24	12	0.1	0.3	4.6	2E+07	1E+07	10	15	0	30	50	2	22	1	200	4.08	1.2	65	1E+04	3
5	20	27	24	12	0.1	0.3	4.6	2E+07	1E+07	10	15	0	30	50	2	22	1	290	4.08	1.2	65	1E+04	3
6	-18	15	24	12	0.1	0.3	4.6	2E+07	1E+07	10	15	0	30	50	3	22	1	200	4.08	1.2	65	1E+04	3
7	13	25	24	12	0.1	0.3	4.6	2E+07	1E+07	10	15	0	30	50	2	22	1	200	4.08	1.2	65	1E+04	3
8	28	30	24	12	0.1	0.3	4.6	2E+07	1E+07	10	15	0	30	50	2	22	1	200	4.08	1.2	65	1E+04	3
9	0	21	24	12	0.1	0.3	2.7	2E+07	1E+07	10	15	0	30	50	2	22	1	200	4.08	1.2	65	1E+04	3
10	0	21	24	12	0.1	0.3	3.7	2E+07	1E+07	10	15	0	30	50	2	22	1	200	4.08	1.2	65	1E+04	3
11	0	21	24	12	0.1	0.3	5.5	2E+07	1E+07	10	15	0	30	50	2	22	1	200	4.08	1.2	65	1E+04	3
12	0	21	24	12	0.1	0.3	6.4	2E+07	1E+07	10	15	0	30	50	2	22	1	200	4.08	1.2	65	1E+04	3
13	0	21	24	12	0.1	0.3	4.6	2E+07	1E+07	5	15	0	30	50	2	22	1	200	4.08	1.2	65	1E+04	3
14	0	21	24	12	0.1	0.3	4.6	2E+07	1E+07	8	15	0	30	50	2	22	1	200	4.08	1.2	65	1E+04	3
15	0	21	24	12	0.1	0.3	4.6	2E+07	1E+07	12	15	0	30	50	2	22	1	200	4.08	1.2	65	1E+04	3
16	0	21	24	12	0.1	0.3	4.6	2E+07	1E+07	15	15	0	30	50	2	22	1	200	4.08	1.2	65	1E+04	3
17	0	21	24	12	0.1	0.3	4.6	2E+07	1E+07	10	7	0	30	50	2	22	1	200	4.08	1.2	65	1E+04	3
18	0	21	24	12	0.1	0.3	4.6	2E+07	1E+07	10	22	0	30	50	2	22	1	200	4.08	1.2	65	1E+04	3
19	0	21	24	12	0.1	0.3	4.6	2E+07	1E+07	10	15	0	25	50	2	18	1	200	3.82	1.2	65	1E+04	3
20	0	21	24	12	0.1	0.3	4.6	2E+07	1E+07	10	15	0	40	50	2	29	1	200	4.60	1.2	65	1E+04	3
21	0	21	24	12	0.1	0.3	4.6	2E+07	1E+07	10	15	0	45	50	2	33	1	200	4.86	1.2	65	1E+04	3
22	0	21	24	12	0.1	0.3	4.6	2E+07	1E+07	10	15	0	60	90	2	44	1	200	5.63	1.2	65	1E+04	3
23	-22	14	24	12	0.1	0.3	4.6	2E+07	1E+07	10	15	0	30	50	3	22	2	200	4.08	1.2	65	1E+04	3
24	-40	8	24	12	0.1	0.3	4.6	2E+07	1E+07	10	15	0	30	50	5	22	2	200	4.08	1.2	65	1E+04	3
25	-40	8	24	12	0.1	0.3	4.6	2E+07	1E+07	10	15	0	30	50	6	22	3	200	4.08	1.2	65	1E+04	3
26	0	21	24	12	0.1	0.3	4.6	2E+07	1E+07	10	15	0	48	50	2	35	1	200	3.00	1.2	65	1E+04	3
27	0	21	24	12	0.1	0.3	4.6	2E+07	1E+07	10	15	0	64	50	2	47	1	200	3.50	1.2	65	1E+04	3
28	0	21	24	12	0.1	0.3	4.6	2E+07	1E+07	10	15	0	80	90	2	59	1	200	4.00	1.2	65	1E+04	3
29	0	21	24	12	0.1	0.3	4.6	2E+07	1E+07	10	15	0	80	90	2	59	1	200	4.50	1.2	65	1E+04	3
30	0	21	24	12	0.1	0.3	4.6	2E+07	1E+07	10	15	0	30	50	2	22	1	200	4.08	1.2	65	1E+04	3
31	0	21	24	12	0.1	0.3	4.6	2E+07	1E+07	10	15	0	30	50	2	22	1	200	4.08	1.2	65	1E+04	3
32	0	21	24	12	0.1	0.3	4.6	2E+07	1E+07	10	15	0	30	50	2	22	1	200	4.08	1.2	65	1E+04	3
33	0	21	24	12	0.1	0.3	4.6	2E+07	1E+07	10	15	0	30	50	2	22	1	200	4.08	1.2	65	1E+04	3
34	0	21	24	12	0.1	0.3	4.6	2E+07	1E+07	10	15	0	30	50	2	22	1	200	4.08	1.2	65	1E+04	3

APPENDIX C

Calculation Steps for Slab-On-Grade Methods

BRAB Method

The undrained shear strength was measured as about 200 kPa. In this BRAB concludes that there is no need for stiffening beams. However, for the purpose of this case history, we will proceed with the BRAB design procedure.

$$\frac{q_u}{w} = \frac{200}{10} = 20 \; not \; within \in [2.5, 7.5]$$

The slab should be designed with reinforcement and stiffening beams.

The climate rating index in College Station is 20 ($C_w = 20$), and the plasticity index $PI = 40\%$.

The soil support index is graphically determined as follows,

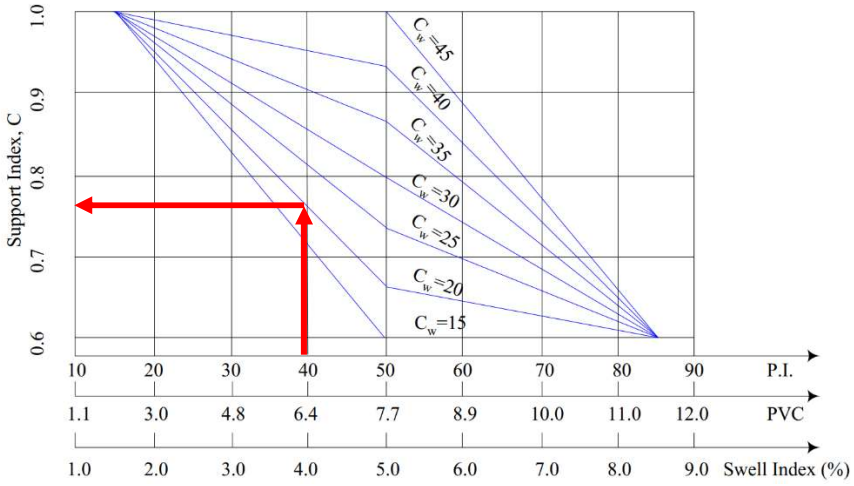

The support index $C = 0.76$

Considering that this is a one-story building and that there is no heavily loaded columns, the ratio of the concentrated load distributed on the slab to the distributed load on the slab is assumed to be $w_c/w = 0.1$

$$\because C = 0.76 > 0.65 - 0.1 = 0.55$$

$$\therefore C = C_{reduce} = \left(2.5 - \frac{q_u}{w}\right)\left[0.13 - 0.2\left(\frac{w_c}{w} + C\right)\right] + \left(0.65 - \frac{w_c}{w}\right)$$

$$= \left(2.5 - 20\right)\left[0.13 - 0.2\left(0.1 + 0.76\right)\right] + \left(0.65 - 0.1\right)$$

$$= 1.285$$

The "reduced" support index is even larger than the original value because of the high value of undrained shear strength. For the purpose of case history, use the original support index C=0.76 for further calculation. The maximum moment and shear force for the design load and the soil conditions are calculated as follows.

$$M_{\max} = \frac{wL^2L'\left(1-C\right)}{8} = \frac{10 \times 38.1^2 \times 18.3 \times \left(1-0.76\right)}{8} = 7969.339kN \cdot m$$

$$V_{\max} = \frac{wLL'\left(1-C\right)}{2} = \frac{10 \times 38.1 \times 18.3 \times \left(1-0.76\right)}{2} = 836.68kN$$

The width of the beam is fixed at 1ft and the spacing in both directions is 12 ft.

The design criterion $\frac{\Delta_{max}}{L} = 360$ is adopted in this case, where the maximum deflection is given by

$$\Delta_{\max} = \frac{wL^4L'\left(1-c\right)}{48EI}$$

The moment inertia I is calculated as

$$I = \frac{1}{12}b_w h^3$$

$$\frac{wL^4L'\left(1-c\right)}{48EI} < \frac{L}{360} \rightarrow h > \sqrt[3]{\frac{wL^4L'\left(1-c\right) \times 360 \times 12}{n \times 48EL \times b_w}}$$

Where n is the number of beams, in the long direction

$$n = \left\lceil \frac{18.3}{3} \right\rceil + 1 = 7$$

Thus,

$$h > \sqrt[3]{\frac{wL^4L'(1-c)\times 360\times 12}{7\times 48EL\times b_w}}$$

$$h > \sqrt[3]{\frac{10\times 38.1^4\times 18.3\times(1-0.76)\times 360\times 12}{6\times 48\times 20\times 10^6\times 38.1\times 0.3}}$$

$$h > 1.82m$$

For construction purposes, the 1.8m depth of beam is adapted to both long and short direction.

BRAB Method with TxASCE Modification

The TxASCE modification limits the length of the slab to 50 ft and reduces the elastic modulus of concrete E from 3000000 psi to a creep modulus of 1500000 psi. The calculation is then repeated as above, and the depth of the beam becomes 2.9 ft (0.88m).

WRI Method

Note: Because the design curve is based on imperial unit, calculation is performed based on imperial unit.

The slope of the construction site is 0. The slope correction factor is therefore $C_5 = 1$.

The consolidation correction factor based on $q_u = 30\ psi \times 0.072 tsf/psi = 2.16\ tsf$, $C_0 = 0.9$

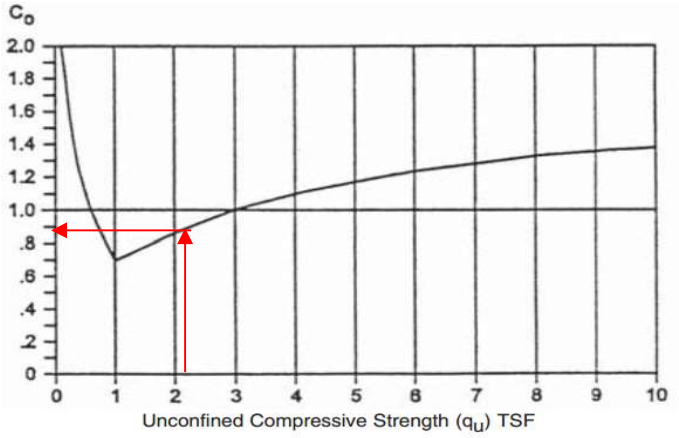

The effective plasticity index PI_0 is calculated as

$$\begin{aligned} PI_0 &= PI \times C_5 \times C_0 \\ &= 40 \times 1 \times 0.9 \\ &= 36\% \end{aligned}$$

The climate rating index in College Station is $C_w = 20$. Based on the climate rating index and the effective plasticity index, the spacing and the cantilever distance for the beam can be determined from the design curve.

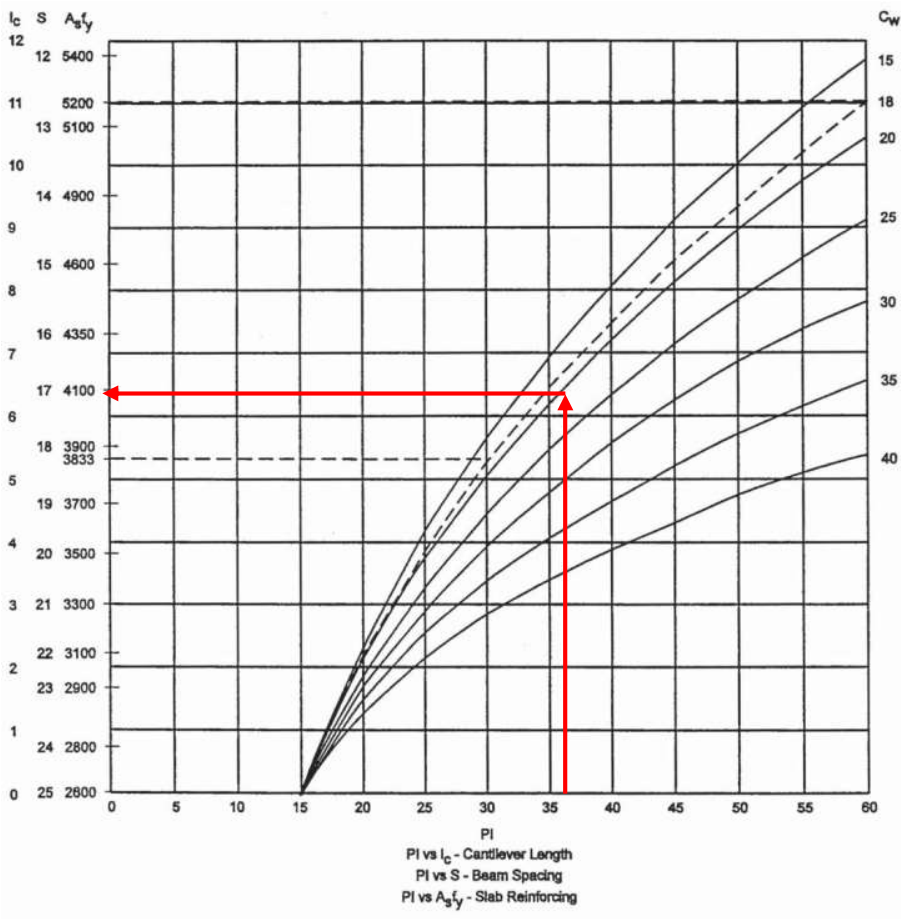

Thus, the cantilever length for the design slab is 6.5 ft, and the spacing of the beam is 17 ft. And the cantilever length is modified based on the actual length of the slab which is $125\ ft \times 60\ ft$

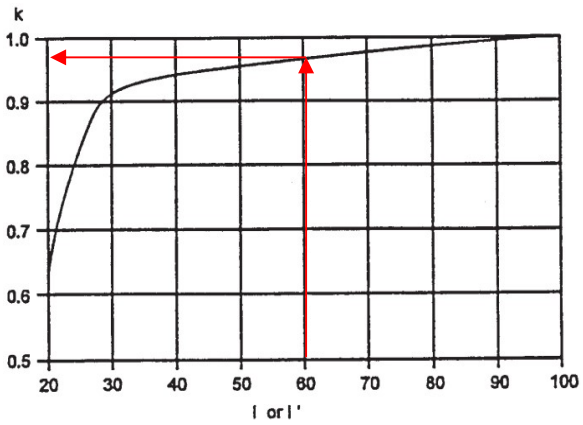

The modification factors for the long and the short side of the slab are 1 and 0.96 respectively, and the modified cantilever length is 6.5 ft and 6.24 ft.

For the beams in the long direction, the number of beams is

$$n = \left\lceil \frac{60}{17} \right\rceil + 1 = 5$$

The maximum moment and shear force are calculated as follows

$$M_{\max} = \frac{wL'\left(L_c\right)^2}{2} = \frac{1.45 \times 144 \times 60 \times \left(6.5\right)^2}{2} = 264.654 kips \cdot ft$$
$$V_{\max} = wL'L_c = 1.45 \times 144 \times 60 \times 6.5 = 81.432 kips$$

The depth of the beam can then be directly calculated as

$$d = \sqrt[3]{\frac{664ML_c}{B}} = \sqrt[3]{\frac{664 \times 264.65 \times 6.5}{5 \times 1 \times 12}} = 26.7in = 2.2ft$$

Thus, the depth of beam design by WRI method is 2.2 ft (0.67m).

WRI with TxASCE Modification

The TxASCE modification limits the length of the slab to 50 ft and the minimum length of cantilever to 6 ft. The modification factor for the cantilever length is 0.95. Thus, the modified cantilever length is 6.175 ft in both directions of the slab.

The number of beams n is calculated as

$$n = \left\lceil \frac{50}{17} \right\rceil + 1 = 4$$

The maximum moment and shear force are changed as follows

$$M_{\max} = \frac{wL'\left(L_c\right)^2}{2} = \frac{1.45 \times 144 \times 50 \times \left(6.175\right)^2}{2} = 199.041 kips \cdot ft$$
$$V_{\max} = wL'L_c = 1.45 \times 144 \times 50 \times 6.175 = 64.467 kips$$

The depth of the beams is then calculated as

$$d = \sqrt[3]{\frac{664ML_c}{B}} = \sqrt[3]{\frac{664 \times 199.041 \times 6.175}{4 \times 1 \times 12}} = 2.14 ft = 0.65 m$$

AS 2870 Method

The Thornthwaite index in College Station is 0. According to the standard recommendation, the depth of suction change will be 1.8 m. However, a suggested value from Abdelmalak (Abdelmalak, R., & Briaud, J. L., 2016) is 2.4m, which is adopted in the calculation.

The depth of the cracking zone is assumed to be 1/3 of the depth of suction change. Thus, the depth of the cracking zone is 0.8m.

The shrinkage index I_{ps} in the AS 2870 method is defined as the percentage of vertical strain per unit change in suction, (%/pF). The suction compressibility index is defined as the change in volumetric strain per unit suction change. The average value of the suction compressibility index provided in Abdelmalak and Briaud (2016) is 20 %/pF. The shrinkage index is taken as one third of the volumetric index as the soil shrinks in all three directions. Thus, the shrinkage index is $(20/3 \approx)7\%$.

The shrinkage behavior is different in the cracked zone and in the uncracked zone. The AS 2870 method provides a factor α to modify the shrinkage index $I_{pt} = I_{ps} \times \alpha$.

The suction variation at the ground surface is assumed to be 2pF together with a linear decrease with depth down to the bottom of the suction change zone.

The depth of the suction change zone is divided into 10 segments for further calculation. The different values of the shrinkage index and of the suction variation are summarized in the table below. The movement of segment i, $y_{s,i}$, is calculated as

$$y_{s,i} = \Delta u \times I_{pt} \times h_i$$

$y_{s,i}$	the movement of segment i
Δu	Change of suction
I_{pt}	Shrinkage index
h_i	Height of segment i

e.g.

Segment	Mid-depth	α value	Shrinkage index	Δu	y_s
	m	--	%/pF	pF	mm
S1	0.12	1	7	1.9	31.92
S2	0.36	1	7	1.7	28.56
S3	0.6	1	7	1.5	25.20
S4	0.84	1.83	12.82	1.3	40.01
S5	1.08	1.78	12.49	1.1	32.97
S6	1.32	1.74	12.15	0.9	26.25
S7	1.56	1.69	11.82	0.7	19.85
S8	1.8	1.64	11.48	0.5	13.78
S9	2.04	1.59	11.14	0.3	8.02
S10	2.28	1.54	10.81	0.1	2.59
				Sum	229.15

The deflection of the slab Δ is limited to 1/400 as recommended by the AS 2870 method for a masonry veneer structure. Thus, considering the long side of the slab.

$$\Delta = \frac{38.1 \times 1000}{400} = 95.25mm$$

$$\frac{y_s}{\Delta} = \frac{229.15}{95.25} = 2.4$$

And the short side of the slab

$$\Delta = \frac{18.3 \times 1000}{400} = 45.75mm$$

$$\frac{y_s}{\Delta} = \frac{229.15}{45.75} = 5$$

The unit stiffness determined by the design curve are as follows,

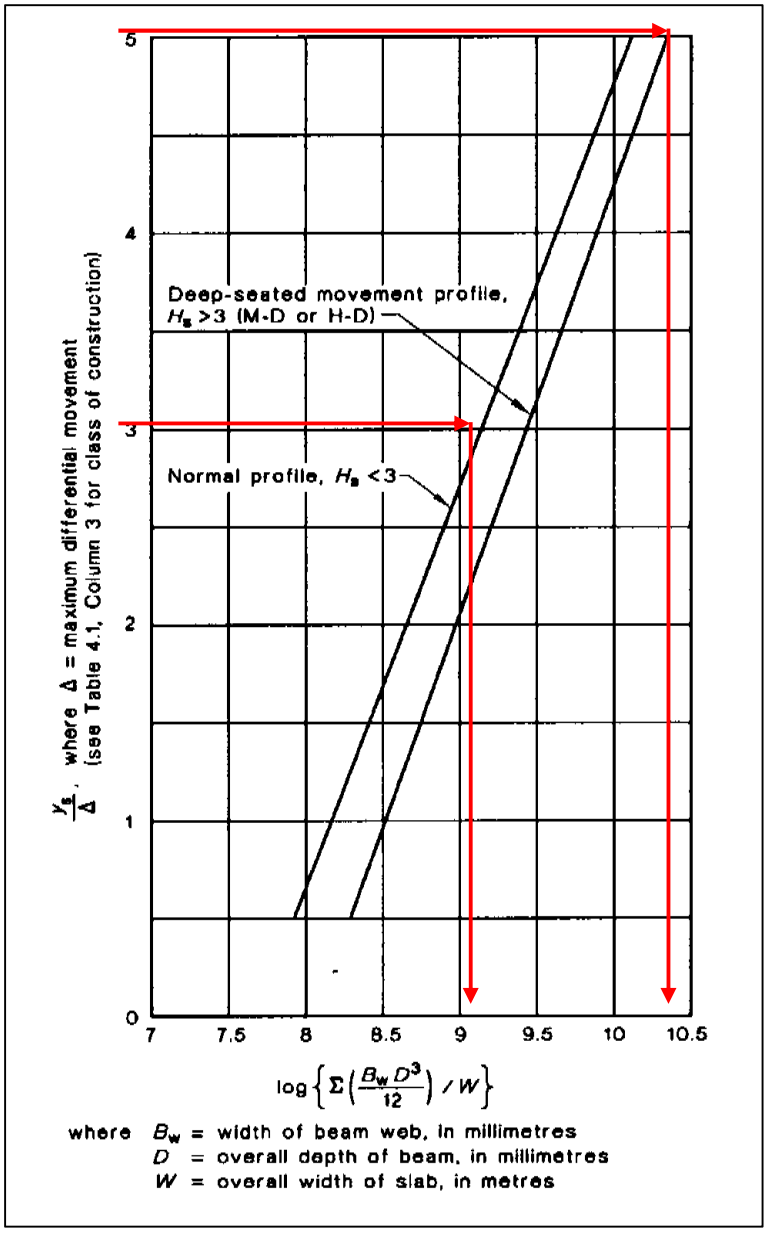

$$\log\left[\sum\left(\frac{B_w D^3}{12}\right)/W\right] = 8.8$$

Considering the deflection in the long direction together with $B_w = 0.3m, and\ W$ =18.3m, D can be determined. Assuming the spacing of the beams is equal to 3.6m (12ft). The number of beams in the short direction is 6.

$$\log\left[6\times\frac{0.3\times1000\times D^3}{12}/18.3\right]=8.8$$

$$D=0.425m$$

Considering the deflection in the short direction together with $B_w = 0.3m$, $W = 38.1m$ and the number of beams in the long direction being 12

$$\log\left[12\times\frac{0.3\times1000\times D^3}{12}/38.1\right]=10.1$$

$$D=1.17m$$

For practical consideration, the depth of the beam used is 1.17m in both directions.

PTI Method

Note: because empirical method is applied, all the calculation is performed based on imperil unit.

The PTI method can be divided into two main parts: the soil movement part and the structural part.

1. ***Soil movement determination***

The plasticity index is $PI = 40\%$, and the liquid limit is $LL = 58\%$
The percentage of fine particles is assumed to be $\%f_c = 20\%$

Note: ($\%f_c = percentage\ of\ soil\ passing\ 2\ \mu m\ sieve / percentage\ of\ soil\ passing\ 75 \mu m\ sieve$)

The mineral composition of the soil is graphically determined by PI and LL in the chart below and is classified as zone 1.

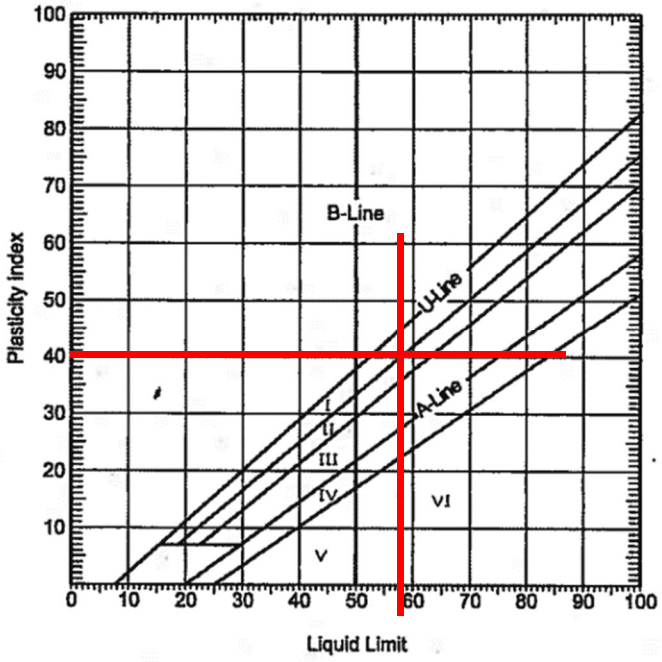

The percent change in soil volume per unit change in soil suction for 100% fine clay γ_0 is graphically determined by the ratio $(PI/\%f_c =)2$ and $(LL/\%f_c =)2.9$. Thus, $\gamma_0 = 0.35$

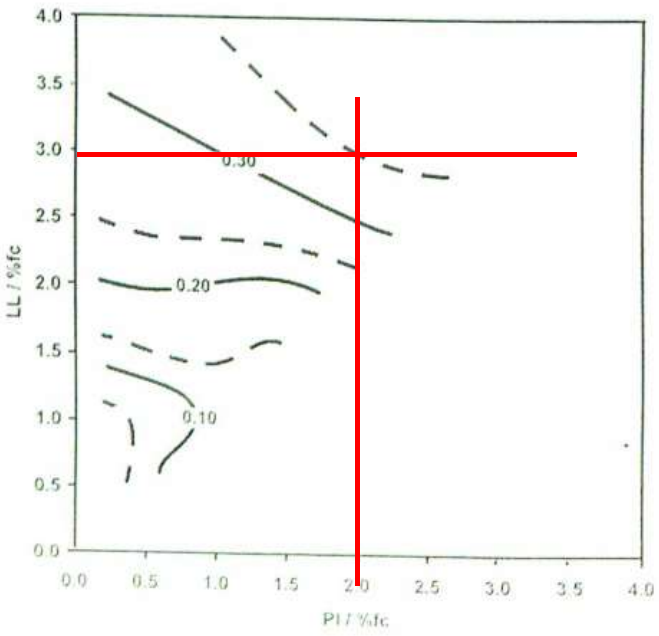

The suction compression index γ_h, defined as the change of soil volume per unit suction for 100% fine clay modified by the actual percentage of fine particle is calculated for both swelling and shrinkage behavior

$$\begin{aligned}\gamma_{h,swell} &= \gamma_0 e^{\gamma_0}\left(\%f_c/100\right)\\ &= 0.35\times e^{0.35}\times 0.2\\ &= 0.099\end{aligned}$$

$$\begin{aligned}\gamma_{h,shrink} &= \gamma_0 e^{-\gamma_0}\left(\%f_c/100\right)\\ &= 0.35\times e^{-0.35}\times 0.2\\ &= 0.049\end{aligned}$$

The slope of the soil water retention curve for this soil is calculated as follows, assuming that the percentage finer than sieve #200 is 50% $((\% - \#200) = 50\%)$

$$\begin{aligned}S_s &= -20.29 + 0.1555LL - 0.117PI + 0.0684\left(\% - \#200\right)\\ &= -20.29 + 0.1555\times 58 - 0.117\times 40 + 0.0684\times 50\\ &= -12.531\end{aligned}$$

Calculate the unsaturated diffusion coefficient α, where swelling refers to edge lift and shrinking refers to center lift.

$$\begin{aligned}\alpha_{swell} &= 0.0029 - 0.000162 \times S_s - 0.0122 \times \gamma_{h,swell} \\ &= 0.0029 - 0.000162 \times -12.531 - 0.0122 \times 0.099 \\ &= 3.72 \times 10^{-3}\end{aligned}$$

$$\begin{aligned}\alpha_{shrink} &= 0.0029 - 0.000162 \times S_s - 0.0122 \times \gamma_{h,shrink} \\ &= 0.0029 - 0.000162 \times -12.531 - 0.0122 \times 0.049 \\ &= 4.33 \times 10^{-3}\end{aligned}$$

Determine the fabric factor F_f, which is the modification factor applied to the unsaturated diffusion coefficient for the presence of roots. In this calculation $F_f = 1.2$.

The modified unsaturated diffusion coefficient is then calculated

$$\alpha'_{swell} = 3.72 \times 10^{-3} \times 1.2 = 4.46 \times 10^{-3}$$
$$\alpha'_{shrink} = 4.33 \times 10^{-3} \times 1.2 = 5.20 \times 10^{-3}$$

The Thornthwaite Moisture Index, I_m is 0

The edge moisture variation distance e_m is graphically determined as follows

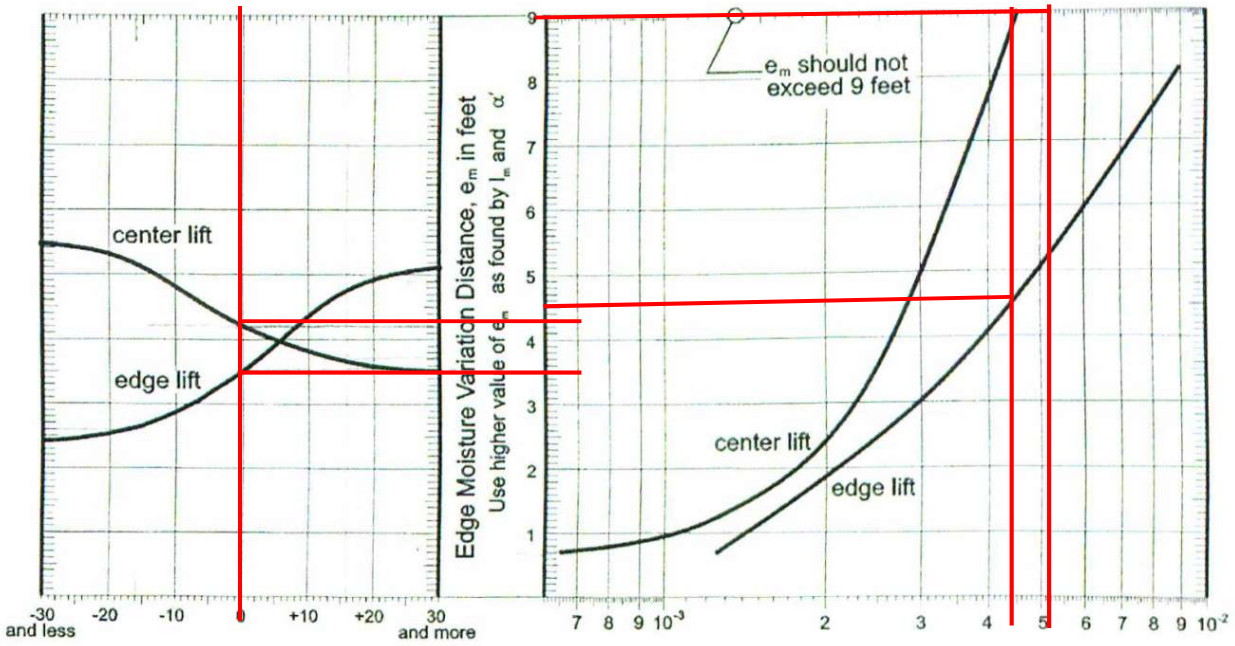

$$e_{m,center}\left(I_m\right) = 4.2\,ft$$
$$e_{m,edge}\left(I_m\right) = 3.5\,ft$$

And

$$e_{m,center}\left(\alpha'_{shrink}\right) = 9\,ft$$
$$e_{m,edge}\left(\alpha'_{swell}\right) = 4.8\,ft$$

Use the larger value of the e_m values, thus

$$e_{m,center} = 9\,ft$$
$$e_{m,edge} = 4.8\,ft$$

The equilibrium suction for the soil refers to the most common suction condition and is determined by the Thornthwaite Moisture Index as shown below.

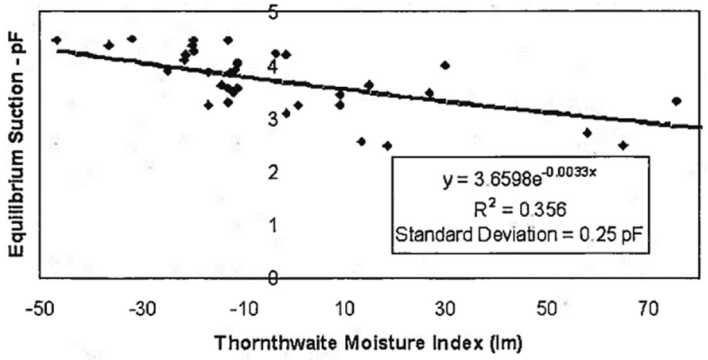

For $I_m = 0$,

$$Equilibrium\ suction = 3.66\,pF$$

We assume that the driest suction and the wettest suction are equal to 4.5 and 3 pF.

The stress change factor (SCF) is the factor quantifying the amount of maximum unrestrained differential soil movement induced by the suction change.

	Final Controlling Suction at Surface, pF						
Equilibrium Suction	2.5	2.7	3	3.5	4	4.2	4.5
2.7	3.2	0	-4.1	-13.6	-25.7	-31.3	-40
3	9.6	5.1	0	-7.5	-18.2	-23.1	-31.3
3.3	11.7	12.1	5.1	-2.6	-11.5	-15.8	-23.1
3.6	27.1	20.7	12.1	1.6	-5.7	-9.4	-15.8
3.9	38.1	30.8	20.7	7.3	-1.3	-4.1	-9.4
4.2	50.4	42.1	30.8	14.8	3.2	0	-4.1
4.5	63.6	54.7	42.1	23.9	9.6	5.1	0

$$SCF-edge = 13.82$$
$$SCF-center = -14.52$$

The maximum unrestrained differential soil movement y_m is calculated as

$$\begin{aligned} y_{m,edge} &= (SCF-edge)\gamma_{h,swell} \\ &= 13.82 \times 0.099 \\ &= 1.37in \end{aligned}$$

$$\begin{aligned} y_{m,center} &= (SCF-center)\gamma_{h,shrink} \\ &= -14.52 \times 0.049 \\ &= -0.71in \end{aligned}$$

In a summary, the soil movement is as follows.

	Center lift	Edge lift
e_m	9 ft	4.8 ft
y_m	0.71 in	1.37 in

2. ***Structural design***

The shape factor, SF, is used to determine the regularity of the foundation,

$$SF = \frac{Perimeter^2}{Area} = \frac{2(125+60)}{125 \times 60} = 0.05 < 24$$

The foundation is therefore considered to be regular, and no additional modification is necessary to the footprint.

Lets try a distance from the edge of the foundation to the maximum moment point $\beta = 8ft$. In the long direction

$$L = 125\,ft > 6\beta = 48\,ft$$

Then we will use the smaller value of 48 ft for further calculations.

For the center lift condition, for a service line load $P = 1000\ lb/ft$, and for a design criterion $C_\Delta = 360$, the beam depth h is calculated as

$$h = \left(\frac{\left(y_m L\right)^{0.205} S^{1.059} P^{0.523} e_m^{1.296} C_\Delta}{4560 z} \right)^{0.824}$$

$$= \left(\frac{\left(0.71 \times 125\right)^{0.205} 12^{1.059} 1000^{0.523} 9^{1.296} 360}{4560 \times 48} \right)^{0.824}$$

$$= 19.44in$$

In the short direction

$$L = 60\,ft > 6\beta = 48\,ft$$

$$h = \left(\frac{\left(0.71 \times 60\right)^{0.205} 12^{1.059} 1000^{0.523} 9^{1.296} 360}{4560 \times 48} \right)^{0.824}$$

$$= 17.18in$$

In this case, we will try a beam depth of 36 in

Sectional properties are summarized as following

	Long direction	Short direction
Depth of beam, h (in)	36	36
Width of beam, b_w (in)	12	12
Number of beams	6	12
Total width of beams, (in)	72	144
Thickness of slab, (in)	4	4

For beams in the long direction

Section	Area (in^2)	y (in)	Ay (in^3)	Ay^2 (in^4)	I_0 (in^4)
Slab (60x12x4)	2880	-2	-5760	11520	3840
Beam (72x32)	2304	-16	-36864	589824	196608
Sum:	5184	--	42624	601344	200448

$$y_t = \sum Ay / \sum A = 42624 / 5184 = 8.22in$$
$$I = \left(\sum Ay^2 + \sum I_0\right) - Ay_t^2 = 601344 + 200448 - 5184 \times 8.22^2 = 451517.41in^4$$
$$S_t = I / y_{top} = 451517.41 / 8.22 = 54929.126in^3$$
$$S_b = I / y_{bottom} = 451517.41 / \left(36 - 8.22\right) = 16253.33in^3$$

For beams in the short direction

Section	Area (in^2)	y (in)	Ay (in^3)	Ay^2 (in^4)	I_0 (in^4)
Slab (125x12x4)	6000	-2	-12000	24000	8000
Beam (144x32)	4608	-16	-73728	1179648	393216
Sum:	10608	--	85728	1203648	401216

$$M_L = A_0\left[B\left(e_m\right)^{1.238} + C\right]$$

$$y_t = \sum Ay / \sum A = 85728 / 10608 = 8.08in$$
$$I = \left(\sum Ay^2 + \sum I_0\right) - Ay_t^2 = 1203648 + 401216 - 10608 \times 8.08^2 = 912057.629in^4$$
$$S_t = I / y_{top} = 912057.629 / 8.08 = 112878.42in^3$$
$$S_b = I / y_{bottom} = 912057.629 / \left(36 - 8.08\right) = 32666.82in^3$$

Center lift design ($e_m = 9ft, y_m = 0.71\ in$)

Moment calculations

Long direction

Where

$$A_0 = \frac{1}{727}\left[L^{0.013} S^{0.306} h^{0.688} P^{0.534} {y_m}^{0.193}\right]$$

$$0 \le e_m \le 5 \qquad \begin{cases} B = 1 \\ \mathrm{C} = 0 \end{cases}$$

$$5 < e_m \qquad \begin{cases} B = \dfrac{y_m - 1}{3} \le 1.0 \\ C = \left[8 - \dfrac{P - 613}{255} \right] \dfrac{4 - y_m}{3} \ge 0 \end{cases}$$

Thus,

$$\begin{aligned} A_0 &= \frac{1}{727} \left[L^{0.013} S^{0.306} h^{0.688} P^{0.534} y_m{}^{0.193} \right] \\ &= \frac{1}{727} \left[125^{0.013} 12^{0.306} 36^{0.688} 1000^{0.534} 0.71^{0.193} \right] \\ &= 1.38 \end{aligned}$$

$$B = \frac{y_m - 1}{3} = \frac{0.71 - 1}{3} = -0.097 \le 1.0$$

$$C = \left[8 - \frac{P - 613}{255} \right] \frac{4 - y_m}{3} = \left[8 - \frac{1000 - 613}{255} \right] \frac{4 - 0.71}{3} = 7.11 \ge 0$$

$$\begin{aligned} M_L &= A_0 \left[B \left(e_m \right)^{1.238} + C \right] \\ &= 1.38 \left[-0.097 \left(9 \right)^{1.238} + 7.11 \right] \\ &= 7.78 \, ft \cdot kips \, / \, ft \end{aligned}$$

Also, for a distance $e_m = 5\ ft$, the moment will be

$$\begin{aligned} M_L &= A_0 \left[B \left(e_m \right)^{1.238} + C \right] \\ &= 1.38 \left[\left(5 \right)^{1.238} \right] \\ &= 10.12 \, ft \cdot kips \, / \, ft \end{aligned}$$

Use $M_L = 10.12\ ft \cdot kips/ft$.

Short direction

For the case where the long side of the slab (LL) divided by the short side of the slab (LS)>1.1

$$M_s = \frac{(58 + e_m) M_L}{60}$$
$$= \frac{(58+9)7.78}{60}$$
$$= 8.69\, ft \cdot kips / ft$$

Also, for a distance $e_m = 5\ ft$, the moment will then be

$$M_s = \frac{(58 + e_m) M_L}{60}$$
$$= \frac{(58+5)10.12}{60}$$
$$= 10.63\, ft \cdot kips / ft$$

Use $M_s = 10.63\ ft \cdot kips/ft$

Now we need to compare the actual stress with the allowable stress under the service load. The allowable concrete tensile and compressive stress are determined as follows

$$f_t = 6\sqrt{f'_c} = 6\sqrt{3000} = 329\, psi = 0.329 ksi$$
$$f_c = 0.45 f'_c = 0.45 \times 3000 = 1350\, psi = 1.35 ksi$$

Long direction

Tension at the top

$$f = -\frac{M_L}{S_t} = -\frac{10.12 \times 60 \times 12}{54929.126} = 0.133 ksi < 0.329 ksi \text{ Ok!}$$

Compression at the bottom

$$f = \frac{M_L}{S_b} = \frac{10.12 \times 60 \times 12}{16253.33} = 0.448 ksi < 1.35 ksi \text{ Ok!}$$

Short direction

$$f = -\frac{M_s}{S_t} = -\frac{10.63 \times 125 \times 12}{54929.126} = 0.29 ksi < 0.329 ksi \text{ Ok!}$$

$$f = \frac{M_L}{S_b} = \frac{10.63 \times 125 \times 12}{16253.33} = 0.98 ksi < 1.35 ksi \text{ Ok!}$$

Compare the stiffness of the slab

Long direction

$$\beta = \frac{1}{12}\sqrt[4]{\frac{E_{cr}I}{E_{soil}}} = \frac{1}{12}\sqrt[4]{\frac{1500000 \times 451517.41}{1000}} = 13.44\,ft$$

$$6\beta = 80.66 < 125 \therefore Z_L = 80.66\,ft$$

$$E_{cr}I_L \geq 18000 M_L L_s C_\Delta Z_L$$

$$I_L \geq \frac{18000 M_L L_s C_\Delta Z_L}{E_{cr}} = \frac{18000 \times 10.12 \times 60 \times 360 \times 80.66}{1500000} = 211579.57 in^4$$

$$I = 451517.41 >> I_L = 211579$$

Stiffness is OK in long direction

Short direction

$$\beta = \frac{1}{12}\sqrt[4]{\frac{E_{cr}I}{E_{soil}}} = \frac{1}{12}\sqrt[4]{\frac{1500000 \times 912057.629}{1000}} = 16.03\,ft$$

$$6\beta = 96.16 > 60 \therefore Z_s = 60\,ft$$

$$I_L \geq \frac{18000 M_s L_L C_\Delta Z_s}{E_{cr}} = \frac{18000 \times 10.63 \times 125 \times 360 \times 60}{1500000} = 344412 in^4$$

$$I = 912057.629 >> I_L = 344412$$

Stiffness is OK in short direction

Shear calculations

Long direction

The expected service shear load is calculated as follows

$$\begin{aligned} V_L &= \frac{L^{0.09} S^{0.71} h^{0.43} P^{0.44} y_m^{0.16} e_m^{0.93}}{1940} \\ &= \frac{125^{0.09} 12^{0.71} 36^{0.43} 1000^{0.44} 0.71^{0.16} 9^{0.93}}{1940} \\ &= 3.31 kips / ft \end{aligned}$$

$$V = \frac{V_L W}{nbh} = \frac{3.31 \times 60 \times 1000}{6 \times 12 \times 36} = 76.62 psi$$

The permissible shear stress is

$$V_c = 1.7\sqrt{f'_c} = 1.7\sqrt{3000} = 93.11 psi > 76.62 psi$$

Shear stress is ok in the long direction

Short direction

The expected service shear load is calculated as follows

$$\begin{aligned} V_s &= \frac{L^{0.19} S^{0.45} h^{0.2} P^{0.54} y_m^{0.04} e_m^{0.97}}{1350} \\ &= \frac{60^{0.19} 12^{0.45} 36^{0.2} 1000^{0.54} 0.71^{0.04} 9^{0.97}}{1350} \\ &= 2.32 kips / ft \end{aligned}$$

$$V = \frac{V_s W}{nbh} = \frac{2.32 \times 125 \times 1000}{12 \times 12 \times 36} = 55.94 psi$$

The permissible shear stress is

$$V_c = 1.7\sqrt{f'_c} = 93.11 psi > 55.94 psi$$

Shear stress is ok in the short direction

Edge lift design ($e_m = 4.8ft, y_m = 1.37$ in)

Long direction

$$\begin{aligned} M_L &= \frac{S^{0.1} \left(he_m\right)^{0.78} y_m^{0.66}}{7.2 L^{0.0065} P^{0.04}} \\ &= \frac{12^{0.1} \left(36 \times 4.8\right)^{0.78} 1.37^{0.66}}{7.2 \times 125^{0.0065} 1000^{0.04}} \\ &= 8.96 kips / ft \end{aligned}$$

Short direction

For the length of the long side divided by the length of the short side >1.1

$$M_s = h^{0.35}\left[\left(19+e_m\right)/57.75\right]M_L$$
$$= 36^{0.35}\left[\left(19+4.8\right)/57.75\right]8.96$$
$$= 12.94 kips/ft$$

Long direction

Tension at the top

$$f = -\frac{M_L}{S_t} = -\frac{8.96\times 60\times 12}{54929.126} = 0.117 ksi < 0.329 ksi \text{ Ok!}$$

Compression at the bottom

$$f = \frac{M_L}{S_b} = \frac{8.96\times 60\times 12}{16253.33} = 0.397 ksi < 1.35 ksi \text{ Ok!}$$

Short direction

$$f = -\frac{M_s}{S_t} = -\frac{12.94\times 125\times 12}{54929.126} = 0.353 ksi > 0.329 ksi \text{ Failure}$$

$$f = \frac{M_L}{S_b} = \frac{12.94\times 125\times 12}{16253.33} = 1.194 ksi < 1.35 ksi \text{ Ok!}$$

Shear calculation

Long direction

The expected service shear load is calculated as follows

$$V_L = \frac{L^{0.07}h^{0.4}P^{0.03}e_m^{0.16}y_m^{0.67}}{3S^{0.015}}$$
$$= \frac{125^{0.07}36^{0.4}1000^{0.03}4.8^{0.16}1.37^{0.67}}{3\times 12^{0.015}}$$
$$= 3.69 kips/ft$$

$$V = \frac{V_L W}{nbh} = \frac{3.69\times 60\times 1000}{6\times 12\times 36} = 85.33 psi$$

The permissible shear stress is

$$V_c = 1.7\sqrt{f'_c} = 1.7\sqrt{3000} = 93.11psi > 85.33psi$$

Shear stress is ok in the long direction

Short direction

The expected service shear load is calculated as follows

$$V_L = \frac{L^{0.07} h^{0.4} P^{0.03} e_m^{0.16} y_m^{0.67}}{3S^{0.015}}$$
$$= \frac{60^{0.07} 36^{0.4} 1000^{0.03} 4.8^{0.16} 1.37^{0.67}}{3 \times 12^{0.015}}$$
$$= 3.5kips / ft$$

$$V = \frac{V_s W}{nbh} = \frac{3.5 \times 125 \times 1000}{12 \times 12 \times 36} = 84.39psi$$

The permissible shear stress is

$$V_c = 1.7\sqrt{f'_c} = 93.11psi > 84.39psi$$

Shear stress is ok in the short direction

Thus, because the beam depth is too small according to the bending moment requirements in the short direction, the beam depth is increase to 3.5ft (1.07m), with a spacing of 12ft (3.65m).

TAMU-SLAB method

The calculations start by assuming a beam depth $D = 1m = 3\ ft$, a beam width $b = 0.3m = 1\ ft$ and a beam spacing $S = 3.5m\ (12\ ft)$. Then the equivalent depth is calculated.

$$Sd_{eqv}^3 = bD^3 \rightarrow d_{eqv} = \sqrt[3]{\frac{bD^3}{S}}$$

$$d_{eqv} = \sqrt[3]{\frac{bD^3}{S}} = \sqrt[3]{\frac{0.3\times 1^3}{3.5}} = 0.44m$$

The water content variation is taken from Briaud (2013), a reasonable estimate of the water content variation in College Station is 5.8% at the edge of the slab. The depth of the active zone is kept as 2.4 m as in the other calculations.

$$\begin{aligned} I_{s-w} &= H \times \Delta w_e \\ &= 2.4 \times 0.058 \\ &= 0.14m \end{aligned}$$

The design parameters can then be read on the design charts using the value of I_{s-w}

Edge drop (shrink)

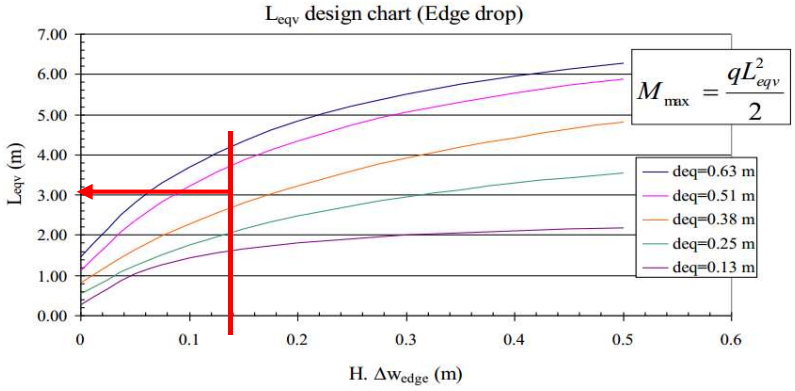

$L_{eqv} = 3m$

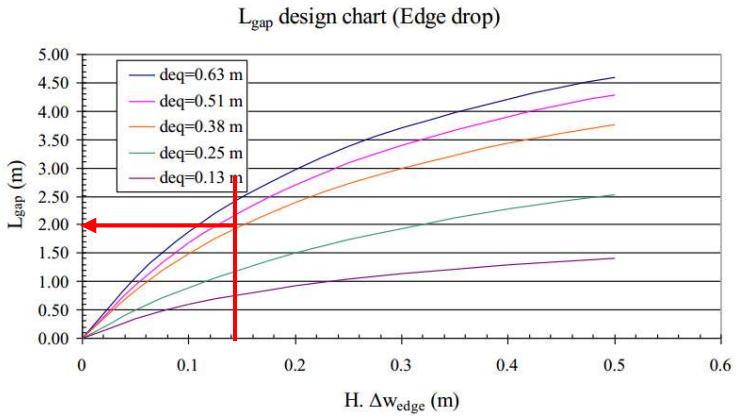

$L_{gap} = 2\ m$

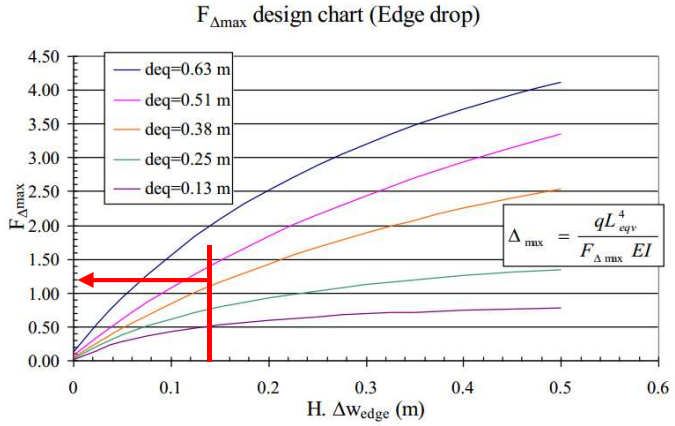

$F_{\Delta max} = 1.2$

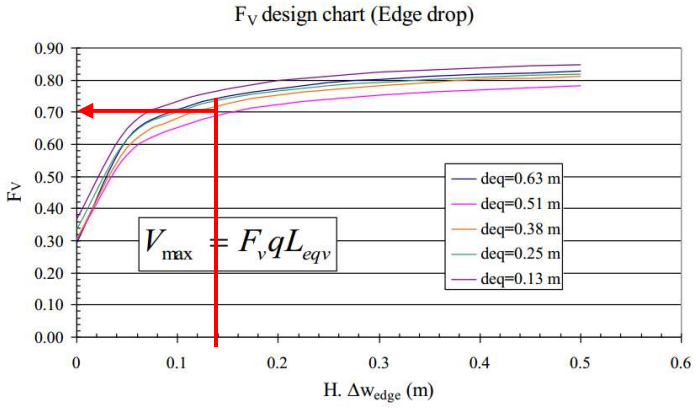

$F_v = 0.7$

Edge lift (swell)

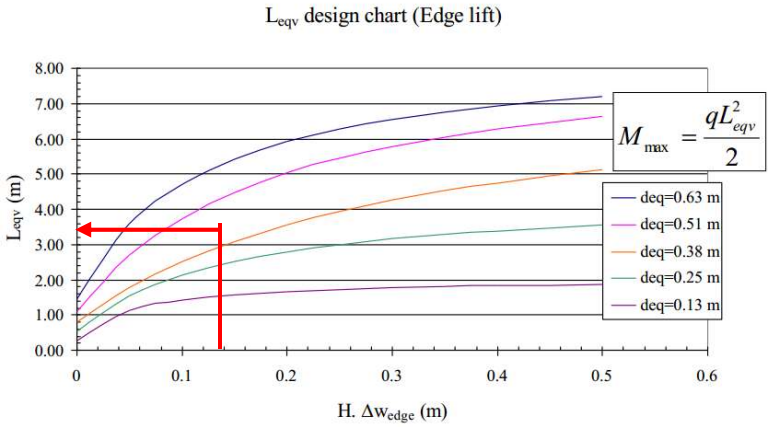

$L_{eqv} = 3.2m$

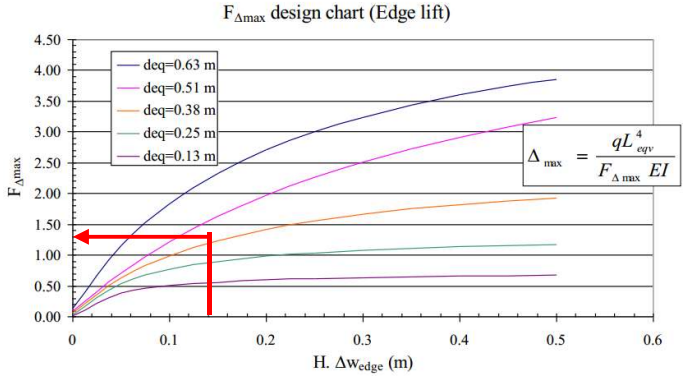

$F_{\Delta max} = 1.4$

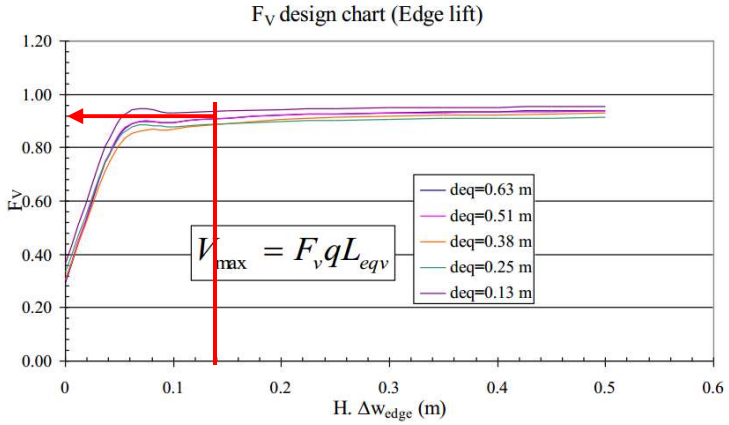

$F_V = 0.88$

The reduction factor due to the length of the slab and the depth of the active zone is shown in the figure below. Since L/2H is larger than 2, there is no need to apply a reduction factor.

$$\frac{L}{2H} = \frac{38.1}{2 \times 2.4} = 7.93$$

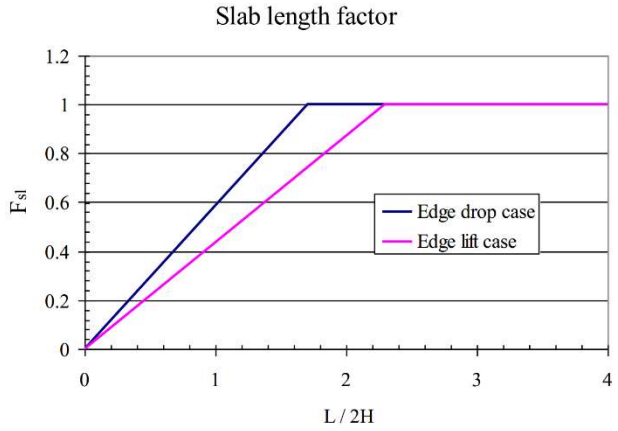

The design uniform load is 208 psf (10kPa), the elastic modulus of concrete is 20 GPa, thus the maximum allowable deflection Δ_{all} is calculated as

$$\Delta_{all} = \frac{L_{eqv}}{360} = \frac{3 \times 1000}{360} = 8.33mm$$

The maximum deflection Δ_{max} is

$$\Delta_{\max} = \frac{qL_{eqv}^4}{F_{\Delta \max} EI_{cr}}$$

Where q is the design uniform load applied to the spacing between two beams, E is the elastic modulus of concrete and I_{cr} is the critical moment inertia of beam taken as one half of the moment intertia of the beam I. By assuming the depth of beam is 1ft (0.9144m), I is calculated as,

$$I = \frac{bh^3}{12} = \frac{0.3 \times 0.9144^3}{12} = 0.0191m^4$$

Edge drop

$$\Delta_{\max} = \frac{qL_{eqv}^4}{F_{\Delta\max} EI_{cr}} = \frac{10 \times 12 \times 0.3048 m / ft \times 3^4}{1.2 \times 20 \times 10^6 \times 0.0191/2} = 0.0129 m = 12.9 mm \text{ Failed!}$$

Edge lift

$$\Delta_{\max} = \frac{qL_{eqv}^4}{F_{\Delta\max} EI_{cr}} = \frac{10 \times 12 \times 0.3084 m / ft \times 3.2^4}{1.4 \times 20 \times 10^6 \times 0.0191/2} = 0.0145 m = 14.5 mm \text{ Failed!}$$

Therefore, the beam depth needs to be increased. Finally, a beam depth of 1.1m is found to satisfy the distortion requirement.